Uncertainty Propagation and Global Sensitivity Analysis in Multi-layered Hydrogeological Models of Flow and Lifetime Expectancy

thesis presented at the

Faculty of Sciences

Center for Hydrogeology and Geothermics (CHYN)

University of Neuchâtel, Switzerland

for the degree of

Doctor of Sciences

presented by

Grégory Deman

accepted on the recommendation of

Prof. Pierre Perrochet - University of Neuchâtel
Dr Jaouher Kerrou - University of Neuchâtel
Prof. Bruno Sudret - ETH Zürich
Dr Abdelhakim Benabderrahmane - Andra, Châtenay-Malabry, France

Defended on October 1, 2015

UNIVERSITÉ DE NEUCHÂTEL

Faculté des sciences
Secrétariat-décanat de Faculté
Rue Emile-Argand 11
2000 Neuchâtel - Suisse
Tél: + 41 (0)32 718 2100
E-mail: secretariat.sciences@unine.ch

IMPRIMATUR POUR THESE DE DOCTORAT

La Faculté des sciences de l'Université de Neuchâtel autorise l'impression de la présente thèse soutenue par

Monsieur Grégory DEMAN

Titre:

"Uncertainty propagation and global sensitivity analysis in multi-layered hydrogeological models of flow and lifetime expectancy"

sur le rapport des membres du jury composé comme suit:

- Prof. Pierre Perrochet, Université de Neuchâtel, directeur de thèse
- Dr Jahouer Kerrou, Université de Neuchâtel, co-directeur de thèse
- Prof. Bruno Sudret, ETH Zürich
- Dr Abdelhakim Benabderrahmane, ANDRA, Châtenay-Malabry, France

Neuchâtel, le 11 novembre 2015

Le Doyen, Prof. B. Colbois

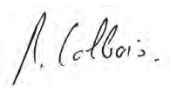

Contents

Acknowledgements

Cinq années de collaboration active au sein du Centre d'Hydrogéologie et de Géothermie de l'Université de Neuchâtel ont permis de donner naissance à la présente thèse de doctorat. C'est avec déférence que je tiens à témoigner ici de ma profonde gratitude envers celles et ceux sans qui elle n'aurait sans doute pas vu le jour.

Mes premiers mots iront pour mes parents, Annie et Marc, qui ont su me donner force et courage tout au long de ma vie, qui m'ont offert leur amour, leur confiance et leur soutien sans faille depuis mes premiers instants. Mes frères, Jérémy et Guillaume, sans qui je ne saurais être "*celui du milieu*" ; ils sont ma joie, ma fierté, mon engagement et ma récompense. À feu mes grand-parents, à mes oncles, tantes, cousins et cousines: quel bonheur de vous savoir toujours à mes côtés !

Le Docteur Jaouher Kerrou, co-directeur de cette thèse, fut un superviseur consciencieux sachant faire preuve d'une rigueur scientifique inouïe: l'apanage des grands instructeurs. Sa véhémence pour la découverte scientifique en font un chercheur d'exception. Je fus honoré de la confiance qu'il m'a témoigné, et du prestige d'être devenu son premier "Docteur".

En qualité de directeur de thèse, le Professeur Pierre Perrochet m'aura transmis bien plus qu'un large savoir scientifique. La patience, l'humilité et la compassion sont les plus grands enseignements qu'il aura su me transmettre. Guide magnanime, il est pour beaucoup un mentor et, pour moi, un véritable ami.

Mécène des travaux présentés ci-après, le Docteur Abdelhakim Benabderrahmane m'enseigna par-dessus tout le pragmatisme: médication prescrite aux chercheurs atteints de "*fièvre académicienne*" ; dont j'espère à présent être immunisé à vie.

Le Professeur Bruno Sudret est, à mes yeux, l'archétype du scientifique avant-gardiste. L'étude des méthodes qu'il développe à l'ETH m'ont apporté le changement de paradigme que j'avais si longtemps recherché. Ma gratitude se tourne vers Katerina Konakli, collaboratrice à l'ETH, dont la bonté ne saurait trouver d'égal dans ma mémoire. Je lui dédie cette thèse, en remerciement de notre fructueuse collaboration.

Les Docteurs William Becker et Stefano Tarantola du *Joint Research Centre of the European Commission* resteront à jamais les protagonistes du grand mystère de ces cinq années. Aujourd'hui encore je m'interroge sur les raisons qui les ont poussés à suivre l'idée saugrenue du statisticien autodidacte hautement inexpérimenté que j'étais ; idée qui aura finalement aboutie sous la forme d'un chapitre dans cette thèse.

Un grand merci à Laurent Tacher pour sa bonne humeur lors des séances Andra, et à Fabien Cornaton pour rappeler qu'après l'effort vient le réconfort (à la Taverne Neuchâteloise). Merci à Philippe Renard, homme de science qui sait rester Homme avant tout.

Durant ces années j'ai pu partager le bonheur de vivre sur les contreforts du Jura helvétique avec les amis du CHYN et de Neuchâtel: Cec' (spéléologue waterproof), Lucio (le doigt de la raison), Lorienne (nana-schiste au cœur d'or), Frank (skieur 5 étoiles), François (Paco-nnemara), Yoan (Impartial sur la torrée), Geoffrey & Lilou (pouet-pouet & môman), Martin & Dylan (accord en Là majeurs), Dom' & Andrea (Unix pour toujours).

Mais aussi Claire, Damian, Giona, Stefan(o) & Charlotte, Lukas, Schnaps, Guillaume & Ghazal, Jeanne & Marius, Fabio, Paul, Antoine, Julien, Nicolas, Luca, Pierik, Jess', Jérôme, Didier, Juju, Hub', Raoul, Samy, Vince, Léa, Cybèle, Alice, Oliver, Axa, Daniel, Ellen, Michiel, Roberto, Christian, Félix, Mitra, Romain & Nadège, Félie, Marco & Veronica, la famiglia Piccioli/Bobbià, Pupi, Hawaï et tous les autres.

À tous les zycos de l'AZYNE: merci de m'avoir permis de passer mes nerfs sur les tomes et les cymbales.

Une pensée chaleureuse pour mes amis de Fontanès, de Montpellier, de Grenoble, de Melbourne et de Fréjus ; dont la liste serait aussi longue que ce manuscrit si j'omettais les virgules...

Mes derniers mots iront pour la femme de ma vie: Alessandra Bobbià. Bien plus qu'Un amour, bien plus que Mon amour, elle est l'Amour: envers chaque chose, chaque être et en chaque instant. Elle fut la voix de la raison quand je perdis la mienne, elle croit en moi lorsque je peine à m'élever.

Tu m'as révélé un beau matin de février alors que je ne rêvais plus que d'espoir. Oui, c'est la vérité: nous aurions bien plus à aimer maintenant que l'on ne s'accorderait à y croire.

Ti amo farfalla mia !!!

Keywords

Design of Experiment (DoE), Global Sensitivity Analysis (GSA), multi-layered hydrogeological model, groundwater flow, mean lifetime expectancy (MLE), radioactive wastes disposal, Meuse/Haute-Marne project.

Mots-clés

plan d'expérience, Analyse de Sensibilité Globale (ASG), modèle hydrogéologique multicouche, flux d'eau souterraine, espérance de vie moyenne (EVM), stockage de déchets radioactifs, projet Meuse/Haute-Marne.

Abstract

English

The main focus of this thesis is the uncertainty propagation (UP) and global sensitivity analysis (GSA) in complex hydrogeological numerical models. Various methods are presented with applications on numerical models for the groundwater flow and *mean lifetime expectancy* (MLE) in the scope of Andra's (French National Radioactive Waste Management Agency) project for the geological disposal of high-level and intermediate-level long-lived radioactive wastes in France.

First, a state of the art is provided for the theory of uncertainty propagation and for the methodologies of sensitivity analyses in a broad sense. Methods for UP are provided from 2-levels Factorial Designs to quasi-random samplings : Latin Hypercube Designs and Low-Discrepancy Sequences. GSA techniques encompass screening methods such as the Morris Measures and the *Derivative-based Global Sensitivity Measures* (DGSM), and also the so-called Sobol' indices based upon the variance decomposition, or analysis of variance (ANOVA), of the response of interest. Meta-modelling techniques such as polynomial regression and Polynomial Chaos Expansions (PCE) meta-models are described. They are employed as surrogate models for UP and GSA purpose at negligible computational-costs. A comparison of GSA techniques upon various complex analytical test-functions was undertaken with the purpose of determining a relevant method to be employed in the context of "screening" out unimportant variables in computer-intensive, high-dimensional models. The DGSM proved to be highly effective for such purposes.

Secondly, a numerical model of groundwater flow and lifetime expectancy is employed for assessing the effect of uncertain advection-dispersion parameters and their spatial distributions upon the MLE from a target zone inside the domain. The model is a 2-dimensions synthetic cross-section of the eastern region of the Paris Basin (Meuse/Haute-Marne sector), where Andra is prospecting a highly impermeable layer from Callovo-Oxfordian age (COX) for the construction of an underground disposal facility for the radioactive wastes. This model was used as an exploratory tool for sensitivity analysis methods applied upon numerous sets of uncertain hydrodynamic and dispersion parameters in 15 layers. The uncertainty characterizing the permeability-porosity values in aquifer formations encompassing the COX have proved to add much of variability to the MLE calculated from the target zone. The model also served at exploring the effect of the spatial variability of permeability-porosity parameters in two main aquifer sequences on the groundwater flow rates and MLE in the model. The variabilities of the output responses are mainly due to the uncertainty upon the means and variances of the permeability-porosity distributions, as well as the longitudinal correlation lengths, in each sequence.

Then, a 3-dimensions high-definition hydrogeological model representing the Meuse/Haute-Marne sector in the eastern region of the Paris Basin is a more comprehensive numerical model incorporating realistic geometries, fractures, heterogeneities and discontinuities encountered on field. A sensitivity analysis of the MLE from a given zone located in the middle of the COX layer was performed by perturbing the hydraulic conductivities and porosities values in fourteen hydrogeological formations resulting from calibrated flow model against measured hydraulic head and taking into account measured hydraulic conductivity and porosity values. The uncertain permeability-porosity parameters in the aquifer formations from Bathonian in the Dogger sequence, and Rauracian-Sequanian in the Oxfordian sequence, have strong and rather non-linear effects on the variability of the output response of interest.

The methodologies for UP and GSA employed in the present thesis have proved to be very efficient when applied to large hydrogeological models of groundwater flow and MLE. In particular, quasi-random sampling methods offer a flexible frame for providing the uncertainty distribution of the output response of interest at low computational costs. Screening techniques provide a fast estimation for the overall contribution of each input variable to the variability of the output. Meta-modelling techniques such as PCE proved highly accurate in individualising the low- and high-order effects of each input variable upon the output response of interest.

The application to the Andra's project gives insights on the priority to carefully define the hydraulic conductivity fields in the aquifer sequences of Oxfordian and Dogger ages encompassing the host formation. The formations with the highest groundwater fluxes are particularly pointed out, specifically those closest to the host layer. A diminution of the uncertainty characterizing the spatial variability of hydraulic conductivity values in these formations may reduce the uncertainties in the predictive modelling of groundwater flow and solute transport in the frame of the risk and safety analysis of Andra's project for the geological disposal of radioactive wastes in the Meuse/Haute-Marne sector.

Français

L'objectif principal de cette thèse est la propagation d'incertitude (PI) et l'analyse de sensibilité globale (ASG) de modèles numériques hydrogéologiques complexes. Diverses méthodes sont présentées avec une application aux modèles numériques de calcul d'écoulement d'eau souterraine et d'*espérance de vie moyenne* (EVM) dans le cadre du projet de l'Andra (Agence Nationale pour la gestion des Déchets Radioactifs) relatif au stockage géologique de déchets radioactifs de moyenne et haute activité à vie longue en France.

En premier lieu, un état de l'art établit la théorie de la propagation d'incertitude et les méthodes d'analyse de sensibilité au sens large. Parmi les méthodes de PI sont mentionnés les plans factoriels à 2 niveaux et les échantillonnages quasi-aléatoires : Hypercubes Latins et suites à discrépance faible. Les techniques d'ASG comprennent des méthodes de criblage tels que les mesures de Morris et les *Derivative-based Global Sensitivity Measures* (DGSM), elles comprennent aussi les indices de Sobol' basés sur la décomposition de la variance, ou analyse de la variance (ANOVA), de la réponse d'intérêt. Les techniques de meta-modelling comme les régression polynomiales et les Expansions de Polynômes du Chaos (EPC) sont décrites. Elles sont employées comme modèles de substitution pour la PI et l'ASG à des coûts de calculs négligeables. Une comparaison de techniques d'ASG appliquées à diverses fonctions analytiques test a été entreprise avec l'objectif de déterminer une méthode adaptée pour le criblage de variables non-significatives dans les modèles à hautes-dimensions et forts coûts de calculs. La DGSM a démontrée une grande efficacité pour de telles applications.

Dans une seconde partie, un modèle numérique d'écoulement souterrain et d'espérance de vie est utilisé pour l'estimation de l'effet de paramètres d'advection-dispersion incertains, et leurs distributions spatiales, sur l'EVM depuis une zone cible dans le domaine. Le modèle est une coupe verticale synthétique en 2-dimensions de la région Est du Bassin de Paris (secteur Meuse/Haute-Marne), où l'Andra étudie une couche hautement imperméable âgée du Callovo-Oxfordien (COX) pour l'établissement d'un centre de stockage souterrain pour les déchets radioactifs. Ce modèle a été utilisé comme outil d'exploration pour les méthodes d'analyse de sensibilité appliquées à divers groupes de paramètres hydrodynamiques et de dispersion dans 15 couches hydrogéologiques. L'incertitude relative aux valeurs de perméabilité-porosité dans les formations aquifères enserrant le COX induit une grande variabilité sur l'EVM calculée depuis la zone cible. Le modèle a aussi été employé pour estimer l'effet de la variabilité spatiale des paramètres perméabilité-porosité dans deux séquences aquifères principales sur les débits d'eau et l'EVM dans le modèle. Les variabilités des réponses sont principalement dues à l'incertitude sur les moyennes et variances des distributions de perméabilité-porosité, ainsi que sur les longueurs de corrélation longitudinales, dans chaque séquence.

Puis, un modèle hydrogéologique de haute définition en 3-dimensions représentant le secteur de Meuse/Haute-Marne dans la partie orientale du Bassin de Paris incorpore des géométries réalistes, les fractures, les hétérogénéités et les discontinuités rencontrées sur le terrain. Une étude de sensibilité de l'EVM depuis une zone localisée au centre de la couche hôte du COX a été effectuée par une perturbation des conductivités hydrauliques et porosités de quatorze formations hydrogéologiques. Les incertitudes sur les paramètres de perméabilité-porosité des formations aquifères du Bathonien dans le Dogger, et du Rauracien-Séquanien dans l'Oxfordien, ont une influence forte et relativement non-linéaire sur la variabilité de la réponse d'intérêt.

Les méthodes pour la PI et l'ASG employés dans la présente thèse ont prouvé leurs grandes efficacités dans leurs applications aux modèles hydrogéologiques d'écoulement souterrain et d'EVM. En particulier, les échantillonnages quasi-aléatoires offrent un cadre flexible pour obtenir la distribution d'incertitude de la réponse d'intérêt à de faibles coûts de calculs. Les méthodes de criblage fournissent une estimation rapide de la contribution d'ensemble de chaque variable d'entrée du modèle à la variabilité de la réponse. Les techniques de meta-modelling comme les EPC ont prouvé leur grande précision pour individualiser les effets de bas et de hauts rangs de chaque variable d'entrée sur la réponse d'intérêt.

Les applications liées au projet de l'Andra offrent un aperçu de la priorité à donner à une définition précise des champs de conductivité hydraulique dans les séquences aquifères de l'Oxfordien et du Dogger enserrant la couche hôte potentielle. Une attention particulière est à donner aux formations présentant les flux d'eau souterraine les plus importants, notamment les formations proches de la couche hôte. Une diminution de l'incertitude relative à la variabilité spatiale des valeurs de conductivité hydraulique dans ces formations permettrait de réduire les incertitudes liées à la modélisation prédictive de flux d'eau souterraine et de transport de soluté dans le cadre de l'analyse de risque et de sûreté liée au projet de l'Andra pour le stockage géologique de déchets radioactifs dans le secteur Meuse/Haute-Marne.

Chapter 1

Introduction

1.1 Motivations and state of the research

In the field of earth and water sciences, methodological and technical developments have been made to better comprehend and represent the geological structures and the physico-chemical processes associated to the groundwater flow and mass migration in the subsurface. Boreholes logs, geophysical surveys, well tests and laboratory measurements on core samples are examples of scientific investigations ordinarily achieved for defining the geometries and physics of the underground media. Even though the accuracy of such measurements can be argued, the main issue in industrial and academic studies typically concerns the unexplored sections of the natural systems. Whether it is for the purpose of extraction of natural resources, for civil engineering projects, for the geological storage of pernicious components, or simply with concern to a sustainable development, geological and hydrogeological systems are often difficult to comprehensively describe. When dealing with environmental policy requirements and/or when seeking the optimization of production operations, it becomes essential to account for the uncertainty regarding the conceptualization of the problem.

When undertaking the characterization of a real-case surface and/or subsurface domain, scientists are often oriented toward the use of numerical modelling, where complex geometrical structures can be designed and where groundwater flow and mass transport partial differential equations can be addressed through numerical integration schemes. However, the imprecise/incomplete knowledge of the structures and spatial distributions of physico-chemical parameters in the underground system compels the modeller to make a number of approximations and assumptions in the development of a numerical model. Indeed, due to the arduousness in collecting data in the underground and in completing an accurate representation of the structures and processes, it generally occurs that a given quantity of interest is affected by a relative uncertainty.

Once the conceptual model is built, calibration techniques may be employed through inverse modelling to reproduce as precisely as possible the field measurements by estimating the parameters distributions with a particular attention to zones of the model where the lack of data is significant. From there, a given model output of interest can be obtained deterministically. But, as a consequence of the assumptions and approximations made in the construction and calibration of the numerical model, the prediction or estimation of a given output quantity should be treated stochastically. The propagation of the uncertainty characterizing the model's layout and parametrization becomes then of major importance in order to estimate the outcomes associated to these assumptions and approximations. This procedure is often referred to as Uncertainty Analysis (UA), and Monte-Carlo (MC) methods are specifically dedicated to this task. Assuming that any parameter at any location in the model can be affected by a relative uncertainty, every parameter field can be treated as a stochastic variable characterized by a statistical distribution. The MC methods are employed to evaluate a given quantity of interest using different, equally probable, models, thus producing a statistical distribution for the output quantity. The latter can then be explored in the frame of a Risk Analysis (RA) for evaluating the needs and costs associated to a specific development program. In the last decades, a wide number of methods were developed for sampling the factors' uncertainty ranges as uniformly and as regularly as possible. These methods, often referred to as Quasi Monte-Carlo (QMC) sampling techniques, have the great advantage to provide a rather rigorous representation of the variability of the output response resulting from the uncertainty in the input factors.

When one is particularly interested in assessing the contribution of each uncertain factor to the variability of a given output response of interest, a Sensitivity Analysis (SA) is specifically advocated. From local to global techniques, the SA makes use of specific sampling techniques to address the sensitivity of a given output response quantity to the uncertainty characterizing each individual input factor considered. In particular, variance-based SA techniques apportion the total variance of the output response into partial variances attributed to each uncertain factor.

It must be mentioned, however, that the user shall always keep in mind the relativity of the problem posed. Fixed variables are deterministic and cannot be accounted for in a UA or SA exercise. This feature might lead to a biased estimation of the total variance of the output response in cases where these variables have a relative uncertainty, even minor, but with a large influence on the response quantity of interest. Moreover, the definition of the variables' uncertainties, through uncertainty ranges and probability density functions (PDF), are determinant in the outcome of the UA and SA. When more data become available, the variabilities of the input factors can be adjusted and thus modify the results of the uncertainty propagation. This is typically the goal of any SA with a *Factor Prioritization* setting : determine which factor shall be further quantified in priority for obtaining the highest reduction of the

variance of the response quantity. Besides, the results of a SA must always be considered relatively to the output response under study, *i.e.* with the exact same definition of input parameters, a SA upon two different output responses may lead to two different sensitivity estimates.

For many years, the petroleum industry has employed UA and SA techniques in the predictive modelling of hydrocarbon production. As an example, Feraille and Marrel (2012) provided a good comparison of uncertainty propagation techniques with various SA methods applied on a numerical model of hydrocarbon reservoir. Applying on a fractured reservoir model, Khosravi et al. (2012) employed a MC sampling for drawing response surfaces from which they extracted the most significant parameters on pressure drop and recovery factor changes.

In the last decades the geological disposal for mid to long-lived radioactive wastes has become a major issue worldwide. With regard to the geological disposal in argillaceous rocks, a consortium of state agencies manages numerous projects through scientific collaborations, research and development (NEA and OECD, 2009). The application of SA in the frame of radioactive waste repositories with focus on mass transport in the subsurface is a challenging task because of the complexity of the physico-chemical processes addressed, and because of the related large time scales.

In the frame of the Yucca mountain project (U.S. project for the geological disposal of long-lived radioactive wastes) and the Waste Isolation Pilot Plant (WIPP), Jon C. Helton has provided a number of major contributions to the development of SA applications (Helton, 1993; Helton et al., 1996, 2012, 2014). As an example, Draper et al. (1999) performed a SA over the simulation of a radionuclide chain transport in the underground and toward the biosphere. In their article, Ciriello et al. (2013) applied a meta-model based SA for estimating the effect of parameters characterizing heterogeneous fields in the migration of radionuclide.

In the scope of the geological repository for high-level (HL) and intermediate-level long-lived (IL-LL) radioactive wastes, Andra (French National Radioactive Waste Management Agency) has studied for more than 15 years the potentiality of a 500 meters deep, highly-impermeable, claystone formation from Callovo-Oxfordian (COX) age in the vicinity of Bure (Haute-Marne, France). Regulatory and statutory legislations establish the risk and safety management framework and, specifically, the "Loi Bataille" (Bataille Law) in 1991 and its extension in 2006 stipulate that *"all radioactive waste management activities must comply with environmental and health protection regulations, taking into account the rights of future generations"* (Delay et al., 2007). With this scope, Andra built a 3-dimensions geological model and later a 3D Finite Elements (FE) integrated regional-local groundwater flow model for the entire Paris Basin (ANDRA, 2005, 2012b). The numerical model was built and calibrated over more than 2000 borehole measurements. For instance, Benabderrahmane et al. (2014) successfully employed uncertainty propagation techniques for calibration purposes. The 3D model is intended to provide predictive estimates of groundwater flow and mass transport in the complex subsurface volume of the Paris Basin. However, it is acknowledged that the numerical model is affected by a relative uncertainty regarding, notably, the parameters distributions in the various geological entities of the model. It follows that performing thorough sensitivity analyses for the flow and transport processes is of major importance in order to fully comprehend the risks associated to the long-term disposal of radioactive materials in the subsurface of the Paris Basin.

1.2 Goal of the thesis

The main objectives of the present research work were to explore various UA and SA techniques with concern to their respective performances, advantages and limitations in the context of computationally demanding models. Relevant methodologies were sought in application to groundwater flow and groundwater age numerical models in the general frame of the project for the geological repository of radioactive wastes in the underground media of the Paris Basin.

A stochastic estimation of a given response of interest in large hydrogeological numerical models encompassing many uncertain parameters may require a considerable amount of model evaluations that can become prohibitive. Thus, the achievement of UA and SA requires the identification of the most relevant methods to reduce the computational burden for the stochastic estimation of the response of interest. Many years of development of UA and SA methods constrain the experimenters to the choice of an appropriate methodology to be applied to their own case of study. The wide range of methods can sometimes be misleading and comparative studies are of major interest for helping the experimenters in their choice for a relevant methodology according to their needs and wants.

A first step in UA and SA is often related to the identification of parameters that have little influence on the variability of the response of interest, at the lowest possible computational cost. This procedure is referred to as *"screening"* and has the purpose of limiting the number of uncertain variables to the most significant ones for a further comprehensive stochastic evaluation of the response of interest. Many techniques can be employed for screening analyses, however to date, these methods have not been compared to show their relative performances. Based on this statement, a theoretical comparative study of screening techniques was undertaken with a special concern to screening out unimportant variables at the lowest possible computational cost in the context of computer-demanding, high-dimensional models.

In the frame of risk and safety analyses related to projects of underground disposals for radioactive wastes, hydrogeological numerical models are employed to perform groundwater flow and mass transport simulations, sometimes over large extensions of space and time. When accounting for the uncertainty characterizing various parameters in these large numerical models, stochastic estimations of hydrogeological processes in the underground media may imply thousands of model evaluations, which is often impracticable. Assuming a steady-state groundwater flow in the domain allows a fast estimation of the average time required for any solute, at any position in the domain, to reach a limit of the latter. This output is called the *mean lifetime expectancy* (MLE) and incorporates the advection-dispersion-diffusion equation (ADE) into its formulation so that the ageing process can be assimilated to a mass transport process and thus meets the requirements for risk and safety analyses.

The present application of UA and SA upon the complex multi-layered hydrogeological system in the general frame of the Andra project considered the MLE of water molecules located in a specific region of the potential host-layer from Callovo-Oxfordian (COX) age. However, as a consequence of its high resolution, the performance of an UA and a SA using exclusively the high-resolution 3D hydrogeological model is computationally intensive. A 2D synthetic case was built and parametrized upon geological and hydrogeological datasets deriving from literature, and a target zone was specified in a deep impermeable layer assimilated to the COX layer. This numerical model was employed for the exploration of UA and SA methods at low computational costs with two different scopes. The first scope was to encompass a large set of uncertain hydrodynamic and dispersion parameters and to evaluate the performance of QMC sampling schemes for estimating the uncertainty distribution of the MLE in the target zone. The performance of a metamodel-based sensitivity analysis was then studied with regard to its accuracy in individualising the effect of each uncertain parameter onto the output response. A second scope was to apply UA and SA techniques to stochastic realisations of the spatial heterogeneity of permeability-porosity values in two major aquifer sequences. The groundwater discharge rates at the outlets of the aquifer sequences and the MLE in the target zone stand for the responses analysed through a metamodel-based SA. The study aimed at evaluating the relevance of the methodology in dealing with stochastic realisations of heterogeneous permeability-porosity fields. The exploration of UA and SA techniques upon the 2D synthetic case was carried out to provide valuable insights on the performances of the methodologies at low computational costs. The results may allow reducing the computational burden for similar applications with the high-resolution 3D model.

A real-case application of UA and SA was achieved upon the MLE calculated from the potential disposal site within the COX layer, employing a refined extraction of the high-resolution 3D integrated model of the Paris Basin. The UA applied on the perturbation of the hydraulic conductivities and porosities values in fourteen hydrogeological formations with the objective of providing an estimation of the most influential hydrogeological layers on the output response of interest. Whereas the methodological applications on the 2D model employed a single SA method, the 3D real-case application was intended to compare the results of two different SA techniques : a screening method and a metamodel-based technique decomposing the variance of the model output response distribution.

1.3 Organisation of the thesis

Throughout the present manuscript various UA and SA methods are employed upon theoretical, methodological and real-case applications. The thesis starts with a general introduction of many UA and SA techniques, provides then a theoretical comparison of some of the latests SA techniques for screening purposes, and follows with the applications of relevant methodologies upon numerical models of groundwater flow and groundwater lifetime expectancy simulations. Finally, a real-case application of UA and SA techniques on a refined extraction of the 3D model of the Paris Basin is presented. Conclusions and outlooks complete the present manuscript.

For a coherent reading of the present thesis, the reader is advised that each chapter is self-dependent, so that they can be read independently from the whole manuscript.

The first chapter defines the notions of uncertainty and sensitivity analysis. The definition of uncertainty ranges in a statistical sense is introduced and various methods of random and quasi-random uncertainty propagation techniques are presented. The 2-levels Full Factorial Design represents the most elementary uncertainty propagation technique, and its development to the Fractional Factorial Design (FFD) was achieved with the purpose of reducing the computational demand for UA and SA. Random and quasi-random uncertainty propagation techniques provide more flexible frames for applications of UA and SA. Random samplings involve Monte-Carlo sampling schemes whereas quasi-random samplings were developed to provide a more uniform sampling in the uncertainty distribution of each individual parameter. Two types of quasi-random samplings are presented: the Latin Hypercube Designs (LHD) and the Low-Discrepancy Sequences (LDS) with their respective specificities. Three major types of SA methods are described in a second section: derivative-based, variance-based and metamodel-based techniques. The three types provide sensitivity indices indicating the influence of each individual uncertain parameter on the output response. Derivative-based techniques derive sensitivity indices as the ratio of the change in the output response to the change in a single input parameter, the other parameters remaining fixed to a given value. The variance-based techniques rely on the functional decomposition of the variance of the output response into sums of partial variances attributed to each uncertain parameter and their multiple interactions. Metamodels are mathematical expressions employed as surrogate models that reproduce the behaviour of the simulator at negligible costs. Sensitivity indices for each parameter and their interactions are derived from the mathematical expression itself. For each SA method presented in this chapter, references to publications related to hydrological and hydrogeological surveys are provided.

The second chapter of the thesis provides a theoretical comparison of SA techniques with focus on screening high-dimensional and time-consuming models (*i.e.* identifying uncertain variables having a low influence on the variability of the model output). The study compares the relative performances of four methods providing the global effect of each uncertain parameter on the output response. The SA methods considered were the Sobol' total sensitivity indices, the Morris Measures, the *Derivative-based Global Sensitivity Measures* (DGSM), and a fourth derivative-based measure being a variation of the DGSM. The methods were compared upon three analytical test-functions selected purposely as having different characteristics regarding dimensionality, nonlinearity, continuity and so forth. The experiments are set so that two groups of parameters, a group a significant and a group of insignificant parameters, are sought to be individualized within a limited number of model evaluation using each individual SA technique. This chapter provides valuable insights upon various SA techniques that can be used for screening high-dimensional models.

The third chapter introduces a vertical 2-dimensions synthetic numerical model of groundwater flow and mean lifetime expectancy of water molecules. The geometry and parametrization of the model is described and the framework for a conservative sensitivity analysis is given. In a first step, porosity-permeability parameters were considered uncertain in 15 homogeneous hydrogeological layers. Then, 78 uncertain input factors were considered, appending the Euler angle of the hydraulic conductivity tensor, the longitudinal dispersion parameter, the hydraulic gradients in three zones, the anisotropy in the hydraulic conductivity and in the dispersion tensors. In both steps, the MLE from a target zone (TZ) in the middle layer of the model stands for the output response of interest. The uncertainty propagation was undertaken by means of Latin Hypercube Designs on the basis of which sparse-Polynomial Chaos Expansions meta-models were constructed. The latter were then employed for the straightforward estimation of Sobol' sensitivity indices. The methodology employed in this chapter is discussed with regard to the estimation, at low computational costs, of the relative effects of uncertain advective-dispersive parameters on the MLE from the TZ in a high-dimensional UP and SA study.

In a fourth chapter, the 2D synthetic model was employed for the uncertainty propagation of parameters governing the spatial distributions of permeability-porosity parameters in two aquifer sequences : the means and variances of Gaussian distributions of hydraulic conductivity values within each sequence, the longitudinal and vertical correlation lengths, and a fifth factor related to the connectivity of high permeability-porosity values within the sequence. The uncertainties characterizing these 10 parameters (5 for each sequence) were propagated upon the outflowing rates at the aquifer sequences discharge boundaries, and upon the MLE calculated at the TZ. The study relies upon random realisations of heterogeneous fields, hence the statistical moments (mean and standard-deviation) of the distributions of the latter model responses actually stand for the output responses of interest. A two-levels Fractional Factorial Design was employed to propagate the parameters' uncertainties and each statistical index of

the output responses was analysed through a regression-based sensitivity analysis. This chapter is a complement to the study of the third chapter, providing valuable insights upon the role of parameters defining the spatial variability of permeability-porosity parameters upon the MLE from the TZ. The study estimates the effectiveness of the methodology, at low computational costs, in evaluating the variability of the statistical distributions of model outputs arising from random realisations of heterogeneous fields.

The last chapter of this manuscript provides a real-case application of UA and SA upon a refined extraction of the 3D high-resolution hydrogeological model of the Paris Basin. Consistency with the previous methodological studies is maintained by performing the sensitivity analysis of the MLE from a central location in the highly-confining COX layer, which is deemed to become the host layer for the geological disposal of radioactive wastes in France. The uncertainty propagation was undertaken through a perturbation of hydraulic conductivity and porosity values in 14 hydrogeological layers resulting from calibrated flow model against measured hydraulic head and taking into account measured hydraulic conductivity and porosity values. Latin Hypercube Designs were employed for the uncertainty propagation and two sensitivity analyses techniques were used: the derivative-based Morris Measures and a regression-based analysis of variance. Results and outlooks are provided for further UA and SA studies applied in the frame of the risk and safety analysis related to the project of the deep geological repository of radioactive wastes in the underground media of the eastern Paris Basin.

A conclusive section discusses the findings of the present research efforts with a main focus on the scientific contribution of UA and SA studies, especially when applied to computationally demanding hydrogeological numerical models. Advantages and limitations of the methodologies applied in this thesis are presented with respect to their applications on the 2D and 3D numerical models. Perspectives are offered for further studies focusing on the calibration and sensitivity analyses in the numerical modelling of flow and mass transport processes in the subsurface of the eastern Paris Basin.

Chapter 2

Methodologies of uncertainty and sensitivity analyses

2.1 Forewords

In the frame of the Uncertainty Analysis (UA) and the Sensitivity Analysis (SA), any given phenomenon is seen as a variable resulting from the combined effect of various input factors. When inputs and output are quantifiable through measurements, analytical and numerical modelling can be employed to produce estimations or even predictions of the given phenomenon, called *response quantity*, as a function of its governing factors.

As a consequence of incomplete/imprecise knowledge, the input factors are characterized by uncertainties regarding their spatial and/or temporal distributions, they are then considered as statistical *variables* defined through their marginal *probability density function* (PDF). The purpose of an UA is then to propagate these uncertainties upon the output quantity of interest, which becomes therefore a statistical variable itself, also characterized by its PDF. Examples of applications of UA are found in industry (de Rocquigny et al., 2008; Helton et al., 2006), healthcare programs (Lopez et al., 2006; Stinnett et al., 1998), economy (Lawson, 1985) and environmental studies (Hanley and Spash, 1993; Duncan, 1972).

In practice, the UA makes use of the so-called *design of experiment* (DoE), or *experimental design* (Fisher, 1935; McKay et al., 1979; Sacks et al., 1989; Helton and Davis, 2003), to evaluate the response quantity for various combinations of inputs variables. The most basic DoE's, the Factorial Designs, may only consider the extremes of the uncertainty ranges of the input variables whereas some algorithms enable specific combinations of input parameters values selected from their marginal PDF. These combinations are set as to explore as uniformly as possible the joint PDF and provide a comprehensive representation of the uncertainty distribution of the output quantity. In risk and safety analyses, the PDF of the output quantity of interest is analysed through decision-making programs by considering the implications associated to the probability of occurrence of a given response quantity. The notion of uncertainty ranges and probability density functions (PDF), as well as examples of DoE's, are provided in Section 2.2.

A Sensitivity Analysis (SA) (Saltelli et al., 2008) has the purpose to provide insights on the contribution of each uncertain input variable on the variability of the output quantity of interest. Broadly speaking, a SA focuses on the existing correlations between the marginal PDF of each input variable and the PDF of the output quantity to determine which input variables are most responsible for the variability of the output quantity, and even specifically determining whether the inputs are positively or negatively correlated to the output quantity, *i.e.* does an increase of the input value raises the output quantity, or inversely. Thus, indeed, a SA is necessarily operated in a step following the definition of an appropriate DoE. Saltelli et al. (2004) propose three approaches in the performance of any SA depending on the goal to achieve: the *Factor Prioritization* (FP), the *Factor Fixing* (FF), and the *Factor Mapping* (FM) settings. In his article, Neumann (2012) provided a comparison of some of the latest SA techniques with focus on these three approaches.

Assume that the exact value of a given variable could be provided, the variance of the output quantity would reduce from a certain amount which is estimated through the *main effect* of the variable (Saltelli and Tarantola, 2002) (see Section 2.3.3). Accordingly, the FP setting has the purpose to determine which variable could be further quantified to obtain the largest reduction of the variance of the output quantity.

Depending on the nature and configuration of the problem, it might happen that some uncertain input variables, characterized by low *total effects* (see Section 2.3.3), have little influence on the variance of the output quantity. The FF setting is thus oriented toward identifying these variables that can be fixed at any value within their own range of uncertainty without significantly affecting the output response quantity. This may be particularly useful when the purpose is to reduce the number of uncertain input variables to be investigated in a further analysis, the insignificant variables being considered as deterministic.

The FM setting can be regarded as an exploration tool that makes use of specific SA methods to determine how the combined effect of input variables can be responsible for driving the output response toward a specific value or region. In other words, the FM setting is dedicated to understanding the model behaviour with regard to the relative effect of each specific variable.

Many SA techniques were developed in the last decades (Hamby, 1994; Homma and Saltelli, 1996; Saltelli et al., 2004, 2008; Iooss and Lemaître, 2015). Qualitative methods offer a fast ranking of the input variables with regard to their relative contribution to the variability of the output response quantity. They are generally employed in the frame of the FF setting and the computation of sensitivity measures require limited efforts. Quantitative estimates address the variables' influence in terms of partial variances of the response quantity. They are especially used in the frame of the FP setting, but they can also be applied within the FF or the FM settings although it must be noted that they generally require higher efforts than

qualitative methods. In the realization of any SA, one is exposed to potential errors to be circumvented (Saltelli et al., 2004): Type I errors are defined as qualifying an important variable as non-influential whereas Type II errors are associated to the identification of a variable as significantly influential when it is not. Then, Type III errors are related to a framing error, an erroneous definition of the problem (*e.g.* incorrect bounds for an input variable) where the results of the SA would be of little help.

The Morris method (Morris, 1991; Campolongo et al., 2007, 2011) and the Derivative-based Global Sensitivity Measures (DGSM) (Kucherenko et al., 2009; Sobol' and Kucherenko, 2009; Lamboni et al., 2013) are examples of qualitative techniques which produce dimensionless sensitivity indices for each input variable by computing the derivative of the response quantity with respect to a change in the input variable. The Morris method is described in Section 2.3.1 while the computation of the DGSM is briefly exposed in Section 2.3.2.

The variance decomposition of the output quantity into partial variances provide sensitivity measures known as the Sobol' indices (Sobol', 1993; Saltelli et al., 2004) which address the fraction of the total variance of the response quantity to be attributed to each variable or variables' interactions. These variance-based sensitivity measures are obtained through various methods: the Fourier Amplitude Sensitivity Test (FAST) (Cukier et al., 1978) and its extended version (eFAST) (Saltelli and Bolado, 1998; Saltelli et al., 1999), the Random Balance Design (RBD) (Tarantola et al., 2006), the Homma-Ishigami-Saltelli-method (HIS) (Saltelli, 2002), the Sobol' algorithm (Sobol' et al., 2007), the Jansen's method (Jansen, 1999; Saltelli et al., 2010), and others. The formulation of the functional decomposition of the output response is given in Section 2.3.3 with the definition of the *main*, *second-order* and *total* effects of input variables.

The development of *meta-models*, also called *proxy* or *surrogate* models, has brought an alternative to evaluating the response quantity with an expensive model by replacing it with a mathematical expression aimed at computing the output response quantity at negligible costs. Thus, meta-models can be used to generate thousands of output quantity values when the "true" model is too expensive to be run extensively ; thus producing a comprehensive PDF for the output response of interest. Moreover, through the mathematical expression of the meta-model, it is possible to extract sensitivity indices for each input variable as well as for interactions between input variables. Regression meta-models (Kleijnen, 1997; Myers et al., 1989; Sacks et al., 1989), kriging meta-models (Santner et al., 2003; Oakley and O'Hagan, 2004), Gaussian process meta-models (Marrel et al., 2009), High-Dimensional Model Representation (HDMR) (Rabitz and Aliş, 1999; Li et al., 2001; Sobol', 2003) or Polynomial Chaos Expansion (PCE) models (Sudret, 2008; Blatman and Sudret, 2010b, 2011) are commonly employed to achieve such tasks. Methods for the construction of regression and PCE meta-models are given together with the computation of sensitivity indices in Sections 2.4.1 and 2.4.2 respectively.

2.2 Experimental design

2.2.1 Definition of the uncertainty ranges

Let us consider a scalar response quantity $y = \mathcal{M}(\boldsymbol{x})$, where $\mathcal{M}$ is a deterministic, error-free "forward model" and $\boldsymbol{x} = \{x_1, \dots, x_k\}' \in \mathbb{R}^k, k \geq 1$, is a vector with k mutually independent random variables. Each input variable x_i can be expressed through its statistical distribution and, more precisely, through its probability density function (PDF) f_{x_i}. When performing an UA or a SA, the *nominal case* refers to the situation where every variable is sampled at its mean value, or median value of its PDF.

The uncertainty affecting the input vector $\boldsymbol{x}$ is then accounted for in the joint probability density function:

$$f_{\boldsymbol{x}}(\boldsymbol{x}) = \prod_{i=1}^{k} f_{x_i}(x_i) \tag{2.1}$$

The vector $\boldsymbol{x}$ represents then a random combination of input factors' quantities and can be seen as a point mapped into the hyperspace $f_{\boldsymbol{x}} \longmapsto \mathcal{H}^k$. The selection of N points in $\mathcal{H}^k$ can be expressed as a matrix $\boldsymbol{X}$, called the *experimental matrix*. Hence, the vector $\boldsymbol{y} = \{y_1, \dots, y_N\}' \in \mathbb{R}^N, N \geq 1$ is the set

of response quantities of interest which results from the processing of $\boldsymbol{X}$. The statistical distribution of the response quantity, represented through its PDF $f_{\boldsymbol{y}}$, can be further analysed in the frame of an UA and/or a SA.

2.2.2 Factorial design

Introduced by statistician Ronald A. Fisher (Fisher, 1935), the factorial design was specifically dedicated to the achievement of real experiments in the fields of agriculture, chemistry or industry, where the uncertain variables are characterized by bounded ranges and/or discrete quantities. However, it may also be employed in the frame of analytical and numerical modelling, involving the evaluation of a model $\mathcal{M}(\boldsymbol{x})$ as a function of uncertain input factors, even if they are continuous factors.

The factorial design relies on the definition of finite levels associated to real quantities for each uncertain variable (Box et al., 2005). Let us consider a two-level factorial design where, for a given variable, level -1 (or simply '$-$') is assimilated to a low quantity whereas level +1 (or simply '+') is assimilated to a high quantity. When considering k variables, the combination of all possible levels yields a so-called *full factorial design* involving $N = 2^k$ model evaluations.

As an example, a two-level full factorial design with $k = 3$ variables requires $N = 2^3 = 8$ experiments as in the following table:

Table 2.1: Two-level full-factorial design with $k = 3$ input factors.

	x_1	x_2	x_3
Experiment # 1	-1	-1	-1
Experiment # 2	+1	-1	-1
Experiment # 3	-1	+1	-1
Experiment # 4	+1	+1	-1
Experiment # 5	-1	-1	+1
Experiment # 6	+1	-1	+1
Experiment # 7	-1	+1	+1
Experiment # 8	+1	+1	+1

Using this kind of DoE, the experimental matrix $\boldsymbol{X}$ presented in Table 2.1 is a Hadamard matrix (Goupy, 2001) with orthogonal properties verifying $\boldsymbol{X'X} = N\mathbf{I}$, where $\mathbf{I}$ is the identity matrix and $\boldsymbol{X'}$ is the transpose of matrix $\boldsymbol{X}$.

Let us now consider the combined effect, or *interaction effect*, of input variables on the output response. The effect of factors taken 2-by-2 is referred to as *two-ways* interactions. Similarly, *three-ways* or even higher-order interactions can be estimated. Resuming the above case with $k = 3$ variables, interaction effects can be added to the Table 2.1 and correspond to the product of the levels for each variable accounted for in the interaction term. For instance, considering experiment #1 in Table 2.1, the product of the levels of the variable x_1 and x_2 is positive (+), whereas the product of the levels of the variable x_1, x_2 and x_3 is negative (-). The mean effect of the uncertain input variables on the output response is estimated through the mean I, which is included in the following matrix as a column of '+':

Table 2.2: Matrix of regressor effects in a full-factorial design with $k = 3$ input factors.

	I	x_1	x_2	x_3	$\{x_1, x_2\}$	$\{x_1, x_3\}$	$\{x_2, x_3\}$	$\{x_1, x_2, x_3\}$
Exp. # 1	+	−	−	−	+	+	+	−
Exp. # 2	+	+	−	−	−	−	+	+
Exp. # 3	+	−	+	−	−	+	−	+
Exp. # 4	+	+	+	−	+	−	−	−
Exp. # 5	+	−	−	+	+	−	−	+
Exp. # 6	+	+	−	+	−	+	−	−
Exp. # 7	+	−	+	+	−	−	+	−
Exp. # 8	+	+	+	+	+	+	+	+

Table 2.2 can be seen as the *matrix of regressor effects* $\boldsymbol{\mathcal{X}}$ (see Section 2.4.1) and is dedicated to the construction of meta-models. The variables and their interactions are referred to as *regressors* in the frame of meta-modelling. Through a SA, these regressors can be used to estimate the main, or linear, effect of each variable or interaction. Note however that the underlying assumption of a two-level design (Table 2.2) is that the relationship between the regressors and the output response is linear.

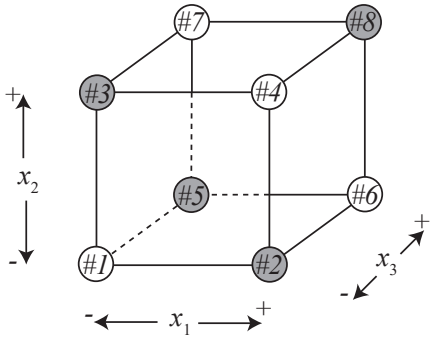

Figure 2.1: Two levels full (every point) and fractional-factorial designs (either white or gray points) for $k = 3$ factors.

With an increasing number of input variables, the required number of model evaluations can quickly become impracticable, particularly when high computational efforts are involved in each evaluation of $\mathcal{M}$. The Plackett-Burman (PB) design (Plackett and Burman, 1946) proposes an alternative by extracting individual rows from matrix $\boldsymbol{X}$ and re-building blocks of equal size while keeping the orthogonal properties between the blocks. The size and number of blocks is related to the *Resolution* chosen by the user. Figure 2.1 illustrates, for $k = 3$ factors, the experimental points in a two-level full factorial design where $2^3 = 8$ experiments are considered. Considering the sets of either white or gray points separately define two blocks of $2^{3-1} = 4$ experiments referred to as *fractional factorial designs* (FFD). A Resolution III is illustrated here, it means that the 3-way interaction $\{x_1, x_2, x_3\}$ is used as a *generator* to confound effects and to generate the FFD.

Table 2.3: Two fractional-factorial designs with $k = 3$ input factors and two-ways interactions.

	I	x_1	x_2	x_3	$\{x_1, x_2\}$	$\{x_1, x_3\}$	$\{x_2, x_3\}$	$\{x_1, x_2, x_3\}$
Exp. # 5	+	−	−	+	+	−	−	+
Exp. # 2	+	+	−	−	−	−	+	+
Exp. # 3	+	−	+	−	−	+	−	+
Exp. # 8	+	+	+	+	+	+	+	+
Exp. # 1	+	−	−	−	+	+	+	−
Exp. # 6	+	+	−	+	−	+	−	−
Exp. # 7	+	−	+	+	−	−	+	−
Exp. # 4	+	+	+	−	+	−	−	−

The two matrices of regressor effects $\boldsymbol{\mathcal{X}}$, corresponding to either the white points or the gray points in Figure 2.1, are represented in Table 2.3. In the upper block of Table 2.3, the levels of I are identical to those of $\{x_1, x_2, x_3\}$. Besides, the levels of x_1 are identical to those of the interaction $\{x_2, x_3\}$, and similarly x_2 is related to $\{x_1, x_3\}$ and x_3 to $\{x_1, x_2\}$. Hence, with this FFD of Resolution III, the effect of each input variable can be confounded with that of a two-ways interaction, whereas the mean effect can be confounded with the effect of the three-ways interaction. This confounding process is called *aliasing*. So, for a given *alias*, the sensitivity index obtained with this strategy represents the effect of factor x_i, to which it may be added the effect of every other term confounded, or *aliased*, with it. As it becomes impracticable to separate the confounded effects it is usually assumed that interaction effects, and particularly high-order ones, are negligible with respect to main effects of variables. This assumption is referred to as the *"sparsity of effect principle"* (Montgomery, 2006). Under this assumption, the sensitivity index represents broadly the effect of the variable x_i solely. Note however that a FFD of

Resolution I or II confounds the main effect of some variables with the main effect of other variables, the interpretation may become complex in such cases. In the lower block of Table 2.3, the same relationships hold but are opposite: $I = -\{x_1, x_2, x_3\}$, $x_1 = -\{x_2, x_3\}$, $x_2 = -\{x_1, x_3\}$ and $x_3 = -\{x_1, x_2\}$. This means that the estimated effect for the variable x_i includes its actual main effect from which is subtracted the effect of the confounded interaction. Assuming negligible interaction effects, the sensitivity index obtained can be attributed to the main effect of variable x_i. For further information regarding aliasing techniques and resolution of the FFD, the reader is referred to the books from Box et al. (2005) and Goupy (2001).

Other types of two-levels or three-levels DoE exist in the literature, the reader is referred to Box and Draper (1987) for an extensive presentation of the various types of DoE with their applications.

2.2.3 Space-filling designs

In this section, the hyperspace $\mathcal{H}^k$ defined in Section 2.2.1 is assimilated to a unit hypercube $[0\ ;\ 1]^k$ by considering the probability range of the cumulative distribution function (CDF) associated to each individual input variable.

A simple random sampling is often referred to as Monte-Carlo sampling (MCS) (Robert and Casella, 2005), in reference to the act of gambling and recording results in a real casino. The random MCS algorithm does not guaranty a proper filling of $\mathcal{H}^k$, potentially creating regions with clusters of sampling points and other regions with no samples at all. This could be problematic when the uncovered region contains major informations on the behaviour of the model. Oppositely, over-sampling regions which provide little information on the variability of response of interest can be seen as a waste of energy. It is however admitted that MCS methods reasonably fill the hyperspace $\mathcal{H}^k$ when a relatively large number of samples is achieved or when dealing with high dimensional problems. This issue is often designated as the *"curse of dimensionality"*.

When an experimenter is willing to obtain a reliable estimation of the uncertainty characterising a quantity of interest within a limited number of experiments, the use of *space-filling* designs is advocated. The Latin Hypercube Sampling (LHS) (McKay et al., 1979; Iman and Conover, 1980), for instance, provides a flexible frame for sampling variables and yields a good spreading of the sampling points. The algorithm is based on the partitioning of each variable's range into N cells, N being the number of experiments specified by the user. For each variable, one random sample is taken into each cell and compiled into a vector of size N. By assembling the k vectors, one obtains an experimental matrix $\boldsymbol{X}$ of size $(N \times k)$. Many developments were done to optimize the LHS according to various criteria (Dette and Pepelyshev, 2010). As an example, Johnson et al. (1990) proposed to optimize the LHS in order to either minimize the maximum distance between any two sampling points (*minimax* criteria) or maximize the minimum inter-points distance (*maximin* criteria). Given as another example of space-filling designs, Owen (1998a) proposed the Latin Supercube Sampling (LSS) for optimizing the sampling scheme when dealing with high-dimensional problems.

The Low Discrepancy Sequences (LDS) (Niederreiter, 1988) are space-filling designs specifically dedicated to optimizing the equidistribution of samples. These sequences provide deterministic sampling points and are often referred to as *quasi Monte-Carlo* methods. The Halton, Faure, Hammersley and Sobol' sequences enter this category of sampling strategies where the sampling points are directly derived from pre-established matrices. Hence, the main difference with other space-filling designs is that there is no algorithm designing the experimental matrix, *i.e.* for a given k and N there is only one possible experimental matrix.

Figure 2.2 illustrates the MCS, the LHS and the Sobol' LDS in a 2 dimensional hyperspace (*i.e.* $k = 2$) for $N = 64$ sampling points. Note that to obtain the highest performances with Sobol' LDS (Sobol', 1967), the sampling size N has to be a power of 2 ; regardless the number k of factors. For the sake of argument it was chosen to meet $N = 2^6$ for each sampling method illustrated in Figure 2.2.

As seen, the MCS creates clusters and gaps in the sampling space $[0\ ;\ 1]^2$ whereas the LHS provides a more uniform sampling. The LDS consists however in series of deterministic samples' coordinates and the sampling is thus more regular than with the two other sampling schemes. Recent studies have undertaken the comparison of these experimental designs with regard on the convergence rates of sensitivity indices. The Sobol' LDS have proven to be more efficient than the LHS (Kucherenko et al., 2011) and the LSS (Tarantola et al., 2012) for producing reliable sensitivity indices at low sample size.

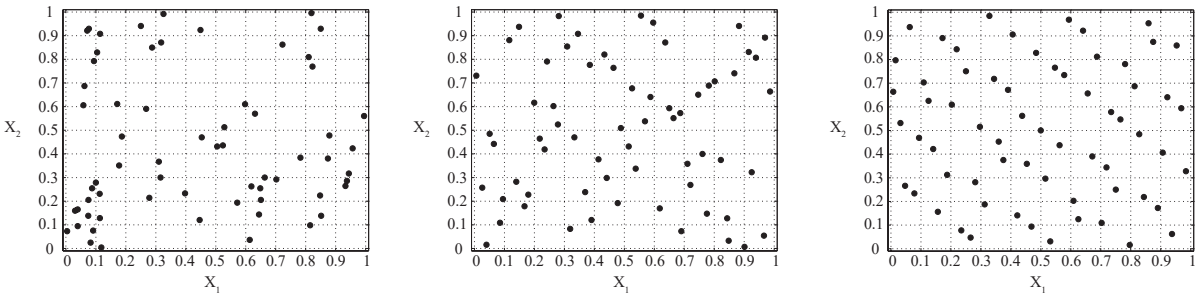

Figure 2.2: Comparison of the Monte-Carlo sampling (left), the latin hypercube sampling (center) and the Sobol' sequence (right) for $k = 2$ factors and $N = 64$ samples.

2.3 Sensitivity analysis methods

2.3.1 The Morris importance measures

The experimental matrix employed for the computation of Morris' importance measures is a specific application of the *one-at-a-time* principle. The latter consists in selecting a point $\boldsymbol{x}$ in $\mathcal{H}^k$ and shift each variable x_i, one-at-a-time, to another value in its uncertainty range while keeping the other variables fixed at their values. The change in the output quantity is directly related to the shift in x_i and calculating a simple derivative provides a sensitivity measure for x_i.

In the method originally proposed by Morris (Morris, 1991), and further developed by Campolongo and co-workers (Campolongo et al., 2007), the hyperspace $\mathcal{H}^k$ is discretized into a regular grid with deterministic and equally spaced levels in each dimension; the number of levels being provided by the experimenter, say 4 discrete levels yields $[0, \frac{1}{3}, \frac{2}{3}, 1]$. A starting point $\boldsymbol{x}^*$ is selected randomly onto the grid and each uncertain variable is shifted consecutively to another level by a fixed increment $\boldsymbol{\Delta}$, say $\frac{2}{3}$. This creates a so-called *trajectory* in $\mathcal{H}^k$ which consists in $N = k + 1$ experiments, k being the number of variables.

As an example, the following matrix $\boldsymbol{X}$ illustrates one Morris' trajectory for $k = 3$ variables with the above-mentioned discretization and increment, and considering a starting point $\boldsymbol{x}^*$ which coordinates would be $[\frac{1}{3}; \frac{2}{3}; 0]$:

$$\boldsymbol{X} = \begin{bmatrix} 1/3 & 2/3 & 0 \\ 1 & 2/3 & 0 \\ 1 & 0 & 0 \\ 1 & 0 & 2/3 \end{bmatrix} \tag{2.2}$$

The same procedure can be repeated R times and each trajectory would yield a single sensitivity measure for each variable. Thus, at the cost of $N = R(k + 1)$ experiments, one obtains R sensitivity measures per input variable that can be treated through the first two moments of the distribution (mean and standard deviation).

In their article, Campolongo et al. (2011) proposed using a similar strategy relying on a different sampling scheme, using *radial samples* (RS) instead of trajectories. A strategy for building RS from LDS is given in (Saltelli et al., 2010) where both the starting point and the shifted values for each input variable derive from the deterministic sampling points provided in the Sobol' LDS (Section 2.2.3). The sampling strategy starts with R Sobol' LDS in $2k$ dimensions, the resulting matrix is split into a matrix $\mathbf{A}$ that contains the first k dimensions and a matrix $\mathbf{B}$ that contains dimensions $k+1$ to $2k$. To create the radial sample we shall consider each row r of matrix $\mathbf{A}$ as a starting point $\boldsymbol{x}_r^*$. By replacing alternatively each element of the vector $\boldsymbol{x}_r^*$ by the elements of $\mathbf{B}$ (*i.e.* $\mathbf{B}(r, i)$) we create a matrix $\mathbf{A_B}$. In the following $\mathbf{A}_\mathbf{B}^{(i)}$ will refer to the row where all columns are from $\mathbf{A}$ except the i-th column which derives from $\mathbf{B}$.

To circumvent occurrences where $\mathbf{A}(r,i) = \mathbf{B}(r,i)$, as it happens for small values of r, Campolongo et al. (2011) proposed extracting a matrix $\mathbf{B}$ from lower rows in the Sobol' LDS. Using this strategy, no discretization of $\mathcal{H}^k$ is assumed and the increment Δ_i differs for each input x_i. According to Campolongo et al. (2011) the use of a varying increment Δ_i contributes to a better identification of the irregularity of the output response with respect to the input variables. In addition, the space-filling properties of the LDS also provide a better spreading of the sampling points into $\mathcal{H}^k$ and can thus better capture the general behaviour of the model under study.

Figure 2.3 exhibits one Morris' trajectory according to the matrix 2.2 and one radial sample based on Sobol' LDS. For each sample set the starting point $\boldsymbol{x}^*$ is indicated.

It clearly appears that the Morris' trajectory relies on fixed levels and uses uniform shifts to sample each point. As mentioned before, this regularity might be disadvantageous in cases where non-monotonicity and strong non-linearities are acknowledged in the response function. Instead, the RS based on Sobol' LDS can better examine the response function by sampling starting points $\boldsymbol{x}^*$ more uniformly within the hyperspace and making use of variable increments to sample the shifted points.

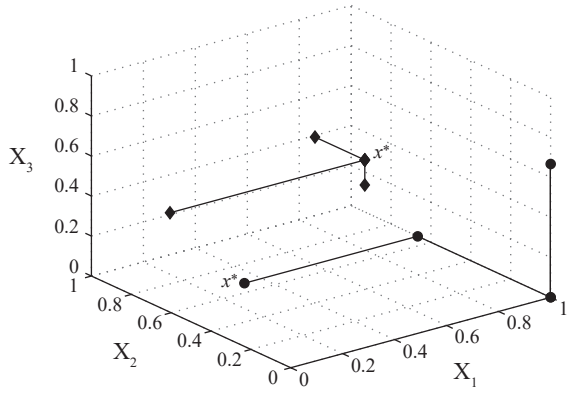

Figure 2.3: Morris' trajectory (dots) and radial sample based on Sobol' LDS (diamonds) for $k = 3$ factors.

For a single radial sample, one can derive an *elementary effect* EE_i for each input variable x_i by computing the ratio between the change in model output and the increment Δ_i:

$$EE_i = \frac{\mathcal{M}(x_1, \ldots, x_i + \Delta_i, \ldots, x_k) - \mathcal{M}(x_1, \ldots, x_i, \ldots, x_k)}{\Delta_i} \tag{2.3}$$

Let us now consider R radial samples having different starting points $\boldsymbol{x}_r^*$, $r = 1, \ldots, R$. One obtains then R elementary effects $EE_i^{(r)}$ for each input variable x_i. The arithmetic mean of the absolute value of all elementary effects $EE_i^{(r)}$ (Campolongo et al., 2007) provides a global sensitivity measure for the variable x_i. In case of non-monotonicity of the relationship between input x_i and the output, EE_i's of opposite signs do not cancel each other. In integral form the Morris measure writes:

$$\mu_i^* = \int_{\mathcal{H}^k} \left| \frac{\partial \mathcal{M}(\boldsymbol{x})}{\partial x_i} \right| d\boldsymbol{x} \tag{2.4}$$

Considering the set of R elementary effects for the variable x_i, the standard deviation σ_i of the $EE_i^{(r)}$ provides a measure of the non-linearity of the relationship between the input factor and the output response: the higher the standard deviation the more non-linear the relationship. This second Morris measure reads:

$$\sigma_i = \left[\int_{\mathcal{H}^k} \left(\left| \frac{\partial \mathcal{M}(\boldsymbol{x})}{\partial x_i} \right| - \mu_i^* \right)^2 d\boldsymbol{x} \right]^{1/2} \tag{2.5}$$

Using the RS method described hereinabove, the Morris measure from Eq. 2.4 comes down to the following matrix expression:

$$\mu_i^* = \frac{1}{R}\sum_{r=1}^{R}\left|EE_i^{(r)}\right| = \frac{1}{R}\sum_{r=1}^{R}\left|\frac{\mathcal{M}(\mathbf{A})_r - \mathcal{M}(\mathbf{A}_\mathbf{B}^{(i)})_r}{(\mathbf{A})_r - (\mathbf{A}_\mathbf{B}^{(i)})_r}\right| \tag{2.6}$$

The overall effect of the input variables x_i, including all-order effects as well as interaction effects, is captured by μ_i^*. The reader should note that similarities exists between μ_i^* and the total Sobol' index (S_i^{tot}) developed in the next section although, to date, no formal proof has been provided (Saltelli et al., 2004; Campolongo et al., 2007, 2011; Kucherenko et al., 2009).

References to case studies employing Morris Measures

The Morris importance measures were employed in many studies related to hydrological and hydrogeological processes. In their article, Van Griensven et al. (2006) implemented a comprehensive sensitivity analysis using the model of a river catchment in Ohio for controlling the water flow and quality at several locations. In their study, they estimated the Morris sensitivity measure for a long list of uncertain soil, groundwater, riverbed and hydrologic parameters and they concluded that the uncertainty regarding water quality is mainly related to hydrologic factors. Using a three-layered groundwater model for modelling the transport and degradation of pesticides from a river toward a pumping well in Switzerland, Malaguerra et al. (2013) employed the Morris method to assess the sensitivity of the geometry of geological layers as well as hydrodynamic parameters. Sun et al. (2012) performed a sensitivity analysis over the hydrological model of a river catchment in south-east Australia with regard to the surface water quality. They notably employed the Morris method as part of a three-phase SA with regard to 6 uncertain input factors related to hydrologic parameters.

2.3.2 Derivative-based Global Sensitivity Measure (DGSM)

Developed as an option for the fast computation of qualitative estimates, the Derivative-based Global Sensitivity Measure (DGSM) relies on the integral of squared derivatives (Sobol' and Kucherenko, 2009):

$$\nu_i = \int_{\mathcal{H}^k}\left(\frac{\partial\mathcal{M}(\boldsymbol{x})}{\partial x_i}\right)^2 d\mathbf{x} \tag{2.7}$$

The method applies to independent random variables and makes use of an experimental design similar to the radial sampling which consists of small shifts in each dimension from given sampled points. The latter can be selected through MC or QMC methods (Section 2.2.3). In the unit hypercube $[0\ ;\ 1]^k$, the recommendation is to shift each factor x_i alternatively from a tiny fixed increment $\Delta = \pm 10^{-5}$ in order to identify strong non-linearities which may possibly be very localised. Indeed, large increments are more likely to "miss" the sharp peaks and locally high gradients in the response function. This may underestimate the effect of a given input variable. So, the computation of ν (Sobol' and Kucherenko, 2009) may use a simple Sobol' sequence as a base. Then, neighbouring points along each dimension need to be set to compute the partial derivatives. Using this experimental design with R initial samples, ν can be estimated with the following expression:

$$\nu_i = \frac{1}{R}\sum_{r=1}^{R}\left(\frac{\mathcal{M}(x_i^{(r)} + \Delta) - \mathcal{M}(x_i^{(r)})}{\Delta}\right)^2 \tag{2.8}$$

where $x_i^{(r)}$ is the value of variable x_i for the r^{th} base sample. For a comprehensive description of the DGSM technique the reader is referred to the articles from Sobol' and Kucherenko (2009) and Kucherenko et al. (2009).

As for the Morris measure μ_i^*, this sensitivity measure accounts for all-order effects as well as interaction effects of the corresponding input variable. Apart from the experimental design, the main difference with the Morris measure is the squaring instead of the absolute value of the derivatives. Thus, $\mu_i^* \leq \sqrt{\nu_i}$ and $\nu_i \leq C\mu_i^*$ if $|\partial\mathcal{M}(x_i)/\partial\mathcal{M}(x_i)| \leq C$, C being a constant. Kucherenko et al. (2009) confronted the DGSM with the Morris importance measure upon various types of test-functions. Based on MC and QMC integration methods, the DGSM has proven to be much faster and more accurate than the Morris method although in many instances the Morris measure can still stand as a good compromise between efficiency and accuracy.

A relation with the total sensitivity index S_i^{tot} introduced in the following section is given in Eq. 2.22-2.23. In their conclusions, Sobol' and Kucherenko (2009) recommend however a special caution for highly nonlinear functions where the ranking of important factors using DGSM may steer toward false conclusions.

References to case studies employing DGSM

The DGSM method is a quite recent technique and not many publications related to geological or hydrogeological surveys can be found. Though, it has already been successfully employed for the screening of horizontal and vertical permeability parameters in a high-dimensional reservoir model used to predict oil and gas production (Touzani and Busby, 2014).

2.3.3 ANOVA decomposition and Sobol' indices

For the sake of clarity a scalar response $y = \mathcal{M}(\boldsymbol{x})$ is considered in the sequel (*i.e.* $N = 1$) but the following holds for each component of $\boldsymbol{y}$. As in the previous section, the hyperspace $\mathcal{H}^k$ is assimilated to the unit hypercube $[0\ ;\ 1]^k$.

In the remainder, $\boldsymbol{x}_{\sim i}$ denotes the vector of all input variables except variable x_i. The vector can be written as follows:

$$\boldsymbol{x}_{\sim i} = (x_1, \ldots, x_{i-1}, x_{i+1}, \ldots, x_k) \tag{2.9}$$

Similarly, the vector $\boldsymbol{x}_{\sim i,j}$ denotes the vector of all input variables which are different from i and j. In a generalized version, the subset $\boldsymbol{u} = \{i_1, \ldots, i_s\} \subseteq \{1, \ldots, k\}$ are index sets and $\boldsymbol{x}_{\boldsymbol{u}} = (x_{i_1}, \ldots, x_{i_s})$ denotes the sub-vector of $\boldsymbol{x}$ containing only the components that belong to u.

The functional decomposition of y into summands of increasing dimensions relies on the following assumptions (Hoeffding, 1948):

- A1: the input variables x_i $(i = 1, 2, \ldots, k)$ are independent random variables uniformly distributed in the unit interval,
- A2: the relation $\mathbb{E}[\mathcal{M}^2(\boldsymbol{x})] < +\infty$ holds,
- A3: the ratio $\frac{\partial\mathcal{M}(\boldsymbol{x})}{\partial x_i}$ is square integrable.

When the above assumptions are valid, the functional decomposition of $\mathcal{M}(\boldsymbol{x})$ is :

$$\mathcal{M}(\boldsymbol{x}) = \mathcal{M}_0 + \sum_{i=1}^{k} \mathcal{M}_i(x_i) + \sum_{1 \leq i \leq j}^{k} \mathcal{M}_{i,j}(x_i, x_j) + \cdots + \mathcal{M}_{1,2,\ldots,k}(\boldsymbol{x}) \tag{2.10}$$

where $\mathcal{M}_0$ is a constant and the functions of the above decomposition can be developed as follows:

$$\mathcal{M}_0 = \int_{\mathcal{H}^k} \mathcal{M}(\boldsymbol{x}) d\boldsymbol{x},$$

$$\mathcal{M}_i(x_i) = \int_{\mathcal{H}^{k-1}} \mathcal{M}(\boldsymbol{x}) d\boldsymbol{x}_{\sim i} - \mathcal{M}_0,$$

$$\mathcal{M}_{i,j}(x_i, x_j) = \int_{\mathcal{H}^{k-2}} \mathcal{M}(\boldsymbol{x}) d\boldsymbol{x}_{\sim i,j} - \mathcal{M}_i(x_i) - \mathcal{M}_j(x_j) - \mathcal{M}_0,$$

$$\ldots \tag{2.11}$$

Equivalently, when considering all and every non-empty subset $\boldsymbol{u}$ of variables, Eq. 2.10 re-writes:

$$\mathcal{M}(\boldsymbol{x}) = \mathcal{M}_0 + \sum_{\boldsymbol{u} \neq \emptyset} \mathcal{M}_{\boldsymbol{u}}(\boldsymbol{x}_{\boldsymbol{u}}) \tag{2.12}$$

and for all $p = 1, 2, \ldots, s$, and any indices $1 \leq i_1 < i_2 < \cdots < i_s \leq k$ and $s = 1, 2, \ldots, k$, the unicity condition for Eq. 2.10 is granted by (Sobol', 1993):

$$\int_0^1 \mathcal{M}_{i_1, i_2, \ldots, i_s}(x_{i_1}, x_{i_2}, \ldots, x_{i_s})\, dx_{i_p} = 0 \tag{2.13}$$

It follows from Eq. 2.11 and Eq. 2.13 that the terms in Eq. 2.10 are orthogonal.

The first-order partial variance of the output response quantity associated to the input variable x_i reads:

$$V_i = \mathbb{V}[\mathcal{M}_i(x_i)] = \int_{\mathcal{H}^k} \mathcal{M}_i^{\,2}(x_i)\, d\boldsymbol{x} \tag{2.14}$$

For a subset $\boldsymbol{u}$ of variables, the relation holds:

$$V_{\boldsymbol{u}} = \mathbb{V}[\mathcal{M}_{\boldsymbol{u}}(\boldsymbol{x}_{\boldsymbol{u}})] = \int_{\mathcal{H}^k} \mathcal{M}^2_{i_1, \ldots, i_s}\, (x_{i_1}, \ldots, x_{i_s})\, d\boldsymbol{x} \tag{2.15}$$

and the total variance V_y of the response quantity writes:

$$V_y = \mathbb{V}[\mathcal{M}(\boldsymbol{x})] = \int_{\mathcal{H}^k} \mathcal{M}^{\,2}(\boldsymbol{x}) d\boldsymbol{x} - \mathcal{M}_0^2 \tag{2.16}$$

Squaring and integrating over $\mathcal{H}^k$ leads to the ANOVA (Analysis of Variance) decomposition of the output response quantity (Sobol', 1993):

$$V_y = \sum_{i=1}^{k} V_i + \sum_{1 \leq i \leq j}^{k} V_{i,j} + \cdots + V_{1,2,\ldots,k} = \sum_{u \neq \emptyset} V_u \tag{2.17}$$

When accounting for the first and high-order effects of the variable x_i, including every interaction with all other variables, the partial variance related to all and every subset that include x_i can be computed as.

$$V_i^{tot} = \sum_{u \in \mathcal{I}_i} V_u \tag{2.18}$$

where the sum $\sum_{\mathcal{I}_i}$ applies to all the subsets of variables with indices $1 \leq s \leq k$ that include the variable x_i.

The global sensitivity index for variable x_i (Sobol', 1993, 2001; Saltelli et al., 2004) is often referred to as the *main*, or *first-order* effect, of variable x_i. It stands as a measure of the linear effect of the variable x_i itself on the variance of the output response y. It is simply computed as the ratio:

$$S_i = \frac{V_i}{V_y} \tag{2.19}$$

Likewise, considering a subset u of variables the global sensitivity index writes:

$$S_{\boldsymbol{u}} = \frac{V_{\boldsymbol{u}}}{V_y} \tag{2.20}$$

Hence, the *second-order* indices, S_{ij}, describe influences from pairs of input variables $\{x_i, x_j\}$ on the output quantity, and higher-order indices describe the combined influence from larger sets of input variables.

The total sensitivity indices, S_i^{tot}, is given by (Homma and Saltelli, 1996; Saltelli et al., 2004) and is often used for the ranking of variables. Computed as the following ratio, it is a measure of the overall effect of the variable x_i, including its interactions with other variables:

$$S_i^{tot} = \frac{V_i^{tot}}{V_y} \tag{2.21}$$

If and only if $S_i^{tot} = 0$, the variable x_i can be interpreted as having no influence at all on the output response y. Note also that in general $0 \leq S_i \leq S_i^{tot} \leq 1$. For a purely linear model the sum of all S_i's equals one, whereas the further this sum to unity the larger the non-linearity of the model.

The ANOVA decomposition introduced hereinabove holds if the input variables are independent. Correlated input variables can be treated similarly, however the case is not discussed here and the reader is referred to (Xu and Gertner, 2008; Li et al., 2010) for a meaningful description of the methods.

Sobol' and Kucherenko (2009) established the link between the DGSM ν_i and the total sensitivity index S_i^{tot} for independent random variables:

$$S_i^{tot} \leq \frac{\nu_i}{\pi^2 V_y} \tag{2.22}$$

In the case where variable x_i follows a Gaussian distribution with variance σ_i^2, the relation 2.22 rewrites:

$$S_i^{tot} \leq \frac{\nu_i \sigma_i^2}{V_y} \tag{2.23}$$

Lamboni et al. (2013) provided equivalent inequalities linking S_i^{tot} and ν_i for a large class of probability distributions. In comparison to the computational cost for the total sensitivity indices, they also proved that the DGSM reduces from 10 to 100 the number of model evaluations required for a reliable estimation of the sensitivity of the input variables; this feature becoming more significant when dealing with small dimensionalities in models with weak interactions among input variables.

References to case studies employing Sobol' indices

In the context of nuclear waste repository, the Level E benchmark model has been widely employed to compare the performances of sensitivity analysis techniques (Saltelli and Sobol', 1995; Homma and Saltelli, 1996; Saltelli et al., 2000). The model simulates the underground migration of a radionuclide chain over geologic time scales to predict the radiologic dose to the atmosphere. Considering non-correlated and correlated parameters, Saltelli and Tarantola (2002) estimated the first-order and total sensitivity indices for 21 uncertain input factors governing the migration and degradation of radionuclide in the Level E model.

In a simulation of radioactive gas release from a nuclear facility in France, Iooss et al. (2006) performed a sensitivity analysis over 6 input variables related to the food chain for the computation of the annual dose of radionuclide to human beings. In their study, a regression meta-model is employed as a surrogate model to compute the total Sobol' indices for each uncertain variable.

2.4 Meta-modelling

As stipulated in Section 2.1, meta-models are mathematical expressions aimed at reproducing the behaviour of the "true" model $\mathcal{M}$ at negligible computational costs. Their construction is based upon the experimental matrix $\boldsymbol{X}$ and the corresponding vector of output quantity $\boldsymbol{y}$. Since they can be employed to produce "estimated" output quantities at negligible costs, they are often used to generate a comprehensive PDF for the output quantity, $f_{\boldsymbol{y}}$. Another feature of the meta-models is that their mathematical expression can be examined to derive sensitivity indices for each input variable and interaction between input variables. The following introduces two types of meta-models: polynomial regression and Polynomial Chaos Expansion meta-models.

2.4.1 Polynomial regression meta-models

The polynomial regression meta-model formulation follows the Hoeffding decomposition of Eq. 2.10, and the variance decomposition of Eq. 2.17, by decomposing the response quantity into a sum of functions that involve unknown coefficients β. In the following, the linear or high-order effects of input variables, as well as the interactions between variables, are referred to as *regressors* accounted for into the matrix of regressor effects $\boldsymbol{\mathcal{X}}$ introduced in Section 2.2.2. Involving linear and interaction terms, a regression meta-model approximating the scalar response y writes (Box and Draper, 1987; Draper and Smith, 1998):

$$\mathcal{M}^{REG}(\boldsymbol{x}) = \beta_0 + \sum_{i=1}^{k} \beta_i \, x_i + \sum_{1 \leq i < j}^{k} \beta_{ij} \, x_i \, x_j + \cdots + \beta_{1,\ldots,k} \, \boldsymbol{x} + \varepsilon \tag{2.24}$$

where the β_i are unknown coefficients associated to each variable x_i, β_{ij} to each two-ways interaction $\{x_i \times x_j\}$, and so on. β_0 is the mean of the regression function and ε is the *error* of the approximation.

The magnitude of the β coefficients is proportional to the influence of the associated regressor in the regression meta-model, and it can thus be seen as a sensitivity measure for the respective effect of the variable or interaction. The magnitude of the error provides a measure for the goodness of fit of the meta-model approximation on the response data, the reliability of the sensitivity estimates is thus related to its magnitude.

The number of regressors that can be included in a regression meta-model depends on the type and size of the experimental design employed to propagate the model's uncertainties. Note that computing every regressor in Eq. 2.24 requires 2^k model evaluations. A two-level design (Section 2.2.2), for instance, can be employed to construct a regression meta-model which may include linear (first-order) terms only. In such case, the regression coefficient associated to each variable can be interpreted as the change in output when the input increases by one unit while all other input variables remain fixed to their values.

When a multi-linear regression meta-model, without interactions, is believed to reliably approximate the true model $\mathcal{M}$ (*e.g.* for a $R^2 > 0.7$, see Eq. 2.35), the standardization of the coefficients β_i associated to each variable may be used to provide a sensitivity measure (Hamby, 1994). The standardized regression coefficients (SRC) are simply computed as:

$$SRC_i = \widehat{\beta}_i \sqrt{\frac{\mathbb{V}(x_i)}{\mathbb{V}(\boldsymbol{y})}} \tag{2.25}$$

where $\mathbb{V}(x_i)$ is the variance of the statistical distribution associated to the input variable x_i, and $\mathbb{V}(\boldsymbol{y})$ is the variance of the model output responses. Note that $\widehat{\beta}_i$ denotes the estimated coefficient β_i associated to the factor x_i, as expressed further below. The advantage of the standardization is that it deletes the effect of units to consider every variable on an equal level. The SRC_i are distributed on [-1 ; +1] where their absolute magnitudes are indications of their respective influence on the response quantity. Specifically, the SRC_i represents the change in the output quantity resulting from a perturbation of the variable x_i by a fixed fraction of its variance. The sign of the SRC_i also indicates whether the associated input variable is proportionally (+) or inversely (-) related to the response quantity.

Applying a two-level design, interaction terms can be added into the matrix of regressor effects $\boldsymbol{\mathcal{X}}$ to introduce curvature into the response function. According to the *sparsity-of-effect* principle (Montgomery, 2006) first-order effects of variables and low-order interaction effects are more likely to be responsible for the variance of the response quantity. As a reminder, the use of a fractional-factorial design confounds the

terms in Eq. 2.24, and the decoupling requires to complete the remaining experiments of the full-factorial design.

In situations where the experimental design provides a number of samples taken not only on the boundaries but within the hyperspace $\mathcal{H}^k$, using space-filling designs for instance (Section 2.2.3), the regression meta-model may also include regressors related to high-order effects of input variables. Considering quadratic and cubic terms as well as two-ways interactions, a multivariate regression meta-model builds:

$$\mathcal{M}^{REG}(\boldsymbol{x}) = \beta_0 + \sum_{i=1}^{k} \beta_i \, x_i + \sum_{i=1}^{k} \beta_{ii} \, x_i^2 + \sum_{i=1}^{k} \beta_{iii} \, x_i^3 + \sum_{1 \leq i < j}^{k} \beta_{i,j} \, x_i \, x_j + \varepsilon \tag{2.26}$$

So, in a general matrix formulation, a regression meta-model reads:

$$\boldsymbol{y} = \mathcal{M}(\boldsymbol{X}) = \boldsymbol{\mathcal{X}}\boldsymbol{\beta} + \boldsymbol{\varepsilon} \tag{2.27}$$

where $\boldsymbol{\mathcal{X}}$ is the matrix $(N \times P)$ of regressor effect, $\boldsymbol{\beta}$ is the vector $(P \times 1)$ of regression coefficients to be estimated and $\boldsymbol{\varepsilon}$ is the vector $(N \times 1)$ of residuals; N being the number of model output responses composing the vector $\boldsymbol{y}$. As illustrated in Tables 2.2 and 2.3, the matrix $\boldsymbol{\mathcal{X}}$ may include P columns to assess the main effect of the k input variables, plus the mean I, and possibly interactions or high-order effects as in Eq. 2.26.

The ordinary least-squares (OLS) estimation of the coefficients β is the solution that minimizes the sum of squared errors:

$$L = \boldsymbol{\varepsilon}'\boldsymbol{\varepsilon} = (\boldsymbol{y} - \boldsymbol{\mathcal{X}}\boldsymbol{\beta})'(\boldsymbol{y} - \boldsymbol{\mathcal{X}}\boldsymbol{\beta}) \tag{2.28}$$

Note that a key assumption of the OLS regression analysis is that the errors ε_i are independent, and the set of errors $\boldsymbol{\varepsilon}$ follows a Gaussian distribution with zero mean and constant variance.

The linear unbiased estimator of $\boldsymbol{\beta}$ is computed as:

$$\widehat{\boldsymbol{\beta}} = \left(\boldsymbol{\mathcal{X}}'\boldsymbol{\mathcal{X}}\right)^{-1} \boldsymbol{\mathcal{X}}\boldsymbol{y} \tag{2.29}$$

A minimum of $N = P$ model evaluation is required to solve Eq. 2.29 but in practice a number $N > P$ is employed to avoid singularity in the information matrix $(\boldsymbol{\mathcal{X}}'\boldsymbol{\mathcal{X}})$. From the above estimated coefficients, the *estimated* response vector is given by:

$$\widehat{\boldsymbol{y}} = \mathcal{M}^{REG}(\boldsymbol{\mathcal{X}}) = \boldsymbol{\mathcal{X}}\widehat{\boldsymbol{\beta}} \tag{2.30}$$

From which the vector of *residuals*, or "observed errors", is:

$$\boldsymbol{e} = \boldsymbol{y} - \widehat{\boldsymbol{y}} = \mathcal{M}(\boldsymbol{X}) - \mathcal{M}^{REG}(\boldsymbol{\mathcal{X}}) \tag{2.31}$$

Quality of the meta-model

Considering the residuals of the meta-modelling approximation, the computation of the sum of squares of the residuals (SS_e) and the *Mean Square Error* (MSE) provide an estimate of the goodness of fit of the regression approximation:

$$SS_e = \boldsymbol{e}'\boldsymbol{e} = \sum_{i=1}^{N} (y_i - \widehat{y}_i)^2,$$

$$MSE = \frac{SS_e}{df_e} = \frac{SS_e}{N - P} \tag{2.32}$$

where y_i and $\widehat{y}_i$ are the "true" and "estimated" response quantities for the i^{th} experiment, and df_e is called the degree of freedom of the residuals. These estimators measure the fraction of the variance of the response quantity that remains unexplained by the regression meta-model. Note also that adding unimportant regressors into the regression meta-model formulation can increase the MSE and thus deteriorate the quality of the estimates for the response quantity of interest. For estimating the goodness of fit, some analysts prefer the use of the *Root Mean Square Error* ($RMSE$), which is simply computed

at the square root of the MSE and has the advantage to be expressed in the same units than the output quantity.

The sum of squares of the regression (SS_r) and its associated *Mean Square due to Regression* MSR are computed as:

$$SS_r = \sum_{i=1}^{N} (\widehat{y}_i - \bar{y})^2,$$

$$MSR = \frac{SS_r}{df_r} = \frac{SS_r}{P-1} \tag{2.33}$$

where $\bar{y}$ is the mean value of the "true" response quantities and df_r is called the degree of freedom of the regression meta-model.

Thus, the total sum of squares (SS_t) is the sum of squares of the deviations of each observation y_i from the mean $\bar{y}$ of the N output response quantities. With an associated total degree of freedom $df_t = N-1$, SS_t is simply computed as:

$$SS_t = SS_r + SS_e = \sum_{i=1}^{N} (y_i - \bar{y})^2 \tag{2.34}$$

A popular index for estimating the goodness of fit of the regression function is the coefficient of multiple determination R^2 (Dodge, 2008). Distributed on [0 ; 1] it expresses the percentage of the variance of the output response explained by the regression meta-model:

$$R^2 = 1 - \frac{SS_e}{SS_t} = \frac{SS_r}{SS_t} = \frac{\sum_{i=1}^{N} (\widehat{y}_i - \bar{y})^2}{\sum_{i=1}^{N} (y_i - \bar{y})^2} \tag{2.35}$$

According to Saltelli et al. (2004), a meta-model with a $R^2 > 0.7$ can be considered as being representative enough of the input-output relationship and can thus be used in an UA or SA. It is however recognized that R^2 increases as more regressors are considered in the regression meta-model, regardless whether the additional regressors are statistically significant in the model or not. Ezekiel (1930) proposed an *adjusted* coefficient of multiple determination R^2_{adj} as a more reliable measure of the quality of the regression:

$$R^2_{adj} = 1 - \frac{N-1}{N-P-1}(1 - R^2) \tag{2.36}$$

The great advantage of R^2_{adj} over R^2 is that it will decrease when insignificant regressors are added into the regression function. This can be especially useful when the optimization of the regression is sought through stepwise regression procedures (see the following Section 2.4.1).

One common issue regarding meta-modelling is the capacity of the meta-model to provide reliable estimates for untested variables' combinations, *i.e.* for unsampled regions in $\mathcal{H}^k$. The predictive abilities of the meta-model can be assessed with the *jackknife error* (Miller, 1974) from which the square sum is generally known as the *predicted residual sum of squares* (PRESS) or *leave-one-out error* (LOO) (Allen, 1971).

Let us consider the jackknifed matrix $\boldsymbol{\mathcal{X}}^{(-i)}$ as the matrix of regressor effects $\boldsymbol{\mathcal{X}}$ from which the i^{th} row has been removed. Concurrently, the jackknifed vector $\boldsymbol{y}^{(-i)}$ is the vector of $N-1$ output responses where the i^{th} observation is omitted. Regression coefficients are estimated with Eq. 2.29 but using the matrix $\boldsymbol{\mathcal{X}}^{(-i)}$ and the vector $\boldsymbol{y}^{(-i)}$, the meta-model would then write:

$$\widehat{\boldsymbol{y}}^{(-i)} = \mathcal{M}^{REG}\left(\boldsymbol{\mathcal{X}}^{(-i)}\right) = \mathcal{M}^{\mathrm{REG}\setminus i} \tag{2.37}$$

The jackknife residual is computed as:

$$J_i = y_i - \widehat{y}_{(i)} = \mathcal{M}\left(\boldsymbol{x}^{(i)}\right) - \mathcal{M}^{\mathrm{REG}\setminus i}\left(\boldsymbol{x}^{(i)}\right) \tag{2.38}$$

where $\widehat{y}_{(i)}$ is the response quantity estimated with meta-model $\mathcal{M}^{\mathrm{REG}\setminus i}$ for the i^{th} vector $\boldsymbol{\mathcal{X}}^{(i)}$ of regressor effects in $\boldsymbol{\mathcal{X}}$.

The LOO is defined as:

$$Err_{LOO} = \frac{1}{N}\sum_{i=1}^{N} J_i^2 = \frac{1}{N}\sum_{i=1}^{N} (y_i - \widehat{y}_{(i)})^2 \tag{2.39}$$

Note that Stone (1974) and Geisser (1974) proposed a generalisation of the LOO, both using a set of m response data to predict the remaining $n - m$ responses.

The predictive power of the meta-model can be easily estimated through the Q^2 statistic (Wold, 1982):

$$Q^2 = 1 - \frac{\text{PRESS}}{SS_{t_{(i)}}} = 1 - \frac{\sum_{i=1}^{N}(y_i - \widehat{y}_{(i)})^2}{\sum_{i=1}^{N}(y_i - \bar{y}^{(-i)})^2} \tag{2.40}$$

where $\bar{y}^{(-i)}$ is the mean value of the output responses when the i^{th} observation is omitted. This estimator may approach $-\infty$ when clusters of experimental points appear into the hyperspace $\mathcal{H}^k$, which denotes the poor quality of the meta-model in predicting values in unsampled regions. However, the Q^2 coefficient may approach unity as the sampling points in $\mathcal{H}^k$ are well-spaced (Quan, 1988) and as the meta-model represents accurately the true model $\mathcal{M}$.

Stepwise procedures

Stepwise procedures (Helton, 1993; Draper and Smith, 1998; Carley et al., 2004; Storlie and Helton, 2008a) consist in searching iteratively the optimal regression meta-model that best approximates the true model and provides the best predictions. The backward elimination, forward selection and stepwise regression are three different procedures to select the most significant subset of regressors according to a quality criteria selected by the experimenter.

Let us consider a full regression meta-model involving P regressors, according to the choice of the experimenter. At each step of the stepwise procedures, a regression meta-model including a number Q, $1 < Q \leq P$, of regressors (the mean β_0 being always included) is constructed. Following the experimenter's choice, a quality criteria is computed: MSE, RMSE, R^2, R^2_{adj}, PRESS, Q^2, or others. At the end of the procedure, the sub-model of Q regressors that provided the best quality criteria may be employed as surrogate model for UA or SA purposes.

The general framework of the backward elimination consists in removing terms from the full meta-model of P regressors, one after the other and from the most insignificant to the most significant regressor in the regression function. In practice, the procedure starts with a full regression model that include the P regressors, chosen by the experimenter. At the first step, each regressor is discarded alternatively from the meta-model and the performances of each sub-model of $Q = P - 1$ regressors are calculated. The second step initiates with the model at $P - 1$ regressors having provided the best quality criteria. The same iterative removal is carried out to identify the $Q = P - 2$ regressors in the regression that yield the highest quality criteria. The procedure continues so on until a regression meta-model including $Q = 2$ regressors, the mean β_0 and the most significant regressor, is achieved. From there, all the possible meta-models are compared and that yielding the highest quality criteria is conserved. An example of backward elimination procedure using a regression meta-model with $P = 3$ regressors is provided in Appendix A.

The forward selection is antagonist to the backward elimination. At the first step a regression meta-model includes the mean β_0 solely and adds alternatively one of the $P - 1$ other regressors, the regressor yielding the highest quality criteria is kept for the next steps. The second step starts with $Q = 2$ regressors in the regression: the mean β_0 and the most significant regression term identified in the first step. The iterative inclusion of one of the remaining $P - Q$ regressor allows selecting the second most significant regressor in the regression function. The procedure continues so on until a regression meta-model including the P regressors is achieved. Like in the backward elimination procedure, all the possible regression meta-models are compared and that yielding the best quality criteria is conserved for further analysis.

The stepwise regression procedure is an intermediary algorithm that adds/removes many regressors at one time according to the partial Fisher F-statistic or to the Student t-statistic (Dodge, 2008) associated to each term included in the regression. A each step, if the partial statistic of a regressor is less than a given cut-off value C_{out}, chosen by the experimenter, the regressor is discarded from the meta-model. Although it is not compulsory, the stepwise regression procedure can also consider a threshold C_{in} for including regressors, the choice of a $C_{in} > C_{out}$ making more difficult to add than to remove regressors. The advantage of the stepwise regression in comparison to backward or forward procedures is that any regressor added/removed at earlier steps may be discarded/included in the current step because of its

relationship with other regressors in the equation (Carley et al., 2004).

As a reminder, the construction method for multivariate regression meta-models introduced in this section considers independent input variables. For an extension toward correlated variables, Xu and Gertner (2008) provide a good description of the method for computing correlated and uncorrelated sensitivity measures for each input variable using a multi-linear regression meta-model.

References to case studies employing regression-based sensitivity analyses

In the frame of the European projects of underground disposal facilities for high-level radioactive wastes, Marivoet et al. (1997) reported the results of various sensitivity analyses of predictive modellings of radionuclide transport from underground repositories toward the biosphere. The EVEREST project focused on three rock salt repository projects in Netherlands, France and Germany, a granite site in France, and two clay-rock sites in France and Belgium. Monte-Carlo samplings and LHS were employed to propagate the uncertainties characterizing the input variables. Stepwise regression procedures, mainly based on linear regression meta-models, and SRC were employed to address the sensitivity of various conceptual and physical variables governing the maximum dose of radionuclide reaching the biosphere.

Similarly, Draper et al. (1999) carried out a sensitivity analysis upon 6 different scenarios of radionuclide migration from a hypothetical underground radioactive waste disposal toward the atmosphere. Treating up to 36 uncertain variables they estimated the uncertainty regarding the maximum dose of radionuclide to reach the biosphere. Regression meta-models including quadratic and interaction terms were notably employed to address the influence of each input variable on the model output. They noticed that including high-order terms in the regression function yields a better fit of the response function.

Building a regression meta-model upon the response data obtained through a LHS, Helton and Davis (2003) estimated the sensitivity of a two-phase fluid flow from an underground radioactive waste repository (U.S. WIPP project) with respect to 31 uncertain variables. Stepwise procedures were applied to estimate the most significant variables in the regression meta-model and to rank the input variables. Other regression-based sensitivity analyses of the WIPP project can be found in the literature (Helton, 1999; Helton et al., 2005). Similar works were also carried out for the U.S. Yucca mountain project for the geological repository of long-lived radioactive waste (Arnold et al., 2003; Helton et al., 2012, 2014).

2.4.2 Polynomial chaos expansion meta-models

In the present section, the methodology for constructing a meta-model is given for a scalar response y, however it applies to the entire set of output response quantity. As previously, the hyperspace is assimilated to the unit hypercube $[0\ ;\ 1]^k$.

For mutually independent random variables in $\boldsymbol{x}$ the scalar quantity y can be expanded onto an orthogonal polynomial basis (Soize and Ghanem, 2004; Blatman and Sudret, 2011) producing series often referred to as *polynomial chaos* expansion (PCE):

$$y = \mathcal{M}(\boldsymbol{x}) = \sum_{\alpha \in \mathbb{N}^k} a_\alpha \Psi_\alpha(\boldsymbol{x}) \tag{2.41}$$

where the deterministic coefficients a_α are unknown and Ψ_α are products of k monodimensional polynomials:

$$\Psi_\alpha(\boldsymbol{x}) = \prod_{i=1}^{k} \psi_{\alpha_i}(x_i) = \psi_{\alpha_1}(x_1) \times \psi_{\alpha_2}(x_2) \times \cdots \times \psi_{\alpha_k}(x_k) \tag{2.42}$$

where $\psi_{\alpha_i}(x_i)$ denotes a polynomial of degree α_i in the i^{th} input variable.

Various types of orthogonal polynomials can be employed in Eq. 2.42 depending on the prior assumption about the statistical distribution attributed to each variable x_i. For example, Hermite polynomials

are employed for Gaussian distributions, Jacobi polynomials are associated to beta distributions, Legendre polynomials to uniform distributions and Laguerre polynomials to gamma distributions (Abramowitz and Stegun, 1964; Xiu and Karniadakis, 2002).

The total number of model evaluations required to compute the PC expansion increases prohibitively fast with the number of terms included in the latter. Thus, in order to reduce the computational burden for the PC expansion, a truncation of Eq. 2.41 is operated after P terms, leading to a so-called *sparse* PC expansion. The number of terms in the sparse PCE is then $P = \frac{(p+k)!}{p!k!}$. Doing so, the p-degree PC approximation of $\mathcal{M}(\boldsymbol{x})$ writes:

$$y \cong \mathcal{M}^{PCE}(\boldsymbol{x}) = \sum_{\alpha=0}^{P-1} a_\alpha \Psi_\alpha(\boldsymbol{x}) \equiv \boldsymbol{a}'\boldsymbol{\Psi}(\boldsymbol{x}) \tag{2.43}$$

where $\boldsymbol{a}$ is the vector of P unknown coefficients a_α, and $\boldsymbol{\Psi}(\boldsymbol{x})$ gathers the P k-dimensional orthogonal basis $\Psi_\alpha(\boldsymbol{x})$ of degree not exceeding p.

The set of P terms can be determined by an appropriate truncation scheme. As an example, a hyperbolic truncation scheme based on the q-quasi-norm (Blatman and Sudret, 2011) can be employed to select the terms satisfying the condition:

$$|| \boldsymbol{\alpha} ||_q = \left(\sum_{i=1}^{k} \alpha_i^q \right)^{1/q} \leq p \tag{2.44}$$

for appropriate $0 \leq q \leq 1$ and $p \in \mathbb{N}$. The selection of a low value for q favours the inclusion of the main effects and low-order interactions effects of input factors, which are likely to be the most significant effects on the output response.

Two methods are commonly employed to determine the expansion coefficients a_α: the *spectral projection* method (Ghiocel and Ghanem, 2002; Le Maître et al., 2002) and the *regression* method (Choi et al., 2004; Sudret, 2008). The first evaluates the coefficients by projecting the model response against each individual basis function, each coefficient is thus recast as a multidimensional integral computed either by simulation or quadrature methods. The second estimates the coefficients by minimization of the mean squared error computed as the difference between the *estimated* response and the *true* response. Similar to the OLS regression (Eq. 2.28) the best set of coefficients is found by minimizing:

$$\widehat{\boldsymbol{a}} = \arg\min \left\{ \mathbb{E}\left[\left(\mathcal{M}(\boldsymbol{x}) - \mathcal{M}^{PCE}(\boldsymbol{x}) \right)^2 \right] \right\} \tag{2.45}$$

It has been proven that the regression method converges faster with respect to the number of model evaluation (Berveiller, 2005; Blatman, 2009) and it will be considered in the following. A *sparse* PCE is defined as a PCE meta-model where only the non-zero coefficients are selected, thus reducing the number of terms in the meta-model representation. This can be obtained by evaluating the coefficients a_α with the *Least Angle Regression* (LAR) method (see Efron et al., 2004; Blatman and Sudret, 2011 for further details).

Considering the whole set of response quantities $\boldsymbol{y}$, Eq. 2.45 rewrites:

$$\widehat{\boldsymbol{a}} = \left(\boldsymbol{\Psi}'\boldsymbol{\Psi} \right)^{-1} \boldsymbol{\Psi}'\boldsymbol{y} \tag{2.46}$$

where $\boldsymbol{\Psi}$ is called the *data matrix* and the product $\boldsymbol{\Psi}'\boldsymbol{\Psi}$ is called the *information matrix*. A minimum of $N = P$ model evaluation is required to solve Eq. 2.46.

Estimating the coefficients of the PC expansion for the entire experimental design $\boldsymbol{X}$ yields the following PC *approximation* of the response quantities:

$$\widehat{\boldsymbol{y}} = \mathcal{M}^{PCE}(\boldsymbol{X}) = \widehat{\boldsymbol{a}}'\boldsymbol{\Psi}(\boldsymbol{X}) \tag{2.47}$$

The quality of the PC expansion can be estimated by means of the *leave-one-out* error (Blatman and Sudret, 2011) or the Q^2 statistic. Let us consider the vector of response quantities $\boldsymbol{y}^{(-i)}$ where the i^{th} observation has been removed, the PC approximation built from the latter is:

$$\widehat{\boldsymbol{y}}^{(-i)} = \mathcal{M}^{PCE}\left(\boldsymbol{X}^{(-i)} \right) = \mathcal{M}^{\mathrm{PCE}\setminus i} \tag{2.48}$$

where $\boldsymbol{X}^{(-i)}$ is the experimental design where the i^{th} experiment has been discarded; *i.e.* the vector $\boldsymbol{x}^{(i)}$ is extracted from the full experimental matrix $\boldsymbol{X}$.

The assessment of the goodness of fit of the PCE meta-model upon the "true" output responses can be carried out by estimating the approximation error as in Eq. 2.32-2.34. The coefficient of multiple determination R^2 can be computed as in Eq. 2.35, or the adjusted version R^2_{adj} of Eq. 2.36.

The performances of the PCE meta-model for predicting unsampled regions in $\mathcal{H}^k$ can be estimated through the jackknife residual (Eq. 2.38) and the LOO as in Eq. 2.39. Note also that the Q^2 statistic can be computed as in Eq. 2.40 to provide a normalized index of the predictive performances of the PCE approximation.

An iterative procedure based on stepwise regression procedures (Blatman and Sudret, 2010b, 2008) is generally employed to provide the most robust PCE metamodel by seeking the degree p and the q-quasi-norm which produces the best quality criteria. The stepwise procedures are similar to that introduced in Section 2.4.1.

2.4.3 Sobol' indices from PCE meta-models

Let $\mathcal{A}$ be a non-empty subset of $\mathbb{N}^k$, the truncated PCE meta-model of Eq. 2.47 can be written as:

$$\widehat{\boldsymbol{y}} = \mathcal{M}^{\mathrm{PCE}}_{\mathcal{A}}(\boldsymbol{X}) = \sum_{\boldsymbol{\alpha}\in\mathcal{A}} \widehat{a}_\alpha \Psi_\alpha(\boldsymbol{X}) \tag{2.49}$$

Let $\mathcal{I}_{i_1,\ldots,i_s}$ be the set of $\boldsymbol{\alpha}$-tuples in $\mathcal{A}$ such that the polynomials Ψ_α only depend on the input variables $\{x_{i_1},\ldots,x_{i_s}\}$, where $\{i_1,\ldots,i_s\}$ are index sets. The decomposition of the output response quantities into summands of polynomial functions writes:

$$\begin{aligned}\mathcal{M}^{\mathrm{PCE}}_{\mathcal{A}}(\boldsymbol{X}) = \widehat{a}_0 + \sum_{i=1}^{k}\sum_{\boldsymbol{\alpha}\in\mathcal{I}_i} \widehat{a}_\alpha\Psi_\alpha(x_i) + \sum_{1\le i_1<i_2}^{k}\sum_{\boldsymbol{\alpha}\in\mathcal{I}_{i_1,i_2}} \widehat{a}_\alpha\Psi_\alpha(x_{i_1,i_2}) \\ + \cdots + \sum_{\boldsymbol{\alpha}\in\mathcal{I}_{1,\ldots,k}} \widehat{a}_\alpha\Psi_\alpha(\boldsymbol{X})\end{aligned} \tag{2.50}$$

Whereas the computation cost of a response quantity with the true model $\mathcal{M}(\boldsymbol{x})$ can be relatively high, especially when it requires a numerical solution involving partial differential equations, a PCE meta-model can serve as a surrogate model to compute response quantities at a negligible computational cost. For instance, the mean and variance of the distribution of response quantities can be estimated straightforwardly:

$$\begin{aligned}\hat{\mu}_y &= \mathbb{E}\left[\mathcal{M}^{\mathrm{PCE}}_{\mathcal{A}}(\boldsymbol{x})\right] = \widehat{a}_0 \ , \\ \hat{\sigma}^2_y &= \mathbb{V}\left[\mathcal{M}^{\mathrm{PCE}}_{\mathcal{A}}(\boldsymbol{x})\right] = \sum_{\alpha=1}^{P-1} \hat{a}^2_\alpha\, \mathbb{E}\left[\Psi^2_\alpha(\boldsymbol{x})\right] = \widehat{V}_y\end{aligned} \tag{2.51}$$

where $\widehat{V}_y$ stands for the estimated variance of the model output with the PCE meta-model. Due to the orthogonality of the PC basis, the total variance can be recomputed as:

$$\widehat{V}_y = \sum_{\alpha\in\mathcal{A}} \widehat{a}^2_\alpha \tag{2.52}$$

Then, an estimate of the partial variance attributed to each variable can be computed as:

$$\widehat{V}_i = \sum_{\boldsymbol{\alpha}\in\mathcal{A}_i} \widehat{a}^2_\alpha \qquad \mathcal{A}_i = \{\boldsymbol{\alpha}\in\mathcal{A} : \alpha_i > 0, \alpha_{i\neq j} = 0\} \tag{2.53}$$

For any given subset $\boldsymbol{u}$ of variables as in 2.3.3, the subset $\mathcal{A}_{\boldsymbol{u}} = \{\boldsymbol{\alpha}\in\mathcal{A} : \alpha_w \neq 0 \text{ if and only if } w\in\boldsymbol{u}\}$. The estimated partial variance attributed to this subset of variables is :

$$\widehat{V}_{\boldsymbol{u}} = \sum_{\boldsymbol{\alpha}\in\mathcal{A}_{\boldsymbol{u}}} \widehat{a}^2_\alpha \tag{2.54}$$

and the estimated all-order partial variance attributed to the variable x_i, including every interaction with other variables writes:

$$\widehat{V}_i^{tot} = \sum_{\boldsymbol{\alpha} \in \mathcal{I}_i} \widehat{a}_\alpha^2 \tag{2.55}$$

where $\mathcal{I}_i$ denotes the set of all indices which include the variable x_i:

$$\mathcal{I}_i \equiv \{\boldsymbol{\alpha} \in \mathbb{N}^k : 0 \leq |\alpha| \leq p, \alpha_i \neq 0\} \tag{2.56}$$

The Sobol' sensitivity indices of any order can computed according to the ratios of partial to total variance, as in Section 2.3.3.

References to case studies employing PCE-based sensitivity analyses

Recent applications of PCE-based sensitivity analyses in the fields of hydrologic and hydrogeologic studies can be found in the literature. Fajraoui et al. (2012) employed a sparse PCE meta-model to address the global sensitivity analysis and parameter optimization of two reactive transport problems in aqueous phases. Laloy et al. (2013) provided a comprehensive study of a high-dimensional groundwater model where they employed PCE meta-models to explore the posterior parameters distributions at negligible computational costs. Ciriello et al. (2013) constructed a PCE meta-model over the responses of a radionuclide transport in a random heterogeneous aquifer. The authors derived Sobol' indices from the PCE model for three parameters: the partition coefficient, the longitudinal dispersivity and the correlation length of log-conductivity in the heterogeneous media.

Chapter 3

A comparison of sensitivity analysis methods for screening[1]

[1] This chapter is under revision for an upcoming submission as article.

3.1 Introduction

Models are becoming more complex and computationally demanding: they may include dozens or even hundreds of input variables and analyse as many outputs. Knowledge of the input variables is often limited and, when dealing with numerous uncertain variables, sensitivity analysis (SA) is widely employed to quantify the contribution to the uncertainty in the model output from individual inputs and groups of inputs.

One way of classifying problem types faced in sensitivity analysis is by dimensionality (the number of input variables of a model), and model run time (the computational time required to execute a computer model for a given set of input) — see Figure 3.1. When the dimensionality and run-time of a model are both low, performing sensitivity analysis is relatively straightforward — a typical approach would be to run the model many thousands of times in order to estimate Sobol' sensitivity indices via the Monte Carlo method (Sobol', 2001). If the run time of the model is low, but the number of variables is high, the Monte Carlo method is usually still appropriate since its cost increases linearly with dimensionality. On the other hand, if the dimensionality is low, but the run-time of the model is high, an emulator-based approach is usually adopted. This involves building a mathematical approximation of the model (typically a Gaussian Process (Oakley and O'Hagan, 2004; Becker et al., 2012), Polynomial Chaos Expansion (Sudret, 2008) or state-dependent parameter regression (Ratto et al., 2007)) using a limited number of model runs as "training data", then estimating sensitivity indices using the emulator, which can be run a great number of times for a negligible computational cost.

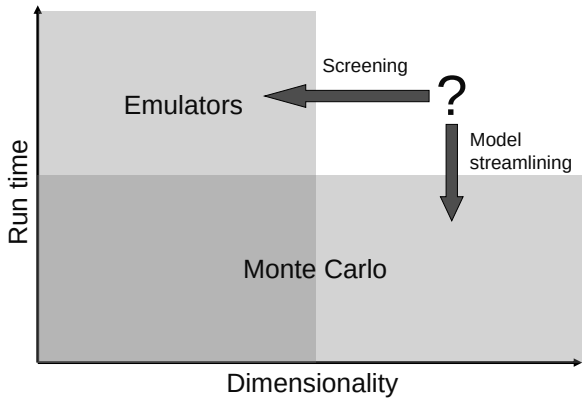

Figure 3.1: A classification of problems in sensitivity analysis by dimensionality and run time.

Although there is extensive literature on the emulator problem in sensitivity analysis, there is relatively little that deals with the very common situation where one has both a high dimensionality *and* a high run time. In such cases, fitting an emulator is generally impractical because the computational cost of doing so tends to increase exponentially with the dimensionality. Furthermore, the model cannot be run enough times for a Monte Carlo analysis. In general, one is left with one of two approaches: either to somehow streamline the model to make it run faster, thereby bringing it within reach of the Monte Carlo method, or somehow reducing the dimensionality of the problem. Although the first approach can often be fruitful, it is only a viable option if one is the developer of the model; besides, the run time might already have been minimised. This paper focuses on the second strategy, which is often called "screening" or "factor fixing".

Screening aims to answer the question, *"Which inputs could be fixed to any value within their range of uncertainty without significantly affecting the uncertainty of the model output(s)?"* Screening is usually associated with the elementary effects method (Morris, 1991; Campolongo et al., 2007), but to the knowledge of the authors there is no theoretical or empirical evidence which shows that the elementary effects method consistently performs better at low sample sizes than other measures of sensitivity. The objective of this paper is therefore to compare the performance of the absolute mean measure μ^* from the elementary effects method, on a high-dimensional problem at small sample size, against two other

measures of sensitivity, the well-known Sobol' total sensitivity indices S^{tot} (Homma and Saltelli, 1996) and a derivative-based global sensitivity measure (DGSM) ν (Sobol' and Kucherenko, 2009). Note that in (Campolongo et al., 2007, 2011) it is acknowledged that μ_i^* has some similarities with S^{tot}, although no formal proof has been provided. On the other hand, there is a solid proof of a link between ν and S^{tot} (Sobol' and Kucherenko, 2009; Kucherenko et al., 2009; Sobol' and Kucherenko, 2010). In this work we discuss the close link between the three measures, and propose a variation of the DGSM measure which is included in the testing.

Because screening and factor fixing is primarily interested in sorting influential from non-influential variables, we assess the performance of each measure in terms of Type I and Type II errors, rather than using the error between estimated and analytical values of each measure, as for example in Tarantola et al. (2012). Type I error occurs when a truly important variable is wrongly qualified as non-influential; Type II error, on the other hand, is when a variable is wrongly identified as influential when it is not.

The remainder of this paper is organised as follows: in Section 3.2 the three SA measures considered in this study are briefly introduced. We refer however to the vast literature available for further details on the measures, limiting the description to the most relevant features with respect to the present topic. In Section 3.3, the test functions are introduced and the results of the sensitivity measures are given with some discussion. Finally, an overview of the main findings and conclusions is in Section 3.4.

3.2 Measures of sensitivity and sampling

3.2.1 Measures of sensitivity

Let us denote by $x_1, x_2, \ldots, x_k$ the input variables of a computer model f, defined over the unit hypercube $\mathcal{H}^k$, and with y being the output of the model, such that $y = \mathcal{M}(x_1, x_2, \ldots, x_k)$.

Any point $\boldsymbol{x}_j = x_{1j}, x_{2j}, \ldots, x_{kj}$ in the hypercube represents a given set of values for the k input variables, for which the model output y_j can in turn be evaluated. A single model evaluation (or model run) can take very different computational time, from nanoseconds to hours, or even days. Hence, it is important, especially in the latter case, to be able to obtain accurate sensitivity measures with the minimum number of model runs.

A well known sensitivity measure S_i^{tot} is the *total order sensitivity index*, which is defined as (Homma and Saltelli, 1996),

$$S_i^{tot} = 1 - \frac{V_{\boldsymbol{x}_{\sim i}}[E_{x_i}\left(y \mid \boldsymbol{x}_{\sim i}\right)]}{V(y)} = \frac{E_{\boldsymbol{x}_{\sim i}}[V_{x_i}\left(y \mid \boldsymbol{x}_{\sim i}\right)]}{V(y)} \tag{3.1}$$

where $V(\cdot)$ denotes the variance operator, $E(\cdot)$ the expected value, and $\boldsymbol{x}_{\sim i}$ the set of all input variables except x_i. The total order sensitivity index measures the contribution to $V(y)$ of a given input x_i, as well as all its interactions of any order with other variables. It has to be distinguished from the *first order sensitivity index* S_i which measures the linear contribution of the variable x_i to $V(y)$. The sum $\sum S_i = 1$ $(i = 1, ..., k)$, for purely linear models whereas $\sum S_i \ll 1$ for strongly nonlinear models.

Let us generate a set of N sampling points, $\boldsymbol{x}_1, \boldsymbol{x}_2, ..., \boldsymbol{x}_N$, randomly sampled from $\mathcal{H}^k$. This may be expressed in a design matrix $\mathbf{X}$ of N rows and k columns, which is used to estimate all the sensitivity measures here.

Letting $\boldsymbol{x}_j^{(i)}$ and $\boldsymbol{x}_j^{(i')}$ be, respectively, a point in the input space, and a point that differs from $\boldsymbol{x}_j^{(i)}$ only in the value of x_i, an estimator of the numerator of S_i^{tot} (V_i^{tot}) is as follows (Jansen, 1999; Saltelli et al., 2010),

$$\hat{V}_i^{tot} = \frac{1}{2N}\sum_{j=1}^{N}\left|\mathcal{M}(\boldsymbol{x}_j^{(i')}) - \mathcal{M}(\boldsymbol{x}_j)\right|^2. \tag{3.2}$$

The absolute value notation here is used for consistency with the other estimators presented here. The $\boldsymbol{x}_j$ therefore correspond to the points from $\mathbf{X}$, and the $\boldsymbol{x}_j^{(i')}$ represent random shifts in the x_i direction.

Another widely-used measure of sensitivity is the mean of absolute elementary effects, which is estimated as (Campolongo et al., 2011),

$$\hat{\mu}_i^* = \frac{1}{N}\sum_{j=1}^{N}\frac{\left|\mathcal{M}(\boldsymbol{x}_j^{(i')}) - \mathcal{M}(\boldsymbol{x}_j)\right|}{|x_{ji}^{(i')} - x_{ji}|}. \tag{3.3}$$

Here, x_{ji} denotes the i^{th} coordinate of $\boldsymbol{x}_j$, so that the denominator of (3.3) is equal to the difference in x_i between $\boldsymbol{x}_j^{(i)}$ and $\boldsymbol{x}_j^{(i')}$.

The final measure used in this study is part of a set of sensitivity measures called "derivative-based global sensitivity measures" (DGSM). The measure is the integral of squared derivatives, *i.e.* $\nu_i = \int_{\mathcal{H}} (\partial y/\partial x_i)^2 d\boldsymbol{x}$. This may be estimated as (Sobol' and Kucherenko, 2009),

$$\hat{\nu}_i = \frac{1}{N} \sum_{j=1}^{N} \frac{\left| \mathcal{M}(\boldsymbol{x}_j^{(i'')}) - \mathcal{M}(\boldsymbol{x}_j) \right|^2}{|\delta|}, \tag{3.4}$$

where $\boldsymbol{x}_j^{(i'')}$ is a point that differs from $\boldsymbol{x}_j$ only by a small increment δ of x_i, in order to give an estimate of $\frac{\partial y}{\partial x_i}$ at each point $\boldsymbol{x}_j$. This increment is kept fixed for all j, and is recommended as $\delta = 1 \times 10^{-5}$ when sampling with respect to the unit hypercube.

Notice that the three measures share a number of similarities. The first is that they are all estimated using random samples in $\mathcal{H}^k$, with perturbations in each x_i direction. This results in a so-called "radial design" which consists of N "stars" in the input space, each having a point from $\mathbf{X}$ at its centre (see Figure 3.2). Hence, for N radial samples, the total number of model runs is $N_T = N(k+1)$. In the cases of S_i^{tot} and μ_i^*, the perturbations are large and random, whereas in the estimator of ν_i they are small and kept constant.

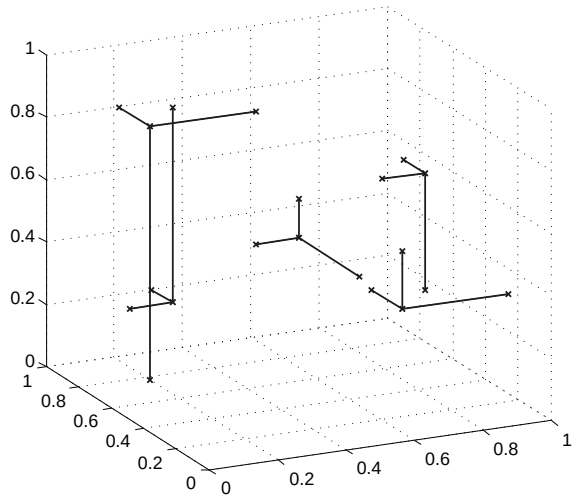

Figure 3.2: An illustration of a radial sampling design with large perturbations, with $N = 5$ and $k = 3$.

Next, all three measures use the difference between $\boldsymbol{x}_j^{(i)}$ and $\boldsymbol{x}_j^{(i')}$ (or $\boldsymbol{x}_j^{(i'')}$) as a basis for measuring sensitivity – for S_i^{tot} and ν_i this is the squared difference, whereas for μ_i^* it is the absolute difference. Finally, the estimators for μ_i^* and ν_i both use the difference in x_i as a denominator, whereas S_i^{tot} does not use this information.

The similarities and differences between these three measures led us to propose a fourth measure which is a variation of ν_i, which we call ξ_i. This is defined as,

$$\hat{\xi}_i = \frac{1}{N} \sum_{j=1}^{N} \frac{\left| \mathcal{M}(\boldsymbol{x}_j^{(i'')}) - \mathcal{M}(\boldsymbol{x}_j) \right|}{|\delta|}, \tag{3.5}$$

i.e. it uses the absolute value in the numerator, rather than the squared value. The aim here is simply to see whether the use of the absolute value, as opposed to the squared value, can help in the ranking of variables.

3.2.2 Sampling

All the measures of sensitivity discussed here require a random sample in $\mathcal{H}^k$ as a basis[2]. In practice however, many practitioners of sensitivity analysis use *quasi-random* numbers in place of pseudo-random numbers, to increase the rate of convergence of the estimators (see for example Caflisch (1998)). In the last decades many techniques have been studied. Among these, latin hypercube sampling (LHS) (McKay et al., 1979; Iman et al., 1981) and latin supercube sampling (LSS) (Owen, 1998a) were developed for the design of real experiments, whereas low-discrepancy sequences (LDS), such as the Sobol' sequence (Sobol', 1967), were thought to address the problem of numerical integration. Recent studies have undertaken the comparison of these experimental designs with regard to the convergence rates of sensitivity indices; Sobol' sequences have proven to be more efficient than both LHS (Kucherenko et al., 2011), LSS (Tarantola et al., 2012) and simple Monte Carlo sampling at low sample size. Moreover, Sobol' sequences can be enhanced by adding new sampling points in the experimental design while keeping the sampling in $\mathcal{H}^k$ as uniform as possible — as such they have probably become the sequence of choice for the majority of practitioners of global SA. In this work, we therefore test both the Sobol' sequence as well as (pseudo-)random numbers as a basis for comparison.

3.3 Numerical experiments

The aim of the tests performed here is to simulate as closely as possible the setting for a screening analysis. In our opinion, the characteristics of a screening experiment are as follows: first, the dimensionality of the problem is high, *i.e.* there are at least around 30 variables, and possibly hundreds (or even thousands). Second, the number of model runs that can be performed is low, perhaps in the region of a few hundred at most. Finally, the objective of the analysis is to separate "significant" variables (those that significantly influence the output of the model) from "insignificant" variables. In other words, we are not necessarily interested in obtaining precise values of sensitivity measures; rather we are primarily interested in sorting the variables into two groups: the influential group, and the non-influential group. The reasoning behind this is that a screening analysis is often followed by a more detailed sensitivity analysis on the remaining set of significant variables, perhaps using an emulator.

To reflect this setting, we use several test functions as the basis of comparison that have different characteristics regarding dimensionality, nonlinearity, continuity and so forth. Test functions are used because we know *a priori* the true ranking of the input variables; additionally, they are very cheap to evaluate. For each function, we set a certain fraction γ of the input variables to be of higher influence, and the remaining fraction $1-\gamma$ of variables to be of lower influence (the exact sensitivity is controlled by the parameter values in each case).

Our experiments are then set as follows. Let $k_{\text{high}} = \lfloor \gamma k \rfloor$, *i.e.* the number of input variables that are set as high influence, and $k_{\text{low}} = k - k_{\text{high}}$. In each test function, the variables are set such that $\{S_1^{tot} = S_2^{tot} = ... = S_{k_{\text{high}}}^{tot}\} \gg \{S_{k_{\text{high}}+1}^{tot} = S_{k_{\text{high}}+2}^{tot} = ... = S_k^{tot}\}$. In other words, the first k_{high} variables are set to have equal and high sensitivities, and the remainder to have equal and low sensitivities.

Now let r_i be the ranking of the i^{th} variable by one of the sensitivity measures defined previously, where ranking runs in descending order, *i.e.* $r_i = 1$ is ranked as the most influential variable, and $r_i = k$ is the least. Our measure of error, Z, is as follows,

$$Z = \frac{1}{k_{\text{high}}} \sum_{i=1}^{k_{\text{high}}} 1(r_i > k_{\text{high}}), \tag{3.6}$$

where $1(\cdot)$ is the count function. This metric therefore measures the fraction of influential variables that are ranked outside the top k_{high} variables by the sensitivity measure. This is purely a measure of sorting the variables into high and low importance groups, and gives no regard to precise rankings or possible cutoff values that might be used to select high importance from low importance variables, since in our experience, what is a "high importance" variable is usually subjective and problem-dependent.

[2]Strictly speaking, these are *pseudo-random* numbers because computer algorithms cannot output truly random numbers, but they exhibit most of the properties of random numbers.

In order to capture the average performance, for each test function investigated, 50 repetitions are made. In the case of random numbers this is simply done by drawing 50 independent samples of random numbers. For the Sobol' sequence, the sample is randomised by applying a random shift in each dimension, following the approach of Owen (1998b). Additionally, each function is tested at values of $N = 1, 2, ..., 10$, which resulted in total sample sizes N_T ranging from $N_T = 31$ for $N = 1$ and $k = 30$, to $N_T = 1010$, when $N = 10$ and $k = 100$.

In the following, the results displayed are from random sampling unless otherwise stated. This is because the relative performance (that is, how well each measure performs compared to the others) when using random numbers as opposed to the Sobol' sequence is almost identical, therefore we have used random numbers to illustrate the results since they are likely more generally applicable, as they do not impose any structure on the sampling. In Section 3.3.4 we do however briefly summarise the relative performance with the Sobol' sequence, which shows that Sobol' sampling does further improve the performance of all the measures.

3.3.1 G^* function

The G^* test function, defined in (Saltelli et al., 2010) has the following form:

$$G^* = G(x_1, x_2, \ldots, x_k, a_1, a_2, \ldots, a_k, \delta_1, \delta_2, \ldots, \delta_k, \alpha_1, \alpha_2, \ldots, \alpha_k) = \prod_{i=1}^{k} g_i^*$$

$$g_i^* = \frac{(1+\alpha_i)\,|2(x_i + \delta_i - \mathbf{I}[x_i + \delta_i]) - 1|^{\alpha_i} + a_i}{1 + a_i} \tag{3.7}$$

where a_i, δ_i and α_i are parameters which can be chosen to obtain different behaviour of the function, and $\mathbf{I}[x_i + \delta_i]$ is the integer part of $(x_i + \delta_i)$. The relative importance of the inputs $(x_1, x_2, \ldots, x_k)$ in the G^* function is controlled by the magnitude of a_i, and the nonlinearity by α_i. The parameter δ_i is simply a shift parameter which is set to zero in this work since we anyway take random replications of samples.

To illustrate the influence of the parameters, Figure 3.3 shows plots of $g^*(a, \alpha, \delta)$ for various values of a, α and δ. From left to right, the coefficient a is doubled from 1 to 4 where each graph compares the influence of doubling α from 1 to 4. The higher a, the lower the amplitude of g^*, and the lower the importance of the corresponding input. The coefficient α acts on the curvature of the bottom part of the g^* function, thus maximizing the slope toward the high values. The shift parameter δ defines the location of the maximum of the g^* function, but has no effect on the importance of the corresponding input.

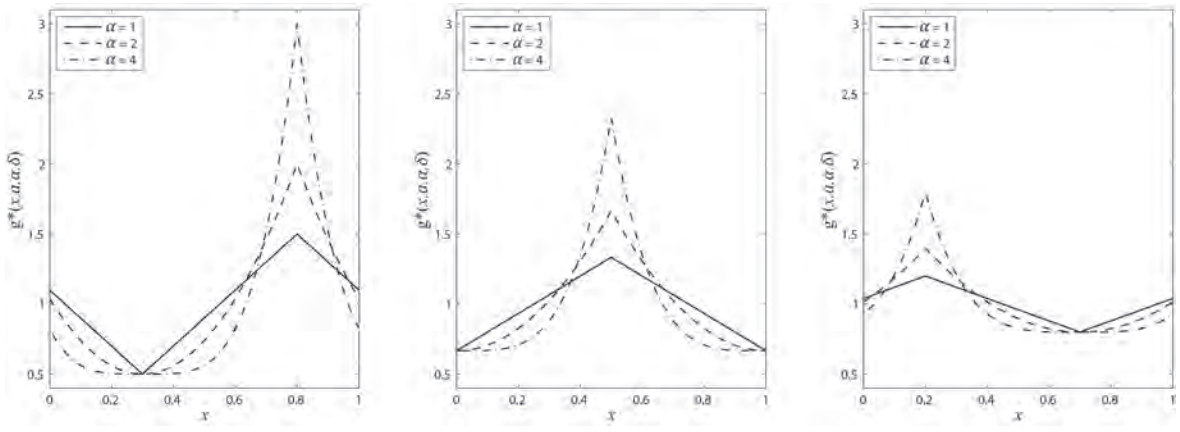

Figure 3.3: (left) $g^*(a, \alpha, \delta)$ for $a = 1$, $\delta = 0.2$, $\alpha = 1, 2, 4$. (middle) $g^*(a, \alpha, \delta)$ for $a = 2$, $\delta = 0.5$, $\alpha = 1, 2, 4$. (right) $g^*(a, \alpha, \delta)$ for $a = 4$, $\delta = 0.8$, $\alpha = 1, 2, 4$.

In order to provide a range of comparisons for the various measures of sensitivity, the G^* function was adjusted to various different dimensionalities and parameter values. The dimensionality was set to $k = 30, 50, 75, 100$ to represent various dimensionalities that might be encountered in a screening analysis. The parameter α was also set to $\alpha = 1, 2, 3$ to test at various values of nonlinearity. Finally the a_i coefficients were set in two scenarios: the first a low-interaction with $a_{\text{high}} = 3$ and $a_{\text{low}} = 10$, resulting in, for illustration, $\sum S_i = 0.805$ at $k = 30$ and $\alpha = 2$. The second scenario set $a_{\text{high}} = 1$ and $a_{\text{low}} = 2$, which at the same k and α values gives $\sum S_i = 0.151$, *i.e.* strong interactions between input variables. Figure 3.4 shows a plot of the G^* function for $k = 2$, using the coefficients from the latter case.

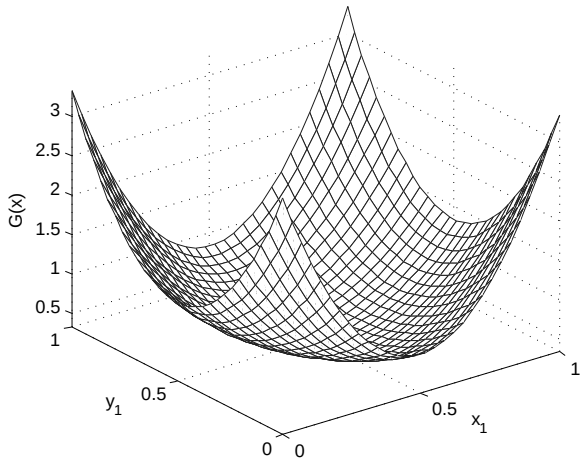

Figure 3.4: Plot of G^* function for $k = 2$, $a_{\text{high}} = 1$, $a_{\text{low}} = 2$, $\alpha = 2$, $\delta = 0.5$.

Table 3.1 shows the relative performance of the various sensitivity measures on various configurations of the G^* function. The numbers in each sensitivity measure column refer to which measure performed best on average over all sample sizes, at the given parameter values. The table then reveals a number of features. First of all, for a given set of parameters, the dimensionality of the function does not generally impact the relative performance of the sensitivity measures. One can also see that, of the configurations tested, the DGSM measures ν and ξ are generally the best, with ξ having a slightly higher number of successes. Then for all cases the μ^* measure is the third best, followed by S^{tot}, which is last.

More detail can be obtained by examining plots of the error measure Z from (3.6) against N_T, showing the decrease of the error of each measure with total sample size in Figure 3.5. To briefly explain these plots, in Figure 3.5(a), for example, the upper line shows that at a total cost of around 100 model runs, S^{tot} is able to rank the variables so that about 1/3 of the significant variables are identified (in the first k_{high} ranking positions). The DGSM measures, at the same sample size, can identify around 3/4 of the significant variables ($Z = 0.26$ approximately).

Figure 3.5(a) shows the performance at $k = 100$, $a_{\text{high}} = 1$, $a_{\text{low}} = 2$, $\alpha = 2$ and $\gamma = 0.2$, in which it can be seen that the two derivative-based measures perform much better than S^{tot} and μ^*, with a very small difference between ξ and ν. Keeping these parameter values but setting $\alpha = 3$ (which increases the nonlinearity), there is little difference in relative performance (Figure 3.5(b)). When the fraction of influential variables is increased to 0.5, in Figure 3.5(c), the ordering changes slightly, with ξ now performing the best, followed closely by ν. The difference in ranking errors between the DGSM measures and μ^* and S^{tot} is also much less. The same is true in Figure 3.5(d), in which the coefficients are changed to the low-interaction setting. In this case, ξ is the best performer, followed by the other measures in the same order.

Table 3.1: Configuration and performance rankings of experiments with G^* function.

k	a_{high}	a_{low}	α	γ	S^{tot}	μ^*	ν	ξ
30	1	2	2	0.2	4	3	1	2
50	1	2	2	0.2	4	3	1	2
75	1	2	2	0.2	4	3	1	2
100	1	2	2	0.2	4	3	1	2
30	1	2	2	0.5	4	3	2	1
50	1	2	2	0.5	4	3	1	2
75	1	2	2	0.5	4	3	1	2
100	1	2	2	0.5	4	3	2	1
30	1	2	3	0.2	4	3	1	2
50	1	2	3	0.2	4	3	1	2
75	1	2	3	0.2	4	3	1	2
100	1	2	3	0.2	4	3	1	2
30	1	2	3	0.5	4	3	2	1
50	1	2	3	0.5	4	3	2	1
75	1	2	3	0.5	4	3	2	1
100	1	2	3	0.5	4	3	2	1
30	3	10	1	0.2	4	3	1	1
50	3	10	1	0.2	4	3	1	1
75	3	10	1	0.2	4	3	1	1
100	3	10	1	0.2	4	3	1	1
30	3	10	1	0.5	4	3	1	1
50	3	10	1	0.5	4	3	1	1
75	3	10	1	0.5	4	3	1	1
100	3	10	1	0.5	4	3	1	1
30	3	10	2	0.2	4	3	1	2
50	3	10	2	0.2	4	3	2	1
75	3	10	2	0.2	4	3	2	1
100	3	10	2	0.2	4	3	2	1
30	3	10	2	0.5	4	3	2	1
50	3	10	2	0.5	4	3	2	1
75	3	10	2	0.5	4	3	2	1
100	3	10	2	0.5	4	3	2	1
30	3	10	3	0.2	4	3	1	2
50	3	10	3	0.2	4	3	2	1
75	3	10	3	0.2	4	3	2	1
100	3	10	3	0.2	4	3	2	1
30	3	10	3	0.5	4	2	3	1
50	3	10	3	0.5	4	2	3	1
75	3	10	3	0.5	4	2	3	1
100	3	10	3	0.5	4	1	3	2

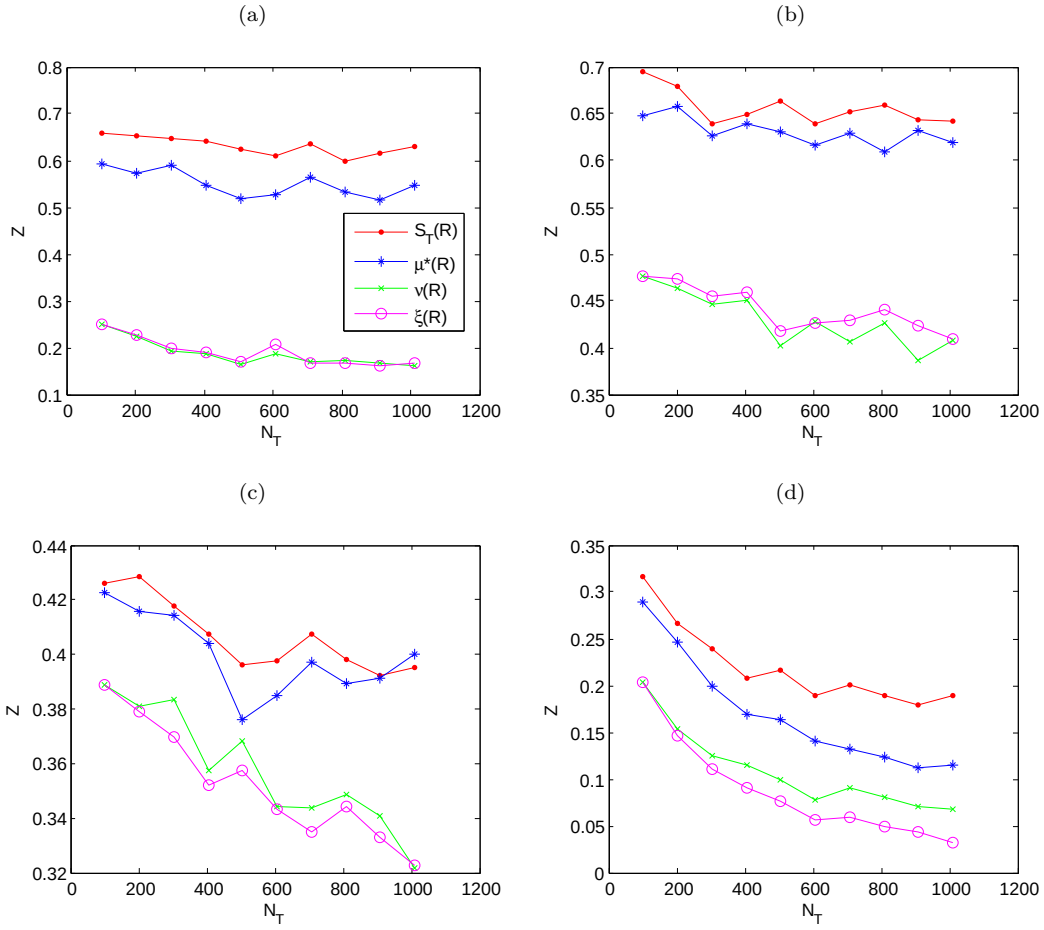

Figure 3.5: Convergence plots for G^* function: (a) $a_{\text{high}} = 1$, $a_{\text{low}} = 2$, $\alpha = 2$, $\gamma = 0.2$; (b) $a_{\text{high}} = 1$, $a_{\text{low}} = 2$, $\alpha = 3$, $\gamma = 0.2$; (c) $a_{\text{high}} = 1$, $a_{\text{low}} = 2$, $\alpha = 2$, $\gamma = 0.5$; (d) $a_{\text{high}} = 3$, $a_{\text{low}} = 10$, $\alpha = 2$, $\gamma = 0.5$; In all cases $k = 100$.

One general feature of these results is that, at least in the G^* function, DGSM measures seem to be more efficient at ranking functions with strong interactions, given the wide gap between ξ and ν and the other two measures. Between the two DGSM measures themselves, there is little discernable difference, although ξ may have a slight advantage. Most likely the reason that DGSM measures perform much better than the other measures on the G^* function is that they are based on a sampling strategy that uses small steps. Given that the G^* function is non-monotonic, it is possible for the large-step samples of μ^* and S^{tot} to "miss" the high gradient of the function in a given dimension by sampling either side of the peak, which might output similar values. With the DGSM sample, this is much less likely to happen because the steps are very small, so the measure is better able to estimate the gradient of the function at a given point. A wider conclusion that can be drawn here then is that DGSM measures should be much more efficient when screening non-monotonic functions.

A related point here is that in the (piecewise) linear case, when $\alpha = 1$, the DGSM measures can perfectly capture the sensitivity, giving error values of $Z = 0$ for all values of N. This is because first, when a function is linear, the gradient at any point can be used to measure its global sensitivity, since the gradient does not change over the input space. Second, although the μ^* measure is also related to the gradient, because it measures across large steps it suffers from the problems related to non-monotonicity, as mentioned previously.

3.3.2 Polynomial additive function

The second function used to compare the three measures was a simple polynomial additive function, of the form,

$$h(\boldsymbol{x}) = \sum_{i=1}^{k} a_i x_i^p, \tag{3.8}$$

where p is the order of the polynomial, and the a_i are weighting coefficients. In this function there are no interactions between variables, so $\sum S_i = 1$. A plot of this function with $k = 2$ is found in Figure 3.6.

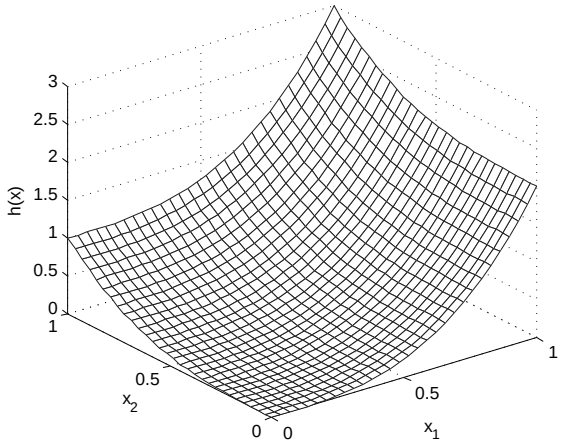

Figure 3.6: Plot of polynomial function for $k = 2$, $a_{\text{high}} = 2$, $a_{\text{low}} = 1$, $p = 3$, $\gamma = 0.5$.

Table 3.2 shows the results of four configurations of the polynomial function, at different dimensionalities. The coefficients are set at $a_{\text{high}} = 2$ and $a_{\text{low}} = 1$ in both cases, but the order of the polynomial is increased from 2 to 3, and the fraction of significant variables from 0.2 to 0.5. In these experiments, the results are quite different from the G^* function – the best measure is now unequivocally μ^*, with ν second best, followed by ξ in the case where $p = 2$, or S^{tot} when $p = 3$.

To see in a little more detail, Figure 3.7 shows two selected plots, the first showing the results of the quadratic function, and the second of the cubic function, with $\gamma = 0.2$ in both cases. These are representative of the relative performance of the other cases in Table 3.2. It is evident first of all that there is not much difference between any of the measures, but the μ^* measure is best by a small margin. In the quadratic case the performance is fairly clearly separated between the four measures, but in the cubic case the performance is extremely similar, with the exception of ξ, which is slightly worse.

Table 3.2: Configuration and performance rankings of experiments with polynomial additive function.

k	a_{high}	a_{low}	p	γ	S^{tot}	μ^*	ν	ξ
30	2	1	2	0.2	4	1	2	3
50	2	1	2	0.2	4	1	2	3
75	2	1	2	0.2	4	1	2	3
100	2	1	2	0.2	4	1	2	3
30	2	1	2	0.5	4	1	2	3
50	2	1	2	0.5	4	1	2	3
75	2	1	2	0.5	4	1	2	3
100	2	1	2	0.5	4	1	2	3
30	2	1	3	0.2	3	1	2	4
50	2	1	3	0.2	3	1	2	4
75	2	1	3	0.2	3	1	2	4
100	2	1	3	0.2	3	1	2	4
30	2	1	3	0.5	3	1	2	4
50	2	1	3	0.5	3	1	2	4
75	2	1	3	0.5	3	1	2	4
100	2	1	3	0.5	3	1	2	4

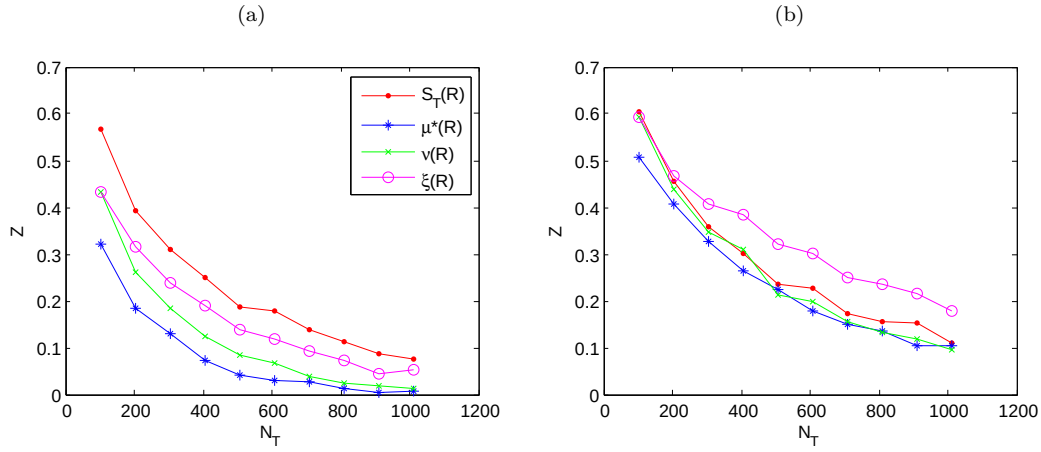

Figure 3.7: Convergence plots for polynomial function: (a) $p = 2$; (b)$p = 3$; In all cases $k = 100$, $a_{\text{high}} = 2$, $a_{\text{low}} = 1$ and $\gamma = 0.2$.

3.3.3 Step function

The final test function is a simple function with a near-discontinuity, of the form,

$$s(\boldsymbol{x}) = \sum_{i=1}^{k} a_i \text{erf}(15(x_i - 0.5)) \tag{3.9}$$

where erf is the error function. This function has a gradient of zero in most places, except around x_i=0.5, at which point the gradient is very steep. This behaviour can be seen in Figure 3.8, where the function is plotted with $k = 2$ for illustration. For the numerical experiments, $a_{\text{high}} = 3$ and $a_{\text{low}} = 1$, with a fraction γ from 0.2 to 0.5 as shown in Table 3.3.

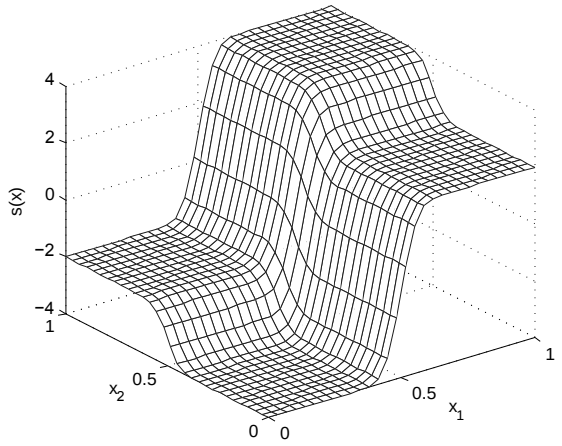

Figure 3.8: Plot of step function for $k = 2$, $a_{\text{high}} = 3$, $a_{\text{low}} = 1$, $\gamma = 0.5$.

The step function was in fact chosen as a counter-example to show the limitations of the DGSM measures. Looking at Table 3.3, the results clearly reflect this. Contrary to the previous two functions, S^{tot} performs the best at all the configurations tested, with the μ^* measure performing second-best, followed by ν and ξ.

More detail can be seen in Figure 3.9 – S^{tot} performs better by quite a large margin. The DGSM measures have a similarly poor performance, and the μ^* measure comes somewhere in the middle. The reason for this ranking is the same as why the ranking is the opposite for the G^* function – the DGSM measures use small steps in each x_i directions, whereas the other two measures use large steps. While

the small steps are an advantage when for identifying a sharp peak in a segment of an otherwise constant function, they are a disadvantage for a function such as the step function, because the sample points need to be very close to the "discontinuity" to see a non-zero gradient (see again Figure 3.8). Indeed, if there were a true discontinuity, the DGSM measures would return sensitivity measures of zero unless the $\boldsymbol{x}_j$ and $\boldsymbol{x}_j^{i''}$ happened to fall either side of the discontinuity. The measures S^{tot} and μ^*, on the other hand, are much more likely to see a change in the function output as a result of their larger steps.

Table 3.3: Configuration and performance rankings of experiments with step function.

k	a_{high}	a_{low}	γ	S^{tot}	μ^*	ν	ξ
30	3	1	0.2	1	2	3	4
50	3	1	0.2	1	2	3	4
75	3	1	0.2	1	2	3	4
100	3	1	0.2	1	2	3	4
30	3	1	0.5	1	2	3	4
50	3	1	0.5	1	2	3	4
75	3	1	0.5	1	2	3	4
100	3	1	0.5	1	2	3	4

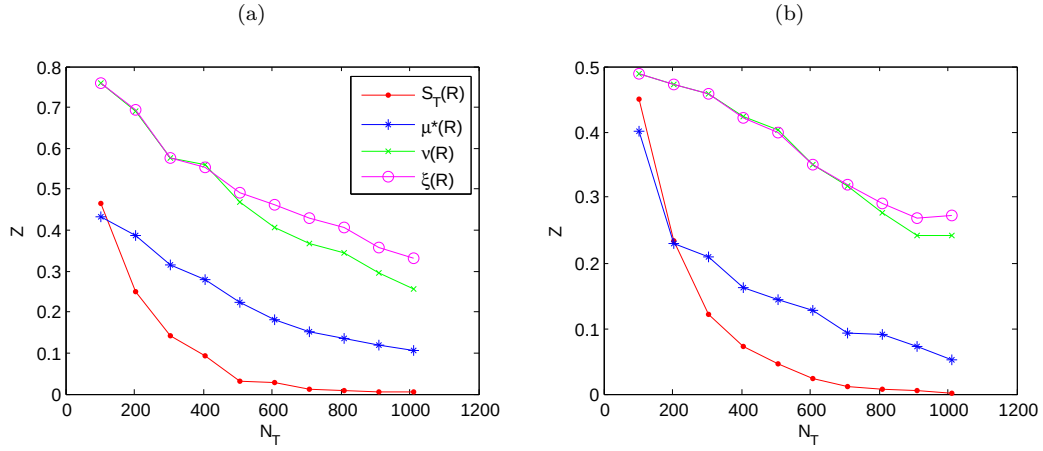

Figure 3.9: Convergence plots for step function: (a) $a_{\text{high}} = 3$, $a_{\text{low}} = 1$, $\gamma = 0.2$; (b) $a_{\text{high}} = 3$, $a_{\text{low}} = 1$, $\gamma = 0.5$; In all cases $k = 100$.

3.3.4 Results with Sobol' sequence

The previous results have only shown the performance of the sensitivity measures using random numbers, since the relative performance of each is nearly identical to that when using the Sobol' sequence. However it is worth briefly examining the differences between using random sampling and the Sobol' sequence. Figure 3.10 shows three selected plots. Clearly, in almost all cases, the use of the Sobol' sequence improves the performance of the sensitivity measures at a given sample size.

For the polynomial function, the improvement is quite consequential, with a practically error-free performance at sample sizes of around 800 upwards, for 100 variables. A lesser, but still significant gain is obtained with the G^* function, but only for the DGSM measures. Finally, the case of the step function is quite interesting. First, the rate of convergence is considerably improved for the DGSM measures, such that at higher sample sizes they actually perform the best. Strangely however, the use of the Sobol' sequence does not actually improve the performance of the S^{tot} measure: on the contrary, it actually makes it worse.

Still, the overriding conclusion is that the Sobol' sequence performs better in almost all cases, and can lead to significant computational savings.

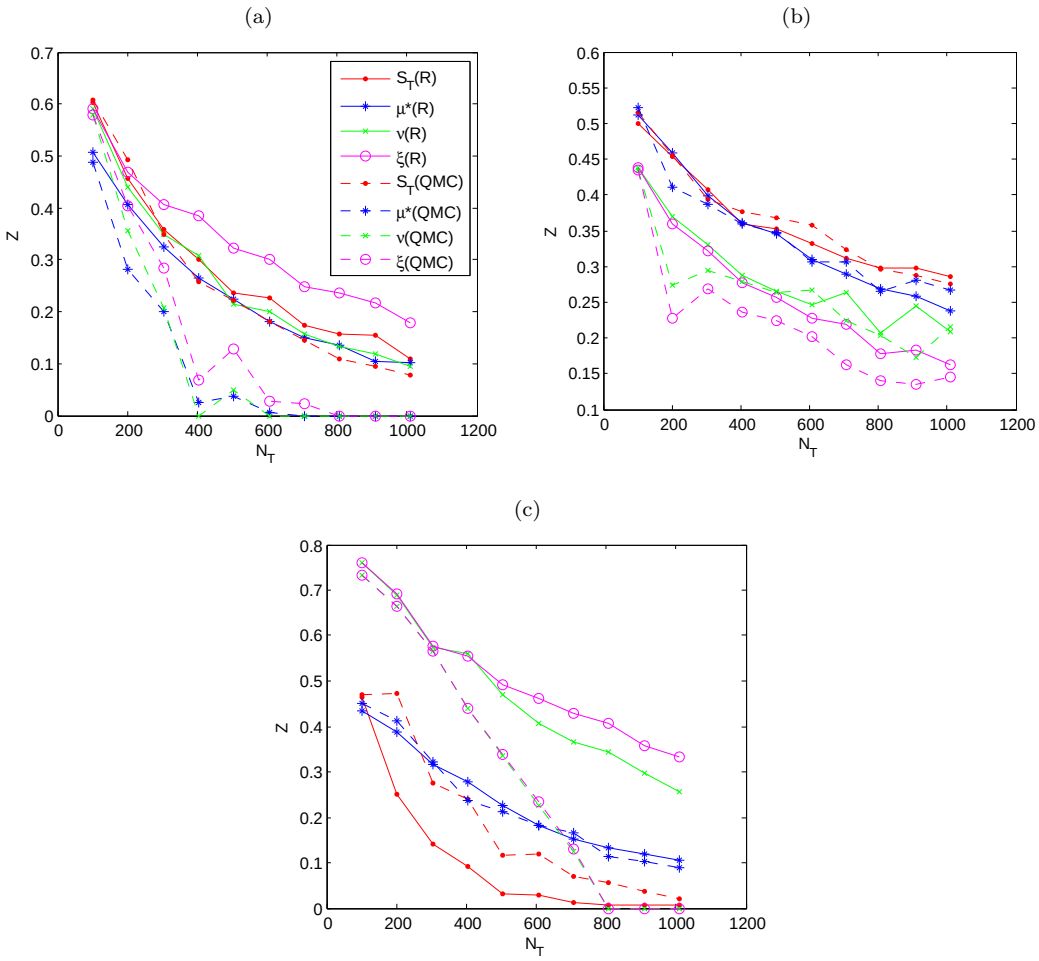

Figure 3.10: Convergence plots for three selected cases, all with $k = 100$ and $\gamma = 0.2$: (a) polynomial function at $a_{\text{high}} = 2$, $a_{\text{low}} = 1$ and $p = 3$; (b) G^* function at $a_{\text{high}} = 3$, $a_{\text{low}} = 10$ and $\alpha = 3$; (c) Step function at $a_{\text{high}} = 3$, $a_{\text{low}} = 1$.

3.4 Discussion and conclusions

By far the most evident conclusion of this work is that there is no "one size fits all" solution to sensitivity analysis, and that the best-performing sensitivity measure in the screening context is very dependent on the type of function or model that is being analysed. This should come as no surprise to those who have experience in sensitivity analysis, or indeed in data analysis as a wider discipline, yet some studies still draw conclusions on the results of a single test function. It is clear from this work that a range of test functions with differing linearity, monotonicity, continuity and interactions should be investigated. Of course, our tests could be extended yet further, but on the basis of this work some useful conclusions can be drawn.

The first thing to note is that DGSM measures performs surprisingly well at low sample sizes, a feature which we do not believe has been specifically investigated to date. On functions such as the G^* function, they actually have a clear advantage, whereas on smoother functions such as the polynomial function, they exhibit comparable performance with the more traditional elementary effects measure. When the function is linear, or piecewise linear, they also provide a much faster convergence than the other measures. Although the step function is a clear counter-example where DGSM measures fail, it is probably safe to say that this kind of response surface is not too common in physical models. However it is worth bearing in mind when analysing a model that has suspected bifurcating behaviour.

The total Sobol' index is not generally efficient at low sample size, and is outperformed by the DGSM measures and the elementary effects measure in most cases, with the exception of the step function. It is not therefore recommended to be used as a screening tool.

The modified DGSM measure proposed in this work had some reasonable success - giving at least comparable performance to the standard DGSM measure, and possibly surpassing it depending on the function. However the performance of the two was generally quite close, therefore it is not possible to say that one is necessarily better than the other without a considerable amount of further testing.

Overall, DGSM measures would seem to be a very useful tool in a screening analysis, as long as their caveats are kept in mind. A safe strategy would be to try to estimate both DGSM measures *and* S^{tot}, although this would require a larger sample which may be impractical.

A further general observation is that the rate of convergence for all the measures here is quite good – even with 100 variables, they can be mostly sorted into high and low influence groups with some few hundreds of runs. Additionally, the test functions here are designed to be taxing – in practice, many physical models do not exhibit strongly nonlinear behaviour. Substantial further computational savings can be obtained by using the Sobol' sequence in place of random numbers, and perhaps further by judicious grouped-screening strategies – see for example Morris (1991).

Chapter 4

Using sparse polynomial chaos expansions for the global sensitivity analysis of groundwater lifetime expectancy in a multi-layered hydrogeological model[1]

[1] This chapter is based on an article that has been submitted to the journal *Reliability Engineering & System Safety*.

4.1 Introduction

With the improvement of computing power, numerical modelling has become a popular tool for understanding and predicting various kinds of subsurface processes addressed in the fields of geology and hydrogeology. However, the incomplete/imprecise knowledge of the underground system frequently compels the modeller to make a number of approximations and assumptions with regard to the geometry of geological structures, the presence of discontinuities and/or the spatial distribution of hydro-dispersive parameters in their models (Renard, 2007). These uncertainties can possibly lead to large variabilities in the predictive modelling of subsurface processes and thus, it becomes of major importance to account for the aforementioned assumptions in the frame of uncertainty and sensitivity analyses. Uncertainty analysis (UA) aims at quantifying the variability of a given response of interest as a function of uncertain input factors, whereas sensitivity analysis (SA) has the purpose to identify the input factors responsible for this variability. Hence, SA determines the key variables to be described in further detail in order to reduce the uncertainty on the predictions of a model.

Methods of SA are typically classified in two categories: local SA and global SA methods. The former investigate effects of variations of the input factors in the vicinity of nominal values, whereas the latter aim at quantifying the output uncertainty due to variations in the input factors in their entire domain. Among several global SA methods proposed in the literature, of interest herein is SA with *Sobol' sensitivity indices*, which belongs to the broader class of variance-based methods (Saltelli et al., 2008). These methods rely upon the decomposition of the response variance as a sum of contributions of each input factor or combinations thereof; unlike regression-based methods, they do not assume any kind of linearity or monotonicity of the model.

Various methods have been investigated for computing the Sobol' indices that were first defined in the article from Sobol' (1993). The reader is also referred to the articles from Archer et al. (1997); Sobol' (2001); Saltelli (2002); Sobol' and Kucherenko (2005); Saltelli et al. (2010) where Monte Carlo simulation is used as a tool to estimate these sensitivity indices. This has revealed extremely costly, although more efficient estimators have been recently proposed (Sobol' et al., 2007; Janon et al., 2013). In the last few years, new approaches using *surrogate models*, also known as *meta-models*, have been introduced in the field of global sensitivity analysis (Storlie et al., 2009; Zuniga et al., 2013). A popular method to compute the Sobol' indices, originally introduced by (Sudret, 2008), is by post-processing the coefficients of the Polynomial Chaos Expansion (PCE) of the response quantity of interest. PCE constitute an efficient UA method in which the key concept is to expand the model response onto a basis made of orthogonal polynomials in the input variables. Once a PCE representation is available, the Sobol' indices can be calculated analytically with elementary operations at almost no additional computational cost. Sparse PCE make the approach even more efficient, as shown in (Blatman and Sudret, 2010b).

In the frame of the stochastic modelling of subsurface flow and mass transport, PCE meta-models have proven to be robust and comprehensive tools in performing SA at low computational cost. As an example, applying a PCE-based global SA upon a fine-grid numerical model of flow and mass transport in a heterogeneous porous medium, Fajraoui et al. (2011) and Younes et al. (2013) established the transient effect of uncertain flow boundary conditions, hydraulic conductivities and dispersivities on solute concentrations at given observation points. Sochala and Le Maître (2013) propagated uncertain soil parameters upon three different physical models of subsurface unsaturated flow. Their study proved the higher efficiency of PCE meta-models, in comparison to a classical Monte-Carlo method, for representing the variability of the output quantity at low computational cost. In the frame of radionuclide transport simulation in aquifers, Ciriello et al. (2013) analysed the statistical moments of the peak solute concentration measured at a specific location as a function of the conductivity field, the dispersivity coefficients and the partition coefficients associated to the heterogeneous media. The comparison of the Sobol' indices obtained for various degree of PCE meta-models showed that low-degree PCE models can yield reliable indices while considerably reducing the computational burden. Formaggia et al. (2013) used PCE-based sensitivity indices to investigate effects of uncertainty in hydrogeological variables on the evolution of a basin-scale sedimentation process. However, the various aforementioned contributions consider simplified models for the description of subsurface flow and mass transport. A more realistic representation of these processes is employed in the present study by using a large-scale simulator.

In the scope of the deep geological storage of radioactive wastes, Andra (French National Radioactive Waste Management Agency) has conducted many studies to assess the potentiality of a clay-rich layer for establishing a mid to long-lived radioactive waste disposal in the subsurface of the Paris Basin. The thick impermeable layer from Callovo-Oxfordian (COX) age has been extensively studied (Delay et al., 2006;

Distinguin and Lavanchy, 2007; Enssle et al., 2011) together with the two major limestone aquifers, in place of the Dogger and the Oxfordian sequences (Brigaud et al., 2010; Linard et al., 2011; Landrein et al., 2013), encompassing the claystone formation. A recent study (Deman et al., 2015) used a high-resolution integrated Meuse/Haute-Marne hydrogeological model (ANDRA, 2012a) to compute the average time for water molecules departing from a given area in the COX to reach the limits of the numerical model. SA over hydro-dispersive parameters in 14 hydrogeological layers proved that the Dogger and Oxfordian limestone sequences have a large influence on the residence time of groundwater. Indeed, advection processes occurring in permeable layers strongly influence the water transit in the subsurface of the Paris Basin, in contrast to the slow-motion diffusive processes taking place in impermeable rocks.

However, the analysis of the effect of uncertainties related to other advective-dispersive parameters, such as boundary conditions, orientations and anisotropies of hydraulic conductivity tensors or magnitudes of dispersion parameters, represents a great effort that cannot be carried out with the integrated model at reasonable computational costs. Addressing the issue of performing UA with the use of high-resolution numerical models of geological reservoirs, Castellini and co-workers (Castellini et al., 2003) established that numerical models built at the coarse scale, but covering a reasonable number of geological and geostatistical features, can be particularly informative in capturing the main subsurface processes at low computational costs.

The present study introduces a vertical two-dimensional multi-layered hydrogeological model representing a simplification of the underground media of the Paris Basin in the vicinity of the site of Bure and does not integrate the complex geometry of the layers, neither does it include the numerous discontinuities or heterogeneities observed in the field. It must be emphasized that the use of this model is focused on numerical issues, sensitivity analysis and calibration purposes and the results cannot be considered with respect to the real situation.

The main objective of the present work is to assess the effect of multiple advective-dispersive parameter on the mean lifetime expectancy (MLE) of water molecules departing from a target zone in the central layer. The MLE corresponds to the average time required for a given solute, taken at a specific location, to reach any outlet of the model. Conservative uncertainty ranges are defined for the input factors analysed in the frame of a SA relying on the estimation of PCE-based Sobol' indices. This study provides a preliminary assessment on the relative effect of factors governing the MLE in the subsurface of the Paris Basin and recommendations are made for the application on the high-resolution integrated Meuse/Haute-Marne hydrogeological numerical model of the Paris Basin.

4.2 The numerical model

4.2.1 Geometry and F.E. mesh

Originally inspired by the COUPLEX numerical model from Bourgeat et al. (2004), the present model stands as a vertical two-dimensional (x-z) cross-section of 25'000 $\times$ 1'040 meters representing a segment of the Paris Basin subsurface. The mesh is discretized into 5 $\times$ 5 meters square elements for a total of 1'040'000 elements. In order to subdivide the domain into entities related to geological formations, the main features of the subsurface were extracted from the lithostratigraphic log of the deep EST433 borehole (Landrein et al., 2013) in the vicinity of the experimental site of Bure (Haute-Marne, France). Therefore, the model consists of 15 hydrogeological layers characterized by tabular geometries, uniform thicknesses and homogeneous parameters. Figure 4.1 summarizes the geometry of the model and gives an overview on the succession and thicknesses of layers.

The bottom layer stands as a 110 m thick low-permeability layer attributed to the Toarcian marl formation (T). Overlying the latter, the succession of carbonate formations from the Dogger sequence is subdivided into 5 layers of which the total thickness attains 250 m in the numerical model. The sequence encompasses the Bajocian (D1) and Bathonian limestones (D3 and D4) representing the main aquifer formations of the Dogger, a clastic dominated interval (*"Marnes de Longwy"*, D2) separating the two. The Dogger sequence is topped with a thin oolithic limestone from Lower Callovian (*"Dalle Nacrée"*, C1), implemented as a 15 m thick layer in the model. The latter marks the transition with the thick, highly impermeable, claystone formation of Callovo-Oxfordian age (C2) of which the thickness reaches

150 m in the model. In the numerical simulations, a target zone (TZ) located in the middle of layer C2 (Figure 4.1) represents the location for the computation of the output quantity of interest.

The low-permeability COX layer is overlaid by a limestone sequence of the Oxfordian age. The latter is incorporated as a 260 m thick formation subdivided into 6 hydrogeological entities. A relatively confining layer from the Upper Argovian (C3ab) rests directly on the COX and is followed by permeable formations of the Rauracian-Sequanian sequence (L1a to L2c). A thick interval of marls and argillaceous limestones from Kimmeridgian age (K1-K2) covers the whole and is implemented as a 160 m thick low-permeability layer. The top layer is a 120 m thick confining formation attributed to the Tithonian (K3). The latter outcrops in the vicinity of Bure.

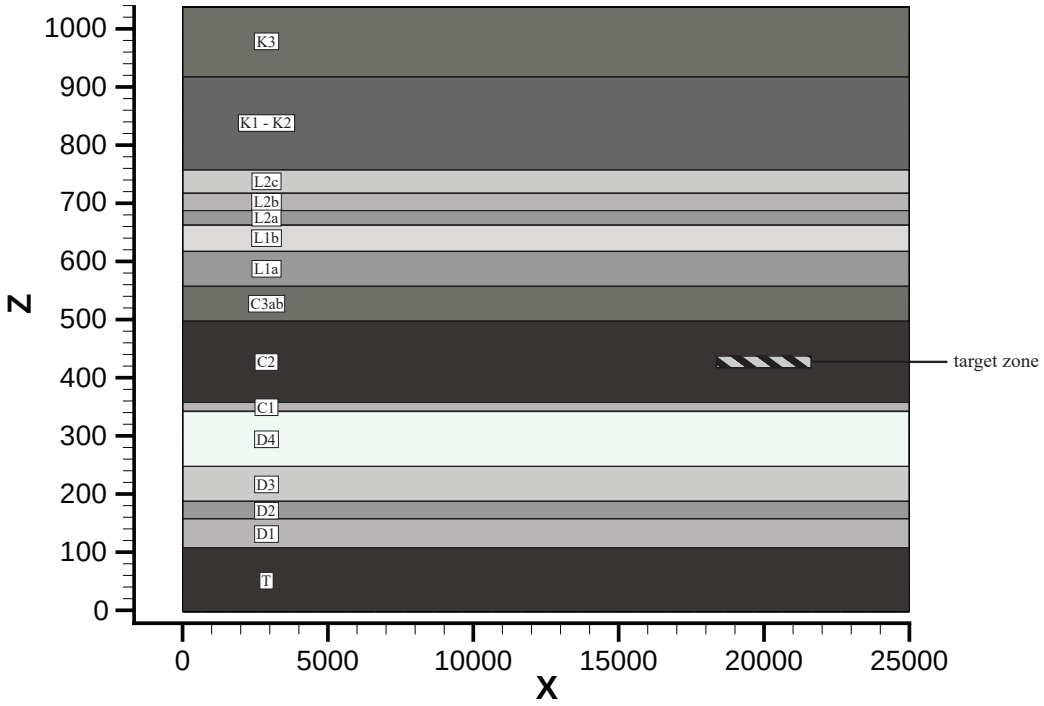

Figure 4.1: Geometry and geological layers with the localization of the target zone (vertical exaggeration: 20).

4.2.2 Governing equations and model outputs

In the numerical simulations the flow is governed by the steady-state equation

$$\nabla \cdot \mathbf{q} = 0, \tag{4.1}$$

where $\mathbf{q} = -\mathbf{K}\ \nabla H$, is the Darcian flux vector [L T^{-1}], $\mathbf{K}$ is the tensor of hydraulic conductivity [L T^{-1}] and H is the hydraulic head [L]. The anisotropy A_K in the components of the tensor of hydraulic conductivity is defined as the ratio between the hydraulic conductivities in the two principal directions: $A_K = K_z/K_x$.

Here, it is assumed that $\mathbf{K}$ has orthotropic properties. Considering a hydraulic conductivity tensor $\mathbf{K}_p$ of which the components are mapped into the Cartesian system and given along their principal direction, X_p, the tensor $\mathbf{K}$ in the global Cartesian space is retrieved by means of the rotation matrix $\mathbf{R}$ with the expression

$$\mathbf{K} = \mathbf{R}^T\ \mathbf{K}_p\ \mathbf{R}. \tag{4.2}$$

For the two-dimensional problem considered, the rotation matrix $\mathbf{R}$ is defined in terms of the Euler angle θ (in degree) as

$$\mathbf{R} = \begin{pmatrix} \cos\theta & \sin\theta \\ -\sin\theta & \cos\theta \end{pmatrix}. \tag{4.3}$$

In the present study, steady-state flow simulations are carried out together with the computation of the lifetime expectancy probability density function (PDF) at any point x in the domain. Under stationary conditions (i.e. steady-state flow), the lifetime expectancy PDF addresses the probability distribution of the time required for a solute, taken at any position x, to leave the domain. In its formulation, the lifetime expectancy PDF assimilates the forward advective-diffusive transport equation (ADE) to the Fokker-Planck (forward Kolmogorov) equation measuring the random motion of solute particles (Uffink, 1989). For more details on the computation of the lifetime expectancy PDF the reader is referred to Cornaton and Perrochet (2006a,b) and Kazemi et al. (2006).

Based on the ADE, the lifetime expectancy PDF is computed using the backward transport equation requiring reversed flow directions ($\mathbf{q} := \text{-}\mathbf{q}$) as well as adjusted downstream boundary conditions. The lifetime expectancy PDF $g_E(x,t)$ at any point x in the domain is then governed by

$$\phi \frac{\partial g_E}{\partial t} = \nabla \cdot (\mathbf{q}\, g_E + \mathbf{D}\, \nabla g_E), \tag{4.4}$$

where ϕ is the effective porosity [-] and where $\mathbf{D}$ is the dispersion tensor

$$\phi \mathbf{D} = (\alpha_L - \alpha_T) \frac{\mathbf{q} \otimes \mathbf{q}}{||\mathbf{q}||} \; + \; \alpha_T \, ||\mathbf{q}|| \, \mathbf{I} \; + \; \phi \, D_m \, \mathbf{I}, \tag{4.5}$$

where $\mathbf{I}$ is the identity matrix, D_m is the coefficient of molecular diffusion [$\mathrm{L}^2\ \mathrm{T}^{-1}$], α_L and α_T are the longitudinal and transverse components of the macro-dispersion tensor [L] respectively. In the present study, the anisotropy in the macro-dispersion tensor is determined with the coefficient: $A_\alpha = \alpha_T / \alpha_L$.

The straightforward computation of the first moment of the lifetime expectancy PDF is the so-called *mean lifetime expectancy* (MLE) $E(x)$ [T] at any position x, governed by

$$-\nabla \cdot (\mathbf{q}\, E + \mathbf{D}\, \nabla E) = \phi, \tag{4.6}$$

where it can be seen that the porosity ϕ [-] acts as the sink term in the aging process.

The target zone (TZ) comprises a set of 1,947 nodes in layer C2, covered by a rectangle which lateral and vertical extensions are x = [18440 ; 21680], z = [425 ; 435] (Figure 4.1). In the present study, the arithmetic mean of $E(x)$ calculated at each of these 1,947 nodes stands for the output response of interest and is used in the subsequent analysis. It can be seen as the average time for a solute originating from the TZ to reach any outlet of the model.

The finite element simulator *GroundWater* (Cornaton, 2007) was employed to solve Eq. 4.1- 4.6 using the Finite Element techniques. A single run of steady-state flow and MLE computation takes about 120 seconds using a parallel solver with 6 CPU.

The reader should note that the use of a 2D vertical model to solve for the hydro-dispersive processes cannot capture correctly the real behaviour of the Paris Basin subsurface because, apart from being a simplified model, it omits the lateral flow and dispersion along the third dimension. This has the effect to underestimate the magnitude of the modelled processes (Kerrou and Renard, 2010). It is however recognized that this bias is equivalent for all the layers considered, thus the interpretation of the SA results obtained with the 2D cross-section may be generalized to a synthetic 3D case employing the same settings.

4.2.3 Flow boundary conditions

The fully saturated model considers stationary flow conditions in a confined aquifer which are implemented as Dirichlet type flow boundary conditions. These flow BCs are imposed on nodes located on top of the numerical model as well as on both lateral limits of the two limestone sequences (Figure 4.2).

Regional piezometric maps based on field measures (Linard et al., 2011, Figures 16 and 17) were used to constrain the hydraulic gradients in both carbonate sequences. The flow BCs imposed on the lateral boundaries of the two limestone sequences derive from a 25km transect starting from the Gondrecourt trough and extending in a North-West direction, the main regional flow direction. The hydraulic gradient

set on top of the model corresponds to the average topographic gradient of the region covered by the transect.

Under these conditions, the general groundwater flow direction is oriented from right to left. The proportions of the total outflowing rates are approximately 2%, 60% and 38% for the top of the model, the Oxfordian and the Dogger discharge boundaries, respectively. In layer C2, the groundwater flows downward in the very right part of the model and then upward in the remainder; with a hydraulic gradient inversion in the vicinity of the TZ (see Figure 4.2). As a summary, the flow BCs are gathered in Table 4.1.

Table 4.1: Flow boundary conditions.

Boundary	Position	Hydraulic head
right Oxfordian	$x = 25000$, $z = [500, 760]$	$H = 305$ m
left Oxfordian	$x = 0$, $z = [500, 760]$	$H = 230$ m
right Dogger	$x = 25000$, $z = [110, 360]$	$H = 295$ m
left Dogger	$x = 0$, $z = [110, 360]$	$H = 275$ m
top of the model	$x = [0, 25000]$, $z = 1040$	$H = 225 + 85x/25000$
elsewhere		*no flow*

To account for uncertainties on the flow BCs, the hydraulic gradients in the two limestone sequence and on the top of the model are considered as uncertain input factors included in the following SA (Section 4.4). A change in the hydraulic gradients may shift the position of the vertical groundwater flux inversion in layer C2, and thus the MLE calculated at the TZ. This feature is explored in Appendix C.

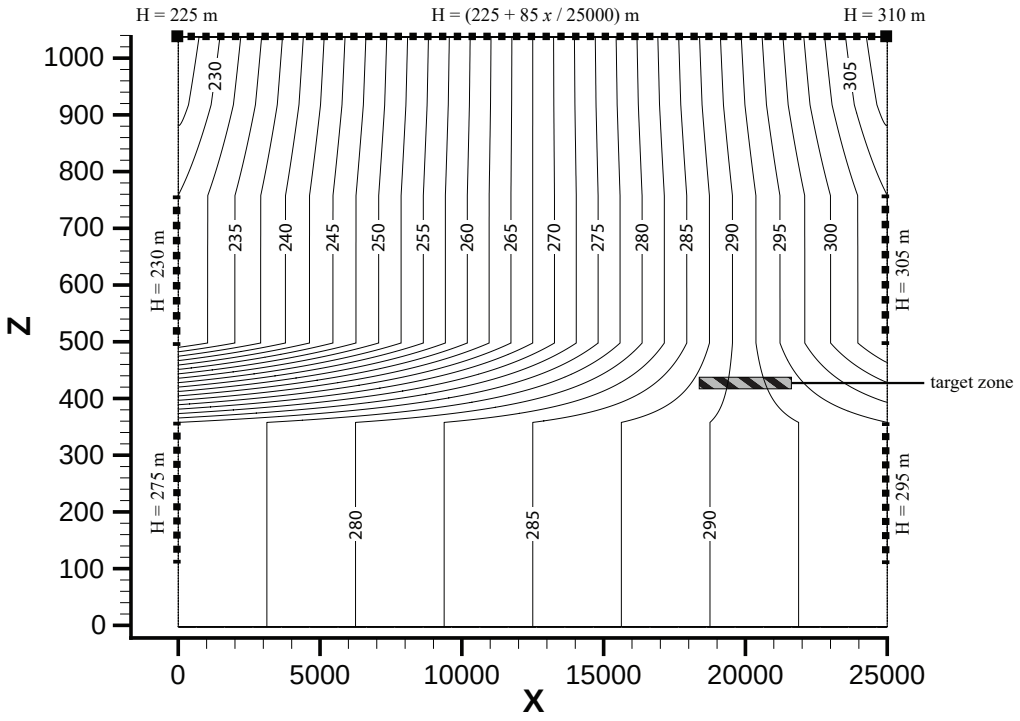

Figure 4.2: Flow boundary conditions and head contours (vertical exaggeration: 20).

4.2.4 Hydraulic conductivity and porosity values

Many studies have undertaken the inventory of hydraulic conductivity (K) and porosity (ϕ) values in the various geological formations of the Paris Basin. For a large number of wells and boreholes within a wide area around the experimental site of Bure, laboratory and field measurements were conducted to provide $\{K, \phi\}$ datasets for the two limestone sequences (Brigaud et al., 2010; Linard et al., 2011; Fourre et al., 2011; Delay and Distinguin, 2004; Delay et al., 2007).

However, very few $\{K, \phi\}$ datasets are available for the four low-permeability formations implemented in the present model (*i.e.* K3, K1-K2, C2 and T). Hence, data extracted from the literature (Cosenza et al., 2002; Delay et al., 2007, 2006; Enssle et al., 2011; Mazurek et al., 2011; Vinsot et al., 2011), and employed in previous modelling efforts (Contoux et al., 2013; de Hoyos et al., 2012; Goncalves et al., 2004), were used to define the uncertainty ranges for the $\{K, \phi\}$ sets in these layers.

In the geological formations of the Oxfordian and Dogger sequences, large variabilities of the $\{K, \phi\}$ couples are noticed with the presence of dependencies (*e.g.* low K and low ϕ values are correlated). However, to simplify the conceptual approach in a first stage, a perfect dependence between $\log_{10}(K)$ and ϕ is defined in each layer by making use of mathematical functions approximating the relationship between these two. Both parameters are referred to as a whole under the name *petrofacies* in the sequel. This approach reduces the computational burden of the subsequent SA by preventing the use of correlation functions between the two uncertain factors. For each layer, the estimated value of hydraulic conductivity $\widehat{K}$ is retrieved through a relationship: $\log_{10}(\widehat{K}) = f(\phi)$. Figures showing the approximation functions fitted on the $\{K, \phi\}$ datasets for each of the 15 layers considered in the synthetic model are provided in Appendix B.

Table 4.2: Nominal values for the porosity (ϕ) and the estimated longitudinal hydraulic conductivity ($\widehat{K}_x$) in the 15 hydrogeological layers.

Layer	$\widehat{K}_x$ [m/s]	ϕ [-]
K3	9.01E−09	0.0100
K1-K2	4.53E−09	0.1150
L2c	1.10E−06	0.1389
L2b	3.46E−07	0.1110
L2a	1.62E−07	0.1139
L1b	1.49E−05	0.1604
L1a	1.17E−06	0.1549
C3ab	4.59E−08	0.0984
C2	1.99E−13	0.1580
C1	1.89E−06	0.0470
D4	1.65E−05	0.0905
D3	1.76E−06	0.1016
D2	2.62E−07	0.0623
D1	3.23E−06	0.0688
T	1.95E−12	0.0810

Although no explicit information is available on the following, the geological formations are believed to feature anisotropic hydraulic conductivity tensors $\mathbf{K}$, *i.e.* anisotropy in the two principal components of the tensor (K_x and K_z) defined as the ratio $A_K = K_z/K_x$. The hydraulic conductivity values deriving from the $\{K, \phi\}$ distributions in each layer are attributed to the longitudinal component of the hydraulic conductivity tensor, K_x. In the nominal case, $A_K = 0.1$ is assumed for every layer of the model.

Preferential flow directions are supposedly taking place within each individual layer. For each, the Euler angle θ defines the orientation of the hydraulic conductivity tensor $\mathbf{K}_p$ in the Cartesian space (see Eq. 4.2-4.3). In the nominal case, $\theta = 0$ degree is assumed in every layer, which corresponds to the two principal components of the hydraulic conductivity tensors $\mathbf{K}_p$ being oriented along the x and z axes. The orientation of the groundwater flux $\mathbf{q}$ in the model is principally due to the static hydraulic gradients ∇H resulting from flow BCs implemented on the edges of the model. Note however that the Euler angle θ may locally change the orientation of $\mathbf{q}$ in a given layer and thus drive the groundwater into adjacent

layers where magnitudes might be different. This phenomenon may have a significant effect on the MLE calculated from the target zone, which is explored in Section 4.4. Illustrations of the univariate effect of this factor on the hydraulic head and MLE distributions throughout the model are provided in Appendix C.

Table 4.2 summarizes the nominal values for ϕ and the corresponding $\widehat{K}_x$ in each of the 15 hydrogeological layers comprised in the model. The values for ϕ correspond to the mean value (or P50 value of the CDF) of the distribution in each layer whereas the values for $\widehat{K}_x$ derive from approximation functions. As a reminder, the present study assumes homogeneous parameters in every layer. Although this feature is unrealistic it is recalled that the purpose of this preliminary study is to bring insights on the global effect of equivalent advective-dispersive parameters in the mutli-layered hydrogeological model and to provide recommendations for a similar application on a high-resolution integrated hydrogeological model of the Paris Basin.

4.2.5 Dispersion parameters

The mean lifetime expectancy formulation (Eq. 4.6) is an advective-dispersive solute transport equation where the longitudinal and transverse components of the macro-dispersion tensor (α_L and α_T respectively) control the particles dispersion. These two uncertain factors depend particularly on the rock type, on the tortuosity of the porous media and also on the scale considered. Homogeneous values of α_L and α_T are set within each layer, with the values $\alpha_L = 15$ m and $A_\alpha = \alpha_T/\alpha_L = 0.1$ considered in the entire numerical model in the nominal case.

As mentioned previously, no decay or adsorption effects are accounted in the computation of the MLE. The coefficient of molecular diffusion is the theoretical self-diffusion coefficient for the water molecule, $D_m = 2.3\ 10^{-9}$ m^2/s.

4.3 Polynomial chaos expansions for sensitivity analysis

Let us denote by $\mathcal{M}$ the computational model describing the behaviour of the considered physical system. Let $\boldsymbol{x} = \{x_1, \ldots, x_k\}$ denote the k-dimensional random input vector with joint PDF $f_{\boldsymbol{x}}(\boldsymbol{x})$ and marginal PDFs $f_{x_i}(x_i)$, $i = 1, \ldots, k$. Due to the input uncertainties represented by $\boldsymbol{x}$, the quantity of interest becomes random. The computational model is thus considered as the map

$$\boldsymbol{x} \in \mathcal{H}^k \subset \mathbb{R}^k \longmapsto y = \mathcal{M}(\boldsymbol{x}) \in \mathbb{R}, \tag{4.7}$$

where $\mathcal{H}^k$ is the support of $\boldsymbol{x}$. In the description of the theoretical framework hereafter, we assume that the components of $\boldsymbol{x}$ are *independent*, which is the case for the model in the present study.

As explained in the Introduction, the aim of global sensitivity analysis is to identity random input variables and combinations thereof with significant contributions to the variability of y, as described by its variance. A concise description of the employed method of PCE-based Sobol' sensitivity indices is given in the following; for further details on the topic, the reader is referred to Sudret (2008) and Blatman and Sudret (2010b). The extension to the case of mutually dependent random variables is presented in Kucherenko et al. (2012); Li et al. (2010).

4.3.1 Sobol' indices

Assuming that the function $\mathcal{M}(\boldsymbol{x})$ is square-integrable with respect to the probability measure associated with $f_{\boldsymbol{x}}(\boldsymbol{x})$, the decomposition of $y = \mathcal{M}(\boldsymbol{x})$ in summands of increasing dimension is given by Sobol' (1993)

$$\mathcal{M}(\boldsymbol{x}) = \mathcal{M}_0 + \sum_{i=1}^{k} \mathcal{M}_i(x_i) + \sum_{1 \le i \le j \le k} \mathcal{M}_{ij}(x_i, x_j) + \ldots + \mathcal{M}_{12\ldots k}(\boldsymbol{x}) \tag{4.8}$$

or equivalently, by

$$\mathcal{M}(\boldsymbol{x}) = \mathcal{M}_0 + \sum_{\boldsymbol{u}\neq\emptyset} \mathcal{M}_{\boldsymbol{u}}(\boldsymbol{x}_{\boldsymbol{u}}), \tag{4.9}$$

where $\mathcal{M}_0$ is the mean value of y, $\boldsymbol{u} = \{i_1, \ldots, i_s\} \subset \{1, \ldots, k\}$ are index sets and $\boldsymbol{x}_{\boldsymbol{u}}$ denotes a subvector of $\boldsymbol{x}$ containing only those components of which the indices belong to $\boldsymbol{u}$. The number of summands in the above equations is $2^k - 1$.

The Sobol' decomposition is unique under the condition

$$\int_{\mathcal{H}^{x_i}} \mathcal{M}_{\boldsymbol{u}}(\boldsymbol{x}_{\boldsymbol{u}}) f_{x_i}(x_i) dx_i = 0, \quad \text{if } i \in \boldsymbol{u}, \tag{4.10}$$

where $\mathcal{H}^{x_i}$ and $f_{x_i}(x_i)$ respectively denote the support and marginal PDF of x_i. Eq. 4.10 leads to the orthogonality property

$$\mathbb{E}\left[\mathcal{M}_{\boldsymbol{u}}(\boldsymbol{x}_{\boldsymbol{u}})\mathcal{M}_{\boldsymbol{v}}(\boldsymbol{x}_{\boldsymbol{v}})\right] = 0, \quad \text{if } \boldsymbol{u} \neq \boldsymbol{v}. \tag{4.11}$$

The uniqueness and orthogonality properties allow decomposition of the variance V_y of y as

$$V_y = \mathbb{V}\left[\mathcal{M}(\boldsymbol{x})\right] = \sum_{\boldsymbol{u}\neq\emptyset} V_{\boldsymbol{u}}, \tag{4.12}$$

where $V_{\boldsymbol{u}}$ denotes the partial variance

$$V_{\boldsymbol{u}} = \mathbb{V}\left[\mathcal{M}_{\boldsymbol{u}}(\boldsymbol{x}_{\boldsymbol{u}})\right] = \mathbb{E}\left[\mathcal{M}^2_{\boldsymbol{u}}(\boldsymbol{x}_{\boldsymbol{u}})\right]. \tag{4.13}$$

The Sobol' index $S_{\boldsymbol{u}}$ is defined as

$$S_{\boldsymbol{u}} = V_{\boldsymbol{u}}/V_y, \tag{4.14}$$

and describes the amount of the total variance that is due to the uncertainties in the set of input parameters $\boldsymbol{x}_{\boldsymbol{u}}$. By definition, $\sum_{\boldsymbol{u}\neq\emptyset} S_{\boldsymbol{u}} = 1$. First-order indices, S_i, describe the influence of each parameter x_i considered separately, also called *main effect*. Second-order indices, S_{ij}, describe influences from pairs of parameters $\{x_i, x_j\}$. Higher-order indices describe the combined influence from larger sets of parameters.

The total sensitivity indices, S_i^{tot}, represent the *total effect* of an input parameter x_i, accounting for its main effect and all interactions with other parameters. They are derived from the sum of all partial sensitivity indices $S_{\boldsymbol{u}}$ that involve parameter x_i, *i.e.*

$$S_i^{tot} = \sum_{\mathcal{I}_i} V_{\boldsymbol{u}}/V_y, \quad \mathcal{I}_i = \{\boldsymbol{u} \supset i\}. \tag{4.15}$$

It follows that $S_i^{tot} = 1 - S_{\sim i}$, where $S_{\sim i}$ is the sum of all $S_{\boldsymbol{u}}$ with $\boldsymbol{u}$ not including i.

Evaluation of the Sobol' indices by Monte Carlo simulation is based on a recursive relationship which requires computing 2^k Monte Carlo integrals involving $\mathcal{M}(\boldsymbol{x})$. Clearly, this is not affordable when the computational model is a time-consuming algorithmic sequence. On the other hand, when PCE of the quantity of interest are available, Sobol' indices can be obtained analytically at almost no additional computational cost.

4.3.2 Polynomial chaos expansions

Computation of Polynomial Chaos Expansions

A PCE approximation of $y = \mathcal{M}(\boldsymbol{x})$ in Eq. 4.8 has the form (Xiu and Karniadakis, 2002)

$$\widehat{y} = \mathcal{M}^{PCE}(\boldsymbol{x}) = \sum_{\boldsymbol{\alpha}\in\mathcal{A}} a_{\boldsymbol{\alpha}} \Psi_{\boldsymbol{\alpha}}(\boldsymbol{x}), \tag{4.16}$$

where $\{\Psi_{\boldsymbol{\alpha}}, \boldsymbol{\alpha} \in \mathcal{A}\}$ is a set of multivariate polynomials that are orthonormal with respect to $f_{\boldsymbol{x}}(\boldsymbol{x})$, with multi-indices $\boldsymbol{\alpha} = (\alpha_1, \ldots, \alpha_k)$, and $a_{\boldsymbol{\alpha}}$ denotes the corresponding polynomial coefficients.

The multivariate polynomials that comprise the PCE basis are obtained by tensorization of appropriate univariate polynomials, *i.e.*

$$\Psi_{\boldsymbol{\alpha}}(\boldsymbol{x}) = \prod_{i=1}^{k} \psi_{\alpha_i}^{(i)}(x_i), \tag{4.17}$$

where $\psi_{\alpha_i}^{(i)}(x_i)$ is a polynomial of degree α_i in the i^{th} input variable belonging to a family of polynomials that are orthonormal with respect to $f_{x_i}(x_i)$. For standard distributions, the associated family of orthonormal polynomials is well-known (*e.g.* a uniform variable with support $[-1, 1]$ is associated with the family of Legendre polynomials), whereas a general case can be treated through an isoprobabilistic transform of $\boldsymbol{x}$ to a basic random vector. The set of multi-indices $\mathcal{A}$ in Eq. (4.16) is determined by an appropriate truncation scheme. In the present study, a hyperbolic truncation scheme is employed, which corresponds to selecting all multi-indices satisfying

$$\| \boldsymbol{\alpha} \|_q = \left(\sum_{i=1}^{k} \alpha_i^q \right)^{1/q} \leq p. \tag{4.18}$$

for appropriate $0 < q \leq 1$ and $p \in \mathbb{N}$ (Blatman and Sudret, 2010a).

Once the basis has been specified, the set of coefficients $\boldsymbol{a} = \{a_{\boldsymbol{\alpha}}, \boldsymbol{\alpha} \in \mathcal{A}\}$ may be computed by minimizing the mean-square error of the approximation over a set of realizations of the input vector, $\boldsymbol{X} = \{\boldsymbol{x}^{(1)}, \ldots, \boldsymbol{x}^{(N)}\}$, called *experimental design*. Efficient solution schemes are obtained by considering the regularized problem

$$\boldsymbol{a} = \underset{\boldsymbol{v} \in \mathbb{R}^{\mathrm{card}\,\mathcal{A}}}{\arg\min} \sum_{i=1}^{N} \left(\mathcal{M}(\boldsymbol{x}^{(i)}) - \sum_{\boldsymbol{\alpha} \in \mathcal{A}} v_{\boldsymbol{\alpha}} \Psi_{\boldsymbol{\alpha}}(\boldsymbol{x}^{(i)}) \right)^2 + C \|\boldsymbol{v}\|_1^2, \tag{4.19}$$

where $\|\boldsymbol{v}\|_1 = \sum_{j=1}^{\mathrm{card}(\mathcal{A})} |v_j|$ and C is a non-negative constant. A nice feature of the above regularized problem is that it provides a *sparse* meta-model by disregarding insignificant terms from the set of predictors. In the present application, we solve Eq. 4.19 using the *hybrid Least Angle Regression* (LAR) method as originally proposed in Blatman and Sudret (2011). Hybrid LAR employs the LAR algorithm (Efron et al., 2004) to select the best set of predictors and subsequently, estimates the coefficients with standard least-squares minimization.

Error estimates

A good measure of the accuracy of PCE is the mean-square error of the residual, $Err_G = \mathbb{E}\left[(y - \widehat{y})^2\right]$, called *generalization error*. In practice, this could be estimated by Monte Carlo simulation using a sufficiently large set of realizations of the input vector, $\boldsymbol{X}_{\mathrm{val}} = \{\boldsymbol{x}^{(1)}, \ldots, \boldsymbol{x}^{(N_{\mathrm{val}})}\}$, called *validation set*. The estimate of the generalization error is given by

$$\widehat{Err}_G = \frac{1}{N_{\mathrm{val}}} \sum_{i=1}^{N_{\mathrm{val}}} \left(\mathcal{M}(\boldsymbol{x}_i) - \sum_{\boldsymbol{\alpha} \in \mathcal{A}} a_{\boldsymbol{\alpha}} \Psi_{\boldsymbol{\alpha}}(\boldsymbol{x}_i) \right)^2. \tag{4.20}$$

The relative generalization error, $\widehat{Err}_G$, is estimated by normalizing $\widehat{Err}_G$ with the empirical variance of $\boldsymbol{y}_{\mathrm{val}} = \{\mathcal{M}(\boldsymbol{x}^{(1)}), \ldots, \mathcal{M}(\boldsymbol{x}^{(N_{\mathrm{val}})})\}$.

However, PCE are typically used as surrogate models in cases when evaluating a large number of model responses is not affordable. It is thus desirable to get an error estimate of Err_G using only the information obtained from the experimental design. One such error measure is the *Leave-One-Out* (LOO) *error* (Allen, 1971). The idea of the LOO cross-validation is to set apart one point of the experimental design, say $\boldsymbol{x}^{(i)}$, and use the remaining points to build the PCE, denoted $\mathcal{M}^{\mathrm{PCE}\setminus i}$. The LOO error is obtained after alternating over all points of the experimental design, *i.e.*

$$\widehat{Err}_{LOO} = \frac{1}{N} \sum_{i=1}^{N} (\mathcal{M}(\boldsymbol{x}^{(i)}) - \mathcal{M}^{\mathrm{PCE}\setminus i}(\boldsymbol{x}^{(i)}))^2. \tag{4.21}$$

Although the above definition outlines a computationally demanding procedure, algebraic manipulations allow evaluation of the LOO error from a *single* PCE based on the full experimental design. Let us denote by h_i the i^{th} diagonal term of matrix $\boldsymbol{\Psi}(\boldsymbol{\Psi}^{\mathrm{T}}\boldsymbol{\Psi})^{-1}\boldsymbol{\Psi}^{\mathrm{T}}$, where $\boldsymbol{\Psi} = \{\boldsymbol{\Psi}_{ij} = \Psi_j(\boldsymbol{x}^{(i)}),\ i = 1, \ldots, N;\ j = 1, \ldots, \mathrm{card}\mathcal{A}\}$. Then, the LOO error can be computed as

$$\widehat{Err}_{LOO} = \frac{1}{N}\sum_{i=1}^{N}\left(\frac{\mathcal{M}(\boldsymbol{x}^{(i)}) - \mathcal{M}^{\mathrm{PCE}}(\boldsymbol{x}^{(i)})}{1-h_i}\right). \tag{4.22}$$

The relative LOO error, $\widehat{err}_{LOO}$, is obtained by normalizing $\widehat{Err}_{LOO}$ with the empirical variance of $\boldsymbol{y} = \{\mathcal{M}(\boldsymbol{x}^{(i)}), \ldots, \mathcal{M}(\boldsymbol{x}^{(N)})\}$. Because this error estimate may be too optimistic, we subsequently employ a corrected estimate, given by Chapelle et al. (2002)

$$\widehat{err}^{*}_{LOO} = \widehat{err}_{LOO}\left(1 - \frac{\mathrm{card}\mathcal{A}}{N}\right)^{-1}\left(1 + \mathrm{tr}((\Psi^{\mathrm{T}}\Psi)^{-1})\right). \tag{4.23}$$

This corrected LOO error is a good compromise between fair error estimation and affordable computational cost.

4.3.3 Sobol' indices from polynomial chaos expansions

Let us consider the PCE $\widehat{y} = \mathcal{M}^{\mathrm{PCE}}(\boldsymbol{x})$ of the quantity of interest $y = \mathcal{M}(\boldsymbol{x})$. It is straightforward to obtain the Sobol' decomposition of $\widehat{y}$ in an analytical form by observing that the summands $\mathcal{M}^{\mathrm{PCE}}_{\boldsymbol{u}}(\boldsymbol{x}_{\boldsymbol{u}})$ in Eq. 4.9 can be written as

$$\mathcal{M}^{\mathrm{PCE}}_{\boldsymbol{u}}(\boldsymbol{x}_{\boldsymbol{u}}) = \sum_{\boldsymbol{\alpha}\in\mathcal{A}_{\boldsymbol{u}}} a_{\boldsymbol{\alpha}}\boldsymbol{\Psi}_{\boldsymbol{\alpha}}, \tag{4.24}$$

where $\mathcal{A}_{\boldsymbol{u}}$ denotes the set of multi-indices that depend *only on* $\boldsymbol{u}$, *i.e.*

$$\mathcal{A}_{\boldsymbol{u}} = \{\boldsymbol{\alpha}\in\mathcal{A} : \alpha_k \neq 0 \text{ if and only if } k\in\boldsymbol{u}\}; \tag{4.25}$$

clearly, $\cup\mathcal{A}_{\boldsymbol{u}} = \mathcal{A}$. Consequently, due to the orthogonality of the PCE basis, the estimated partial variance $\widehat{V}_{\boldsymbol{u}}$ reduces to

$$\widehat{V}_{\boldsymbol{u}} = \mathbb{V}\left[\mathcal{M}^{\mathrm{PCE}}_{\boldsymbol{u}}(\boldsymbol{x}_{\boldsymbol{u}})\right] = \sum_{\boldsymbol{\alpha}\in\mathcal{A}_{\boldsymbol{u}}} {a_{\boldsymbol{\alpha}}}^2, \tag{4.26}$$

whereas the estimated total variance reads

$$\widehat{V}_y = \mathbb{V}\left[\mathcal{M}^{\mathrm{PCE}}(\boldsymbol{x})\right] = \sum_{\boldsymbol{\alpha}\in\mathcal{A}} {a_{\boldsymbol{\alpha}}}^2. \tag{4.27}$$

Accordingly, the Sobol' indices of any order can be obtained by a mere combination of the squares of the PCE coefficients. For instance, the estimated first-order Sobol' indices are given by

$$\widehat{S}_i = \sum_{\boldsymbol{\alpha}\in\mathcal{A}_i} {a_{\boldsymbol{\alpha}}}^2/\widehat{V}_y, \qquad \mathcal{A}_i = \{\boldsymbol{\alpha}\in\mathcal{A} : \alpha_i > 0, \alpha_{i\neq j} = 0\}, \tag{4.28}$$

whereas the estimated total Sobol' indices are given by

$$\widehat{S}^{tot}_i = \sum_{\boldsymbol{\alpha}\in\mathcal{A}^{tot}_i} {a_{\boldsymbol{\alpha}}}^2/\widehat{V}_y, \qquad \mathcal{A}^{tot}_i = \{\boldsymbol{\alpha}\in\mathcal{A} : \alpha_i > 0\}. \tag{4.29}$$

It is evident that once a PCE representation of $y = \mathcal{M}(\boldsymbol{x})$ is available, the complete list of Sobol' indices can be obtained at a nearly costless post-processing of the PCE coefficients requiring only elementary mathematical operations.

4.4 Results and discussion

Figure 4.3 provides an overview of the distribution of the mean lifetime expectancy (MLE) throughout the entire model in the nominal case (see Section 4.2). In this case, the parameters are distributed homogeneously in each of the 15 layers; K_x and ϕ take on the values given in Table 4.2 for each layer, whereas for all layers the anisotropy ratio is $A_K = 0.1$, the Euler angle is $\theta = 0$ degree, the longitudinal component of the macro-dispersion tensor is $\alpha_L = 15$m and the anisotropy ratio is $A_\alpha = 0.1$. The hydraulic gradients follow the boundary conditions settings described in Section 4.2.3.

For the sake of illustrating the univariate influence of each group of uncertain parameters on the hydraulic head distribution and on the MLE throughout the entire numerical model, Appendix C presents and discusses the cases where each group of uncertain factors are set alternatively to their upper/lower uncertainty bounds while all other factors are kept to their nominal values.

Because of its highly confining properties, the middle layer (C2) presents values of MLE $>$ 40,000 years. On average, it takes approximately 75,000 years for a solute departing from the target zone (TZ) to reach any outlet of the model. Much lower MLE values are found in the two aquifer sequences, with the Oxfordian displaying slightly smaller values. The effect of conductive layers is clearly distinguishable as fringes of low MLE values stretch in layers D4, L1a and L1b in particular. As a result of the low permeability in the top two layers (K3 and K1-K2) and the bottom layer (T), water molecules can take more than a 100,000 years to flow through the model.

In the following, we compute the PCE-based Sobol' indices for the MLE at the TZ by implementing the theory presented in Section 4.3. We conduct the analysis in two stages: we begin with a simplified description of the input by accounting for the uncertainty in the petrofacies only (case 1); in the sequel, we consider a higher-dimensional random input encompassing the entirety of hydrodynamic and dispersion parameters described in Section 4.2 as well as the flow BC (case 2). In the following sections, the term "porosity", ϕ, is construed in the discussion of Sobol' indices. Since the values for the hydraulic conductivities are retrieved through approximation functions, the estimation of the sensitivity for the ϕ variables is implicitly associated to that of the $\widehat{K}_x$ variables in the respective layers. This is singularly important when interpreting the Sobol' indices for aquifer formations where the hydraulic conductivity governs the ageing process (see Section 4.4.3). Computations of the PCE and Sobol' indices are performed with the uncertainty quantification software UQLab (Marelli and Sudret, 2014).

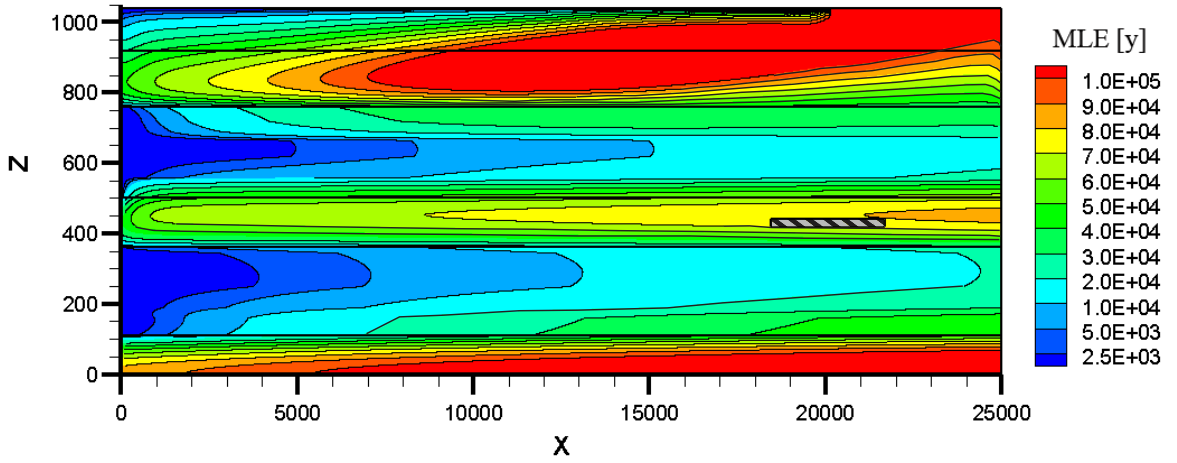

Figure 4.3: Spatial distribution of mean lifetime expectancy in the reference case (vertical exaggeration: 10).

4.4.1 Case 1: 15 input random variables

In the first case, the uncertain input comprises the petrofacies P in each of the 15 layers of the hydrogeological model. As stated before, a deterministic relationship $\log_{10}(\widehat{K}_x) = f(\phi)$ is assumed for each layer, *i.e.* the uncertainty regarding the petrofacies P of a layer is treated through the porosity ϕ, resulting in a

random input vector of dimension $k = 15$. The uncertain porosities are modeled as *independent* uniform random variables, each bounded by the values $\phi^{(min)}$ and $\phi^{(max)}$ listed in Table 4.3 together with the respective coefficients of variation (CoV) and shown graphically in Figure 4.4. Note that the bounds $\phi^{(min)}$ and $\phi^{(max)}$ represent the 1st and 9th deciles of the corresponding CDF derived from porosity values measured in each geological layer. This approach is justified by the presence of local extreme measures that cannot be representative for the whole layer. Bounds for the $\widehat{K}_x$ parameters are also provided in Table 4.3 consistently with the $\log_{10}(\widehat{K}_x) = f(\phi)$ approximation functions, and presented graphically in Figure 4.5.

Table 4.3: Ranges of porosity ϕ with the respective CoV and the estimated permability values $\widehat{K}$ in the 15 geological layers.

Layer	$\phi^{(min)}$ [-]	$\phi^{(max)}$ [-]	CoV	$\widehat{K}_x^{(min)}$ [m/s]	$\widehat{K}_x^{(max)}$ [m/s]
K3	0.0840	0.1160	0.0924	3.3734e-10	2.4078e-07
K1-K2	0.0870	0.1430	0.1406	9.8116e-11	2.0928e-07
L2c	0.1019	0.1759	0.1538	3.6186e-08	2.6212e-06
L2b	0.0645	0.1574	0.2417	8.7318e-10	6.3950e-06
L2a	0.0651	0.1627	0.2474	4.7005e-10	9.9336e-06
L1b	0.1375	0.1833	0.0824	3.4324e-09	2.8913e-04
L1a	0.0991	0.2107	0.2080	3.1165e-08	2.1523e-06
C3ab	0.0747	0.1221	0.1391	7.8488e-09	1.2945e-06
C2	0.1284	0.1876	0.1082	5.0349e-14	6.2570e-13
C1	0.0142	0.0799	0.4031	1.8184e-07	1.6195e-05
D4	0.0237	0.1573	0.4262	1.6408e-07	3.1521e-03
D3	0.0237	0.1795	0.4427	1.7470e-07	4.3539e-06
D2	0.0185	0.1061	0.4059	6.6071e-08	1.7049e-06
D1	0.0191	0.1186	0.4172	6.2552e-08	1.8425e-05
T	0.0696	0.0925	0.0816	1.2325e-13	8.1328e-12

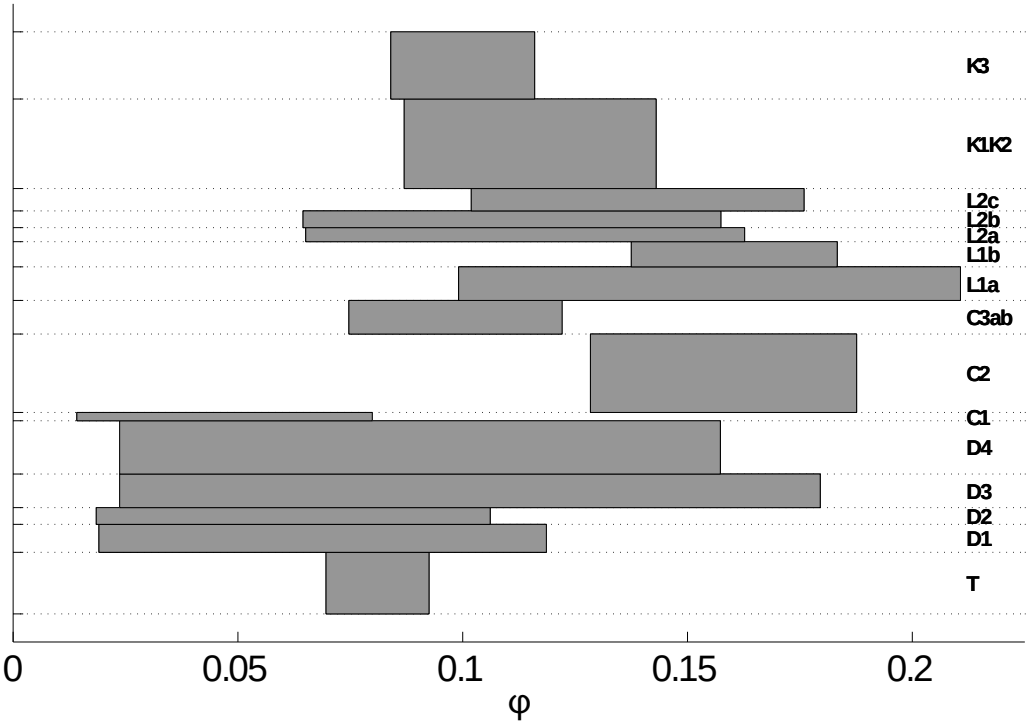

Figure 4.4: Porosity ranges along the model cross-section.

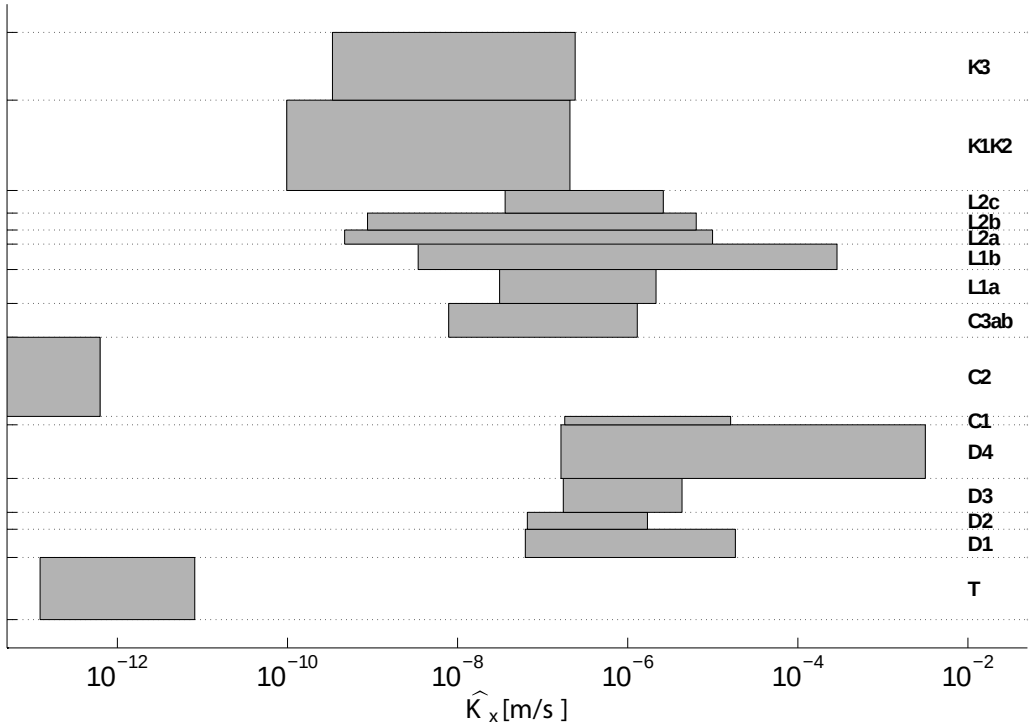

Figure 4.5: Hydraulic conductivity ranges along the model cross-section.

Polynomial Chaos Expansion

To build PCE of the MLE in terms of the 15 input random variables, we use an experimental design comprising $N = 1,000$ points drawn with Latin Hypercube Sampling (LHS) (McKay et al., 1979). LHS is a popular technique for obtaining random experimental designs ensuring uniformity of each sample on the margin input variables $\{x_i, \ldots, x_k\}$. A histogram of the model response at the considered LHS design is shown in Figure 4.6, indicating a positively skewed distribution with the mode situated at MLE $\approx$ 75,000 years.

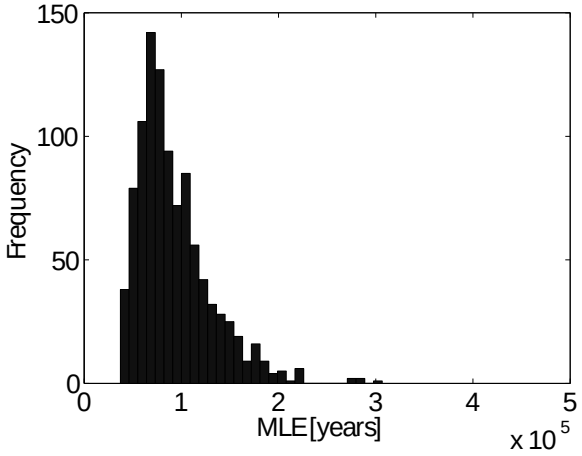

Figure 4.6: Histogram of mean lifetime expectancy values.

We develop two PCE meta-models, respectively denoted 1A and 1B, by applying the procedure in Section 4.3.2, first, on the original scale and then, on the logarithmic transform of the MLE. For both PCE, the candidate basis is determined using a hyperbolic truncation scheme (see Eq. 4.18) with $q = 0.5$. The maximum degree p is varied from 1 to 15 and the optimal sparse PCE is selected by means of the corrected relative LOO error (see Eq. 4.23), simply called LOO error and denoted err_{LOO} hereafter.

When the non-transformed response is considered, the optimal PCE 1A is obtained for $p = 10$ and the corresponding LOO error is $err_{LOO} = 0.0321$. The sparse meta-model includes 166 basis elements, whereas the total number of basis elements for $p = 10$ and $q = 0.5$ (resp. $q = 1$) is $1,656$ (resp. 3.2×10^6). When the logarithmic response is considered, the optimal PCE 1B is obtained for $p = 13$ and the corresponding LOO error is $err_{LOO} = 0.0120$. In this case, the sparse meta-model includes 245 basis elements, whereas the total number of basis elements for $p = 13$ and $q = 0.5$ (resp. $q = 1$) is $3,801$ (resp. 3.7×10^7). For both PCE, the sparse bases involve polynomials in all 15 input variables. The index of sparsity, defined as the number of basis elements in the sparse expansion divided by the size of a full basis ($q = 1$) with the same maximum degree, is $166/3.2 \times 10^6 \approx 5.2 \times 10^{-5}$ for case 1A and $245/3.7 \times 10^7 \approx 6.6 \times 10^{-6}$ for case 1B. These numbers indicate the interest in developing sparse PCE for such analyses.

The left graph of Figure 4.7 compares the values of PCE 1A, $\hat{y}$, with the respective values of the exact model, y, at the input samples of the experimental design; the right graph shows a similar comparison for the exponential transform of PCE 1B. Assessing the relative accuracy of the two meta-models, first, we note that 1B yields a smaller LOO error; furthermore, it results in a smaller dispersion of $\hat{y} - y$ around zero and a better approximation of the exact response at the upper tail of its distribution. However, we should bear in mind that in the subsequent SA, the Sobol' indices obtained from the coefficients of PCE 1B represent contributions to the variance of the *logarithmic* MLE.

Sobol' indices

Figures 4.8 and 4.9 show bar-plots of the first-order and total Sobol' indices of the porosities at the 15 layers using PCE 1A and 1B, respectively. To identify unimportant effects, the threshold of 0.01 is marked with a horizontal dashed line.

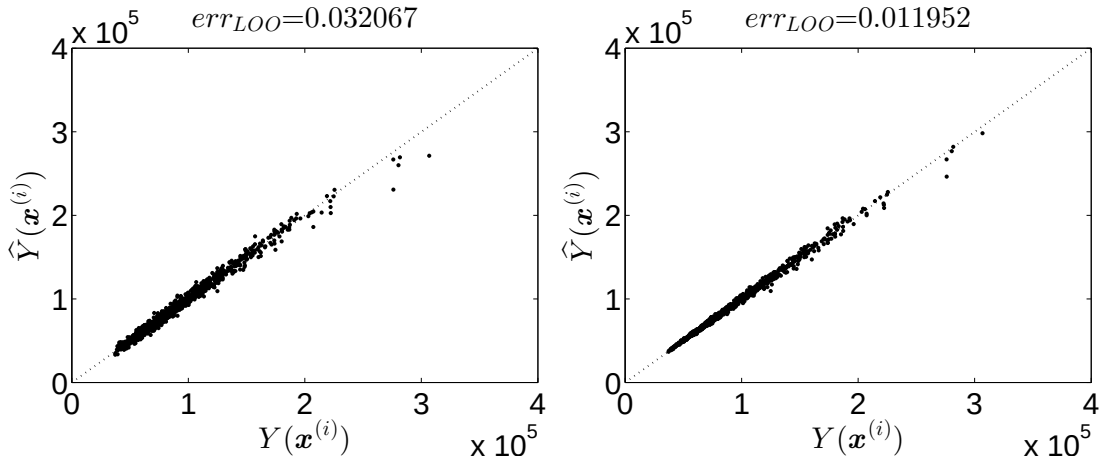

Figure 4.7: Comparison of PCE 1A (left) and the exponential transform of PCE 1B (right) with the actual model response at the experimental design.

Both figures indicate that the variability in the MLE is mainly due to main effects and interactions associated with layers D4, L1b, C3ab and L1a in order of importance in terms of total effects, with layer D4 being clearly dominant. All aforementioned layers are located close to the host layer C2; D4 is the thickest among those and has the highest hydraulic conductivity. The condition $S_i^{tot} > 0.01$ additionally classifies as important layers C1 and D1 for both PCE 1A and 1B, and marginally layers D3 and L2b for PCE 1A only. Note that although C1 is adjacent to the host layer C2, it is associated with smaller total and first-order indices than other neighbouring layers, which may be attributed to its small thickness.

To gain further insight into the effects of the important variables on the model response, we examine the behaviour of first-order summands comprising univariate polynomials only, *i.e.*

$$\mathcal{M}_i(x_i) = \mathbb{E}\left[\mathcal{M}(\boldsymbol{x}|x_i = x_i)\right] \tag{4.30}$$

or equivalently

$$\mathcal{M}_i(x_i) = \sum_{\boldsymbol{\alpha}\in\mathcal{A}_i} y_{\boldsymbol{\alpha}}\Psi_{\boldsymbol{\alpha}}(x_i), \qquad \mathcal{A}_i = \{\boldsymbol{\alpha}\in\mathcal{A} : \alpha_i > 0, \alpha_{i\neq j} = 0\}. \tag{4.31}$$

Figures 4.10 and 4.11 depict such univariate effects considering PCE 1A and 1B, respectively, for the porosities at the six layers classified as important with both meta-models. The scales in the vertical axes in the two figures are different due to consideration of the non-transformed response in one and the logarithmic response in the other. The figures demonstrate that an increasing porosity, and thus an increasing permeability, is associated with a decreasing algebraic contribution to the MLE value, though this relationship is not strictly monotonic for all layers. Despite the different scales, the shapes of respective curves in the two figures demonstrate similar trends. However, we note the presence of higher-order terms for PCE 1B, which is consistent with its higher degree p and lower sparsity as compared to 1A. For both PCE, the sum in Eq. 4.31 tends to include more higher-order terms for the important variables.

For model 1A, main and second-order effects respectively account for 88.5% and 10.3% of the response variance, indicating that the contribution of higher-order effects is merely 1.2%. For model 1B, main and second-order effects respectively account for 94.7% and 4.8% of the response variance, indicating that the contribution of higher-order effects is smaller than 1.0%. For both models, the highest second-order indices involve one of the layers D4 or L1b. Overall, effects from interactions are slightly more significant for the variance of MLE in the original scale.

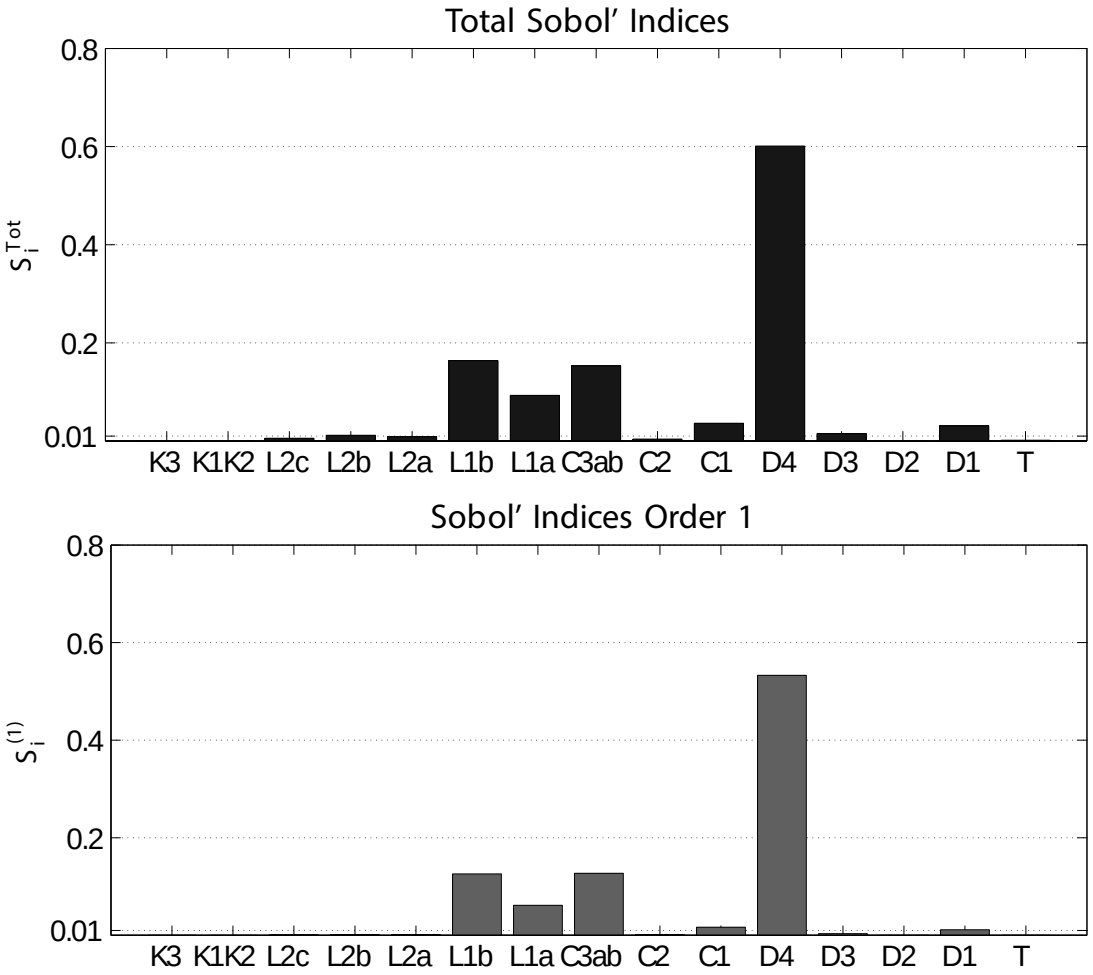

Figure 4.8: Sobol' indices using PCE 1A.

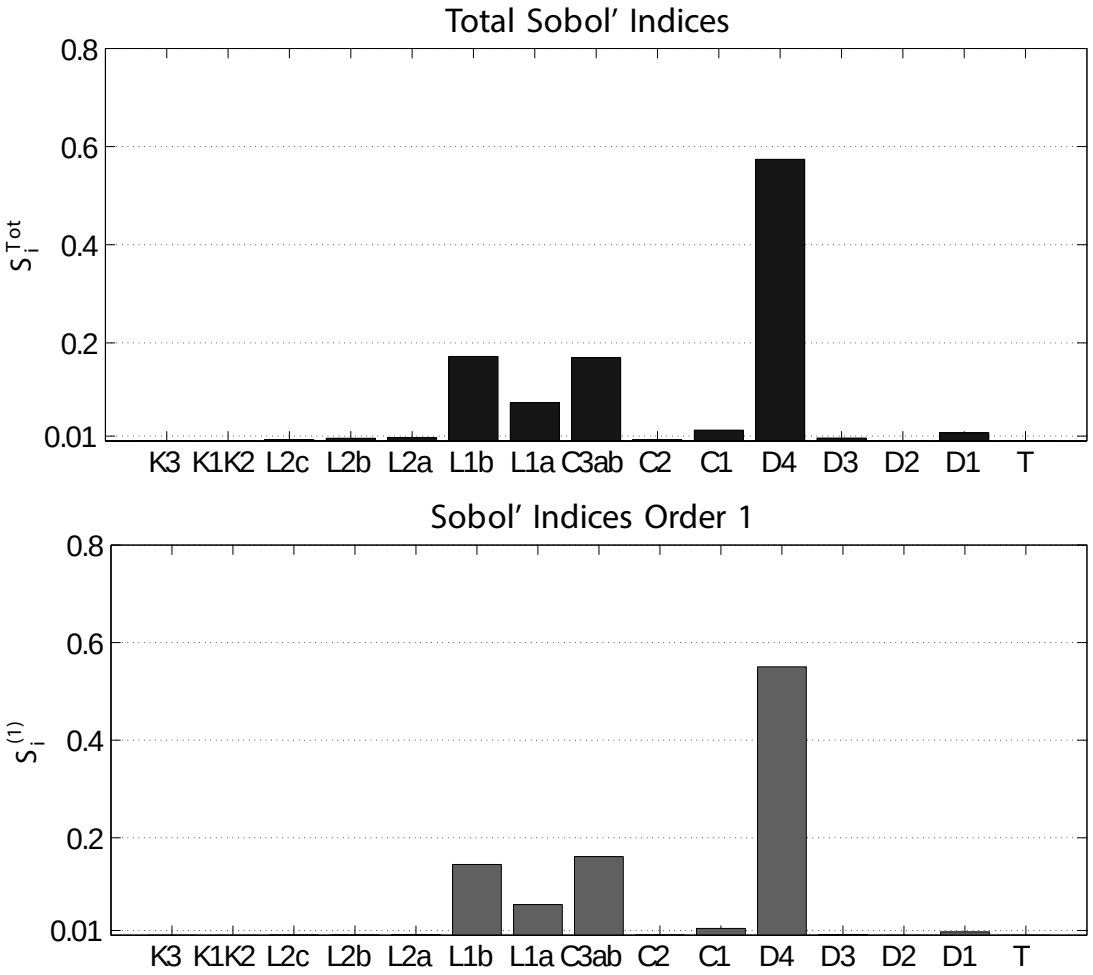

Figure 4.9: Sobol' indices using PCE 1B.

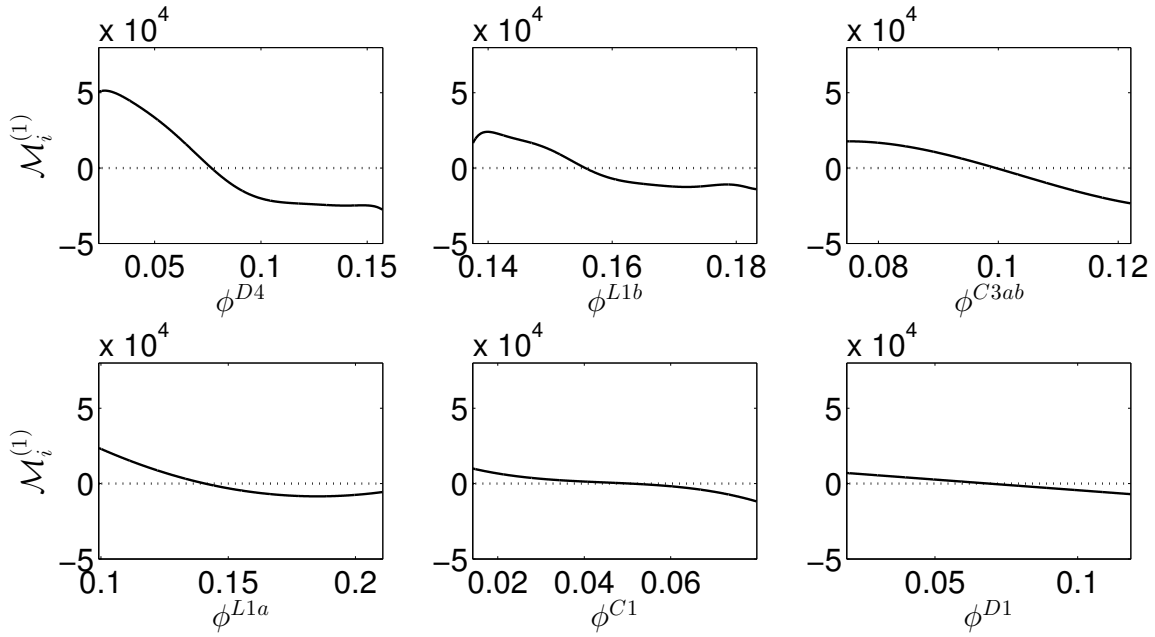

Figure 4.10: Univariate effects of important variables using PCE 1A.

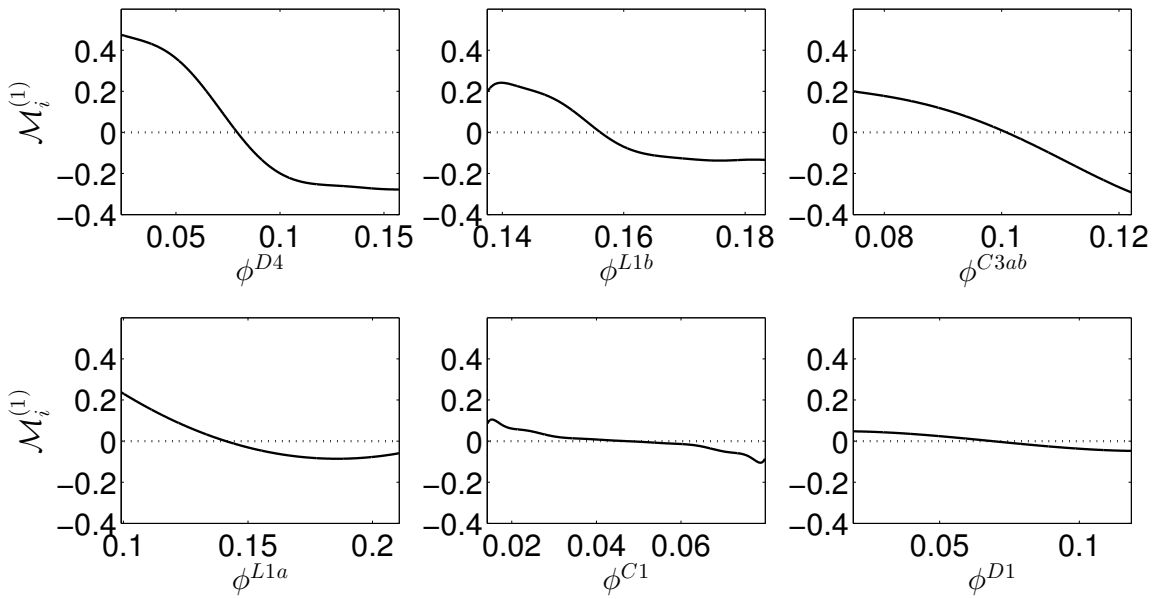

Figure 4.11: Univariate effects of important variables using PCE 1B.

4.4.2 Case 2: 78 input random variables

In case 2, we employ a more detailed description of the input uncertainty. In addition to the petrofacies, the uncertain input in each layer comprises the following four parameters governing the advective-dispersive processes: the anisotropy in the components of the hydraulic conductivity tensor, A_K; the Euler angle of the hydraulic conductivity tensor, θ; the longitudinal component of the dispersivity tensor, α_L; and the anisotropy in the longitudinal and vertical components of the dispersivity tensor, A_α. As in case 1, a deterministic relationship $\log_{10}(\widehat{K}_x) = f(\phi)$ is assumed for each layer. Furthermore, the uncertain input includes the hydraulic gradients, ∇H, at three zones: the Dogger sequence, the Oxfordian sequence and the top of the model, respectively denoted zone 1, zone 2 and zone 3. In total, the model subsumes $k = 78$ *independent* input random variables upon the MLE of water molecules outflowing from the TZ in the middle of layer C2.

The uncertain porosities, and the associated hydraulic conductivities, are modeled as in case 1. Due to the lack of explicit information, each of the parameters A_K, θ, α_L and A_α is identically distributed in the different layers. In particular, the anisotropy ratios A_K and A_α both follow a uniform distribution in [0.01, 1], the Euler angle θ is uniformly distributed in [-30, 30] (in degrees) and the parameter α_L is uniformly distributed in [5, 25] (in meters). The static hydraulic gradients are also uniformly distributed in the ranges given in Table 4.4. These were obtained by applying a perturbation of 20% of the nominal hydraulic gradient within each of the three zones. Although hypothetical, these conservative uncertainty ranges were purposely chosen to provide insights into the behaviour of the multi-layered model.

Table 4.4: Ranges of hydraulic gradient at the three zones of interest.

Zone number	$\nabla H^{(min)}$	$\nabla H^{(max)}$
1	0.00064	0.00096
2	0.00240	0.00360
3	0.00272	0.00408

Polynomial Chaos Expansion

In this case, the available data for building PCE consist of the MLE values for (i) an experimental design of size $N = 2,000$, drawn with LHS and denoted $\boldsymbol{X}$, and (ii) an enrichment of $\boldsymbol{X}$ of equal size $N' = 2,000$, denoted $\boldsymbol{X}'$. The enrichment is built so that the joint set $\{\boldsymbol{X}, \boldsymbol{X}'\}$ forms a LHS experimental design as well. Histograms of the model response for the two sets of input vectors are shown in Figure 4.12. Positively skewed distributions are observed for both output sets, while modes are situated at MLE $\approx$ 85,000 years.

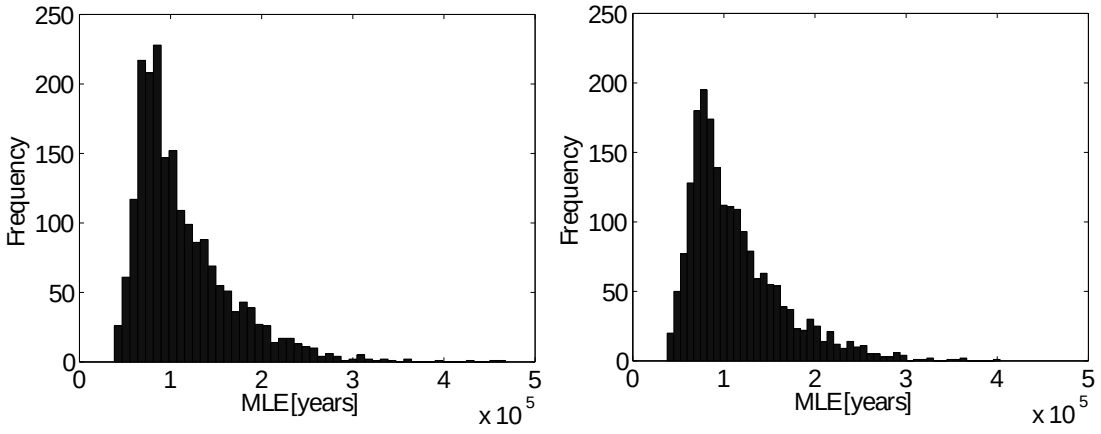

Figure 4.12: Histograms of mean lifetime expectancy values calculated with sets $\mathbf{X}$ (left) and $\mathbf{X}'$ (right).

In the following, we develop PCE based on $\boldsymbol{X}$ and the joint set $\{\boldsymbol{X}, \boldsymbol{X}'\}$. For the set $\boldsymbol{X}$, we consider the MLE response in both the original and the logarithmic scales; in this case, the enrichment $\boldsymbol{X}'$ serves

as a validation set for computing the generalization error (see Section 4.3.2). For all PCE, the candidate basis is determined using a hyperbolic truncation scheme with $q = 0.5$. The maximum degree p is varied from 1 to 15 and the optimal sparse meta-model is selected by means of the LOO error.

The first PCE, denoted 2A, is built using $\boldsymbol{X}$ as the experimental design and considering the response in the original scale. The optimal degree is $p = 8$ and the corresponding LOO error is $err_{LOO} = 0.0565$. The sparse PCE includes 185 basis elements, whereas the total number of basis elements for $p = 8$ and $q = 0.5$ (resp. $q = 1$) is 18,643 (resp. 5.3×10^{10}). Thus, the index of sparsity is $185/5.3 \times 10^{10} \approx 3.5 \times 10^{-9}$. The sparse basis consists of polynomials in 68 out of the 78 total input parameters, meaning that the output does not depend at all on the values of the 10 excluded parameters. Note that 3 out of the 10 excluded parameters are properties of layer T. The generalization error (evaluated with $\mathcal{E}'$) is $err_G = 0.0759$. The left graph of Figure 4.13 compares the values of the meta-model, $\hat{y}$, with the respective values of the exact model, y, at the input samples of the experimental design, $\boldsymbol{X}$. A similar comparison but for the validation set, $\boldsymbol{X}'$, is shown in the right graph of the same figure.

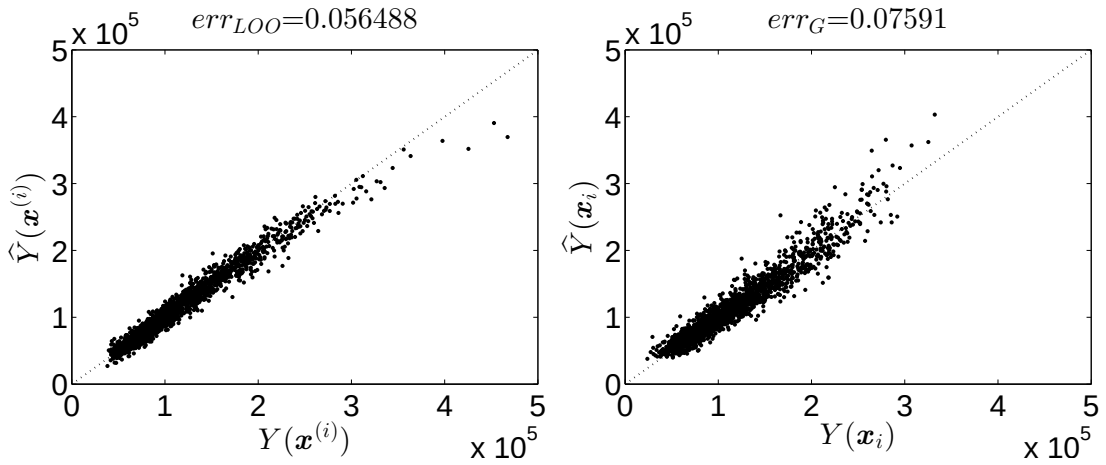

Figure 4.13: Comparison of PCE 2A with the actual model response at the experimental design, $\boldsymbol{X}$, (left) and at the validation set, $\boldsymbol{X}'$ (right).

A second PCE, denoted 2B, is built by using again $\boldsymbol{X}$ as the experimental design, but employing a logarithmic transform of the MLE. The optimal sparse PCE is obtained for $p = 8$ (same degree as for 2A) and comprises 163 basis elements; the corresponding LOO error is $err_{LOO} = 0.0287$. The sparse basis consists of polynomials in 65 out of the 78 total input parameters; note that 6 out of the 13 excluded parameters are dispersivity anisotropy ratios (A_α). The resulting generalization error for the MLE response in the original scale (considering the exponential transform of the obtained PCE) is $err_G = 0.0452$, which is slightly lower than that of PCE 2A. The left and right graphs of Figure 4.14 compare the exponential transform of PCE 2B with the exact model response at $\boldsymbol{X}$ and $\boldsymbol{X}'$, respectively.

Finally, we use as experimental design the joint set $\{\boldsymbol{X}, \boldsymbol{X}'\}$ consisting of $N + N' = 4,000$ points. The optimal PCE is obtained for $p = 10$ and the corresponding LOO error is $err_{LOO} = 0.0384$. The sparse PCE comprises 312 basis elements and has an index of sparsity $312/4.5 \times 10^{12} \approx 6.9 \times 10^{-11}$. The only two parameters excluded from the sparse basis are A_K^{L2b} and α_L^T. The comparison between the meta-model, denoted 2C, and the exact model response at the input samples of the experimental design, $\{\boldsymbol{X}, \boldsymbol{X}'\}$, is shown in Figure 4.15.

Assessing the relative accuracies of the three meta-models, we note that all have LOO errors of the same order of magnitude, with the smallest error corresponding to PCE 1B. Because it is of interest to limit the number of costly evaluations of the exact hydrogeological model, an experimental design comprising 2,000 points is deemed most appropriate. We therefore conduct SA for the MLE response by post-processing the coefficients of PCE 2A and 2B and compare the results. We should bear in mind that the Sobol' indices obtained from the coefficients of 2B represent contributions to the variance of the *logarithmic* MLE.

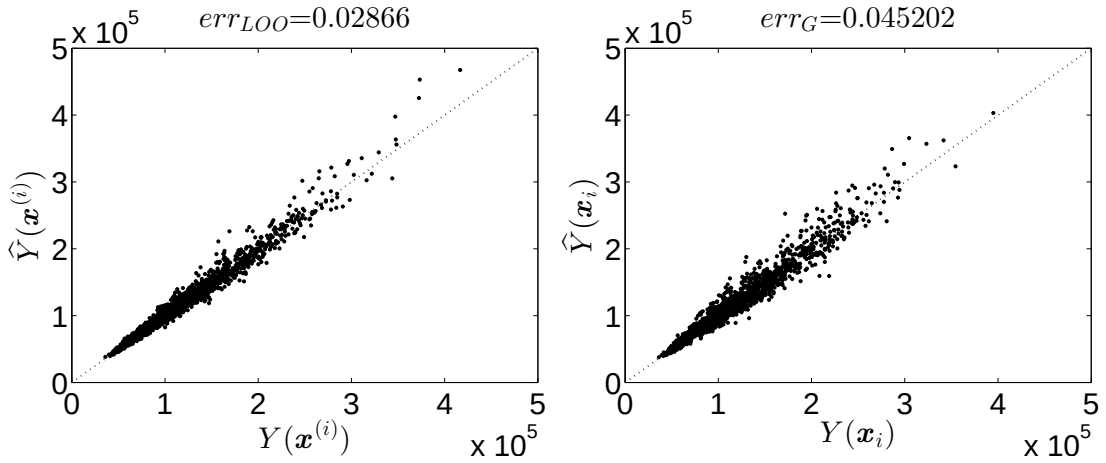

Figure 4.14: Comparison of exponential transform of PCE 2B with the actual model response at the experimental design, $\boldsymbol{X}$, (left) and at the validation set, $\boldsymbol{X}'$ (right).

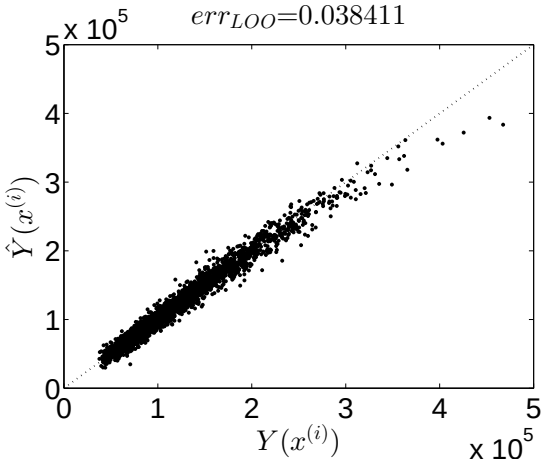

Figure 4.15: Comparison of PCE 2C with the actual model response at the experimental design, $\{\boldsymbol{X}, \boldsymbol{X}'\}$.

Sobol' indices

Figures 4.16 and 4.17 show bar-plots of the total and first-order Sobol' indices for PCE 2A and 2B, respectively. In each graph, bar-plots of the ten largest indices are presented in descending order. The superscripts on the parameter symbols on the horizontal axes denote layer names or zone numbers. To identify unimportant effects, the threshold of 0.01 is marked with a horizontal dashed line.

A first observation is that both PCE lead to the same ranking of the five variables with the highest total indices. These are the porosities of layers D4, C3ab, L1b, L1a and C1 in order of importance, with the porosities of layer D4 being the by-far dominant. For both PCE, these are also the variables with the highest first-order indices following the same ranking. Note that PCE 1A and 1B identified the same five layers as most significant in terms of both total and main effects, which indicates the consistency of the analyses in cases 1 and 2. However, the ranking of layers C3ab and L1b in terms of the total indices is interchanged in the two cases; also, layers D4 and C1 have slightly higher contributions in case 2. Employing the criterion $S_i^{tot} < 0.01$ to sort out unimportant variables, the porosities of the aforementioned five layers comprise the only important parameters for both 2A and 2B. Univariate effects for these variables follow similar trends as in case 1 and are thus not shown. The screening allows one to consider 73 out of 78 parameters as unimportant, meaning that they could be given a deterministic value without affecting essentially the predicted MLE.

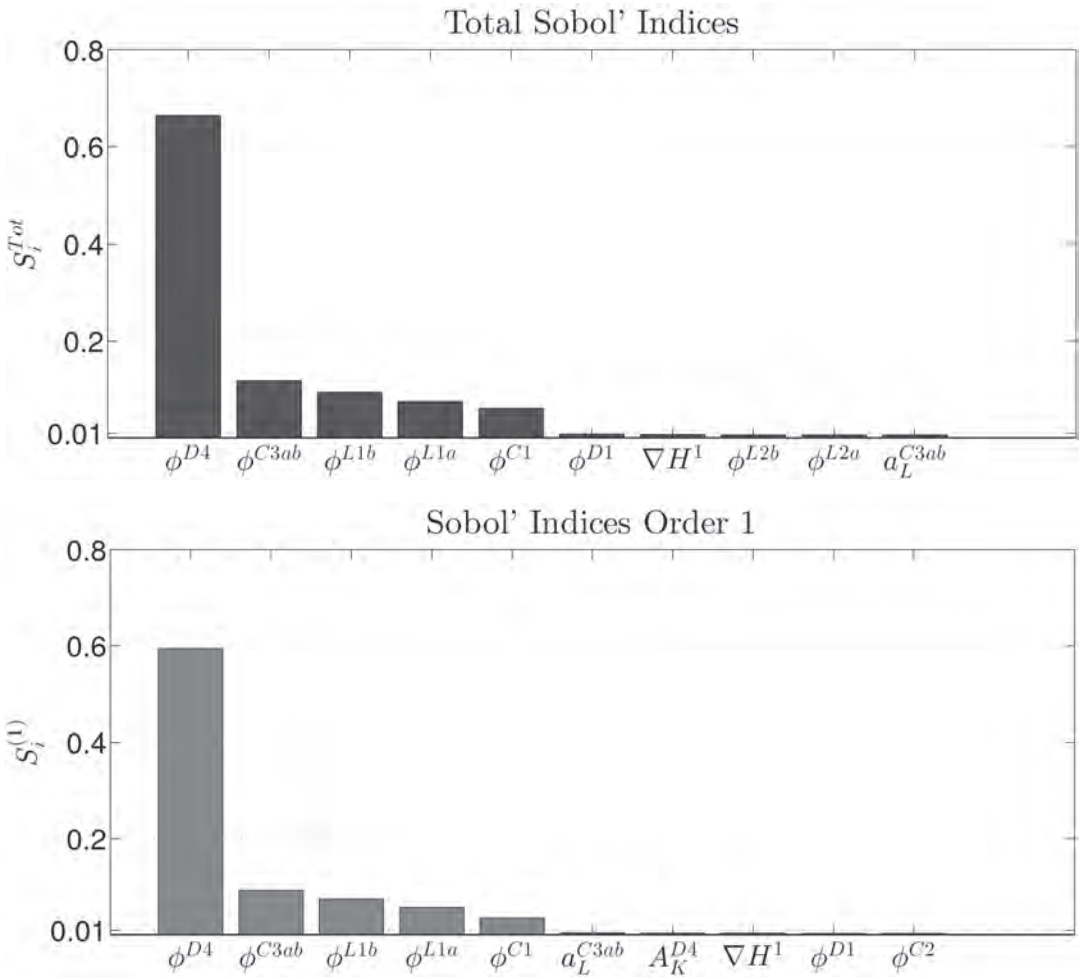

Figure 4.16: Sobol' indices using PCE 2A.

Let us now examine higher-order effects. For both PCE, the largest second-order effects comprise interactions between the five porosities classified above as important and involve one of the layers D4 or L1b; their sum explains 10.9% and 4.2% of the total variance for PCE 2A and 2B, respectively. Overall, second-order effects are slightly less important for the logarithmic response than for the response in the original scale, which is consistent with the results in case 1. Contributions of higher than second-order effects are practically zero.

The above analysis indicated that among the set of random variables, only the porosities of certain layers are important for explaining the response variance. Because of the assumed relationship between porosity and hydraulic conductivity in each layer, the Sobol' indices for the ϕ variables are also indicative of the importance of $\widehat{K}_x$ in the respective layers. Accordingly, in the subsequent discussion of the SA results (Section 4.4.3), we will interpret the variability of MLE in terms of joint effects of the petrofacies P.

For a more in-depth investigation of the contributions of the different types of hydro-dispersive parameters, Table 4.5 lists the sums of the first-order indices per type of property over all layers or zones of the considered cross-section. According to this table, the added main effects of the porosities account for approximately $87\% - 93\%$ of the response variance for the two PCE, whereas the added main effects of all remaining input random variables account for a mere $2.5\% - 2.8\%$. We note the slightly higher contributions of main effects for 2B and the zero main effects of A_α for both PCE.

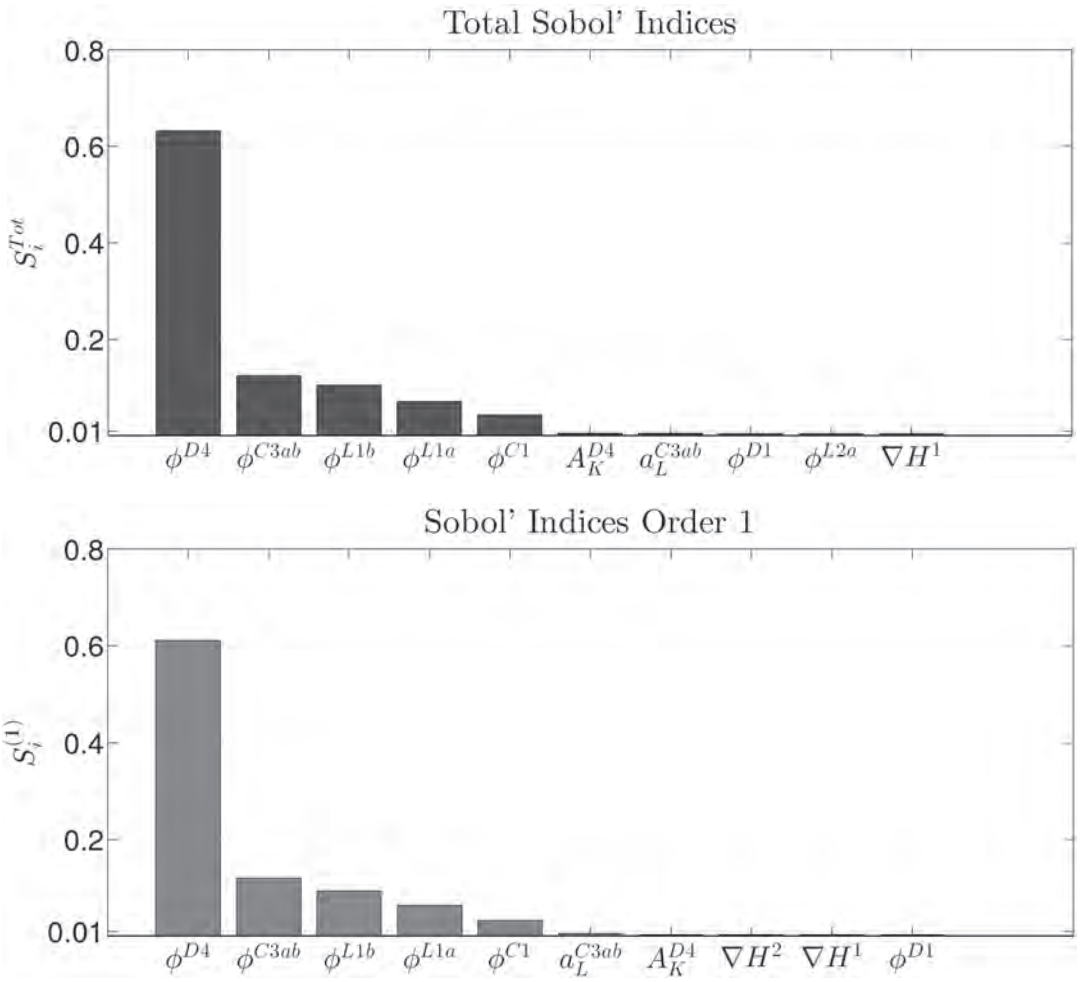

Figure 4.17: Sobol' indices using PCE 2B.

Table 4.5: Sums of first-order Sobol' indices over all layers per type of property.

meta-model	ϕ	A_K	θ	α_L	A_α	∇H
2A	0.8664	0.0088	0.0029	0.0076	0	0.0057
2B	0.9302	0.0096	0.0032	0.0088	0	0.0061

4.4.3 Discussion of results

In both cases 1 and 2, the petrofacies of aquifer formations have the largest effects on the variability of the MLE at the TZ. For layers D4 and L1b in particular, for which the upper bounds of the hydraulic conductivity ranges are the highest (see Table 4.3, Figure 4.5), strong advective processes within their own volume may reduce the overall groundwater residence time in the model. Besides, the wider the ranges of $\widehat{K}_x$ values in these permeable formations, the higher are the contributions of the respective petrofacies to the variability of the MLE. The position of the layers relatively to layer C2 is also relevant: the further the layer is, the lower is its effect on the MLE of water molecules departing from the TZ. Layer L1a, which is the first aquifer encountered in the Oxfordian sequence (at a distance of 60 meters from layer C2), has a significant effect on the output variance, whereas layers D2 and D3 that have similar $\widehat{K}_x$ ranges have much smaller contributions.

The three most significant aquifer formations, namely D4, L1b and L1a, have a rather non-linear univariate effect on the output response (Figures 4.10 and 4.11). Substantial changes in the response quantity are observed with small shifts in the ranges of low porosity and permeability values, revealing the effect of the balance between advective and dispersive-diffusive transport processes. But for higher

porosity-permeability values advective fluxes prevail, thus yielding more linear and moderate changes in the response function.

The relatively large uncertainty range and high upper-bound value of permeability for layer D1 results in a marginal effect on the response variability in case 1 (see Figures 4.8 and 4.9). The uncertainty in the petrofacies of this layer influences linearly or nearly linearly and rather moderately the transit time of water molecules from the TZ (see Figures 4.10 and 4.11). However, accounting for uncertain dispersion processes and groundwater fluxes in case 2 may reduce the quantity of water molecules departing from the TZ and reaching layer D1, thus lessening the contribution of P^{D1} to the variance of the output quantity, which becomes unimportant with respect to the threshold $S_i^{tot} < 0.01$.

The petrofacies of semi-permeable formations, P^{C3ab} and P^{C1}, are also significantly influencing the variability of the MLE at the TZ. By isolating layer C2 from major aquifer formations, they buffer solute intrusions into the Oxfordian and Dogger aquifer sequences, thus acting like a geological barrier. Figures 4.10 and 4.11 show that their univariate effects on the output quantity are relatively non-linear despite their limited amplitude.

We underline that the petrofacies of the host layer attributed to the Callovo-Oxfordian claystone (P^{C2}) are insignificant with regard to the MLE variability. Slow diffusive processes take place into highly impermeable rocks, which induces large values of the MLE response. Modifying the magnitudes of advective-dispersive transport processes in layer C2 does not add a significant variability to the time required for solutes to leave the layer's volume.

The magnitude of the transverse advective fluxes in each layer is related to the respective value of K_z, in which the uncertainty is accounted for through the anisotropy ratio A_K. Although A_K represents the second most influential group of factors, considering added effects from all layers (see Table 4.5), the uncertainty in this property adds a small amount of variability to the MLE ($< 1\%$) compared to the petrofacies ($\approx 90\%$). We note however that factor A_K^{D4} is only marginally excluded from the important factors when PCE 2B is considered (see Figure 4.17). Indeed, for the highest $\widehat{K}_x$ values, strong advective fluxes take place within the layer's volume. Under the assumption of strong transverse fluxes ($A_K^{D4} \to 1$), solutes can be oriented toward neighbouring layers where slower fluxes occur, thus raising the MLE.

For each layer, the Euler angle θ could deviate groundwater fluxes from an orientation parallel to the x-axis and toward the main discharge boundaries, thus raising the variability of the response. Although it could be assumed as especially influential in the most advective layers, the total contribution of this group of uncertain factors to the variance of the MLE is negligible in comparison to that of the petrofacies P (see Table 4.5).

In aquifer formations, the effects of the uncertainty regarding the macro-dispersion tensors upon the response quantity, *i.e.* the magnitude (α_L) and anisotropy (A_α) of the tensors, are concealed by the strong effect of petrofacies on the advective part of the transport processes (see Table 4.5). We note however that the longitudinal component of the macro-dispersion tensor in layer C3ab (α_L^{C3ab}) appears among the ten factors with the highest total Sobol' indices for both PCE 2A and 2B. The anisotropy ratios, A_α, have no contribution at all to the response variance when considered independently; the uncertainty in these factors contributes to the variability of MLE only through interaction terms.

The sensitivity of the MLE with respect to flow BCs considered in the model is directly related to the magnitude and orientation of the advective fluxes in the entire model. In the case of high gradients in both limestone sequences, the advective solute transport processes would raise within their volume, and thus reduce the MLE. Table 4.5 indicates that the three random hydraulic gradients have a small added effect on the output variance. Note however that the total Sobol' index for the hydraulic gradient in the Dogger sequence (∇H^1) belongs to the ten highest indices for both PCE 2A and 2B. The uncertainty regarding this factor can alter the advective processes occurring notably in layer D4, which has the far highest contribution to the variance of the MLE calculated at the TZ.

4.5 Conclusions

The model introduced in this paper stands as a two-dimensional vertical cross-section of the subsurface of Paris Basin in the vicinity of Bure (Haute-Marne). While encompassing most of the hydrogeological features of the underground media, it was simplified with regard to geometries, discontinuities, fractures and heterogeneities. This numerical model is intended to explore the behaviour of a complex multi-layered hydrogeological system at low computational cost and to provide insights into the effect of uncertain parameters upon various types of model output.

Sensitivity Analysis (SA) was carried out for two cases of modelling the input uncertainty. For the sake of simplicity, homogeneous parameters were assumed within each of the 15 hydrogeological layers comprising the model in both cases. In case 1, only the petrofacies, P, regarded as the couple permeability-porosity, $\{K, \phi\}$, were considered uncertain. In case 2, the uncertain factors at each layer included four additional hydro-dispersive parameters: the anisotropy ratio and the orientation of the hydraulic conductivity tensor, A_K and θ respectively, the magnitude and anisotropy ratio in the macro-dispersion tensor, α_L and A_α respectively; additionally, the hydraulic gradients, ∇H, in three zones of the numerical model were considered random, summing up to 78 uncertain input factors.

In the present study, a target zone (TZ) located within the middle layer (C2) of the model provides the output response of interest. Latin Hypercube Sampling was employed to address the propagation of the uncertainty from the input factors upon the mean lifetime expectancy (MLE) of water molecules departing from the TZ. Polynomial Chaos Expansion (PCE) meta-models were used to compute the Sobol' sensitivity indices for each input factor at low computational costs. Sparse PCE proved particularly efficient in providing fairly accurate representations of the MLE in terms of the considered high-dimensional input. The accuracy was enhanced when the PCE were fitted to the logarithmic MLE.

Focusing on the effects of petrofacies solely, case 1 demonstrated the large contributions of aquifer formations to the variance of the model output. In particular, (i) the closer the aquifer formation to layer C2, (ii) the thicker the layer, (iii) the wider the ranges of the petrofacies and (iv) the higher the upper bound of the hydraulic conductivity range, the larger were the effects of the petrofacies on the variability of the response. Investigation of the univariate effects of petrofacies highlighted that for these permeable formations, the response is more sensitive to changes occurring within low porosity-permeability ranges. Hence, within a certain range of $\{K, \phi\}$ values, the dispersive-diffusive processes counterbalance with the strong advective fluxes in the ageing process.

The SA results in case 2 showed that the variability of the MLE is almost entirely due to the uncertainty regarding the petrofacies of the hydrogeological layers. The other hydro-dispersive parameters are insignificant for explaining the response variance and may be considered as deterministic factors in future works. SA in cases 1 and 2 were consistent in identifying the layers of which the petrofacies are important.

In formations characterized by highly advective processes, the longitudinal hydraulic conductivities applying in the main groundwater direction have large contributions to the MLE variability. The two semi-confining formations encompassing the C2 layer buffer the transfer of solute from the latter toward the further aquifer sequences. Besides, it is acknowledged that longitudinal dispersion processes occurring within their own volume also retard the solute transfer toward the adjacent aquifers. Because of the diffusion-dominated transport processes occurring within its volume, the petrofacies of the highly-confining C2 layer have a negligible effect on the variance of the output response.

It is important to remind that the use of a 2D model tends to overestimate the output response of interest by omitting the advection and dispersion along the third dimension. Recognizing this limitation, we underline that the purpose of the synthetic model introduced in this study is to shed light on the relative effects of various uncertain factors governing the advective and dispersive processes in a complex multi-layered hydrogeological system. The authors acknowledge that the methods employed in this study can be applied to a real-case study employing a realistic 3D numerical model.

The sensitivity analysis performed in this work is deemed very informative for future applications with the high-resolution integrated Meuse/Haute-Marne hydrogeological model. In the frame of a real-case uncertainty analysis with concern to a solute transport in the subsurface of the Paris Basin, the authors recommend defining as thoroughly as possible the spatial distributions of hydraulic conductivity values, with a main focus on the large aquifer sequences of Oxfordian and Dogger ages.

Chapter 5

Sensitivity analysis of heterogeneity parameters on groundwater flow and lifetime expectancy, a synthetic case study

5.1 Introduction

In the last decades mathematical and numerical modelling have become comprehensive tools to understand and predict various kinds of environmental issues. Among the large number of available modelling techniques in engineering sciences, one is often compelled to make approximations or assumptions that must be tested and validated. Assuming that model inputs are very often uncertain and varying with space and time, Sensitivity Analysis (SA) techniques (Hamby, 1994; Saltelli et al., 2004) cover a wide range of mathematical and statistical methods to investigate these assumptions and to provide a better understanding of how factors contribute to the variance of the phenomenon under study. Two types of factors my be encountered: continuous factors are variables taking any value within their own range of uncertainty whereas categorical factors are related to conceptual representations of the problem (*e.g.* presence or absence of a certain feature).

In the petroleum and geological storage industry, the subsurface structure and its inherent physico-chemical parameters are often characterized by large uncertainties regarding the geometries of geological formations, geostatistical heterogeneities, discontinuities and/or channelized structures. In this context, geostatistical and numerical models are commonly employed for performing uncertainty propagation in predictive simulations with regard to the extension, orientation or connectivity of the hydrogeological structures.

The literature provides many examples of studies analysing the effect of geological and geostatistical uncertainties on the subsurface flow and hydrocarbon production in the context of highly heterogeneous sedimentary reservoirs. In their paper, Castellini et al. (2003) address the issue of uncertainty assessment with the use of high-resolution heterogeneous numerical models of geological reservoirs. They established that models built at the coarse scale, but covering a reasonable number of geological and geostatistical features, can be particularly informative in capturing the main processes occurring in the subsurface at low computational costs. Using the numerical model of a sedimentary reservoir in Azerbaijan, Choi et al. (2007) performed a SA using a Design of Experiment (DoE) coupled with the Response Surface Methodology (RSM) and the Analysis of Variance (ANOVA) to underline the effect of parameters controlling the interlayer connectivity and the flow paths tortuosity on oil recovery and gas production. Applying the same methodology on fictitious oil reservoirs, de Jager and co-workers (de Jager et al., 2009; Van Doren et al., 2007) showed that the variance of the predicted flow in the reservoir is influenced by variogram-based parameters such as the sill and the mean permeability of the heterogeneous field. They also established that the connectivity of channels prevails over their geometry with regard to their individual effects on the variance of the predicted flow.

In the frame of geostatistical simulation of geological reservoirs for CO_2 storage, Oladyshkin et al. (2012) made use of arbitrary polynomial chaos expansion to compute Sobol' indices which quantify the effect of factors defining the spatial heterogeneity of geological features and the groundwater flow velocity on contaminant transport. They proved that the longitudinal flow velocity is mainly responsible for the peak time of concentration at a given location whereas the peak level of the mean concentration is rather dependent on the level of heterogeneity and correlation length scale of the log-conductivity values in the heterogeneous media. Li and Zhang (2014) made use of a three-levels DoE combined with RSM for screening continuous and categorical factors in a heterogeneous hydrogeological numerical model simulating CO_2 injection. Their results showed the large influence of the level of hydraulic conductivity heterogeneity on the extension of the CO_2 plume in the reservoir.

In the context of the geological disposal for radioactive wastes, Pan and co-workers (Pan et al., 2009, 2011; Ye et al., 2007) carried out a SA over heterogeneous parameters for flow and transport simulations in the unsaturated zone of the Yucca Mountain (U.S. project for long-lived radioactive waste geological repository). Their studies notably showed that layer-scale prevails over local-scale heterogeneities of hydraulic conductivity in regard to their effects on the variance of the travel time of solutes in the subsurface.

In the scope of the French project for the geological disposal of radioactive wastes Deman et al. (2015) used a high-resolution integrated hydrogeological model of the region Meuse/Haute-Marne (France) (ANDRA, 2012a) to compute the average time for water molecules departing from a given area in the potential host clay-layer from Callovo-Oxfordian (COX) to reach the limits of the model's domain. The analysis of the effect of the uncertainty on permeability-porosity parameters in 14 hydrogeological layers in the underground Paris basin proved that the two aquifer sequences of Dogger and Oxfordian ages have a greater influence than the impermeable layers on the residence time of water in the underground. Indeed, advection processes occurring in permeable layers strongly influence the residence time of waters in

the subsurface of the Paris basin in comparison to the slow motion dispersion-diffusion processes taking place in impermeable rocks. The Dogger and the Oxfordian aquifer sequences are both affected by a large spatial variability of permeability-porosity parameters. Preliminary sensitivity tests were carried out (Kerrou et al., 2012) to qualify the effect of spatial heterogeneity on groundwater flow and transport prediction; however making use of systematic SA methods is a great task to achieve which would require a large amount of computationally expensive numerical simulations.

The main objective of this work is then to design a proper methodology of SA and to offer a preliminary assessment on the relative sensitivity of factors governing the spatial heterogeneity of permeability-porosity parameters in the Oxfordian and Dogger aquifer sequences. In the present work, the spatial distribution of porosity values is defined as a function of the distribution of hydraulic conductivity values. For each sequence, 5 factors are tested: the mean and standard deviation of the distribution of hydraulic conductivity parameters within the sequence, the correlation lengths of the log-conductivity values along dimensions x and z, and the connectivity of the geological structures featuring high hydraulic conductivity values. The method employed in this study relies on the DoE coupled with the RSM and ANOVA techniques to provide sensitivity indices in the scope of screening unimportant variables.

The first part of the chapter introduces a vertical 2-dimensions synthetic model of the Meuse/Haute-Marne region with its parameterization. The methodology for generating heterogeneous structures is described and the formulations of the output responses of interest are also reported. The second part introduces the uncertain factors under study together with the methods of DoE, RSM and ANOVA to compute the sensitivity indices for each factor. Then, results are discussed and recommendations are provided for further applications on complex hydro-systems.

5.2 The model of groundwater flow and mean lifetime expectancy

5.2.1 Layout of the numerical model

The present model was inspired by the COUPLEX model (Bourgeat et al., 2004), a vertical 2D flow and mass transport model used to simulate the release of radionuclide from a fictitious nuclear waste repository located inside a deep underground clay layer. The mesh of the present model, already introduced in Chapter 4, was discretized into 5×5 meters square elements in a two-dimensional $(x - z)$ cross section of 25'000 $\times$ 1'040 meters. The succession and thicknesses of hydrogeological structures derive from the lithostratigraphic log of the deep EST433 borehole (Landrein et al., 2013); the latter being located in the vicinity of the experimental site of Bure (Haute-Marne, France). All layers are horizontal with uniform thicknesses with a 140m highly impermeable clay formation, attributed to the Callovo-Oxfordian (COX) age, lying in the centre of the model. The Oxfordian limestone sequence overlies the COX and is confined under two thick low-permeability layers from Kimmeridgian (K1 - K2) and Tithonian age (K3). The Dogger limestone sequence is located under the COX, overlying a thick marl formation attributed to the Toarcian age (T). Figure 5.1 summarizes the geometry of the model and gives an insight on the thickness of each layer. A target zone is indicated as the location from which is calculated the mean lifetime expectancy formulated further below.

5.2.2 Governing equations and model outputs

Groundwater outflowing from the aquifer sequences

In the model the flow is considered to be incompressible and single-phased. Hence, the steady-state forward divergence-free flow field writes:

$$\begin{aligned} \nabla \cdot \mathbf{q} &= 0 \\ \mathbf{q} &= -\mathbf{K}\, \nabla H \end{aligned} \tag{5.1}$$

where $\mathbf{q}$ is the flux vector [L T^{-1}], H is the hydraulic head [L], and $\mathbf{K}$ is the tensor of hydraulic conductivity [L T^{-1}].

The groundwater flow rate Q_o [L^3 T^{-1}] outflowing from the left lateral limit (Figure 5.1) of either heterogeneous aquifer sequence is taken as the output of interest used in the subsequent SA. They are computed as:

$$Q_o = -\int_{\Gamma^+} \mathbf{q}\, d\Gamma^+ \tag{5.2}$$

where Γ^+ stands for the discharge boundary of either the Oxfordian or the Dogger sequence.

For a given setting of Multi-Gaussian model, many random heterogeneous fields are generated in order to account for the stochastic nature of the field generation method (see Section 5.2.5). Hence, the actual model outputs to be studied in the SA are the first two moments (ensemble mean, μ, and standard deviation, σ) of the distributions of groundwater flow rates obtained from different equally likely realisation random fields.

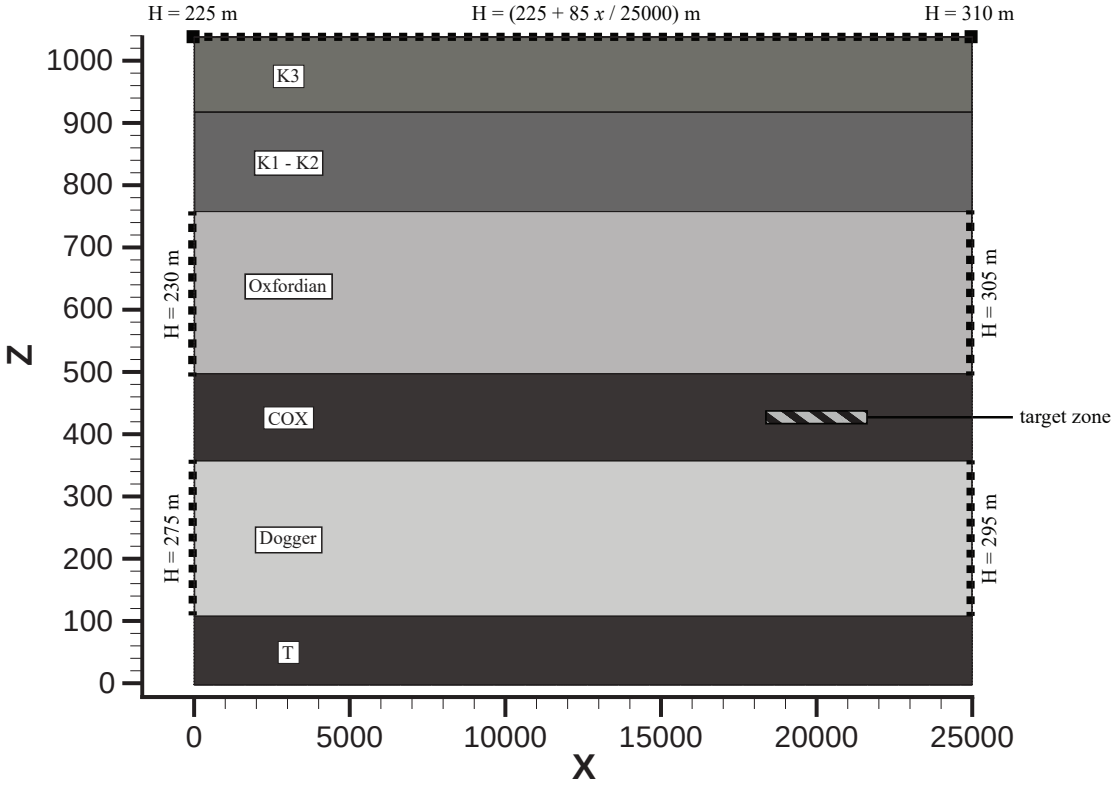

Figure 5.1: Geometry of the model, localization of the target zone and illustration of the flow boundary conditions (vertical exaggeration: 20). K3: Tithonian, K1-K2: Kimmeridgian, T: Toarcian

Mean Lifetime Expectancy from a target zone

Under stationary conditions, the lifetime expectancy probability density function (PDF) at any point x in the domain is the probability distribution of the time required for a solute taken at x to reach any limit of the domain. The formulation applies to conservative and non-reactive tracers and assimilates the forward advective-dispersive transport equation (ADE) to the Fokker-Planck (forward Kolmogorov) equation evaluating the random motion of solute particles (Uffink, 1989).

By reversing the flow direction (**q** := -**q**) the backward transport equation governing the lifetime expectancy PDF, $g_E(x,t)$, is:

$$\phi \frac{\partial g_E}{\partial t} = \nabla \cdot (\mathbf{q}\, g_E + \mathbf{D}\, \nabla g_E) \tag{5.3}$$

where ϕ is the effective porosity [-] and where $\mathbf{D}$ is the dispersion tensor:

$$\phi \mathbf{D} = (\alpha_L - \alpha_T) \frac{\mathbf{q} \otimes \mathbf{q}}{||\mathbf{q}||} \; + \; \alpha_T \, ||\mathbf{q}|| \, \mathbf{I} \; + \; \phi \, D_m \, \mathbf{I} \tag{5.4}$$

where $\mathbf{I}$ is the identity matrix, α_L and α_T are the longitudinal and transverse dispersivities [L] respectively, and D_m is the coefficient of molecular diffusion [L^2 T^{-1}].

As it can be seen in equations 5.3-5.4, no decay or adsorption effects are accounted in the computation of the lifetime expectancy PDF. The computation of the first moment of this PDF is given in Cornaton and Perrochet (2006b,a) and in Kazemi et al. (2006) as the mean lifetime expectancy (MLE) $E(x)$ [T] at any position x:

$$- \nabla \cdot (\mathbf{q}\, E + \mathbf{D}\, \nabla E) = \phi \tag{5.5}$$

where the porosity ϕ [-] acts as the sink term in the aging process.

A set of 1'947 nodes are selected in a rectangle which lateral and vertical extensions are x = [18'440 ; 21'680], z = [425 ; 435] to represent the target zone (TZ). In the present study the arithmetic mean of the $E(x)$ calculated at each of these 1'947 nodes stands for the output response of interest and is used in the subsequent SA.

Again, many heterogeneous fields are generated with the same variogram and Gaussian parameters, and the first two moments of the distribution of MLE for an ensemble realisation stand for the output responses.

The differential equations 5.1-5.5 are solved with the finite element simulator *GroundWater* (Cornaton, 2007). A single simulation of steady-state flow and MLE computation with the synthetic model takes about 120 seconds using a parallel Algebraic Multi-Grid (AMG) solver with 6 CPU using the *lx24-amd64* architecture.

5.2.3 Flow boundary conditions

All layers are assumed to be fully saturated with water and flow boundary conditions are stationary so that the flow solution is independent of time, *i.e.* steady-state flow. Dirichlet type flow boundary conditions (BCs) were set as in Figure 5.1. See Chapter 4 for details on the flow BCs.

The static hydraulic gradients derive from piezometric maps (Linard et al., 2011) where a 25km transect starting from the Gondrecourt trough and extending in the main regional flow direction was considered. The average topographic gradient of the region covered by the transect was used to set the hydraulic gradient on top of the model domain. With the above settings a groundwater flux inversion appears, vertically perpendicular to the target zone: the water flows downward from the Oxfordian to the Dogger sequence through the COX in the very right part of the model and then flows upward.

5.2.4 Dispersion and diffusion parameters

In the simulation of transport processes, accounted for in the mean lifetime expectancy (MLE) formulation presented in Section 5.2.2, the longitudinal and transverse components of the macro-dispersion tensor (α_L and α_T) control respectively the horizontal and transverse expansion of the plume. The study from Chapter 4 proved the lesser effect of these parameters on the MLE calculated from the target zone in the synthetic model. In this study, they are considered as deterministic factors and homogeneous values of α_L = 5m and α_T = 0.1m are set throughout the model. In this work, no decay or adsorption effects are assumed. The coefficient of molecular diffusion throughout the model is the theoretical self-diffusion coefficient for the water molecule, Dm = 2.3 E-9 m^2/s.

5.2.5 Permeability-porosity parameters

Statistical distributions

The isotropic hydraulic conductivity (K_g) and porosity (ϕ) values in the Oxfordian and Dogger sequences were measured on-site and in laboratory for a number of wells and boreholes within a wide area around the experimental site of Bure (Brigaud et al., 2010; Linard et al., 2011; Fourre et al., 2011; Delay and Distinguin, 2004; Delay et al., 2007). The measured data correspond to small volumes of rock and describe well the spatial variability of hydraulic conductivity and porosity values in the aquifers.

A Gaussian distribution was fitted on either dataset, and the first two moments of the Gaussian PDF is used in the subsequent sensitivity analysis. The means ($\mu_{log_{10}(K_g)}$) and variances ($\sigma^2_{log_{10}(K_g)}$) of the two distributions are considered as uncertain input factors. The variance of the Gaussian PDF in the Oxfordian ($\sigma^2_{log_{10}(K_g)} = 1.32$) is larger than in the Dogger ($\sigma^2_{log_{10}(K_g)} = 1.08$) whereas the mean of the Gaussian PDF in the Dogger ($\mu_{log_{10}(K_g)} = -5.57$) is higher than in the Oxfordian ($\mu_{log_{10}(K_g)} = -6.25$).

Table 5.1: geometric mean of the hydraulic conductivity (K_g [m/s]) and porosity (ϕ [-]) in the 6 numerical layers comprised in the model.

Layer	K3	K1-K2	Oxfordian	COX	Dogger	T
K_g [m/s]	9.01 E-09	4.53 E-09	5.51 E-07	2.73 E-13	2.70 E-06	5.11 E-13
ϕ [-]	0.0980	0.1095	0.1319	0.1656	0.0823	0.0764

For the four layers that do not belong to the Dogger and Oxfordian sequences, homogeneous K and ϕ values are attributed throughout the layer as the average K and ϕ values found in the literature (Cosenza et al., 2002; Delay et al., 2007, 2006; Enssle et al., 2011; NEA and OECD, 2009; Mazurek et al., 2011; Vinsot et al., 2011) and used in previous modelling efforts (Goncalves et al., 2004; Contoux et al., 2013; Goncalves et al., 2004; de Hoyos et al., 2012). Table 5.1 summarizes the mean of the K_g and ϕ datasets for each of the 6 hydrogeological formations comprised in the model.

Spatially distributed parameters

By examining the $\{K-\phi\}$ couples measured in the Oxfordian and Dogger sequences (Figure 5.2), a large variability is noted with the presence of correlations(*e.g.* low hydraulic conductivity and low porosity values are associated). But, for the sake of simplicity in the achievement of uncertainty propagation the conceptual approach is simplified in a first stage, defining a perfect dependence between K and ϕ by making use of a polynomial function $\phi = f(K)$ (solid black lines in figure 5.2). This allows considering both parameters at the same time and reduces the computational burden of the subsequent sensitivity analysis.

In the Paris basin the heterogeneous structures can have variable sizes, extensions and connections. Spherical variograms were employed to spatially distribute the $\{K-\phi\}$ values within the aquifer sequences. A key parameter of those variograms is the range, or correlation length, which represent the distance over which the $\{K-\phi\}$ values are correlated in space. This means that similar $\{K-\phi\}$ parameters will be populated together according to that range. The longitudinal correlation length scale λ_x defines the horizontal extent for which $\{K-\phi\}$ values are correlated whereas the vertical correlation length λ_z applies to the vertical dimension. The latter were designed to populate $\{K-\phi\}$ parameters according to the regional depositional setting, *i.e.* divagating tidal channels in a shallow-marine lagoon, of the history of the Oxfordian sequences in which porous horizons developed below sub-basins. Exceptions to this were the basinal facies where an equal lateral variogram of 5000m was used, and in certain specific zones. According to observations from the field (Vincent, 2001; Carpentier, 2004), the size of these depressions does not exceed 1000m and thus a relationship $\lambda_x \times \lambda_z$ of 1'000m $\times$ 50m would be appropriate.

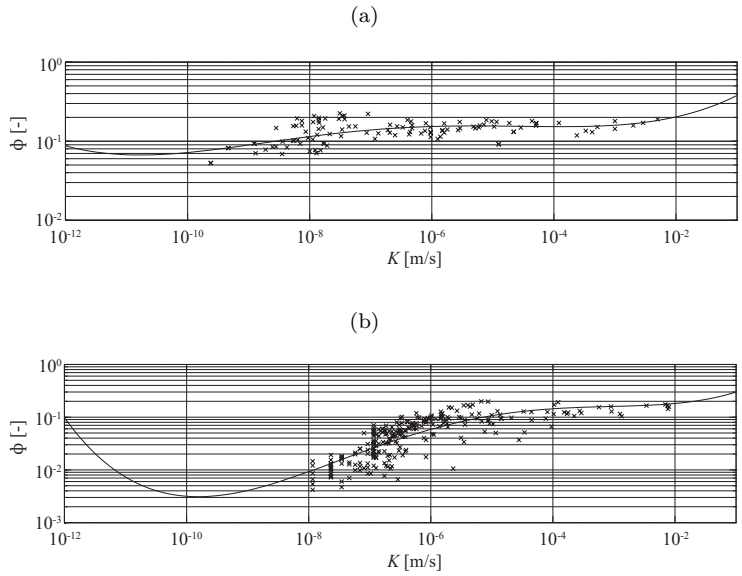

Figure 5.2: Permeability-porosity $\{K - \phi\}$ datasets in the (a) Oxfordian and (b) Dogger sequences with approximation functions.

Multigaussian fields were created, providing the spherical variogram model parameters that are: the sill, the range and the nugget. Normalized multigaussian fields Y_0 with zero mean (μ_{Y_0}) and unitary variance ($\sigma^2_{Y_0}$) were generated in the Oxfordian and Dogger sequences independently using the turning band method (Mantoglou and Wilson, 1982). Due to the stochastic nature of the turning band method, a number of heterogeneous fields must be generated, for every combination of parameters. The real parameters fields are retrieved from the normalized ones with the following expression (Kerrou and Renard, 2010):

$$Y(\mu_Y, \sigma_Y) = (Y_0 - \mu_Y)\frac{\sigma_Y}{\sigma_{Y_0}} + \mu_Y \tag{5.6}$$

where $Y(\mu_Y, \sigma_Y)$ is the transformed random variable with mean equal to μ_Y and a standard deviation equal to σ_Y; these two statistical moments deriving from the K_g datasets.

The hydrogeological formations are assumed to feature anisotropic hydraulic conductivity tensors and preferential flow directions, although no explicit information is available on the latter. Therefore, an anisotropy ratio $K_x/K_z = 0.1$ is assumed in the four homogeneous layer, K_x and K_z being the horizontal and vertical components of the hydraulic conductivity tensor respectively. In each of the two heterogeneous aquifer sequences, the anisotropy ratio is retrieved as the ratio of equivalent hydraulic conductivity values $K_{eq,x}/K_{eq,z}$. These are computed as (Ababou, 1996; Kerrou and Renard, 2010):

$$K_{eq,i} = K_g \exp\left(\sigma_Y^2 \left[\frac{1}{2} - \frac{1}{N}\frac{\lambda_h}{\lambda_i}\right]\right) \tag{5.7}$$

where K_g is the geometric mean of the hydraulic conductivity [L T^{-1}], σ_Y^2 is the variance of the $log_{10}(K_g)$, N is the number of dimensions of the problem, λ_i is the correlation length [L] in dimension i and λ_h is the harmonic mean of the correlation lengths [L].

Limestone formations often display karstic networks where preferential and connected flow paths are acknowledged. The turning band method employed to build the multigaussian fields assumes no specifically connected structures. Hence, the spatial connectivity C of high values in the normalized heterogeneous field is also taken into account in the present study and incorporated as a categorical factor. Broadly speaking, the following transformation transposes the location of the high values to draw path lines in the layer's volume. From the normalized field Y_0 the connected field is obtained with (Zinn and Harvey, 2003):

$$Y_0^C(\mu_{Y_0}, \sigma_{Y_0}) = -\sqrt{2}\,\text{erfinv}\left(2\,\text{erf}\left(\frac{|Y_0|}{\sqrt{2}}\right) - 1\right) \tag{5.8}$$

where Y_0^C is a field with connected high values and having zero mean and unitary variance, erf and erfinv are the error function and its inverse. Every multigaussian field obtained from the turning-band method can then be transformed into its connected form using Eq. 5.8, and then converted from the normalized to the real-values field using Eq. 5.6-5.7. However, it must be mentioned that this transformation applied on hydraulic conductivity parameters raises the equivalent conductivity K_{eq} while preserving the geometric mean K_g of the hydraulic conductivity field (Renard and Allard, 2011; Zinn and Harvey, 2003).

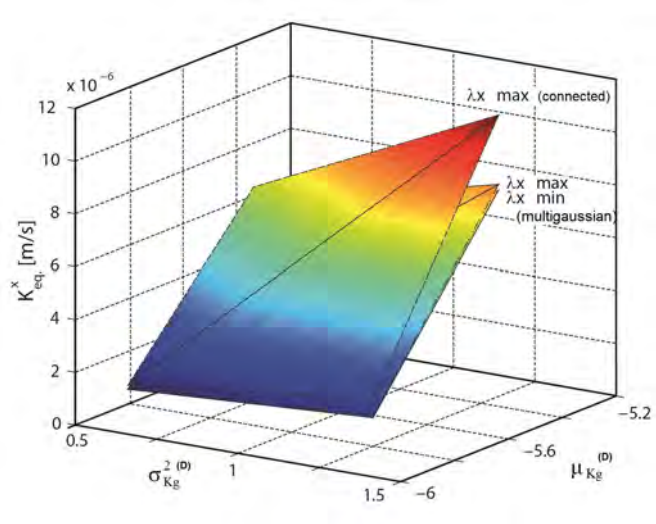

Figure 5.3: Theoretical equivalent permeability K_{eq} in the Dogger sequence as a function of the mean and standard deviation of a Gaussian distribution, for various correlation lengths and considering multigaussian or connected heterogeneous fields.

Figure 5.3 exhibits the theoretical repercussion on K_{eq} in direction x arising from varying the ensemble mean and variance in the Dogger sequence. The values were computed by isolating the sequence from the rest of the model and the uncertainty ranges for the moments of the distribution of K_g values presented in Table 5.2 were employed. Three cases are presented: the analytical K_{eq} computed with Eq. 5.7 for $\lambda_x = 500$m and for $\lambda_x = 8000$m, and the estimated K_{eq} retrieved from reversing Eq. 5.1 for a connected field with $\lambda_x = 8000$m. The uncertainty on the mean $\mu^{(D)}$ and on the variance $\sigma^{2(D)}$ of the Kg distribution in the Dogger sequence modifies K_{eq} by a factor 4 and 1.33, respectively. These raising effects are more significant than the effect of the connectivity C which only increases K_{eq} by a factor 1.25. It is however acknowledged that the presence of various recharge and discharge boundaries in the synthetic model may not strictly reproduce the above observations.

5.3 Methodology of sensitivity analysis

5.3.1 Uncertainty ranges of the input factors

The 5 uncertain input factors governing the characteristics of the heterogeneous fields in each sequence are (Table 5.2): the mean $\mu_{log(K_g)}$ and the variance (the sill of the variogram model) $\sigma^2_{log(K_g)}$ of the Gaussian distributions of hydraulic conductivity values, the longitudinal and vertical correlation lengths scale (the directional ranges of the variogram): λ_x and λ_z, respectively ,and the spatial connectivity C of high permeability-porosity values. In total the following SA studies the effect of $k = 10$ factors upon the groundwater flow rates at the outlet of the aquifer sequences and upon the MLE of water molecules outflowing from the target zone in the COX layer.

Table 5.2: Uncertainty range for the $k = 10$ factors considered in the Sensitivity Analysis (categorical factors in gray).

	$\mu_{log(K_g)}$ [m/s]	$\sigma^2_{log(K_g)}$ [m/s]	λ_x [m]	λ_z [m]	C [-]
Oxfordian	[-6.56 ; -5.96]	[0.50 ; 1.32]	[500 ; 8000]	[15 ; 60]	[without ; with]
Dogger	[-5.87 ; -5.27]	[0.50 ; 1.08]	[500 ; 8000]	[15 ; 60]	[without ; with]

The uncertainty ranges for the means $\mu_{log(K_g)}$ of the Gaussian distributions for $log(K_g)$ were estimated from the confidence interval of global transmissivity values found in Linard et al. (2011, Table 1). From the global values measured in a dozen of deep boreholes it appears that, for both Oxfordian and Dogger sequences, the minimum (resp. maximum) of the confidence interval is on average two times lower (resp. higher) than the mean value. Thus, a quite conservative uncertainty range $[\mu_{log(K_g)} - log(2)$; $\mu_{log(K_g)} + log(2)]$ is applied to the mean value of $log(K_g)$ in the respective aquifer sequence.

The uncertainty ranges on the variance $\sigma^2_{log(K_g)}$ of the Gaussian distributions for $log(K_g)$ in each sequence was set as follows. The variances obtained from the distributions fitted upon K_g datasets in either sequence are thought to be a maximum. In the event of collecting more hydraulic conductivity data in the Oxfordian and Dogger sequences, it is highly expected that the variances would reduce. Thus, a conservative minimum variance $\sigma^2_{log(K_g)} = 0.5$ is assumed in each sequence.

As mentioned previously, when converting the normalized fields into real-values K fields, the porosity values attributed in each mesh element of the two aquifer sequences in the numerical model are retrieved from the respective polynomial equations $\phi = f(K)$ (Figure 5.2).

Since various fields can be obtained with the very same variogram parameters, preliminary tests have shown that the moments of the distributions of the various model outputs stabilize after 20 realisations on average. Hence, a number of 25 random fields were generated for each combination of correlation lengths λ_x and λ_z, and were used in the subsequent analysis. Each of the 25 fields was transformed into its connected field version.

5.3.2 Design of experiment

Considering k uncertain factors, each having its own range of uncertainty, the nominal case is obtained by taking the mean value (or P50 value) for each factor. The basic principle of the uncertainty propagation is to shift each factor *one-at-a-time*, from its nominal value to another value in its own range of uncertainty while keeping the other factors at their nominal values, and to measure the change in the output. Compiling the uncertainty ranges for the k factor builds up a hyperspace H^k which can be explored by means of thorough designs of experiment (DoE). A large number of designs exist in the literature, including space-filling designs such as the Latin Hypercube Sampling (LHS) (McKay et al., 1979), the Latin Supercube Sampling (LSS) (Owen, 1998a) or the Low Discrepancy Sequences (LDS) (Sobol', 1967). However, the latter cannot include categorical input factors in their procedure.

In the event of having both continuous and categorical input factors, the factorial designs are DoE that efficiently explore H^k, thus avoiding the demanding one-at-a-time method. The Plackett-Burman (PB) design (Plackett and Burman, 1946) is a two-level DoE where only the minimum and maximum of the uncertainty ranges are considered, the minimum corresponding to a level -1 and the maximum to a level $+1$. For categorical factors these two levels (-1 and $+1$) correspond to different conceptualization of the problem modifying, for instance, some layout of the model. In the present study all factors are continuous except the connectivity C which depicts the spatial distribution of mesh elements characterized by high permeability-porosity parameters. Two-level designs allow the estimation of main (linear) effects of input factors as well as interaction effects (combined effect of 2 input factors) using the ANOVA setting.

A two-level full-factorial design for the $k = 10$ factors considered in this study would require $2^{10} = 1024$ simulations. Here, a fractional-factorial design (FFD) of resolution V (PB design) was chosen to reduce the computational burden to $N = 2^{10-3} = 128$ model runs. The FFD is a strategy to reduce the size of the experimental matrix by confounding the effect of input factors in the ANOVA decomposition while maintaining the orthogonality of the design matrix (Hadamard matrix) (Plackett and Burman, 1946). Using the ANOVA decomposition with a FFD of resolution V, the main effect of input factors are estimated solely and the two-way interaction effects (combined effect of 2 inputs) are assessed with

the additional effect of higher-order interaction effects (combined effect of 3 or more inputs). So, a prior assumption of negligible three-ways interactions and high-order effects of individual inputs is assumed in the following SA. In other words, the quadratic, cubic or higher effects of single factors as well as the combined effect of 3 or more factors are assumed to insignificantly influence the variability of the model output.

5.3.3 Regression model and ANOVA

Any phenomenon y being a function of k input factors $(x_1, x_2, \ldots, x_k)$ can be expressed with the following mathematical relationship (Hamby, 1994; Saltelli et al., 2004):

$$y = f(\mathbf{x}) = f(x_1, x_2, \ldots, x_i, \ldots, x_k) \tag{5.9}$$

The effect of the input factors and their interactions on the model output can be assessed by decomposing $f(\mathbf{x})$ into a sum of functions (Hoeffding, 1948). In the ANOVA setting, the variance of the output response Y is partitioned into components attributable to first or higher order effects of each input factor x_i as well as their interactions with every other input factor. If the k input factors are mutually independent random variables the ANOVA decomposition writes:

$$\mathbb{V}[y] = \sum_{i=1}^{k} \mathbb{V}_i(y) + \sum_{i<j} \mathbb{V}_{ij}(y) + \sum_{i<j<m} \mathbb{V}_{ijm}(y) + \cdots + \mathbb{V}_{1,2,\ldots,k}(y) \tag{5.10}$$

where $\mathbb{V}_i(y) = \mathbb{V}[\mathbb{E}(y|x_i)], \mathbb{V}_{ij}(y) = \mathbb{V}[\mathbb{E}(y|x_i x_j)] - \mathbb{V}_i(y) - \mathbb{V}_j(y)$, and so on.

The Response Surface Methodology (RSM) (Box and Draper, 1987) is a multivariate regression function fitted upon the responses obtained from any DoE and is meant to reproduce the behaviour of a specific phenomenon in the range of uncertainty of its input factors; thus it can be seen as a metamodel approximating the true function $f(\mathbf{x})$. In a two-level design, only the main (linear) effects and the two-way interactions effects of the factors can be assessed. Considering Eq. 5.10, the RSM based on the PB design is:

$$\hat{Y} = \beta_0 + \sum_{i=1}^{k} \beta_i \, x_i + \sum_{i=1}^{k-1} \sum_{j=i+1}^{k} \beta_{ij} \, x_i \, x_j \tag{5.11}$$

where $\hat{Y}$ is the modelled output response values and β are the coefficients of the RSM. For each input factor and for each interaction of factors, the associated coefficient β represents a measure of the sensitivity of the output response to that factor or interaction. The coefficient of multiple determination $R^2 \in [0, 1]$ assesses the quality of the RSM by addressing the fraction of the total variance of the model output accounted for by the regression function. Saltelli et al. (2004) acknowledge that a regression function with a $R^2 > 0.7$, meaning that 70% of the variance of the model output is explained by the regression, is acceptable for the interpretation of sensitivity indices.

In the scope of screening out unimportant input factors, the Student's t-test (Dodge, 2008) is commonly employed in multivariate linear regression functions. This statistical hypothesis test is carried out to extract the most important factors influencing each of the various model outputs considered in this study.

5.4 Results

5.4.1 Groundwater outflowing from the aquifer sequences

For the sake of argument, Figure 5.4 illustrate one random distribution of $log(K_x)$ values in its multigaussian and connected versions for the nominal case where $\mu_{log(K_g)}$ and $\sigma^2_{log(K_g)}$ correspond to the arithmetic mean of the bounds given in Table 5.2; $\lambda_x = 2000$m and $\lambda_z = 30$m. The corresponding hydraulic head isopiezes throughout the model are displayed in each case.

(a)

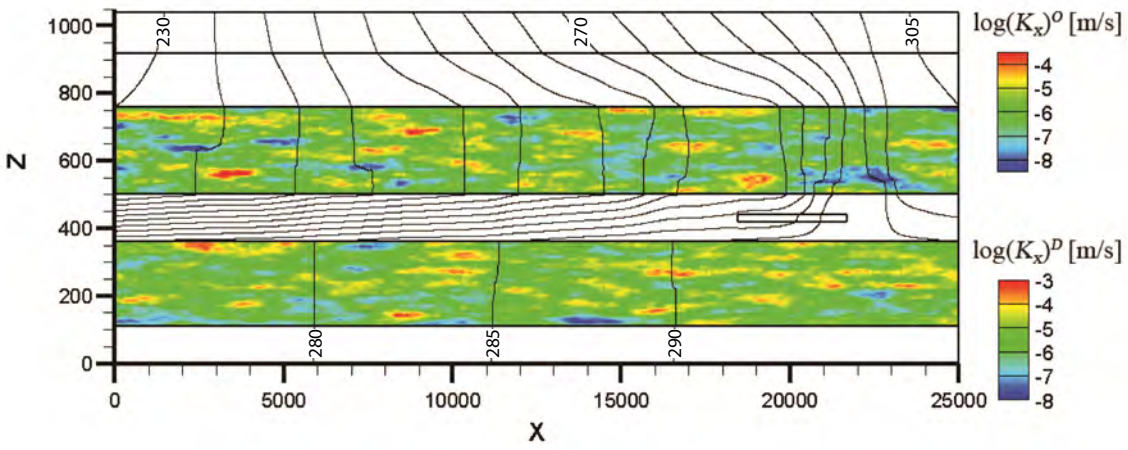

(b)

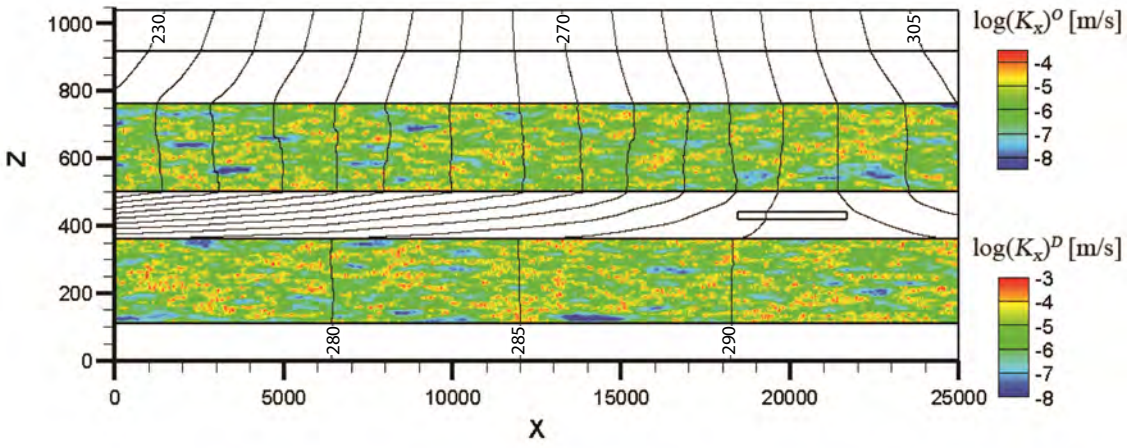

Figure 5.4: Longitudinal conductivity $Log(K_x)$ for a (a) multigaussian and (b) connected field in the nominal case with isopiezes in solid black lines, 5m intervals. (vertical exaggeration: 10 m)

The result of connecting high K parameters on the distribution of hydraulic heads appears clearly by producing more regular isopiezes, whereas with the multigaussian field (Figure 5.4a) the hydraulic gradients is more sensitive to the spatial distribution of K values. More illustrations are provided in Appendix D.1. Again, the presence of connected structures tends to lower the irregularity of the hydraulic heads distribution, and is then thought to homogenise the groundwater fluxes at the discharge boundaries of the aquifer sequences.

Each one of the 128 experiments of the PB design, using an ensemble of 25 random heterogeneous fields, gathers a distribution of groundwater flow rates, $Q_o^{(O)}$ and $Q_o^{(D)}$, at the Oxfordian and Dogger discharge boundaries respectively. The moments, μ_{Q_o} and σ_{Q_o}, of the distributions of groundwater flow rates for either discharge boundary are the output responses analysed through the sensitivity analysis.

The purpose is then to identify which uncertain input parameters are mainly responsible for the variability of the moments of the distributions of $Q_o^{(O)}$ and $Q_o^{(D)}$, or in other words, which uncertain parameters govern the shape of the distributions of $Q_o^{(O)}$ and $Q_o^{(D)}$ that result from an ensemble of 25 random heterogeneous fields.

Based on the 128 experiments, the multivariate regressions metamodels constructed on the means $\mu_{Q_o^{(O)}}$ and standard deviations $\sigma_{Q_o^{(O)}}$ of $Q_o^{(O)}$ yield coefficients $R^2 \approx 0.94$ and $R^2 \approx 0.88$, respectively. A $R^2 \approx 0.94$ and a $R^2 \approx 0.89$ were obtained from regression metamodels built over the means $\mu_{Q_o^{(D)}}$ and standard deviations $\sigma_{Q_o^{(D)}}$, respectively.

Ranked in order of significance, Table 5.3 provides the sets of influential factors upon each individual output response using a Student t-test at a 99% significance level. Similarities are observed in the sensitivity of the moments of the distributions of outflowing rates $Q_o^{(O)}$ and $Q_o^{(D)}$; the following interpretations are then valid for both sequences.

Table 5.3: List of influential factors on each of the six model outputs, sorted with the Student's t-test at 99% significance level.

Response	Influential factors (99% significance level)
$\mu_{Q_o^{(O)}}$	$\sigma^{2(O)}$, $\mu^{(O)}$, $\lambda_x^{(O)}$, $\lambda_z^{(O)}$
$\sigma_{Q_o^{(O)}}$	$\sigma^{2(O)}$, $\lambda_x^{(O)}$, $\mu^{(O)}$, $C^{(O)}$
$\mu_{Q_o^{(D)}}$	$\mu^{(D)}$, $\sigma^{2(D)}$, $\lambda_x^{(D)}$, $\lambda_z^{(D)}$
$\sigma_{Q_o^{(D)}}$	$\sigma^{2(D)}$, $\lambda_x^{(D)}$, $\mu^{(D)}$, $C^{(D)}$
$\mu_{MLE}^{(TZ)}$	$\mu^{(O)}$, $\sigma^{2(O)}$, $\mu^{(D)}$, $\sigma^{2(D)}$, $\lambda_z^{(O)}$, $\lambda_x^{(O)}$, $\lambda_z^{(D)}$, $C^{(O)}$, $C^{(D)}$
$\sigma_{MLE}^{(TZ)}$	$\lambda_x^{(D)}$, $\lambda_x^{(O)}$, $\sigma^{2(D)}$, $\sigma^{2(O)}$, $C^{(D)}$, $\lambda_z^{(D)}$, $\lambda_z^{(O)}$, $C^{(O)}$, $\mu^{(D)}$

A first observation is that only the uncertain heterogeneity parameters in a given aquifer sequence have an influence on the variability of the moments of the distribution of the groundwater flow rates at the respective discharge boundary, *i.e.* the uncertainty on the heterogeneity parameters in the Dogger does not affect the distribution of outflowing rates in the Oxfordian, and reciprocally. This is an obvious consequence of the presence of the thick, highly confining, layer from COX which hinders transverse groundwater fluxes between the two sequences.

The uncertainties on the moments ($\mu_{log(K_g)}$ and $\sigma^2_{log(K_g)}$) of the distributions of hydraulic conductivity values in the aquifer sequences have the greatest influence on the variability of the moments, μ_{Q_o} and σ_{Q_o}, of the distribution of Q_o. The longitudinal correlation lengths, λ_x, have also a relatively large effect on the variability of these moments. In other words, in the respective aquifer sequence, the three uncertain factors are mainly governing the shape of the output distribution of Q_o values resulting from an ensemble of 25 random heterogeneous fields generations. The two-ways interactions implying these three important factors are also significant in the regression metamodels. The sign of their respective regression coefficients indicates that the three uncertain factors and their interactions are proportionally related to both moments of the distribution of Q_o; *i.e.* increasing the magnitude of any of these three factors ($\mu_{log(K_g)}$, $\sigma^2_{log(K_g)}$ and λ_x) raises the moments, μ_{Q_o} and σ_{Q_o}, of the distributions of the outflowing rates at the discharge boundaries.

As shown in Figure 5.3, raising the mean, $\mu_{log(K_g)}$, of the hydraulic conductivity values increases the equivalent K_{eq} and thus the outflowing rate Q_o at the discharge boundaries. The sensitivity analysis indicates that the variability of the moments, μ_{Q_o} and σ_{Q_o}, of the distributions of the outflowing rates is closely related to the uncertain $\mu_{log(K_g)}$ values as interactions with other factors may increase non-linearities into the response function.

With an increasing variance $\sigma^2_{log(K_g)}$, the equivalent permeability K_{eq} raises (Figure 5.3), thus producing higher flow rates at the discharge boundaries. A high $\sigma^2_{log(K_g)}$ produces the occurrence of extreme hydraulic conductivity values, making the flow paths more tortuous and thus increasing the variability of the moments, μ_{Q_o} and σ_{Q_o}, of the distributions of Q_o. The uncertainty characterizing $\sigma^2_{log(K_g)}$ is largely responsible for the variability of the range of Q_o values and high-order effects, including interactions with other factors, are likely to add variability to both moments of the distributions of Q_o.

A large longitudinal correlation length λ_x increases the spatial connectivity of correlated K values over the distance in the main flow direction which has the effect of raising the equivalent permeability K_{eq}

(Figure 5.3). In the event of large λ_x, the spatial distribution of K parameters raises the variability of the moments of the distributions of Q_o. Of course, the combined effect of the longitudinal correlation length λ_x with the statistical moments, $\mu_{log(K_g)}$ and $\sigma^2_{log(K_g)}$, of the Gaussian distribution of K parameters intensifies the latter aspects.

Oppositely, increasing the vertical correlation length, λ_z, tends to reduce the mean outflowing rate at the lateral discharge boundaries, μ_{Q_o}, by raising divergent groundwater fluxes. Again, with respect to the spatial distribution of K parameters this parameter significantly influences the variability of the mean outflowing rates. However, it appears that λ_z has a negligible effect on the variability of the standard deviations σ_{Q_o} of the distributions of Q_o. The uncertainty characterizing the vertical correlation length, λ_z, tends to shift the distributions of Q_o values resulting from the ensemble of 25 random heterogeneous fields, but has no significant effect their standard deviations.

According to the t-test at 99% significance level, the connectivity C of high K values in the aquifer sequences does not add a significant variability to the mean, μ_{Q_o}, of the distributions of outflowing rates while it has a marginal, reducing effect on their standard deviations, σ_{Q_o}. The presence of connected conductive materials tends to have a stabilising effect on the groundwater flow rates at the discharge boundaries regardless of the spatial distribution of K values; thus having a significant, reducing effect, over the standard deviations of the distributions of Q_o. Note however that the insignificant effect of the categorical parameter C is related to the configuration of the present analysis. With regard to the SA settings, the large uncertainty bounds attributed to the other uncertain parameters conceal the potentially large effect of connected structures on the distributions of Q_o.

5.4.2 Mean lifetime expectancy from the COX

Figure 5.5 displays the distribution of MLE values throughout the model for the connected and multigaussian fields in Figure 5.4. Although the connected field presents more homogeneous distributions of MLE values in the aquifer sequences, the distributions from both multigaussian and connected fields are analogous. It should be noted that in the nominal case the MLE of groundwater molecules originating from the target zone (TZ) is approximately 60'000 years. In the aquifer sequences the MLE are much smaller, because of strong advective processes occurring, with values less than 20'000 years and with a Dogger sequence displaying a smaller range of MLE values than the Oxfordian due to its higher mean, $\mu_{log(K_g)}$, of hydraulic conductivity values (Table 5.1).

Appendix D.2 provides illustrations and discusses the MLE distributions for the inferior, nominal and superior values of uncertainty ranges of Table 5.2. Although strong at high correlations lengths and variances of the K distributions, the effect of the spatial distribution of $\{K - \phi\}$ parameters on the distributions of MLE tends to be smoothed by the presence of connected structures.

As in the previous section, each of the 128 experiments of the PB design considers an ensemble of 25 random generations of heterogeneous $\{K - \phi\}$ fields in the Oxfordian and Dogger aquifer sequences. This ensemble yields a distribution of MLE values calculated from the target zone, $MLE^{(TZ)}$, from which the moments, $\mu^{(TZ)}_{MLE}$ and $\sigma^{(TZ)}_{MLE}$, are the output responses considered in the sensitivity analysis. The latter explores then the effect of the 10 uncertain input parameters defining the heterogeneity in the aquifer sequences upon the variability of these two statistical moments. Broadly speaking, the SA aims at determining which uncertain input parameters mostly influence the shape of the distribution of $MLE^{(TZ)}$ values.

The RSM built upon the responses $\mu^{(TZ)}_{MLE}$ and $\sigma^{(TZ)}_{MLE}$ produced a $R^2 \approx 0.99$ and $R^2 \approx 0.97$, respectively. Table 5.3 and Figure 5.6 rank the influential parameters, according to the Student's t-test at 99% significance level, regarding their effect on the moments, $\mu^{(TZ)}_{MLE}$ and $\sigma^{(TZ)}_{MLE}$, of the distribution of MLE values in the target zone.

The MLE is governed by advective-dispersive processes (Eq. 5.3 - 5.5) which, in aquifer formations, are essentially controlled by the distribution of permeability-porosity parameters. The first observation arising from the SA results is that the uncertainties on the moments, $\mu_{log(K_g)}$ and $\sigma^2_{log(K_g)}$, of the Gaussian distributions of hydraulic conductivity values in each sequence have the largest effect on the variability of the mean, $\mu^{(TZ)}_{MLE}$, of the distribution of $MLE^{(TZ)}$ values. The signs of the associated coefficients in the regression metamodel indicate an inverse-proportionality between the input parameters and the mean $\mu^{(TZ)}_{MLE}$ (Figure 5.6 *left*), which indicates that the larger the moments of the Gaussian distributions of

(a)

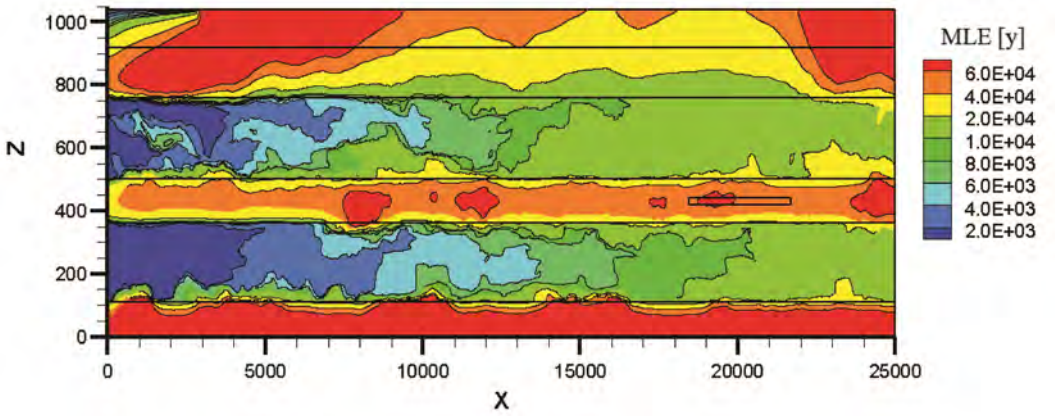

(b)

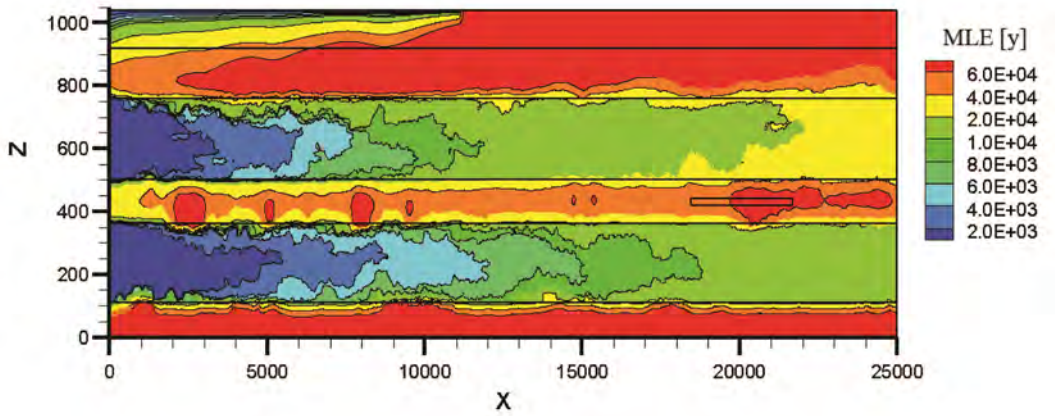

Figure 5.5: Distribution of MLE for a (*a*) multigaussian and (*b*) connected field in the nominal case. (vertical exaggeration: 10 m)

hydraulic conductivity values, the lower the mean of the distribution of $MLE^{(TZ)}$ values.

High values for the mean hydraulic conductivity in each sequence ($\mu^{(O)}$ and $\mu^{(D)}$) raise the overall advective processes within their respective volume. This allows the transported molecules to reach faster the domain's boundaries and thus reduces the mean lifetime expectancy, $MLE^{(TZ)}$, calculated from the target zone. The SA results prove that the effect can be generalised, independently of the random spatial distribution of $\{K-\phi\}$ parameters in the heterogeneous fields.

Large variances of the distributions of $\{K-\phi\}$ parameters in each sequence ($\sigma^{2(O)}$ and $\sigma^{2(D)}$) increase the occurrence of preferential fast-flow paths and thus reduces the mean transit time, $MLE^{(TZ)}$, of water molecules departing from the target zone. The regression metamodel indicates a negative correlation between the variances, $\sigma^{2(O)}$ and $\sigma^{2(D)}$, and the mean, $\mu^{(TZ)}_{MLE}$. Thus, the higher the variances, the stronger the preferential fast-flow paths, the lower the mean of the distribution of $MLE^{(TZ)}$ values.

Note that the variability of $\mu^{(TZ)}_{MLE}$ is principally influenced by the moments of the Gaussian distribution of permeability-porosity parameters in the Oxfordian ($\mu^{(O)}$ and $\sigma^{2(O)}$). This characteristic is due to the static flow boundary conditions applied on the model which produce a groundwater inversion vertically perpendicular to the TZ (Figure 5.4). The major part of the model features groundwater fluxes oriented upward to bring transported molecules into the Oxfordian sequence. Besides, the uncertainty range on $\sigma^2_{log(K_g)}$ is larger in the Oxfordian than in the Dogger, hence giving more variability to $\mu^{(TZ)}_{MLE}$.

The uncertainties on $\mu^{(O)}$ and $\mu^{(D)}$ have lesser influences on the variability of the standard deviation $\sigma^{(TZ)}_{MLE}$ of the distribution of $MLE^{(TZ)}$ values. Obviously, the mean hydraulic conductivity values in each aquifer sequence do not vary the range of $MLE^{(TZ)}$ values resulting from an ensemble of 25 random fields, however the variances, $\sigma^2_{log(K_g)}$, of the hydraulic conductivity values do.

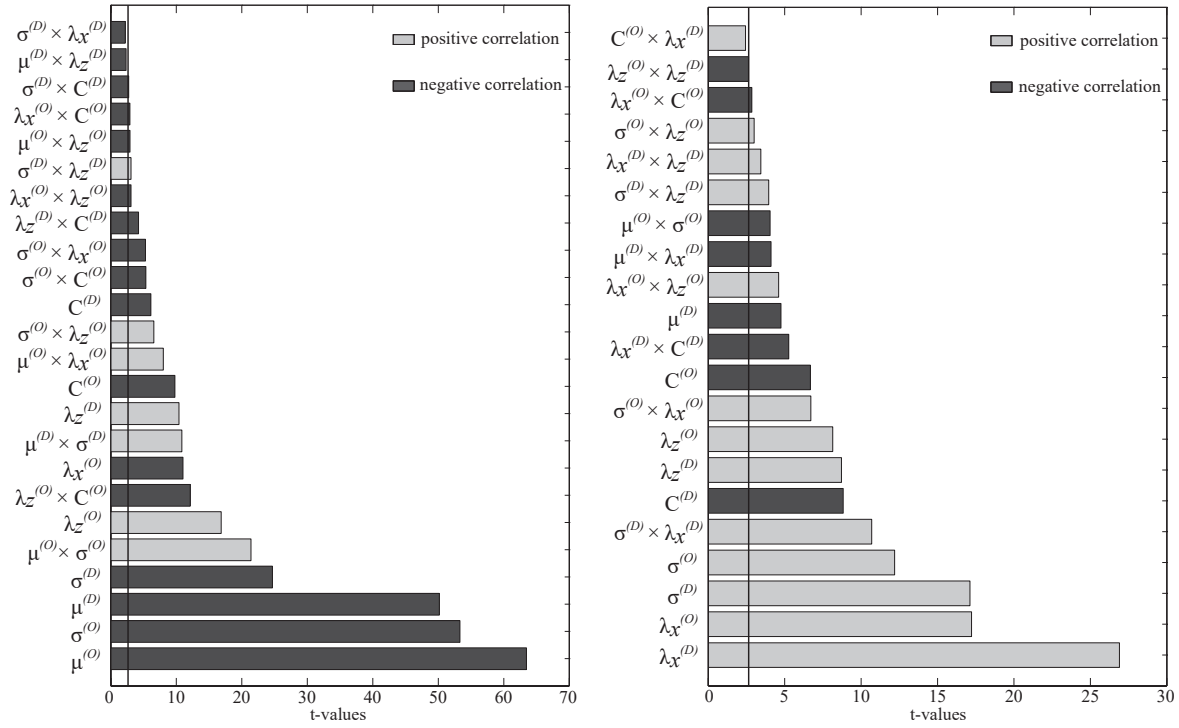

Figure 5.6: Sensitivity of the means $\mu^{(TZ)}_{MLE}$ (left) and standard deviations $\sigma^{(TZ)}_{MLE}$ (right) of the distributions of MLE in the target zone (threshold for the 99% significance level t-test in black solid line).

The longitudinal correlation length in the Oxfordian, $\lambda^{(O)}_x$, adds little variability to the mean $\mu^{(TZ)}_{MLE}$ of the distribution of $MLE^{(TZ)}$ whereas the t-test at 99% significance level rejects the hypothesis of $\lambda^{(D)}_x$ having a significant effect on the variability of $\mu^{(TZ)}_{MLE}$. However, both uncertain longitudinal correlation

lengths have the largest effect on the variability of the standard deviation, $\sigma^{(TZ)}_{MLE}$, of the distribution of $MLE^{(TZ)}$ (Figure 5.6). According to the sign of their corresponding coefficients in the regression metamodel, these parameters are proportionally correlated to $\sigma^{(TZ)}_{MLE}$. Conductive materials extending in the main flow direction are governed by advective processes likely to reduce the transit time of transported molecules. Oppositely, the $MLE^{(TZ)}$ can drastically increase when waters penetrate impermeable materials where the mass transport is dominated by slow dispersive-diffusive processes. With respect to the spatial distribution of $\{K-\phi\}$ parameters, the longitudinal correlation lengths has then the consequence of producing a large variability to $\sigma^{(TZ)}_{MLE}$.

Likewise, the uncertainty on the variances, $\sigma^{2(O)}$ and $\sigma^{2(D)}$, of the Gaussian distributions of K parameters in each sequence has a strong effect on the variability of the standard deviation, $\sigma^{(TZ)}_{MLE}$, of the distribution of $MLE^{(TZ)}$ values. In relation to the random spatial distribution of $\{K-\phi\}$ parameters, the higher the value for $\sigma^{2(O)}$ and $\sigma^{2(D)}$, the higher the standard deviation of the output response distribution. Figure 5.6 also indicates that interactions between λ_x and $\sigma^2_{log_{10}(K_g)}$ have a strong effect on the variability of the standard deviation $\sigma^{(TZ)}_{MLE}$ of the distribution of $MLE^{(TZ)}$ values.

The vertical correlation lengths in the heterogeneous sequences ($\lambda^{(O)}_z$ and $\lambda^{(D)}_z$) are proportionally correlated to both moments of the distribution of $MLE^{(TZ)}$ values. These parameters produce divergent groundwater fluxes and thus retard the water molecules from reaching the domain's boundaries. Note however that their effects are negligible with respect to those of the other uncertain parameters.

According to the t-test at 99% significance level, the spatial connectivity of high $\{K-\phi\}$ parameters ($C^{(O)}$ and $C^{(D)}$) have a significant effect on both moments of the distribution of $MLE^{(TZ)}$ values. By creating connected structures where fast groundwater pathways appear, the mean time required for transported molecules to reach any outlet of the model reduces, thus reducing the mean, $\mu^{(TZ)}_{MLE}$, of the distribution of $MLE^{(TZ)}$. However, the SA results indicate that the connectivities in either aquifer sequence have little effect on $\mu^{(TZ)}_{MLE}$ in comparison to the other significant parameters. By homogenizing the MLE distribution in the two aquifers sequences (Figure 5.5), the presence of connected structures has a lessening effect on the variability of the standard deviation, $\sigma^{(TZ)}_{MLE}$, of the distribution of $MLE^{(TZ)}$ values. As indicated by the sign of the associated coefficients in the regression metamodel (Figure 5.6), this effect is rather significant and underlines the major role of connected structures in reducing the variability of $MLE^{(TZ)}$ values arising from the random field generation.

Finally, it should be noted that the mean, $\mu^{(TZ)}_{MLE}$, of the distribution of $MLE^{(TZ)}$ is more sensitive to the uncertain heterogeneous parameters in the Oxfordian sequence whereas its standard deviation, $\sigma^{(TZ)}_{MLE}$, is more sensitive to the uncertain heterogeneous parameters in the Dogger sequence. Given the configuration of the synthetic model where the hydraulic gradients drive the water molecules from the TZ to the Dogger sequence at first, strong heterogeneities of $\{K-\phi\}$ values in the latter may highly influence the transit of water molecules to the Oxfordian sequence, thus being mostly responsible for the range of $MLE^{(TZ)}$ values. And since most of the transport process occurs in the Oxfordian sequence, its uncertain heterogeneous parameters have a larger influence on the mean of the distribution of $MLE^{(TZ)}$ values.

5.5 Discussion and conclusions

Employing a vertical 2-dimensions synthetic hydrogeological model of a region of the Paris basin, a Sensitivity Analysis (SA) was performed upon variogram parameters and the moments of a Gaussian distribution which define the type and level of heterogeneity of permeability-porosity ($\{K-\phi\}$) values in two large aquifer sequences. The latter are assimilated to the Dogger and Oxfordian limestone formations, and they are separated by a thick impermeable layer (COX) which is the potential host layer for a geological repository of radioactive wastes in France. Data derived from literature were used to constrain the uncertainty ranges for 5 factors in each of the two sequences: the mean and variance of Gaussian distributions, $\mu_{log(K_g)}$ and $\sigma^2_{log(K_g)}$, for the hydraulic conductivity parameters, the longitudinal and vertical correlation lengths (directional ranges in the variogram), λ_x and λ_z, and the spatial connectivity, C, of high $\{K-\phi\}$ values. A two-level Plackett-Burman design of experiment was employed for propagating

the uncertainty of these 10 factors on three model outputs: the steady-state flow rates at the discharge boundary of the Oxfordian and Dogger aquifer sequence, $Q_o^{(O)}$ and $Q_o^{(D)}$, and the mean life expectancy from a target zone, $MLE^{(TZ)}$, which represents the mean time required for water molecules released in a specific zone inside the COX layer to reach any outlet of the model. To account for the stochastic nature of multigaussian field generation, an ensemble of 25 random heterogeneous fields was generated for each combination of uncertain heterogeneous parameters, thus producing a distribution of values for each of the three above-mentioned model's responses. The statistical moments (mean and standard deviation) of these distributions were analysed through a regression-based SA by decomposing the contributions of variables, and interactions between variables, to the total variance of each model output.

With respect to the uncertainty ranges employed in this study, the level of heterogeneity of $\{K - \phi\}$ values in aquifer systems, governed by the variances, $\sigma^2_{log(K_g)}$, of their statistical distributions, is a major factor that influences both the distributions of flow rates at the discharge boundaries of the aquifers sequences, and the distribution of MLE of water molecules originating from the target zone. The means, $\mu_{log(K_g)}$, of the Gaussian distributions of K values in the aquifer sequences also have a strong effect on the distributions of the outflowing rates, $Q_o^{(O)}$ and $Q_o^{(D)}$, at the discharge boundaries of the sequences ; they also influence the mean of the distribution of $MLE^{(TZ)}$ but have almost no effect on its standard deviation. The longitudinal flow velocity in the aquifer sequences is proportional to the longitudinal correlation lengths, λ_x, and has a significant effect on both the flow and ageing processes. In relation to the spatial distribution of $\{K - \phi\}$ values, the longitudinal correlation lengths have the highest influences, among all the uncertain parameters, on the range of $MLE^{(TZ)}$ values resulting from the ensemble of random heterogeneous fields. Oppositely, the vertical correlation length, λ_z, tends to reduce the groundwater fluxes at the discharge boundaries of the aquifer sequences and to raise the $MLE^{(TZ)}$ by favouring divergent groundwater fluxes in the layer's volume. Though, these uncertain parameters have minor effects on the distributions of $Q_o^{(O)}$, $Q_o^{(D)}$ and $MLE^{(TZ)}$. The occurrence of connected structures of high $\{K - \phi\}$ values, related to the connectivity parameter, C, does not strongly influence the statistical distributions of the outflowing rates, $Q_o^{(O)}$ and $Q_o^{(D)}$, nor does it add variability to the distribution of $MLE^{(TZ)}$ values. Connected structures of conductive materials create connected preferential flow paths which tend to homogenise the outflowing rates in the aquifers sequences. Connected structures also stabilize the values for the MLE of transported molecules from the COX deriving from the ensemble of random heterogeneous fields. This has been underlined by the relative, inversely proportional, effect of the parameters C on the standard deviations of the distributions of $Q_o^{(O)}$, $Q_o^{(D)}$ and $MLE^{(TZ)}$. It is however recognised that the effect of connectivity may be concealed by *(i)* the presence of multiple discharge boundaries favouring transverse groundwater fluxes, and *(ii)* the large uncertainty ranges for the other input factors which add much variability to the model outputs.

Some limitations are acknowledged: the flow and transport parameters fixed in this exploration of the model, in particular the fixed flow boundary conditions, can be of major importance on the outcomes of the present SA. Besides, the experimental design employed in this preliminary study did not consider high-order effects of uncertain variables which might be of importance; especially when heterogeneity parameters are close to the superior bounds of their uncertainty ranges.

It must be mentioned that the results presented in the present study cannot be extrapolated to other numerical models, especially not within the frame of the risk an safety analysis related to the Andra project. Nonetheless, for application on the 3D integrated Meuse/Haute-Marne hydrogeological model of the Paris basin, the authors recommend to precisely define the location and extension of the heterogeneities within the two aquifer sequences, and also to properly define the distributions of permeability-porosity values. Following these recommendations would allow a lesser variability of the calculated flow rates and MLE in the predictive simulations of flow and solute transport in the subsurface system of the Paris basin.

A major originality in the present study is in the conceptualisation and implementation of the problem. This work applied a Sensitivity Analysis upon uncertain statistical variables (means and variances) as inputs and as outputs of the model. Such conceptual approaches have not been widely employed so far, and the methodology brought in the present chapter is expected to be useful for performing uncertainty and sensitivity analysis of complex subsurface systems.

Chapter 6

Sensitivity Analysis of groundwater lifetime expectancy to hydro-dispersive parameters: the case of Andra Meuse/Haute-Marne site.[1]

[1]This chapter is published as: *G. Deman, J. Kerrou, H. Benabderrahmane and P. Perrochet, 2015, Sensitivity analysis of groundwater lifetime expectancy to hydro-dispersive parameters: the case of Andra Meuse/Haute-Marne site. Reliability Engineering & System Safety, 134(0):276-286, ISSN 0951-8320, doi: 10.1016/j.ress.2014.08.005.*

6.1 Introduction

For over fifteen years, Andra (French National Radioactive Waste Management Agency) has conducted many studies and field exploration programs to assess the feasibility of a high-level radioactive waste disposal in the thick Callovo-Oxfordian (COX) clay-rich sedimentary layer of the eastern Paris basin (ANDRA, 2005). The host formation has been extensively characterized (Vinsot et al., 2011; Enssle et al., 2011) together with the Oxfordian and Dogger limestone aquifer formations, respectively above and below the COX.

In 2012, Andra has achieved to build an integrated regional-local geological model for the entire Paris basin to study the groundwater flow and solute transport behavior in the multi-layered aquifer system including the Callovo-Oxfordian clay host formation. The distribution of hydro-dispersive calibrated parameters of the groundwater numerical model is referred to as the nominal case of hydraulic head and flow velocity fields. However, such deterministic modeling of groundwater flow and solute transport is very often affected by uncertainties (de Marsily et al., 2005). These uncertainties may be related to all or one of the geometry of the multi-layered system, the boundary conditions and particularly, the parameters values and their spatial variability. In the scope of predictive simulations for risk and safety assessment it becomes of major importance to propagate these uncertainties on a model output under study as a decision-making tool. With many examples of application in environmental studies (Campolongo and Saltelli, 1997; Ciriello et al., 2013; Draper et al., 1999; Helton, 1993; Van Griensven et al., 2006; Malaguerra et al., 2013), sensitivity analysis (SA) techniques are powerful tools commonly employed to achieve such tasks.

The vast collection of SA methods can be broadly divided into two groups: local and global methods. In local sensitivity techniques, or one-at-a-time (OAT) techniques, the change in model output is measured by shifting a single factor from its nominal value while keeping the other factors fixed to their nominal value. A major drawback of this approach is that interactions among factors cannot be detected and non-linearities between input and output variables are difficult to assess (Muleta and Nicklow, 2005). A Global Sensitivity Analysis (GSA) explores more efficiently the multidimensional input space by varying all the factors simultaneously and investigating the variation of the output response as a result of all inputs and their possible interactions. Among classes of GSA methods, very often based on Monte Carlo methods, qualitative screening techniques are used for the investigation of models where more demanding quantitative methods are not affordable due to computational burden. GSA techniques include (1) elementary effect methods such as the Morris method (Campolongo et al., 2007, 2011; Morris, 1991; Pujol, 2009; Santiago et al., 2012), winding stairs (Jansen, 1999), latin hypercube-OAT (Van Griensven et al., 2006), etc. (2) variance-based techniques such as the Sobol' indices (Saltelli, 2002; Sobol', 1993), the Fourier amplitude sensitivity test (FAST) (Cukier et al., 1973; Saltelli et al., 1999), etc. and (3) metamodel-based methods that include regression or correlation based techniques such as the response surface methodology (RSM) and standardized regression coefficients (SRC) (Box and Draper, 1987; Helton and Davis, 2003; Sacks et al., 1989), high dimensional model representation (HDMR) (Li et al., 2002; Rabitz and Aliş, 1999), polynomial chaos expansion (PCE) (Blatman and Sudret, 2010b, 2011; Fajraoui et al., 2011; Sudret, 2008), etc. The elementary effect method is a derivative-based technique used in screening applications. It has the advantage to be efficient at low sample size but it does not allow the distinction between high-order effects of input factors and interactions between factors. In spite of their high computational cost, variance-based techniques are very flexible and the sensitivity indices are easy to interpret since they rely upon the decomposition of the variance of the output into fractions attributed to factors or sets of factors. Metamodel-based methods approximate the model under study with a mathematical expression aimed at capturing the characteristics of the relationship between the input factors and the output response. Depending on their setting they can dissociate for each input factor pure linear effects from high-order effects and from interaction effects at relatively low sample size. However, when dealing with strongly non-linear and complex systems the inaccuracy of the metamodel can lead to misinterpretation of the sensitivity indices.

The main issue in SA is that a given method can possibly lead to qualify an important factor as non-influential (Type I error) or conversely to identify a factor as significantly influent when it is not (Type II error). It becomes then essential to compare the results obtained from various SA techniques before disqualifying any input factor. As part of the problem, the computation of partial differential equations of groundwater and mass transport requiring numerical solution generally involves a computational demand that precludes the realization of a great number of model evaluations. Hence, experimenters should opt for a thorough exploration of the uncertain input space with a limited number of runs in order to

capture the complexity of the inputs-output relationship and minimize the occurrence of Type I and Type II errors. Latin Hypercube Designs (LHD) are a class of space-filling designs introduced in 1979 by McKay et al. (1979) and further optimized according to various criteria (Dette and Pepelyshev, 2010). Many examples of LHD applications can be found in the frame of sensitivity and uncertainty analyses (Van Griensven et al., 2006; Helton and Davis, 2003; Manache and Melching, 2004; Storlie and Helton, 2008a,b). The articles from Campolongo and Saltelli (1997) and Drouet et al. (2011) give constructive comparisons of the performances of SA techniques applied on environmental models of gas emissions to the atmosphere. Both studies showed the efficiency of the derivative-based Morris method at low sample size in comparison with the Sobol' and Extended FAST (EFAST) methods. Regarding groundwater flow and mass transport modeling, Malaguerra et al. (2013) used the Morris method to assess the influence of the geometry and parameterization of a groundwater model simulating the transport of pesticides through the underground media. In the context of nuclear waste disposal many studies can be found in the literature (Helton, 1993; Helton et al., 2000a,b, 2012; Helton and Iman, 1982; Helton et al., 1985). Draper et al. (1999) used a regression-based SA and the EFAST method to predict the radiological dose for humans using a hypothetical underground repository model. Recently, Ciriello et al. (2013) used a PCE metamodel to compute the Sobol' indices for the parameters from a theoretical radionuclide migration through an heterogeneous groundwater model. Most of the above-mentioned studies used a simplified numerical model of groundwater processes (*e.g.* 2 dimensional geometry, homogenous parameters, etc.). However, the use of a complex 3D integrated model is a challenge.

The objectives of the SA applied to Andra's hydrogeological model presented in this chapter are (1) to understand the behavior of the multi-layered system in terms of advection-dispersion of solute throughout the model's domain, (2) to propagate the uncertainty of hydro-dispersive parameters on the model output, and (3) to assess the relative sensitivity of the model output with respect to the hydro-dispersive parameters. The study focuses on the uncertainty relative to couples of hydro-dispersive parameters (the hydraulic conductivity K and the porosity ϕ) in fourteen hydrogeological layers in the local-scale Andra Meuse/Haute-Marne numerical model (ANDRA, 2012a; Deman et al., 2012, 2013). The output variable under study is the average time for a water molecule released from the potential repository emplacement to reach the limits of the model. This output is referred to as mean lifetime expectancy (MLE) and is defined by Cornaton and Perrochet (2006b,a) and Kazemi et al. (2006). The computational cost of the model output precludes the use of variance-based techniques. A screening exercise is then carried out at low sample size by means of the elementary effect method and a comparison is made with regression-based techniques.

The structure of the chapter is as follows. First the structure and parameterization of the numerical model are introduced and the mathematical formulation of the MLE is presented. Then the uncertain hydro-dispersive parameters are listed, the design of experiment using maximin-Latin Hypercube Design (Johnson et al., 1990) is established and the methodologies for the computation of sensitivity indices with the elementary effect and regression-based methods are presented. In the third part the sensitivity indices are interpreted and an insight on the general behavior of the multi-layered system is given. Results are then discusses in the last section of the present chapter with some recommendations and perspectives for possible future work.

6.2 The numerical groundwater flow and mass transport model

6.2.1 Structure and parameterization of the numerical model

The geology of the Paris basin consists of a succession of sedimentary layers covering pre-Cambrian bedrock with more than 3000 m thickness at the center of the basin. The Middle to Upper Jurassic succession encompasses a 150 m thick clay-rich layer from Callovo-Oxfordian (COX) age in the middle of which Andra has established the Underground Research Laboratory (URL) and conducted a number of studies to assess the feasibility of a deep geological repository for high-level radioactive wastes. Geo-hydrological data resulting from a great number of deep investigation boreholes, 400 m to 2000 m in depth, drilled over a 400 km^2 sector around the experimental site of Bure allowed to describe the

groundwater flow and the spatial variability of the hydrodynamic properties of the two main sedimentary formations embedding the COX layer (Linard et al., 2011): the Dogger and Oxfordian sequences, respectively underlying and overlying the COX. The investigation of these two sequences revealed the presence of three main limestone aquifers from Bajocian, Bathonian (Dogger sequence) and Rauracian-Sequanian (Oxfordian sequence) ages (Table 6.1), separated by semipermeable layers.

Gathering and integrating data from borehole logs, seismic profiles and in-situ and laboratory measurements of material properties lead first to a 3-dimensions geological model and later a 3D Finite Elements (FE) integrated regional-local groundwater flow model for the entire Paris basin (Figure 6.1). The model incorporates 27 geological layers from the Lower Triassic to the surface (Tertiary formation) and includes a large number of discontinuities (fractures, faults and troughs) as well as surface hydrographic network. The flow boundary conditions are mainly represented by fixed water levels on specific river network nodes and an average 240 mm/year recharge is integrated by applying source terms on the model's surface.

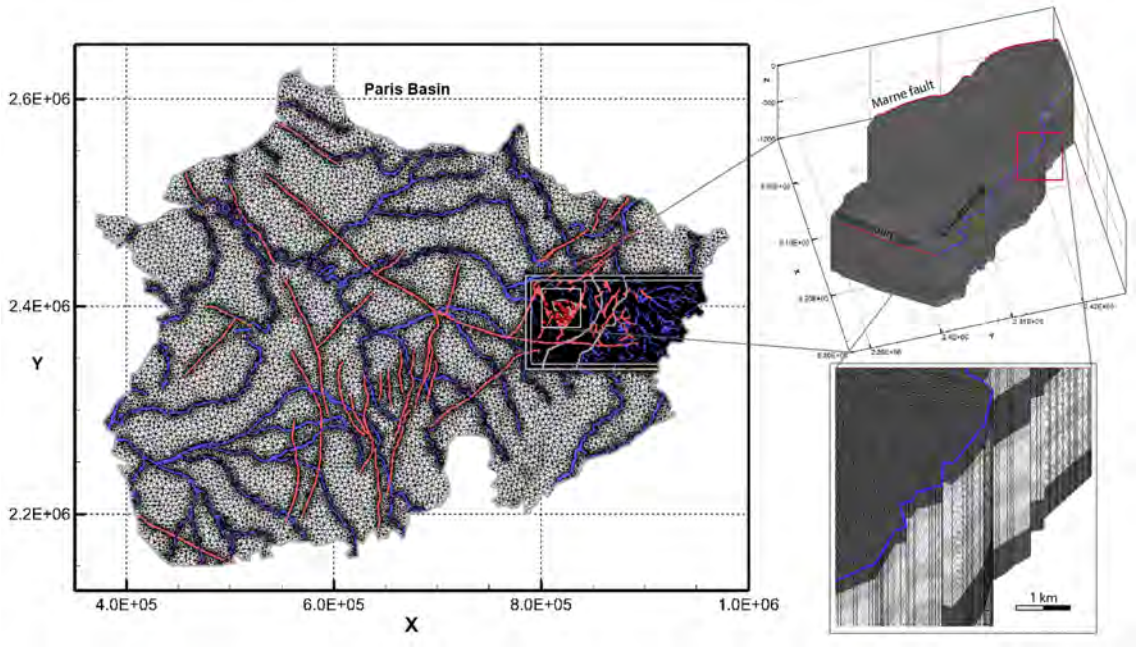

Figure 6.1: Left: Finite elements mesh for the integrated regional-local scale model with focus on the sector-scale model. Refinement is applied on hydrographic networks (blue) and faults (red). Right-up: local scale model with identification of the lateral limits. Right-down: the mesh refinement and regularity is illustrated.

Initial values of hydraulic conductivity and porosity for each of the 27 layers were derived from in-situ and laboratory measurements (ANDRA, 2005). The inverse modeling algorithm PEST (Doherty, 2005) was then used to calibrate the hydro-dispersive parameters with respect to more than 2000 hydraulic head measurements and the maps of observed flow fields . The resulting model and the associated parameters distributions was validated and referred to as the nominal case. More importantly, the region-scale nominal case model was used to supply realistic boundary conditions to the local model used in the present work.

The identification of potential release zones to the surface has allowed the extraction of a 250 km^2 area around the site of Bure from the region-scale model. The local model is bounded to the North-West by the Marne fault, the main potential outlet of the aquifer system, to the North-East by the Ornain valley, to the South-East by the Gondrecourt faults and to the South-West by the Marne valley (Figure 6.1 and Figure 6.2). It comprises 16 layers out of the 27 layers from the regional model and is limited vertically by two semipermeable layers in order to encompass only the most important aquifer formations. The local model was highly refined to perform flow and solute transport simulations and a high discretization of the COX formation is also enforced to improve the stability of the numerical solution of the transport

equation. In summary, the local model consists in 143 numerical layers comprising more than 8 million nodes for about 16 million elements which average thicknesses equal to 5m for a horizontal resolution of 50 to 150 m.

Fixed head boundary conditions were derived from the flow solution of the integrated regional-local model and are applied to nodes located on the external faces of the local model. Table 6.1 gives the nominal values for K and ϕ in the 16 hydrogeological layers composing the local model.

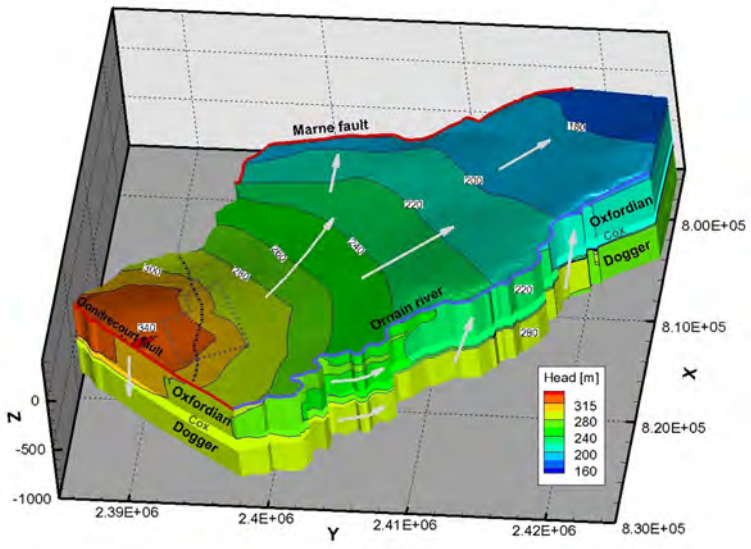

Figure 6.2: Distribution of the hydraulic head [m] on the local-scale model. The black dotted line shows the flow inversion line and the vertical projection of the potential repository emplacement is displayed with a gray dotted-line polygon.(Vertical exaggeration:20).

Table 6.1: nominal values for the hydraulic conductivity (K) and porosity (ϕ) of the 16 hydrogeological layers composing the local model.

	Hydrogeological unit	Type	ID[a]	ϕ [-]	K [m/s]
Malm	Kimmeridgian	Semi-permeable	*NC*	0.1320	9.38E−11
Oxfordian	Top of upper Sequanian	Aquifer	14	0.1585	4.66E−07
	Base of upper Sequanian	Aquifer	13	0.1615	1.16E−06
	Lower Sequanian	Semi-permeable	12	0.1756	4.14E−08
	Upper Rauracian	Aquifer	11	0.1867	2.96E−07
	Lower Rauracian	Aquifer	10	0.2068	1.05E−07
	Upper Argovian	Semi-permeable	9	0.2103	4.64E−11
COX	Lower Argovian	Semi-permeable	8	0.1705	8.00E−13
	Upper Callovian	Semi-permeable	7	0.1681	1.92E−15
Dogger	Lower Callovian (Dalle Nacré)	Semi-permeable	6	0.2043	3.90E−08
	Mid-upper Bathonian	Aquifer	5	0.2043	7.81E−06
	Lower Bathonian	Aquifer	4	0.1999	3.90E−06
	Marnes de Longwy	Semi-permeable	3	0.1878	4.64E−11
	Upper Bajocian	Aquifer	2	0.1878	1.95E−06
	Lower Bajocian	Semi-permeable	1	0.2089	5.79E−08
Lias	Toarcian	Semi-permeable	*NC*	0.2059	1.63E−12

[a] Identification number of the geological layer in the scope of the sensitivity analysis(NC:not considered in the SA exercise).

6.2.2 Model Outputs : Flow and Lifetime Expectancy

Instead of solving time-consuming transient state transport equation, Cornaton and Perrochet (2006b,a) and Kazemi et al. (2006) proposed an alternative by solving a backward-in-time equation providing the lifetime expectancy probability distribution for any single point within a domain under stationary flow conditions. The mean lifetime expectancy (MLE) is the time required for a water molecule, taken somewhere in the model, to reach an outlet of the aquifer system. It equals therefore zero at an outlet and grows as the molecule moves back towards an inlet limit. The formulation is based on the advective-dispersive transport equation (ADE) and it applies to conservative and non-reactive tracers. More precisely, the forward ADE is assimilated to the Fokker-Planck (or forward Kolmogorov) equation analyzing the random motion of solute particles (Uffink, 1989). Hence, the expected resident concentration of a conservative tracer is taken as the probability density function for the location of a particle, at any time. The reader is referred to the articles from Cornaton and Perrochet (2006b,a) for a detailed description of the equations governing the lifetime expectancy probability density function.

Let us consider an aquifer domain in which the velocity field is given by the Darcy law:

$$\mathbf{q} = -\mathbf{K}\,\nabla H \tag{6.1}$$

where $\mathbf{q}$ is the flux vector [L T^{-1}], H is the hydraulic head [L], and $\mathbf{K}$ is the tensor of hydraulic conductivity [L T^{-1}].

Considering a forward divergence-free flow field ($\nabla \cdot \mathbf{q} = 0$), the flow direction is reversed: the flux initially equal to $\mathbf{q}$ becomes -$\mathbf{q}$. The backward transport equation governing the lifetime expectancy PDF at any position x, $g_E(x,t)$, is (Cornaton and Perrochet, 2006b,a; Kazemi et al., 2006):

$$\phi \frac{\partial g_E}{\partial t} = \nabla \cdot (\mathbf{q}\, g_E + \mathbf{D}\, \nabla g_E) \tag{6.2}$$

where ϕ is the effective porosity [-] and where $\mathbf{D}$ [L^2 T^{-1}] is the dispersion tensor:

$$\mathbf{D} = (\alpha_L - \alpha_T)\frac{\mathbf{q} \otimes \mathbf{q}}{||\mathbf{q}||} \;+\; \alpha_T\, ||\mathbf{q}||\, \mathbf{I} \;+\; \phi\, D_m\, \mathbf{I} \tag{6.3}$$

where α_L and α_T are the longitudinal and transversal dispersivities [L] respectively, D_m is the coefficient of molecular diffusion [L^2 T^{-1}] and $\mathbf{I}$ is the identity matrix.

The mean lifetime expectancy $E(x)$ at any position x is obtained by taking the first moment from equation 6.2:

$$-\nabla \cdot (\mathbf{q}\, E + \mathbf{D}\, \nabla E) = \phi \tag{6.4}$$

where it can be seen that the porosity acts as the sink term in the aging process.

The steady-state equations (6.1 - 6.4) were solved with the finite element simulator *GroundWater* (Cornaton, 2007). The flow and mass transport differential equations are solved according to the standard Finite Element Galerkin and the Control-Volume Finite Element techniques. A single simulation run takes about 30 minutes using a parallel solver with 6 CPU using the lx24-amd64 architecture.

Flow solution around the site of Bure for the Dogger and Oxfordian aquifers display a general SSE to NNW horizontal flow direction (Linard et al., 2011). Besides, piezometric levels reveal a vertical flow inversion a few kilometers north-west of the Bure site (Figure 6.2). On the south-eastern part of the area groundwater flows from the Oxfordian toward the Dogger sequence, through the COX, while on the north-western part the waters flow upward.

In the context of our study a selection of 7212 model nodes in the center of the COX formation is aimed to represent the location of the repository. Given that the finite elements located in the repository domain have homogeneous volumes, the arithmetic mean of the MLE at the 7212 nodes was calculated. This average MLE stands for the model output response considered in the context of the SA developed in this chapter.

With regard to transport parameters, a mesh-size dependency with the longitudinal dispersivity is assigned. Using this strategy, the longitudinal dispersivity α_L is set for each mesh element equal to its equivalent diameter. Transverse dispersivity α_T is set to a tenth of the longitudinal dispersivity. The coefficient of molecular diffusion (D_m) is set to 2.3 x 10^{-9} m^2/s and corresponds to that of pure water (H_2O).

Figure 6.3 gives an insight of the lifetime expectancy distribution throughout the model in the nominal case. It takes approximately 2 million years for water molecules located in the potential repository to

reach an outlet of the model (Figure 6.3). Lifetime expectancies are lower in the Dogger and Oxfordian sequences where the relatively high permeabilities of their sedimentary formations favor fast advective fluxes. Because of their highly confining properties the transport process in the COX layers is essentially driven by diffusion. This feature is highlighted by the high values of MLE shown in Figure 6.3b.

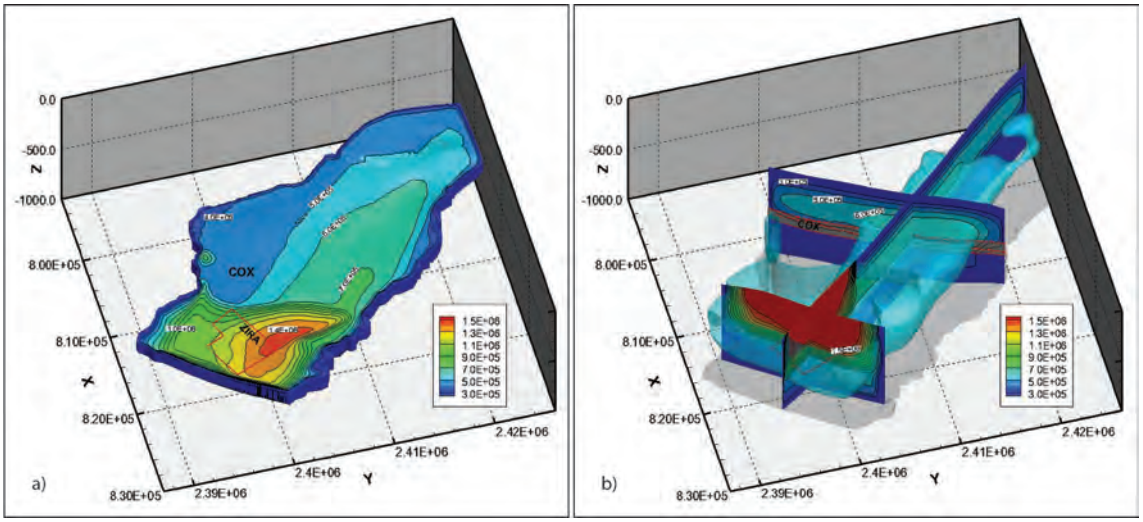

Figure 6.3: Mean lifetime expectancy for the nominal case. (a) 2D horizontal section on top of the COX sequence with a vertical projection of the potential repository emplacement. (b) 2D sections through the 3D volume of the local model.

6.3 Methodology of sensitivity analysis

6.3.1 Uncertain hydro-dispersive parameters

Within each hydrogeological layer considered in the model, the decimal logarithm of the hydraulic conductivity (K [L T^{-1}]) values as well as the natural porosity (ϕ [-]) values follow normal distributions. The Hagen-Poiseuille law for laminar flow through fractured media acknowledges a correlation between both parameters (Ford and Williams, 2007; Louis, 1985), hence parameters K and ϕ within a single layer must be taken jointly when achieving a perturbation of their nominal values (Table 6.1). In the following, the term "petrofacies" will refer to these couples of hydro-dispersive parameters and identification numbers (ID) are assigned to each layer investigated in the SA exercise. The reader should note that the Kimmeridgian and Toarcian layers, located respectively on top and bottom of the local model, are not considered (NC) in the SA exercise but are yet included in the numerical model.

The SA exercise consists in a perturbation of each petrofacies around their nominal value. Based on the observation of the joint distributions for both K and ϕ in each layer, a linear approximation of the Hagen-Poiseuille law can be assumed where the magnitude of the perturbation is minor. Accordingly, the logarithm of the multiplicative factor applied to the K values ($log(K_{mult})$) can be linearly correlated to the multiplicative factor applied to the ϕ values (ϕ_{mult}) using the following empirical relationship:

$$\phi_{mult} = 0.15\, log(K_{mult}) + 1 \tag{6.5}$$

A minor perturbation is assumed when the nominal hydraulic conductivity values are shifted by a factor which does not exceed 10, *i.e.* multiplied or divided by 10. Consequently, and using equation 6.5, the multiplicative factors applied to porosity values fall in [0.85 ; 1.15].

Space-filling designs use algorithms that purposely construct the experimental matrix such that the samples are uniformly spaced within the unit hypercube, thus avoiding clustering of sampling points in any region of the latter. Among the wide collection of space-filling designs the maximin Latin Hypercube

Design (MLHD) (Dette and Pepelyshev, 2010; Johnson et al., 1990) spreads out the experimental points by maximizing the minimum distance between any two points.

Considering the whole set of n experiments to carry out, each of the k input factors follows a uniform distribution $\mathcal{U}(0,1)$ where the sampled levels stand for quantiles of user-defined distributions. To comply with the observed statistical distributions of hydro-dispersive parameters in the model the sampled quantiles are associated to the CDF of a normal distribution $\mathcal{N}(0,1/3)$. Using these settings, and according to the *three-sigma rule* (also known as the *68-95-99.7 rule* or *empirical rule*), the major proportion of the converted samples lie in the interval [-1 ; 1]. To retrieve the multiplicative factors that apply to hydraulic conductivity values, these samples are taken as power exponents of 10. In other words, the normally distributed samples provided from the above sampling scheme are transformed such that the eventual experimental matrix contains a major proportion of samples lying in $[10^{-1}; 10^{1}]$ with a mean value equal to 10^{0}. Using equation 6.5 the corresponding multiplicative factors that apply to the porosity values are recovered and most belong to the interval [0.85 ; 1.15]. The normal distribution does not guarantee that all the multiplicative factors are bounded to the above-mentioned intervals for either K_{mult} or ϕ_{mult} but most are. In the event that a multiplicative factor for K (respectively ϕ) is much larger than 10^{1} (respectively 1.15) or much lower than 10^{-1} (respectively 0.85), the sampling process is reiterated.

6.3.2 Elementary Effects Methodology

The original Morris Method

The method originally proposed in 1991 by Morris (1991) enhanced by Campolongo et al. (2007) is a class of OAT screening technique that belongs to the class of derivative-based global sensitivity analysis (DGSA). By averaging multi-dimensional local measures, this method provides a global sensitivity measure capable of identifying the factors with (1) negligible effects, (2) linear and additive effects or (3) nonlinear and/or interaction effects (Saltelli et al., 2004). Assuming a model with k input factors, the k-dimensional input space Ω is discretized into a regular p-level grid, each level representing a quantile of the Cumulative Distribution Function (CDF) for factor x_i. A starting points $\mathbf{x}^*$ is randomly chosen within Ω and a so-called trajectory is drawn by shifting each factor, one-at-a-time, by a fixed increment Δ, leading to $k+1$ model runs. For each factor x_i, an Elementary Effect (EE_i) is defined as the ratio between the change in model output and the increment Δ:

$$EE_i = \frac{y(x_1, \ldots, x_i + \Delta, \ldots, x_k) - y(x_1, \ldots, x_i, \ldots, x_k)}{\Delta} \tag{6.6}$$

The procedure is repeated r times, considering different starting points $\mathbf{x}_j^*$, $j = 1, \ldots, r$, so that local sensitivities can be integrated to global sensitivity measures for each factor :

- the mean effect μ_i of factor x_i is computed as the average of its $EE_i^{(j)}$ and assesses the global influence of the factor:

$$\mu_i = \frac{1}{r} \sum_{j=1}^{r} EE_i^{(j)} \tag{6.7}$$

- In case of non-monotonicity, the elementary effects $EE_i^{(j)}$ can have opposite signs and cancel each other in the computation of the above sensitivity measure. The arithmetic mean of the absolute value of the $EE_i^{(j)}$ is also considered (Campolongo et al., 2007):

$$\mu_i^* = \frac{1}{r} \sum_{j=1}^{r} |EE_i^{(j)}| \tag{6.8}$$

- the standard deviation of the $EE_i^{(j)}$ provides a measure of how uniform the effects are by highlighting the presence or absence of non-linearities and/or interactions with other parameters:

$$\sigma_i = \sqrt{\frac{1}{r-1}\sum_{j=1}^{r}\left(EE_i^{(j)} - \mu_i\right)^2} \tag{6.9}$$

Factors with negligible effects are characterized by low values of μ_i^* and σ_i. Factors with linear effects present low values of σ_i and high values of μ_i^* while factors with non-linear and/or interaction effects display high values for both. The comparison of $|\mu_i|$ and μ_i^* gives an insight of the monotonicity of the output variable with respect to the input factor x_i, the closer the two variables, the higher the monotonicity.

A new sampling strategy and its application to the petrofacies screening

The procedure proposed in the present chapter is a combination of the Radial Sampling (RS) introduced in Campolongo et al. (2011) and the LH-OAT proposed by Van Griensven et al. (2006). The Latin Hypercube Radial Sampling (LH-RS) starts with a Latin Hypercube Design (here the MLHD) filling the input space and from each sample point $\mathbf{x}_j^*$ a radial trajectory is drawn by shifting each input factor, taken one at a time, by a random perturbation $\Delta_i^{(j)}$ that differs for each factor and for each trajectory. According to Campolongo et al. the use of an increment that is not fixed contributes to a better identification of the irregularity of the output response with respect to the input variables. Besides, no discretization of Ω is achieved in order to leave more flexibility to the design of the RS trajectories. The sensitivity measures are calculated the same way. Figure 6.4 provides a comparison of the designs of trajectories when using the original Morris method and the new LH-RS method proposed in this chapter.

By designing r starting points $\mathbf{x}_j^*$ with a MLHD considering k factors the sampling strategy leads to $N = r(k+1)$ simulations runs. An iterative procedure was introduced in the design of radial trajectories in order to obtain the best spread of sampling points in Ω. The procedure is based on the calculation of distances between trajectories. Using the strategy proposed by Ruano et al. (2012) iterations are executed on the design of radial trajectories, starting with the same set of points $\mathbf{x}_j^*$, until an optimal spread of sampling points is achieved. The resulting experimental matrix, containing quantiles distributed on [0 ; 1], is converted into multiplicative factors according to the procedure presented in the section 6.3.1.

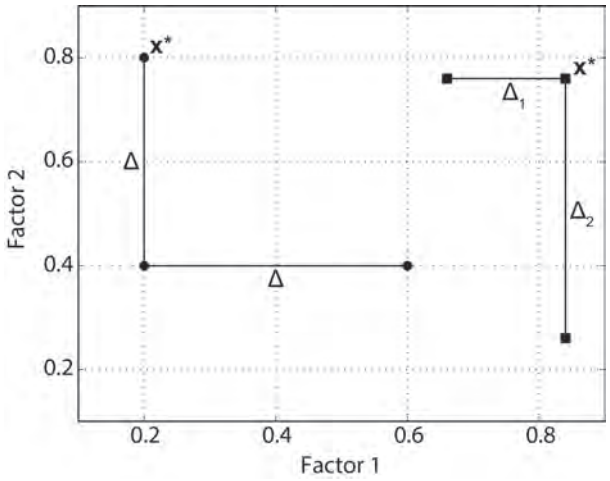

Figure 6.4: illustration with 2 factors of trajectory designs for the Elementary Effect methodology using Morris strategy with fixed increment and discretization of the input space (black dots) and LH-RS strategy with random increments and no discretization (black squares). The $\mathbf{x}^*$ are the initial points for the design of each trajectory.

6.3.3 Regression-based sensitivity analyses

Standardized Regression Coefficients (SRC)

A regression model is a mathematical approximation (or *metamodel*) of the true function $f(\mathbf{x})$ which quality is assessed by the coefficient of multiple determination R^2 (Dodge, 2008). This well-known statistic indicates the amount of variance of the output explained by the regression model and is distributed on [0 , 1]. In matrix notation the multivariate regression equation is written:

$$\mathbf{y} = \boldsymbol{\mathcal{X}}\ \boldsymbol{\beta}\ + \boldsymbol{\varepsilon} \tag{6.10}$$

where $\mathbf{y}$ is the vector of the "true" output responses, $\boldsymbol{\mathcal{X}}$ is the matrix of regressors, $\boldsymbol{\beta}$. is the vector of the regression coefficients, and $\boldsymbol{\varepsilon}$ is the vector of random errors. Saltelli et al. (2006) suggested that a value of R^2 larger than 0.7, indicating that less than 30% of the variance of the output remains unexplained by the regression, is acceptable for a sensitivity analysis based on regression measures.

A regression equation is said to be linear when only the input variables are considered for its construction. When the assumption of linearity between input factors and output response is accepted ($R^2 > 0.7$) the standardization of the coefficients of the linear regression equation can be used as a tool for SA (Helton and Davis, 2003; Storlie and Helton, 2008a; Hamby, 1994; Iooss et al., 2006; Xu and Gertner, 2008). The SRC for the input factor x_i is computed as follows:

$$SRC_i = \mathbf{b}_i \sqrt{\frac{\mathbb{V}(x_i)}{\mathbb{V}(\mathbf{y})}} \tag{6.11}$$

where $\mathbf{b}_i$ is the estimated regression coefficient for the input factor x_i and $\mathbf{Y}$ is the vector of "true" responses. All the SRCs are distributed on the interval [-1 , 1] and the closer the value of SRC_i to zero the lower the influence of parameter x_i on the output. The sign of a SRC indicates whether the input and output variable are proportionally related (*i.e.* positive sign), or inversely related (*i.e.* negative sign).

Response Surface Model (RSM) - Stepwise Regression

A response surface model (RSM) (Box and Draper, 1987; Dodge, 2008; Draper and Smith, 1998) is a regression equation which may involve high-order terms as well as interaction terms to better fit the response data in the event of strong non-linearities or interactions between factors in the inputs-output relationship. Stepwise procedures (Storlie and Helton, 2008a) are techniques used to select the set of regression terms that provides the best fit of the regression function upon the response data. Broadly speaking, stepwise procedures consist in sequentially adding or removing one or more terms from a regression equation and to analyze the accuracy of the fit using the coefficient of multiple determination. Since the R^2 statistic is subject to many disadvantages in the performance of a sequential regression model construction, experimenters frequently use an adjusted coefficient of multiple determination R_{adj} (Carley et al., 2004; Seber, 1977; Manache and Melching, 2008):

$$R_{adj} = 1 - \frac{n-1}{n-p}(1 - R^2) \tag{6.12}$$

where n is the number of output response (or model runs) and p the number of regression coefficients considered in the regression model. The purpose of a stepwise procedure is to generate a regression model that only includes terms significantly reducing the unexplained variance. Similar to the SRCs, the magnitude of the regression coefficients gives an indication of the influence of the associated regression terms on the output response. The sign of a coefficient also indicates whether the associated term is proportionally or inversely related to the output response.

6.3.4 Application to the screening of petrofacies of the local model

In the context of our study a set of $r = 20$ starting points $\mathbf{x}_j^*$ is designed with a MLHD. Considering k =14 factors the LH-RS strategy led to $N = r(k + 1) = 300$ simulations runs. Each sampled point led to a petrofacies combination using the procedure presented in section 6.3.1. The corresponding output responses were used to compute the sensitivity indices with the elementary effect methodology.

Another design of 300 samples was built purely with the MLHD and the corresponding output responses were used to construct the regression and RSM models and calculate the sensitivity indices.

Even with different sampling schemes it is assumed that 300 realizations for each design are sufficient to capture the main features of the model. The simulations of groundwater flow and mass transport were executed concurrently on a 128-processor Linux cluster where a single simulation run takes about 30 minutes using a parallel solver with 6 CPU using the lx24-amd64 architecture.

6.3.5 Savage scores

The objective of a screening exercise is essentially to determine the set of factors that mainly drive a specific phenomenon, but also the set that has no significant effect on the variable under study. It becomes then of importance to compare different SA methods by measuring their degree of agreement. A commonly used tool is the rank transformation, in this procedure the sensitivity indices are simply replaced by their corresponding ranks, *i.e.* rank 1 will be assigned to the most sensitive parameter, rank 2 to the second most sensitive, and so on. For the ranking of parameters with the Elementary Effect method the sensitivity index μ_i^* is used since it stands for a sensitivity measure of the overall influence of the factor x_i on the output response.

The Savage scores are indices computed on ranks and can be employed for the comparison of results obtained from various SA methods (Campolongo and Saltelli, 1997). The indices are calculated as follows:

$$s_i = \sum_{j=w}^{k} \frac{1}{j} \tag{6.13}$$

where w is the rank assigned to an input factor according to the SA method employed. The Pearson correlation measure is then used as an indicator of the agreement between methods.

6.4 Results

6.4.1 Elementary Effects

Results of the EE method are presented in Figure 6.5 and Table 6.2. Figure 6.5 displays the μ_i^* statistics versus the standard deviations σ_i of the EEs for each parameter x_i, where the petrofacies are identified by their ID number. Table 6.2 gives the three sensitivity measures calculated with equation 6.6 - 6.9. A first observation arising from this analysis is that petrofacies having a strong overall influence on the MLE (high μ_i^* value) are also involved in strong interactions with other petrofacies and/or have high-order effects on the output response (high σ_i value); in Figure 6.5 the points lie on the diagonal. Second, the comparison of $|\mu_i|$ and μ_i^* suggests near-monotonous relationship between inputs and output variables (Table 6.2).

The petrofacies P14 has the largest σ_i value, which is also captured in the overall effect sensitivity measure μ_i^*. This makes the top of the Upper Sequanian formation the most influential petrofacies on the MLE according to the EE method. This characteristic is consistent with the general behavior of the model: in the north-western part of the model the groundwater flows upward (Figure 6.2) and higher volumes can potentially leave the model from its upper limit if the confining properties of the top layer are reduced.

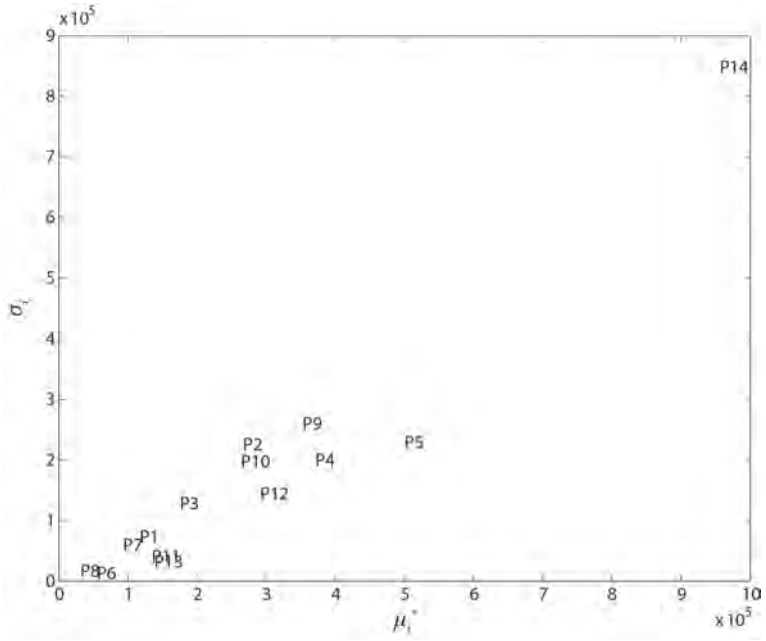

Figure 6.5: Sensitivity measures using the Elementary Effects method for the 14 petrofacies of the local model. Petrofacies are identified by their ID number (see Table 6.1).

Petrofacies from the Bathonian sequence (P4 and P5) are highly sensitive due to the strong advective fluxes occurring in these formations; their hydro-dispersive properties can highly reduce the MLE, as revealed by their high and negatively inclined μ_i values (Table 6.2).

The MLE is inversely related to the petrofacies of the Upper Argovian (P9) semipermeable layer (Table 6.2). This feature is consistent with its confining properties and the proximity of the Rauracian aquifers resting directly above. Indeed, a raise of its hydraulic conductivity facilitates the groundwater fluxes toward the overlying aquifers where advective fluxes reduce the MLE.

Another interesting observation concerns the uncertainty regarding the hydro-dispersive parameters of the semipermeable layers from Lower Bajocian (P1), Marnes de Longwy (P3), Callovian (P6 and P7) and Lower Argovian (P8) which present low sensitivity indices.

Given the general flow trend, where a wide region of the model is governed by ascendant fluxes, and the depth of the Lower Bajocian layer with respect to the COX layer, most of the groundwater travels through the overlying formations which have little retarding effects. The retardation effect of the thin clay layer named Marnes de Longwy (P3) is negligible since it is located between two aquifers, from Bajocian and Bathonian ages, where advective fluxes dominate. Similarly, raising the hydro-dispersive properties of the Lower Callovian (Dalle Nacrée) layer can reduce the MLE (negative μ values) by enhancing the advective-diffusive fluxes toward the Bathonian sequence. However, this thin layer does not manifest a significant influence on the output response.

The petrofacies of the COX formation also have little, inversely related, influence on the MLE. Since diffusion is the dominant transport process in these layers, increasing their very low hydraulic conductivity does not affect the MLE compared to advection-dominant transport found in aquifers.

The low sensitivity indices of the aquifers from Upper Rauracian (P11) and the base of the Upper Sequanian (P13) could be related to their relative positions on either side of the semipermeable layer from Lower Sequanian. Indeed the latter has high sensitivity indices because of its confining properties which prevent waters from flowing upward to the upper limit of the model.

Table 6.2: values of the sensitivity measures, ranks and Savage scores obtained with the EE and the SRC methods

Petrofacies	EE method μ	EE method μ^*	EE method σ	EE method ranks	EE method Savage scores	SRC	SRC ranks	SRC Savage scores
P1	8.06E+04	1.17E+05	7.21E+04	11	0.32	-0.0294	10	0.42
P2	1.96E+05	2.67E+05	2.25E+05	6	0.97	-0.1083	9	0.53
P3	5.83E+04	1.75E+05	1.27E+05	8	0.66	0.0262	11	0.32
P4	-3.07E+05	3.71E+05	1.99E+05	3	1.75	-0.3071	3	1.75
P5	-4.36E+05	5.00E+05	2.28E+05	2	2.25	-0.7133	1	3.25
P6	-4.48E+04	5.52E+04	1.23E+04	13	0.15	-0.1178	8	0.66
P7	2.33E+04	9.31E+04	5.90E+04	12	0.23	0.0015	14	0.07
P8	2.56E+04	3.12E+04	1.59E+04	14	0.07	0.0121	12	0.23
P9	-2.42E+05	3.53E+05	2.59E+05	4	1.42	0.0100	13	0.15
P10	1.79E+05	2.64E+05	1.97E+05	7	0.80	-0.1252	7	0.80
P11	-1.19E+05	1.34E+05	3.95E+04	10	0.42	-0.1792	6	0.97
P12	-1.83E+05	2.91E+05	1.43E+05	5	1.17	-0.3314	2	2.25
P13	-1.30E+05	1.38E+05	3.15E+04	9	0.53	-0.2001	5	1.17
P14	-8.96E+05	9.76E+05	8.47E+05	1	3.25	-0.2864	4	1.42

6.4.2 Standardized Regression Coefficients

A multiple linear regression model was fitted on the obtained responses and yielded an R^2 statistic of 0.87. This relatively high value of R^2 validates the assumption that the inputs-output relationship is pseudo-linear and the use of SRC for SA purpose is adequate. Values and associated ranks of the SRC_i are given in Table 6.2. When focusing on the 5 petrofacies having the highest sensitivity measures, both μ_i^* and SRC_i display the same set except for one. The EE method includes the petrofacies of the Upper Argovian (P9) while the SRC considers the petrofacies of the base of the Upper Sequanian (P13). This divergence could be explained by the specificities of each method: unlike the EE method, the SRC method relies on a linear approximation of the true function and, with a $R^2 = 0.87$, a proportion of 13% of the variance of the output remains unexplained by the multi-linear regression. This could possibly underestimate or overestimate the overall sensitivity of a given factor. However, both methods clearly identify the petrofacies of the Bathonian sequence (P4 and P5) as parameters having a strong influence on the MLE.

It is interesting to note that both methods agree on the lesser effects of the hydro-dispersive parameters of the COX layers on the output response. As mentioned previously, diffusive fluxes dominate the transport process in these formations and a modification of their very low hydraulic conductivity does not have a significant impact on the travel time of water molecules from the potential repository emplacement. Like the EE method, the SRC method acknowledges the strong influence of the petrofacies of the top of the Upper Sequanian layer (P14), reducing the MLE with fluxes oriented toward the upper limit of the model.

6.4.3 Savage scores

The Pearson correlation measure on the Savage scores obtained for the 14 factors with both the EE and SRC methods displays a value of 0.61, which indicates a rather good agreement between the two sensitivity measures. The correlation is investigated in Figure 6.6 and the values of Savage scores are given in Table 6.2. A good agreement is observed for the ranking of petrofacies P4, P5, P12 and also for the parameters displaying lesser influence on the output (*i.e.* P1, P7, and P8). A larger disagreement between methods is observed for petrofacies P14 and P9. This could be explained by the presence of high-order and/or interactions effects which the SRC method fails at identifying whereas the sensitivity measure μ_i^* incorporates (Figure 6.5). These features are investigated in the following section with help of the Response Surface Methodology (RSM).

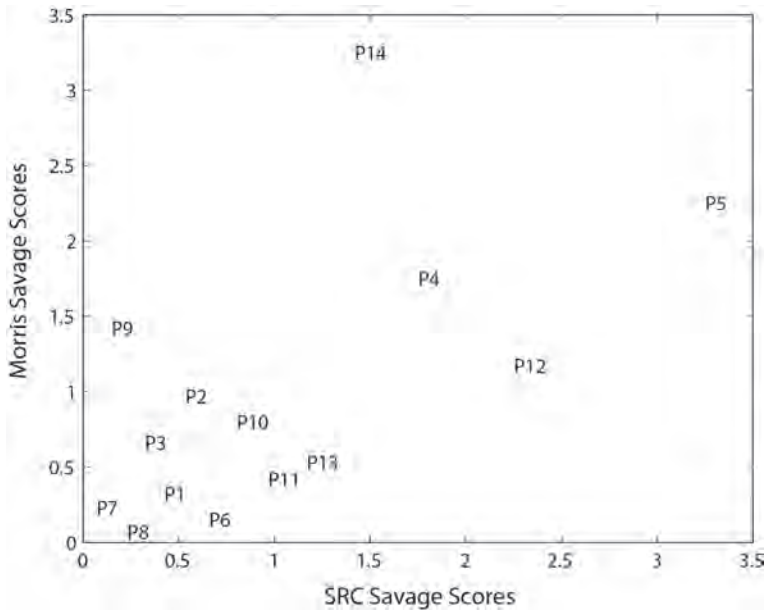

Figure 6.6: cross-validation by Savages Scores for the sensitivity measures obtained with the EE and SRC methods.

6.4.4 Response Surface Methodology - Stepwise Regression

A RSM was built upon the output responses to include high-order and interaction terms. According to expert judgment, interactions between hydrogeological layers that are not adjacent are unlikely to occur, especially if they are not linked. Hence, the regression matrix should only include interaction terms between petrofacies of adjacent layers; which led to 13 interaction terms. Second and third order effects of petrofacies on the output response are highly expected, the corresponding terms have been included in the regression matrix. The resulting mathematical formulation consists of 56 terms, including a constant term, and is of the form of equation 6.10. The associated adjusted coefficient of determination is R_{adj} = 0.929. The Stepwise procedure was applied on this RSM and yielded a model comprising 36 terms, including the constant term. The latter produces a statistic slightly better than with the full regression model; with a R_{adj} = 0.932. The remaining 7% of unexplained variance might be due to higher-order effects or interactions which were not considered; however these aspects are not investigated here. Figure 6.7 gives a ranking of the regression terms according to the magnitude of their associated regression coefficients $\mathbf{b}_i$.

The main feature arising from the observation of the coefficients of the RSM is the presence of strong high-order terms for most of the petrofacies considered in the study. In particular, the petrofacies of the Bathonian sequence (P4 and P5) exhibit strong first, second and third orders effects which dominate the set of sensitive parameters. The results show a positively defined regression coefficient associated to the interaction term P4 - P5 (Figure 6.7).

The petrofacies of the top of the Upper Sequanian (P14), the Lower Sequanian (P12) and the Lower Rauracian (P10) also strongly influence the model's response with linear, and high-orders effects. The three layers belong to the Oxfordian sequence where, as a result of the ascending water fluxes, most of the solute flows toward the model limits. By raising their hydro-dispersive parameters the solute transport is facilitated and the MLE decreases. The linear and high-order effects of the "Marnes de Longwy" sequence (P3) are also captured. Assigning strongly confining properties to this layer decreases the time required for water molecules from the potential repository emplacement to reach an outlet limit.

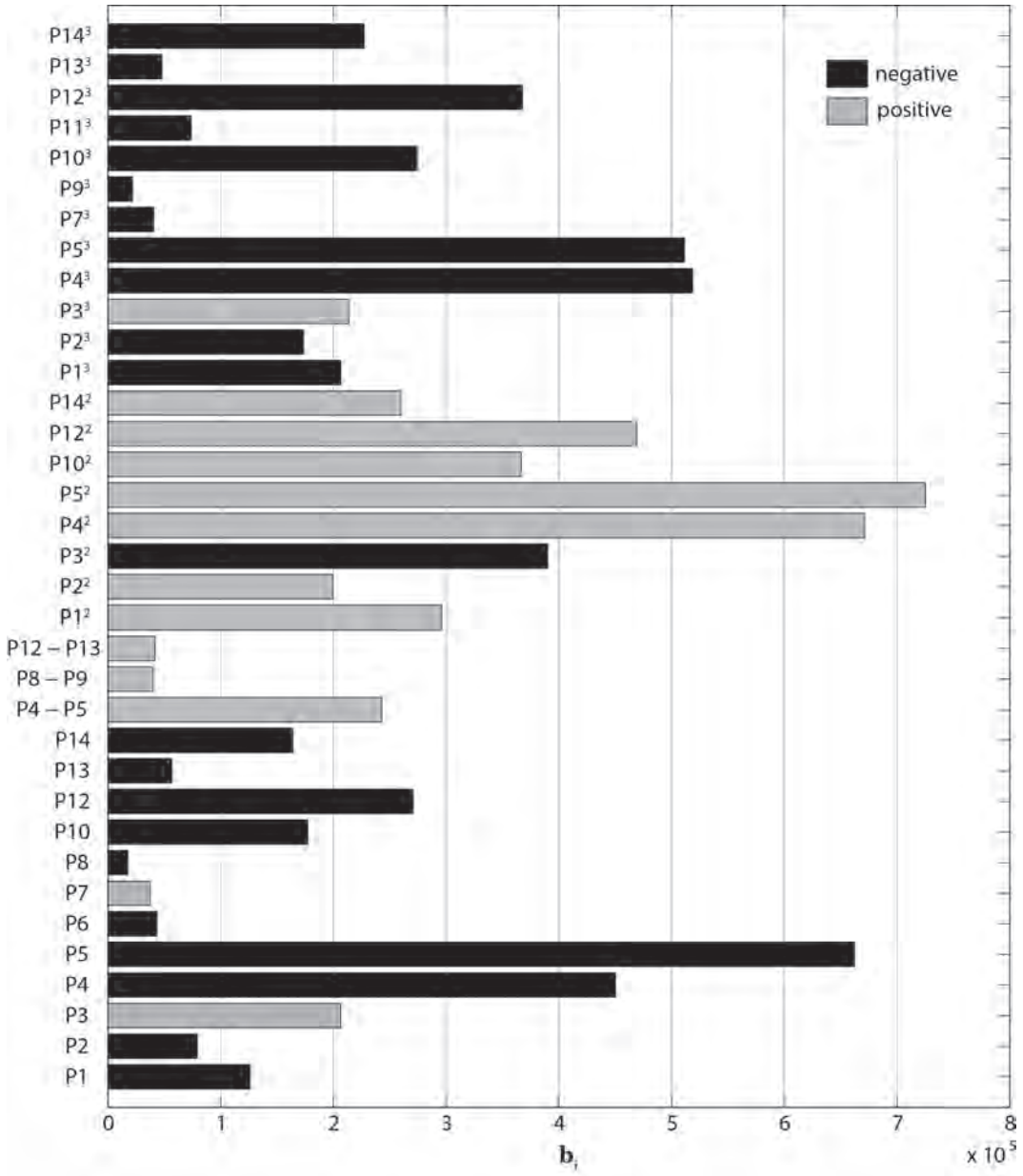

Figure 6.7: histogram of the magnitude of the regression coefficients from the RSM obtained by stepwise procedure.

6.5 Conclusions

The present chapter serves as a preliminary study in the thorough exploration of the hydrogeological numerical model of Andra Meuse/Haute-Marne developed within the framework of the high and intermediate level long lived radioactive waste geological repository project. The computational cost of the numerical model introduced in the presented study is the main restriction to the performance of any sensitivity analysis.

In order to capture the main features of the transport process through the multi-layered system a sensitivity analysis was performed upon uncertain couples of hydro-dispersive parameters (the hydraulic conductivity K and the porosity ϕ) referred to as petrofacies. The variable under study is the mean lifetime expectancy (MLE) defined as the average time for a water molecule, taken from the potential repository emplacement volume, to reach an outlet of the model. The results from a screening exercise using the Elementary Effect methodology with a new sampling strategy, the Latin Hypercube Radial Sampling (LH-RS), were compared to those obtained with regression-based methods.

When considering the Oxfordian sequence, the 250 meters-thick Rauracian-Sequanian aquifer (P10 to P14) represents a great source of variability for the MLE and, according to the sign of their sensitivity indices, the petrofacies of these formations are inversely related to the latter. The transport mechanism being mainly advective in these entities, they can be interpreted as fast-flow paths that reduce the transit-time from the potential repository emplacement to an outlet of the model. Additionally, the RSM coupled with stepwise procedures (Figure 6.7) identified high-order effects of these petrofacies on the output under study. Within the Dogger sequence the two petrofacies of the Bathonian aquifers (P4 and P5) are the most overall sensitive formations with respect to their contribution to the variance of the model output, and both are characterized by large high-orders effects (Figure 6.7). Given the general groundwater flow gradient in the studied domain (Figure 6.2), fluxes crossing the potential repository emplacement enter the Bathonian aquifers where a relatively high advective flux reduces the MLE. In combination, or interaction, the effect is proportionally related to the MLE, which could indicate that, when high hydro-dispersive properties are attributed to both layers, dispersive processes increase and the MLE rises.

According to this study the semi-permeable layers exhibit very little effects on the MLE (Table 6.2 and Figure 6.7). Diffusive transport processes are very slow compared to advective processes, a change of porosity values (and consequently a change in the effective diffusion) in the semi-permeable layers modifies slightly the transit time to surrounding hydrogeological formations. It must be emphasized that layers with confining properties act as barriers where slow dispersive processes take place within their own volume.

The SA methods used in this study disagreed on the magnitude of the effect of the Upper Argovian semi-permeable layer (P9). The EE methodology identifies this petrofacies as part of the five most important factors in the model while regression-based methods barely capture its effect (Table 6.2 and Figure 6.7). Further study might be needed in order to thoroughly interpret its effect on solute transport through the multi-layered system.

In the present study some limitations are acknowledged. It might be of interest to propagate the uncertainty on the boundary conditions distribution throughout the model in order to estimate its influence on the general flow paths. To better capture the individual effects of the two hydro-dispersive parameters a posterior study might consider, for each layer, both parameters K and ϕ separately but assuming correlations between them. The definition of exclusive statistical distributions for each factor, instead of performing a uniform perturbation of their nominal values, should also be undertaken to better comply with field data distributions. Besides, the effective diffusion parameter in each layer could be taken into consideration for a more complete study.

Other SA techniques such as variance-based (Saltelli et al., 2004) could also been applied on the modeled response resulting from a mathematical model; using Polynomial Chaos Expansion for example (Ciriello et al., 2013; Blatman and Sudret, 2010b, 2011; Fajraoui et al., 2011; Sudret, 2008).

Chapter 7

Conclusions

7.1 Main results

This thesis presents thorough descriptions for a wide range of mathematical and statistical methods employed for the performance of uncertainty propagations (UP) within the frame of risk and global sensitivity analyses (GSA). The fields of application for such methods are vast and the present research work focused on relevant methods for the analysis of large and complex multi-layered numerical models of groundwater flow and mean lifetime expectancy. Therefore, the UP and GSA techniques proposed in the present thesis were selected with the goal of achieving accurate estimations at the lowest possible computational costs.

At low dimensionality (*i.e.* few uncertain factors), factorial designs yield estimations of the variability of the output response of interest at very-low costs. Besides, they can incorporate continuous and categorical factors. However, a limitation to these designs of experiment is that a strong assumption of linearity between the inputs and the output is considered. Space-filling designs, such as Latin Hypercube Designs (LHD) and Low-Discrepancy Sequences (LDS), sample uniformly the uncertainty ranges of the input factors and allow flexible sampling sizes. Besides they do not bear any assumption of linearity. However, they can hardly incorporate categorical factors. The GSA techniques presented in the present thesis can be divided into two categories: derivative-based and variance-based techniques. The main advantage of derivative-based methods is that sensitivity estimates are obtained at low computational-costs. The main limitation, however, is that only the global effects of input factors on the output response is estimated, precluding the individualisation of low-order from high-order effects for a given factor. Variance-based methods provide the partial variances of the output response distribution attributed to each factor and factor interaction, allowing the individualisation of low-order and high-order effects. However, the methods rely on large experimental designs, thus potentially high computational costs. Meta-modelling techniques employ a mathematical expression aimed at reproducing the behaviour of the "true" model. The metamodels can then substitute the costly model to perform UP an GSA at negligible computational costs. Polynomial regression techniques provide a simple, robust and flexible framework, Polynomial Chaos Expansions (PCE) metamodels employ more advanced mathematical formulations and allow a straightforward estimation of variance-based sensitivity indices. A major drawback of metamodels arises in the event of having very complex inputs-output relationships when the mathematical expression poorly reproduces the behaviour of the true model ; the UP and GSA deriving from the metamodel may then become unreliable.

It often occurs that numerical models of subsurface processes are computer-intensive and include a large number of uncertain variables. In general, few variables are principally responsible for the variability of the model outputs, and screening techniques are specifically dedicated to identifying the latter at low computational-costs. Chapter 3 compared the convergence rates, at increasing sample sizes, of three commonly employed GSA techniques : the Sobol' indices, the Morris importance measures and the *Derivative-based Global Sensitivity Measures* (DGSM), with regard to their ability to correctly individualise two sets of uncertain parameters (a set of significant and a set of insignificant parameters). A fourth measure was proposed as a combination of the Morris measure and the DGSM. The respective performances of the above techniques were tested upon three complex analytical test-functions and proved the relatively higher efficiency of the DGSM technique. When dealing with high-dimensionality, computationally-demanding numerical models, the theoretical study of Chapter 3 can help in the selection of a relevant method for excluding unimportant variables at low computational cost before achieving a more exhaustive sensitivity analysis.

The numerical models of groundwater flow and and mean lifetime expectancy employed in the present thesis for the applications of UP and GSA methods were related to the French project for the deep geological disposal for mid to long-lived radioactive wastes. In France, Andra is in charge of the engineering and development of an underground facility for the geological disposal of radioactive wastes in a 500m deep highly-confining layer (COX layer) in the subsurface of the Paris Basin. Within this frame, the uncertainty and sensitivity analysis for the flow rates and the mean lifetime expectancy (MLE) of groundwater in the subsurface of the eastern Paris Basin was carried out with the use of two hydrogeological numerical models: a synthetic 2D model and a high-resolution 3D model. The first model was employed for methodological applications of UP and GSA whereas a real-case application was performed upon the 3D model. Both models encompass a number of hydrogeological formations characterized by uncertainties regarding the spatial distributions of hydrodynamic and dispersion parameters ; the 2D model being a simplified version of the 3D model which considers realistic geometries, fractures, faults and spatial heterogeneities. The MLE is a statistical indicator of the average time required for a given solute, from any position in

the domain, to reach any boundary of the model's domain. The formulation of the lifetime expectancy incorporates the advection-dispersion-diffusion equation (ADE) such that the MLE is a relevant indicator in the frame of risk and safety analyses related to the geological disposal of radioactive wastes. Employing either numerical models, the statistical analysis of the variability of the MLE of water molecules departing from a specific zone in the COX layer was undertaken by propagating the uncertainties characterising hydrodynamic and dispersion parameters in the hydrogeological layers.

The study of Chapter 4 employed the 2D synthetic model for a methodological application of UP and GSA methods considering the MLE of water molecules from a target zone (TZ) as the output response of interest. Considering 15 hydrogeological layers with homogeneous parameters, the study analysed the sensitivity of the output response with respect to the uncertainty regarding anisotropy ratios and angles of the hydraulic conductivity tensors, the magnitude of hydraulic conductivity and porosity values, dispersion parameters and hydraulic gradients in the domain. Latin Hypercube Designs were applied for the UP, and sparse-PCE metamodels were employed to derive variance-based sensitivity indices. The methodology proved to be highly effective and flexible for identifying low and high-order effects of uncertain parameters at low computational costs. With respect to the large, conservative, uncertainty bounds considered in the study, the results showed that the longitudinal components of the hydraulic conductivity tensors in aquifer layers have a major contribution to the variability of the MLE in the TZ in comparison to the other uncertain parameters. Indeed, advective transport processes may be strong in these highly conductive layers, and it can greatly influence the transit time of solutes toward discharge boundaries of the model domain. Non-linear effects on the output response were identified, which highlights the balance between advective and dispersive transport processes occurring in certain ranges of permeability-porosity values. Semi-permeable formations encompassing the host layer have a relative influence on the variability of the MLE from the TZ. Advection and dispersion transport processes extending within their own volume raise the output response by retarding the solute intrusion into the more advective aquifer formations from the Oxfordian and Dogger sequences. Although some limitations are recognized, the study shed light on the necessity to define properly the spatial variability of hydraulic conductivity values in aquifer formations ; especially in the Bathonian (Dogger) and Rauracian-Sequanian (Oxfordian) formations, as their role prevail in the transport processes in the subsurface of the Paris Basin.

Chapter 5 studied the sensitivity of the MLE calculated from the TZ, and the outflowing rates at the Oxfordian and Dogger discharge boundaries, with respect to the uncertainty on heterogeneity parameters defining the spatial variability of permeability-porosity values in the Oxfordian and Dogger aquifer sequences. The 2D model was employed for a methodological application of UP and GSA considering uncertainty upon the means and variances of Gaussian distributions of hydraulic conductivity values in the sequences, longitudinal and vertical correlation lengths, and a categorical factor related to the occurrence of connected structures of high hydraulic conductivity values. A two-level Plackett-Burman (PB) design was employed for the UP. Due to the stochastic nature of heterogeneous fields generation, an ensemble of random fields was employed for each combination of uncertain parameters ; thus producing a distribution of values for each output response. From these distributions, the means and standard deviations were extracted, and their variability were analysed through a GSA relying on polynomial regression metamodels. This is one of the uncommon studies that considers the variability of statistical indices (means and variances) as input parameters and as output responses. The methodology proposed in Chapter 5 allowed the UP and GSA of both continuous and categorical factors at a very-low sample size. Since each experiment of the PB design had to be run with an ensemble of random heterogeneous fields, a very limited sample size was a major requirement to keep the computational burden low. Polynomial regression metamodels proved efficient in decomposing the variance of the model outputs as a function of the uncertain parameters and their interactions. With respect to the inputs' uncertainty bounds, the results proved that the extension of heterogeneous geological structures in the main flow direction, determined by the longitudinal correlation length, has a large effect on the variability of the distribution of the flow rates at the discharge boundaries of the aquifer sequences, and also on the variability of the distribution of the MLE calculated from the TZ. The means and variances of the distributions of permeability-porosity values in the aquifer sequences are also highly influencing the variability of the distributions of the model outputs. Besides, the parameter governing the spatial connectivity of high permeability-porosity values tends to homogenise the general behaviour of the model. Note however that the spatial variability of the parameters, associated to the method employed for the random generation of heterogeneous fields, is determinant especially at large correlation lengths and variances of the distributions of permeability-porosity values.

Results arising from the studies of Chapter 4 and Chapter 5 show that highly confining hydrogeological

layers, such as the COX claystone, are characterized by diffusive transport mechanisms responsible for the large time-scales observed in the MLE calculated from the TZ. The GSA results showed that the uncertainties characterizing permeability-porosity parameters in these layers have a negligible influence on the variability of the predictive values for the MLE of water molecules departing from the target zone. Besides, the hydraulic behaviour of the Oxfordian and Dogger aquifer sequences is clearly influenced by the presence of the COX layer limiting the groundwater fluxes between the two. The study of Chapter 5 also confirmed that the heterogeneity parameters of one of the sequences have little effect on the variability of the flow rates at the discharge boundary of the other sequence.

The real-case application on the high-resolution 3D hydrogeological model of the Meuse/Haute-Marne region in Chapter 6 developed a GSA upon the perturbation of the parameters from the calibrated model. The spatially distributed permeability-porosity values in each hydrogeological formation were simultaneously shifted by applying a multiplicative factor to the parameters' values in the entire layer. The output response of interest was the MLE of water molecules from a specific location inside the COX aimed at representing the potential site for the disposal of radioactive wastes. A LHD was employed for sampling the multiplicative factor to apply to each of the 14 layers considered in the study. Two GSA methods were employed: the Morris method and a regression-based decomposition of the variance of the model output. The UP and GSA methods proved to be highly efficient at low computational costs, yielding accurate sensitivity indices and allowing the identification of strong non-linearities in the inputs-output relationship. The variability of the MLE from the COX is strongly correlated to the uncertainty on the hydraulic conductivity values of aquifer formations from Bathonian and Rauracian-Sequanian. This confirms the estimations brought by the 2D synthetic model and validates the use of the latter for further methodological studies on the topic. According to the Morris measures, the variability of the output is influenced by strong high-order effects of permeability-porosity values in the semi-permeable layers encompassing the COX. However, an accurate estimation of these effects would require a more detailed analysis.

In summary, the variability of the MLE of water molecules from the potential site for the disposal of radioactive wastes in the Callovo-Oxfordian claystone in the subsurface of the eastern Paris Basin is mainly related to the uncertainties characterising advective transport processes occurring in the aquifer formations of the Oxfordian and Dogger sequences. A specific attention should then be paid in the definition of the spatial distribution of the hydraulic conductivity values in these aquifers, and also in the semi-permeable formations encompassing the COX layer. The formations closer to the potential host layer require a thorough parametrisation to expect further reductions of the variability of any output response related to the predictive modelling of radionuclide migration in the subsurface of the Paris Basin. With the numerical models employed in the present thesis, the effects of other advection-dispersion parameters may be disregarded in future applications of UP and GSA considering the MLE of water molecules in the potential site for the disposal of radioactive wastes.

The results exposed in the present thesis show the effectiveness, at low computational costs, of UP and GSA techniques for estimating the relative influence of uncertain parametrisation of geological structures on the variability of the MLE in the hydrogeological modelling of complex advective-dispersive processes. The various applications presented in this thesis are thought to be of great contribution for performing risk and safety analyses in relation to the geological disposal of radioactive wastes worldwide. The methodologies for UA and GSA employed in this work are assumed to be very profitable for various applications in the field of earth and water sciences when one is concerned about the variability upon the predictive modelling of complex surface and/or subsurface processes.

7.2 Further outlooks

In the works presented in this thesis, deterministic functions relating the hydraulic conductivity to the porosity were employed to circumvent the use of correlation functions. This strategy was undertaken also to reduce the computational burden by considering these two uncertain factors as a whole. Besides, the investigation of correlated uncertain parameters through sensitivity analysis techniques is a challenge that has only been recently tackled. For instance, Xu and Gertner (2008) proposed a regression-based technique to divide the correlated and uncorrelated contribution of an individual factor to the variance of the model output. However, their method relies on the linearisation of the input-output relationship, which is a strong assumption rarely validated in the hydrogeological modelling of transport processes. Extending the variance decomposition of the model output to the case with dependent input factors,

Kucherenko et al. (2012) proposed a general method for estimating first-order and total Sobol' indices. Still, the method is computationally intensive and an application on large hydrogeological models may be impracticable. Making use of meta-models, based on the High Dimensional Model Representation (HDMR) technique, Zuniga et al. (2013) proved the robustness of the variance decomposition through the coefficients of the polynomial functions for estimating Sobol' indices at low computational costs. Hence, with the 2D synthetic numerical model, the uncertainty regarding the correlated hydraulic conductivities and porosities may be analysed to determine the correlated and uncorrelated contributions to the variance of any output response of interest. This could be made at reasonable computational costs and provide insights on the relevance of decoupling both parameters in a later application on the high-resolution 3D model.

Another challenging field of interest in hydrogeological modelling is to make use of uncertainty propagation and meta-modelling techniques for calibration purpose. Within this frame, Razavi et al. (2012) provided a thorough comparison of two optimizers not involving meta-models and three meta-modelling optimizers using radial basis functions, kriging and neural networks. The application on four highly non-linear test functions and on two real-case studies of water resources modelling showed the relative inefficiency of meta-modelling optimizers in comparison to meta-modelling-independent ones, especially in cases where the response functions are highly non-linear. The authors concluded that *"meta-model-enabled optimizers can be developed that would almost always show computational budget dependent relative performance such that they would be preferred over any meta-model-independent optimizer for at least some limited range of reduced computational budgets"*. Thus, it might be of interest to confront some of the latest meta-modelling techniques, using *e.g.* Polynomial Chaos Expansions meta-models, with optimizers commonly employed for such tasks in calibration procedures upon complex hydrogeological numerical models. As part of the ANDRA project, Benabderrahmane et al. (2014) employed a LHS design coupled with a multivariate regression model to explore an objective function, comprising hydraulic heads and flow rates data, in a calibration exercise. Applying the methods on an extraction of the high-resolution 3D model of the Paris Basin, the outcomes were satisfactory although some theoretical tests and developments would be meaningful to reach higher performances. The methodologies and results are presented in a published article provided in Appendix E.

In conclusion, it must be mentioned that the results of any GSA can be subject to much variability depending on subjective choices regarding the model settings, the set of parameters and their uncertainty ranges. Type III errors, as defined by Saltelli et al. (2008), correspond to a framing error where the use of GSA techniques may lead to erroneous interpretations of the behaviour of the system under study. The subjectivity of the modeller in his choices for characterizing a given object should always be taken into account. Indeed, GSA techniques might also be applied to the most fundamental aspects of the problem, such as the conceptualisation of the model layout, the numerical integration schemes or the level of discretization of the mesh. Furthermore, the selection of empirical PDFs related to each uncertain factor can be of major importance. Arbitrary choices can steer the results of a given GSA toward many distinct outcomes, and this subjectivity must be recognized by all conscientious practitioners. This is the point raised by Saltelli and associate-workers in their publications (Saltelli et al., 2013; Saltelli and Funtowicz, 2014), where they advocate a set of rules to be followed when performing a *"sensitivity auditing of models used in a policy context"*.

Bibliography

Bibliography

Ababou, R. (1996). *Random Porous Media Flow on Large 3-D Grids: Numerics, Performance, and Application to Homogenization*, Volume IMA - 79 of *Mathematics and its Applications: Environmental Studies - Math., Comput. and Statistical Analysis*. Springer, New York.

Abramowitz, M. and I. A. Stegun (1964). Handbook of mathematical functions with formulas, graphs, and mathematical tables. *Mathematics of Computation*.

Allen, D. M. (1971). *The Prediction Sum of Squares as a Criterion for Selecting Predictor Variables*. Technical report - Department of Statistics, University of Kentucky. University of Kentucky.

Anderson, M. P. and W. W. Woessner (1992). *Applied Groundwater Modeling: Simulation of Flow and Advective Transport* (4 ed.). Academic Press.

ANDRA (2005). Dossier 2005 : Référentiel du site de Meuse/Haute-Marne. Tome 1 : Le site de Meuse/Haute-Marne : histoire géologique et état actuel (décembre 2005). rapport ANDRA C.RP.ADS.04.0022.B. Technical report, ANDRA.

ANDRA (2012a). Modèle hydrogéologique intégré région-secteur à l'actuel. Phase II 2010-2012 - Tâche 3: Sensibilité du modèle de référence aux incertitudes sur les paramètres hydro-dispersifs et analyse de risque. Rapport ANDRA C.RP.0CHYN.12.0001. Technical report, ANDRA.

ANDRA (2012b). Modèle hydrogéologique intégré région-secteur à l'actuel. Phase II 2010-2012. Mise à jour, consolidation et exploitation du modèle. Rapport de la tâche 1, mise à jour et consolidation du modèle hydrogéologique de 2009. Rapport ANDRA C.RP.0CHYN.12.0. Technical report, ANDRA.

Archer, G. E., A. Saltelli, and I. M. Sobol' (1997). Sensitivity measures, ANOVA-like techniques and the use of bootstrap. *J. Stat. Comput. Simul. 58*, 99–120.

Archie, G. E. (1942). The electrical resistivity log as an aid in determining some reservoir characteristics. *Trans. Am. Inst. Min. Metall. Engrs 146*, 54–62.

Arnold, B. W., S. P. Kuzio, and B. A. Robinson (2003). Radionuclide transport simulation and uncertainty analyses with the saturated-zone site-scale model at Yucca Mountain, Nevada. *Journal of Contaminant Hydrology 62-63*(0), 401–419.

Becker, W., J. E. Oakley, C. Surace, P. Gili, J. Rowson, and K. Worden (2012). Bayesian sensitivity analysis of a nonlinear finite element model. *Mechanical Systems and Signal Processing 32*, 18–31.

Benabderrahmane, H., J. Kerrou, L. Tacher, G. Deman, and P. Perrochet (2014). Modelling of predictive hydraulic impacts of a potential radioactive waste geological repository on the Meuse/Haute-Marne multilayered aquifer system (France). *Journal of Applied Mathematics & Physics 2*(12), 1085–1090.

Berveiller, M. (2005). *Stochastic finite element analysis: Intrusive and non-intrusive approaches for reliability analysis*. Ph. D. thesis, Université Blaise Pascal - Clermont-Ferrand II.

Beven, K. (2010). *Environmental modelling: An uncertain future?* Taylor & Francis.

Blatman, G. (2009). *Adaptive sparse polynomial chaos expansions for uncertainty propagation and sensitivity analysis*. Ph. D. thesis, Université Blaise Pascal - Clermont-Ferrand II.

Blatman, G. and B. Sudret (2008). Sparse polynomial chaos expansions and adaptive stochastic finite elements using a regression approach. *Comptes Rendus Mécanique 336*(6), 518–523.

Blatman, G. and B. Sudret (2010a). An adaptive algorithm to build up sparse polynomial chaos expansions for stochastic finite element analysis. *Probabilistic Engineering Mechanics 25*(2), 183–197.

Blatman, G. and B. Sudret (2010b). Efficient computation of global sensitivity indices using sparse polynomial chaos expansions. *Reliability Engineering & System Safety 95*(11), 1216–1229.

Blatman, G. and B. Sudret (2011). Adaptive sparse polynomial chaos expansion based on least angle regression. *Journal of Computational Physics 230*(6), 2345–2367.

Boisson, J. Y., L. Bertrand, J. F. Heitz, and Y. Moreau-Le Golvan (2001). In situ and laboratory investigations of fluid flow through an argillaceous formation at different scales of space and time, Tournemire tunnel, southern France. *Hydrogeology Journal 9*(1), 108–123.

Bourgeat, A., M. Kern, S. Schumacher, and J. Talandier (2004). The COUPLEX test cases: Nuclear waste disposal simulation. *Computational Geosciences 8*(2), 83–98.

Box, G. E. P. and N. Draper (1987). *Empirical Model-Building and Response Surfaces*. Wiley Series in Probability and Statistics. Wiley.

Box, G. E. P., J. S. Hunter, and W. G. Hunter (2005). *Statistics for Experimenters: Design, Innovation, and Discovery*. Wiley Series in Probability and Statistics. Wiley-Interscience.

Brigaud, B., B. Vincent, C. Durlet, J. F. Deconinck, P. Blanc, and A. Trouiller (2010). Acoustic properties of ancient shallow-marine carbonates: Effects of depositional environments and diagenetic processes (Middle Jurassic, Paris basin, France). *Journal of Sedimentary Research 80*(9-10), 791–807.

Bursztyn, D. and D. M. Steinberg (2006). Comparison of designs for computer experiments. *Journal of Statistical Planning and Inference 136*(3), 1103–1119.

Caflisch, R. E. (1998). Monte carlo and quasi-monte carlo methods. *Acta numerica 7*, 1–49.

Campolongo, F., J. Cariboni, and A. Saltelli (2007). An effective screening design for sensitivity analysis of large models. *Environmental Modelling & Software 22*(10), 1509–1518.

Campolongo, F. and A. Saltelli (1997). Sensitivity analysis of an environmental model: an application of different analysis methods. *Reliability Engineering & System Safety 57*(1), 49–69.

Campolongo, F., A. Saltelli, and J. Cariboni (2011). From screening to quantitative sensitivity analysis. A unified approach. *Computer Physics Communications 182*(4), 978–988.

Carley, M. K., Y. N. Kamneva, and J. Reminga (2004). Response surface methodology. CASOS technical report CMUISRI-04-136. Technical report, Carnegie Mellon University.

Carman, P. C. (1937). Fluid flow through granular beds. *Transactions of the Institution of Chemical Engineers 15*, 150–166.

Carman, P. C. (1956). Flow of gases through porous media. pp. 182 p.

Carpentier, C. (2004). *Géométries et environnements de dépôt de l'Oxfordien de l'Est du Bassin de Paris*. Ph. D. thesis, Université de Nancy I.

Carrera, J., A. Alcolea, A. Medina, J. Hidalgo, and L. J. Slooten (2005). Inverse problem in hydrogeology. *Hydrogeology Journal 13*(1), 206–222.

Castellini, A., A. Chawathe, D. Larue, J. L. Landa, F. X. Jian, J. L. Toldi, and M. C. Chien (2003). What is relevant to flow? a comprehensive study using a shallow marine reservoir. Houston, Texas, U.S.A. Society of Petroleum Engineers.

Chapelle, O., V. Vapnik, and Y. Bengio (2002). Model selection for small sample regression. *Machine Learning 48*(1), 9–23.

Choi, K., M. Jackson, G. Hampson, A. Jones, and T. Reynolds (2007). Impact of heterogeneity on flow in fluvial-deltaic reservoirs: Implications for the giant ACG field, South Caspian Basin. In E. Conference and E. Europec (Eds.), *EAGE Conference and Exhibition/SPE Europec*, Volume 6, London, UK. 69th European Association of Geoscientists and Engineers Conference and Exhibition: Society of Petroleum Engineers.

Choi, S.-K., R. V. Grandhi, R. A. Canfield, and C. L. Pettit (2004). Polynomial chaos expansion with latin hypercube sampling for estimating response variability. *AIAA Journal 42*(6), 1191–1198.

Ciriello, V., V. Federico, M. Riva, F. Cadini, J. Sanctis, E. Zio, and A. Guadagnini (2013). Polynomial chaos expansion for global sensitivity analysis applied to a model of radionuclide migration in a randomly heterogeneous aquifer. *Stochastic Environmental Research and Risk Assessment 27*(4), 945–954.

Civan, F. (2011). *Porous Media Transport Phenomena*. Wiley.

Contoux, C., S. Violette, R. Vivona, P. Goblet, and D. Patriarche (2013). How basin model results enable the study of multi-layer aquifer response to pumping: the Paris Basin, France. *Hydrogeology Journal 21*(3), 545–557.

Cornaton, F. J. (2007). Groundwater: a 3-d ground water and surface water flow, mass transport and heat transfer finite element simulator. Reference manual. University of Neuchâtel.

Cornaton, F. J. and P. Perrochet (2006a). Groundwater age, life expectancy and transit time distributions in advective-dispersive systems: 1. generalized reservoir theory. *Advances in Water Resources 29*(9), 1267–1291.

Cornaton, F. J. and P. Perrochet (2006b). Groundwater age, life expectancy and transit time distributions in advective-dispersive systems; 2. reservoir theory for sub-drainage basins. *Advances in Water Resources 29*(9), 1292–1305.

Cosenza, P., M. Ghoreychi, G. de Marsily, G. Vasseur, and S. Violette (2002). Theoretical prediction of poroelastic properties of argillaceous rocks from in situ specific storage coefficient. *Water Resources Research 38*(10), 25–1:25–12.

Cukier, R. I., C. M. Fortuin, K. E. Shuler, A. G. Petschek, and J. H. Schaibly (1973). Study of the sensitivity of coupled reaction systems to uncertainties in rate coefficients. I Theory. *The Journal of Chemical Physics 59*(8), 3873–3878.

Cukier, R. I., H. B. Levine, and K. E. Shuler (1978). Nonlinear sensitivity analysis of multiparameter model systems. *Journal of Computational Physics 26*(1), 1–42.

de Hoyos, A., P. Viennot, E. Ledoux, J. M. Matray, M. Rocher, and C. Certes (2012). Influence of thermohaline effects on groundwater modelling - Application to the Paris sedimentary Basin. *Journal of Hydrology 464*, 12–26.

de Jager, G., J. F. M. Van Doren, J. D. Jansen, and S. M. Luthi (2009). An evaluation of relevant geological parameters for predicting the flow behaviour of channelized reservoirs. *Petroleum Geoscience 15*(4), 345–354.

de Marsily, G., F. Delay, J. Goncalves, P. Renard, V. Teles, and S. Violette (2005). Dealing with spatial heterogeneity. *Hydrogeology Journal 13*, 161–183.

de Rocquigny, E. (2012). *Modelling Under Risk and Uncertainty: An Introduction to Statistical, Phenomenological and Computational Methods*. Wiley Series in Probability and Statistics. Wiley.

de Rocquigny, E., N. Devictor, and S. Tarantola (2008). *Uncertainty in Industrial Practice: A Guide to Quantitative Uncertainty Management*. Wiley.

Delay, J. and M. Distinguin (2004). *Hydrogeological Investigations in Deep Wells at the Meuse/Haute Marne Underground Research Laboratory*, Volume 104 of *Lecture Notes in Earth Sciences*, Chapter 26, pp. 219–225. Springer Berlin Heidelberg.

Delay, J., M. Distinguin, and S. Dewonck (2007). Characterization of a clay-rich rock through development and installation of specific hydrogeological and diffusion test equipment in deep boreholes. *Physics and Chemistry of the Earth 32*(1-7), 393–407.

Delay, J., H. Rebours, A. Vinsot, and P. Robin (2007). Scientific investigation in deep wells for nuclear waste disposal studies at the Meuse/Haute Marne underground research laboratory, northeastern France. *Physics and Chemistry of the Earth 32*(1-7), 42–57.

Delay, J., A. Trouiller, and J. M. Lavanchy (2006). Hydrodynamic properties of the Callovo-Oxfordian formation in the East of the Paris Basin: comparison of results obtained through different approaches. *Comptes Rendus Geoscience 338*(12-13), 892–907.

Deman, G., J. Kerrou, H. Benabderrahmane, and P. Perrochet (2012). Parametric uncertainty analysis on a groundwater flow and mass transport model using experimental design and response surface methodology: the case of Andra Meuse/Haute-Marne site. In *Proceedings: 5th International meeting "Clays in Natural and Engineered Barriers for Radioactive Waste Confinement"*.

Deman, G., J. Kerrou, H. Benabderrahmane, and P. Perrochet (2013). Comparison of sensitivity analysis methods applied on a groundwater flow and mass transport model. In *Proceedings: 7th International Conference on Sensitivity Analysis of Model Output*.

Deman, G., J. Kerrou, H. Benabderrahmane, and P. Perrochet (2015). Sensitivity analysis of groundwater lifetime expectancy to hydro-dispersive parameters: The case of ANDRA Meuse/Haute-Marne site. *Reliability Engineering & System Safety 134*(0), 276–286.

Dette, H. and A. Pepelyshev (2010). Generalized latin hypercube design for computer experiments. *Technometrics 52*(4), 421–429.

Diersch, H. J. (2013). *FEFLOW: Finite Element Modeling of Flow, Mass and Heat Transport in Porous and Fractured Media*. Springer Berlin Heidelberg.

Distinguin, M. and J. M. Lavanchy (2007). Determination of hydraulic properties of the Callovo-Oxfordian argillite at the Bure site: Synthesis of the results obtained in deep boreholes using several in situ investigation techniques. *Physics and Chemistry of the Earth 32*(1-7), 379–392.

Dodge, Y. (2008). *The Concise Encyclopedia of Statistics*. Springer.

Doherty, J. (2005). Pest: model-independent parameter estimation. User manual. 5th edition.

Domenico, P. A. and F. W. Schwartz (1998). *Physical and Chemical Hydrogeology*, Volume 1. Wiley.

Draper, D., A. Pereira, P. Prado, A. Saltelli, R. Cheal, S. Eguilior, B. Mendes, and S. Tarantola (1999). Scenario and parametric uncertainty in GESAMAC: A methodological study in nuclear waste disposal risk assessment. *Computer Physics Communications 117*(1-2), 142–155.

Draper, N. and H. Smith (1998). *Applied Regression Analysis*. Wiley Series in Probability and Statistics. Wiley-Interscience.

Drouet, J. L., N. Capian, J. L. Fiorelli, V. Blanfort, M. Capitaine, S. Duretz, B. Gabrielle, R. Martin, R. Lardy, P. Cellier, and J. F. Soussana (2011). Sensitivity analysis for models of greenhouse gas emissions at farm level. case study of N2O emissions simulated by the CERES-EGC model. *Environmental Pollution 159*(11), 3156–3161.

Duncan, R. B. (1972). Characteristics of organizational environments and perceived environmental uncertainty. *Administrative Science Quarterly 17*(3), 313–327.

Efron, B., T. Hastie, L. Johnstone, and R. Tibshirani (2004). Least angle regression. *Annals of Statistics 32*, 407–499.

Enssle, C. P., M. Cruchaudet, J. Croise, and J. Brommundt (2011). Determination of the permeability of the Callovo-Oxfordian clay at the metre to decametre scale. *Physics and Chemistry of the Earth 36*(17-18), 1669–1678.

Ezekiel, M. (1930). *Methods of Correlation Analysis*. J. Wiley & Sons, Incorporated.

Fajraoui, N., T. A. Mara, A. Younes, and R. Bouhlila (2012). Reactive transport parameter estimation and global sensitivity analysis using sparse polynomial chaos expansion. *Water, Air, & Soil Pollution 223*(7), 4183–4197.

Fajraoui, N., F. Ramasomanana, A. Younes, T. A. Mara, P. Ackerer, and A. Guadagnini (2011). Use of global sensitivity analysis and polynomial chaos expansion for interpretation of nonreactive transport experiments in laboratory-scale porous media. *Water Resources Research 47*.

Feraille, M. and A. Marrel (2012). Prediction under uncertainty on a mature field. *Oil & Gas Science and Technology – Rev. IFP Energies nouvelles 67*(2), 193–206.

Fisher, R. A. (1935). *The Design of Experiments*. New York: Hafner Pub. Co.

Ford, D. and P. Williams (2007). *Analysis of Karst Drainage Systems (in Karst Hydrogeology and Geomorphology)*, pp. 145–208. John Wiley & Sons Ltd.

Formaggia, L., A. Guadagnini, I. Imperiali, V. Lever, G. Porta, M. Riva, A. Scotti, and L. Tamellini (2013). Global sensitivity analysis through polynomial chaos expansion of a basin-scale geochemical compaction model. *Computational Geosciences 17*(1), 25–42.

Fourre, E., P. Jean-Baptiste, A. Dapoigny, B. Lavielle, T. Smith, B. Thomas, and A. Vinsot (2011). Dissolved helium distribution in the Oxfordian and Dogger deep aquifers of the Meuse/Haute-Marne area. *Physics and Chemistry of the Earth 36*(17-18), 1511–1520.

Geisser, S. (1974). A predictive approach to the random effect model. *Biometrika 61*(1), 101–107.

Ghiocel, D. and R. Ghanem (2002). Stochastic finite-element analysis of seismic soil-structure interaction. *Journal of Engineering Mechanics 128*(1), 66–77.

Goncalves, J., S. Violette, F. Guillocheau, C. Robin, M. Pagel, D. Bruel, G. de Marsily, and E. Ledoux (2004). Contribution of a three-dimensional regional scale basin model to the study of the past fluid flow evolution and the present hydrology of the Paris basin, France. *Basin Research 16*(4), 569–586.

Goncalves, J., S. Violette, C. Robin, D. Bruel, F. Guillocheau, and E. Ledoux (2004). Combining a compaction model with a facies model to reproduce permeability fields at the regional scale. *Physics and Chemistry of the Earth 29*(1), 17–24.

Goupy, J. (2001). *Introduction aux Plans d'Expériences*. Technique et ingénierie. Dunod.

Hamby, D. M. (1994). A review of techniques for parameter sensitivity analysis of environmental models. *Environmental Monitoring and Assessment 32*(2), 135–154.

Hanley, N. and C. L. Spash (1993). *Cost-benefit Analysis and the Environment*. Cambridge University Press.

Helton, J. C. (1993). Uncertainty and sensitivity analysis techniques for use in performance assessment for radioactive-waste disposal. *Reliability Engineering & System Safety 42*(2-3), 327–367.

Helton, J. C. (1999). Uncertainty and sensitivity analysis in performance assessment for the Waste Isolation Pilot Plant. *Computer Physics Communications 117*(1-2), 156–180.

Helton, J. C., D. R. Anderson, B. L. Baker, J. E. Bean, J. W. Berglund, W. Beyeler, K. Economy, J. W. Garner, S. C. Hora, H. J. Iuzzolino, P. Knupp, M. G. Marietta, J. Rath, R. P. Rechard, P. J. Roache, D. K. Rudeen, K. Salari, J. D. Schreiber, P. N. Swift, M. S. Tierney, and P. Vaughn (1996). Uncertainty and sensitivity analysis results obtained in the 1992 performance assessment for the Waste Isolation Pilot Plant. *Reliability Engineering & System Safety 51*(1), 53–100.

Helton, J. C., J. E. Bean, K. Economy, J. W. Garner, R. J. MacKinnon, J. Miller, J. D. Schreiber, and P. Vaughn (2000a). Uncertainty and sensitivity analysis for two-phase flow in the vicinity of the repository in the 1996 performance assessment for the Waste Isolation Pilot Plant: Disturbed conditions. *Reliability Engineering & System Safety 69*(1-3), 263–304.

Helton, J. C., J. E. Bean, K. Economy, J. W. Garner, R. J. MacKinnon, J. Miller, J. D. Schreiber, and P. Vaughn (2000b). Uncertainty and sensitivity analysis for two-phase flow in the vicinity of the repository in the 1996 performance assessment for the Waste Isolation Pilot Plant: Undisturbed conditions. *Reliability Engineering & System Safety 69*(1-3), 227–261.

Helton, J. C., W. H. Clifford, and C. J. Sallaberry (2012). Uncertainty and sensitivity analysis in performance assessment for the proposed high-level radioactive waste repository at Yucca Mountain, Nevada. *Reliability Engineering & System Safety 107*(0), 44–63.

Helton, J. C. and F. J. Davis (2003). Latin hypercube sampling and the propagation of uncertainty in analyses of complex systems. *Reliability Engineering & System Safety 81*(1), 23–69.

Helton, J. C., F. J. Davis, and J. D. Johnson (2005). A comparison of uncertainty and sensitivity analysis results obtained with random and latin hypercube sampling. *Reliability Engineering & System Safety 89*(3), 305–330.

Helton, J. C., C. W. Hansen, and C. J. Sallaberry (2014). Expected dose and associated uncertainty and sensitivity analysis results for all scenario classes in the 2008 performance assessment for the proposed high-level radioactive waste repository at Yucca Mountain, Nevada. *Reliability Engineering & System Safety 122*(0), 421–435. Special Issue: Performance Assessment for the Proposed High-Level Radioactive Waste Repository at Yucca Mountain, Nevada.

Helton, J. C. and R. L. Iman (1982). Sensitivity analysis of a model for the environmental movement of radionuclides. *Health Physics 42*(5), 565–584.

Helton, J. C., R. L. Iman, and J. B. Brown (1985). Sensitivity analysis of the asymptotic-behavior of a model for the environmental movement of radionuclides. *Ecological Modelling 28*(4), 243–278.

Helton, J. C., J. D. Johnson, C. J. Sallaberry, and C. B. Storlie (2006). Survey of sampling-based methods for uncertainty and sensitivity analysis. *Reliability Engineering & System Safety 91*(10-11), 1175–1209.

Hoeffding, W. F. (1948). A class of statistics with asymptotically normal distributions. *Annals of Mathematical Statistics 19*(3), 293–325.

Homma, T. and A. Saltelli (1996). Importance measures in global sensitivity analysis of nonlinear models. *Reliability Engineering & System Safety 52*(1), 1–17.

Iman, R. L. and W. J. Conover (1980). Small sample sensitivity analysis techniques for computer models with an application to risk assessment. *Communications in Statistics - Theory and Methods 9*(17), 1749–1842.

Iman, R. L., J. C. Helton, and J. E. Y. Campbell (1981). An approach to sensitivity analysis of computer models, Part 1. introduction, input variable selection an preliminary variable assessment. *Journal on Quality Technology 13*(3), 174–183.

Iooss, B. and P. Lemaître (2015). A review on global sensitivity analysis methods. In C. Meloni and G. Dellino (Eds.), *Uncertainty management in Simulation-Optimization of Complex Systems: Algorithms and Applications*. Springer.

Iooss, B., F. Van Dorpe, and N. Devictor (2006). Response surfaces and sensitivity analyses for an environmental model of dose calculations. *Reliability Engineering & System Safety 91*(10-11), 1241–1251.

Jafari, A. and T. Babadagli (2009). A sensitivity analysis for effective parameters on 2D fracture-network permeability. *SPE Reservoir Evaluation & Engineering 12*, 455–469.

Janon, A., T. Klein, A. Lagnoux, M. Nodet, and C. Prieur (2013). Asymptotic normality and efficiency of two Sobol index estimators. *ESAIM: Probability and Statistics*, 1–20.

Jansen, M. J. W. (1999). Analysis of variance designs for model output. *Computer Physics Communications 117*(1-2), 35–43.

Johnson, M. E., L. M. Moore, and D. Ylvisaker (1990). Minimax and maximin distance designs. *Journal of Statistical Planning and Inference 26*(2), 131–148.

Kazemi, G. A., J. H. Lehr, and P. Perrochet (2006). *Groundwater Age*. Wiley.

Kerrou, J., H. Benabderrahmane, and P. Perrochet (2012). Stochastic modelling of the Oxfordian and Dogger aquifers heterogeneity and evaluation of its impacts on the groundwater flow and transport predictions in the Meuse/Haute-Marne area. In *Proceedings: 5th International meeting "Clays in Natural and Engineered Barriers for Radioactive Waste Confinement"*.

Kerrou, J. and P. Renard (2010). A numerical analysis of dimensionality and heterogeneity effects on advective dispersive seawater intrusion processes. *Hydrogeology Journal 18*(1), 55–72.

Khosravi, M., B. Rostami, and S. Fatemi (2012). Uncertainty analysis of a fractured reservoir's performance: A case study. *Oil & Gas Science and Technology – Rev. IFP Energies nouvelles 67*(3), 423–433.

Kleijnen, J. P. C. (1997). Sensitivity analysis and related analyses: A review of some statistical techniques. *Journal of Statistical Computation and Simulation 57*(1-4), 111–142.

Kozeny, J. (1927). Über kapillare Leitung der Wasser im Boden. *Sitzungs-ber. Akad. Wiss. Wien 136*, 271–306.

Kucherenko, S., B. Feil, N. Shah, and W. Mauntz (2011). The identification of model effective dimensions using global sensitivity analysis. *Reliability Engineering & System Safety 96*(4), 440–449.

Kucherenko, S., M. Rodriguez-Fernandez, C. Pantelides, and N. Shah (2009). Monte Carlo evaluation of Derivative-based Global Sensitivity Measures. *Reliability Engineering & System Safety 94*(7), 1135–1148.

Kucherenko, S., S. Tarantola, and P. Annoni (2012). Estimation of global sensitivity indices for models with dependent variables. *Computer Physics Communications 183*(4), 937–946.

Laloy, E., B. Rogiers, J. A. Vrugt, D. Mallants, and D. Jacques (2013). Efficient posterior exploration of a high-dimensional groundwater model from two-stage Markov chain Monte Carlo simulation and polynomial chaos expansion. *Water Resources Research 49*(5), 2664–2682.

Lamboni, M., B. Iooss, A. L. Popelin, and F. Gamboa (2013). Derivative-based Global Sensitivity Measures: General links with Sobol' indices and numerical tests. *Mathematics and Computers in Simulation 87*, 45–54.

Landrein, P., G. Vigneron, J. Delay, P. Lebon, and M. Pagel (2013). Lithology, hydrodynamism and thermicity in the multi-layer sedimentary system intersected by the ANDRA deep borehole of Montiers-sur-Saulx (Meuse, France). *Bulletin De La Societe Geologique De France 184*(6), 519–543.

Lawson, T. (1985). Uncertainty and economic analysis. *The Economic Journal 95*(380), 909–927.

Le Maître, O. P., M. T. Reagan, H. N. Najm, R. G. Ghanem, and O. M. Knio (2002). A stochastic projection method for fluid flow II.: Random process. *J. Comput. Phys. 181*(1), 9–44.

Lee, T. C. (1998). *Applied Mathematics in Hydrogeology*. Environmental engineering: Mathematics. Taylor & Francis.

Li, G., H. Rabitz, P. E. Yelvington, O. O. Oluwole, F. Bacon, C. E. Kolb, and J. Schoendorf (2010). Global sensitivity analysis for systems with independent and/or correlated inputs. *The Journal of Physical Chemistry A 114*(19), 6022–6032.

Li, G., C. Rosenthal, and H. Rabitz (2001). High dimensional model representations. *The Journal of Physical Chemistry A 105*(33), 7765–7777.

Li, G., S.-W. Wang, and H. Rabitz (2002). Practical approaches to construct RS-HDMR component functions. *The Journal of Physical Chemistry A 106*(37), 8721–8733.

Li, S. and Y. Zhang (2014). Model complexity in carbon sequestration: A design of experiment and response surface uncertainty analysis. *International Journal of Greenhouse Gas Control 22*(0), 123–138.

Linard, Y., A. Vinsot, B. Vincent, J. Delay, S. Wechner, R. De La Vaissiere, E. Scholz, B. Garry, M. Lundy, M. Cruchaudet, S. Dewonck, and G. Vigneron (2011). Water flow in the Oxfordian and Dogger limestone around the Meuse/Haute-Marne Underground Research Laboratory. *Physics and Chemistry of the Earth 36*(17-18), 1450–1468.

Lopez, A. D., C. D. Mathers, M. Ezzati, D. T. Jamison, and C. J. L. Murray (2006). Global and regional burden of disease and risk factors, 2001: Systematic analysis of population health data. *Lancet 367*, 1747–1757.

Louis, C. (1985). *Introduction a l'Hydraulique des Roches*. Paris, France: Universite de Paris VI.

Lucia, F. J. (1995). Rock-fabric/petrophysical classification of carbonate pore space for reservoir characterization. *AAPG Bulletin 79*(9), 1275–1300.

Malaguerra, F., H.-J. Albrechtsen, and P. J. Binning (2013). Assessment of the contamination of drinking water supply wells by pesticides from surface water resources using a finite element reactive transport model and global sensitivity analysis techniques. *Journal of Hydrology 476*(0), 321–331.

Manache, G. and C. S. Melching (2004). Sensitivity analysis of a water-quality model using latin hypercube sampling. *Journal of Water Resources Planning and Management-Asce 130*(3), 232–242.

Manache, G. and C. S. Melching (2008). Identification of reliable regression- and correlation-based sensitivity measures for importance ranking of water-quality model parameters. *Environmental Modelling & Software 23*(5), 549–562.

Mantoglou, A. and J. L. Wilson (1982). The Turning Bands Method for simulation of random fields using line generation by a spectral method. *Water Resources Research 18*(5), 1379–1394.

Marelli, S. and B. Sudret (2014). UQLab: a framework for uncertainty quantification in MATLAB. In *Proceedings: 2nd International Conference on Vulnerability, Risk Analysis and Management (ICVRAM2014), Liverpool, United Kingdom*.

Marivoet, J., I. Wemaere, P. Escalier des Orres, P. Baudoin, C. Certes, A. Levassor, J. Prij, K.-H. Martens, and K. Röhlig (1997). The EVEREST project: Sensitivity analysis of geological disposal systems. *Reliability Engineering & System Safety 57*(1), 79–90.

Marrel, A., B. Iooss, B. Laurent, and O. Roustant (2009). Calculations of Sobol indices for the Gaussian process metamodel. *Reliability Engineering & System Safety 94*(3), 742–751.

Mazurek, M., P. Alt-Epping, A. Bath, T. Gimmi, N. W. H., S. Buschaert, P. De Cannière, M. De Craen, A. Gautschi, S. Savoye, A. Vinsot, I. Wemaere, and L. Wouters (2011). Natural tracer profiles across argillaceous formations. *Applied Geochemistry 26*(7), 1035–1064.

McKay, M. D., R. J. Beckman, and W. J. Conover (1979). A comparison of three methods for selecting values of input variables in the analysis of output from a computer code. *Technometrics 21*(2), 239–245.

Miller, R. G. (1974). The jackknife: A review. *Biometrika 61*(1), 1–15.

Montgomery, D. C. (2006). *Design and Analysis of Experiments*. John Wiley & Sons.

Morris, M. D. (1991). Factorial sampling plans for preliminary computational experiments. *Technometrics 33*(2), 161–174.

Muleta, M. K. and J. W. Nicklow (2005). Sensitivity and uncertainty analysis coupled with automatic calibration for a distributed watershed model. *Journal of Hydrology 306*(1-4), 127–145.

Myers, R. H., A. I. Khuri, and J. Carter, W. H. (1989). Response Surface Methodology: 1966-1988. *Technometrics 31*(2), 137–157.

NEA and OECD (2009). *Natural Tracer Profiles Across Argillaceous Formations : the CLAYTRAC Project*. Paris: Nuclear Energy Agency, Organisation for Economic Co-operation and Development.

Neumann, M. B. (2012). Comparison of sensitivity analysis methods for pollutant degradation modelling: A case study from drinking water treatment. *Science of The Total Environment 433*(0), 530–537.

Niederreiter, H. (1988). Low-discrepancy and low-dispersion sequences. *Journal of Number Theory 30*(1), 51–70.

Oakley, J. E. and A. O'Hagan (2004). Probabilistic sensitivity analysis of complex models: a Bayesian approach. *Journal of the Royal Statistical Society B 66*, 751–769.

Oladyshkin, S., F. P. J. de Barros, and W. Nowak (2012). Global sensitivity analysis: A flexible and efficient framework with an example from stochastic hydrogeology. *Advances in Water Resources 37*(0), 10–22.

Owen, A. B. (1998a). Latin supercube sampling for very high-dimensional simulations. *ACM Trans. Model. Comput. Simul. 8*(1), 71–102.

Owen, A. B. (1998b). Monte Carlo, quasi-Monte Carlo, and randomized quasi-Monte Carlo. *Monte Carlo and Quasi-Monte Carlo Methods 2000*, 86–97.

Pan, F., M. Ye, J. Zhu, Y. Wu, B. X. Hu, and Z. Yu (2009). Incorporating layer- and local-scale heterogeneities in numerical simulation of unsaturated flow and tracer transport. *Journal of Contaminant Hydrology 103*(3-4), 194–205.

Pan, F., J. Zhu, M. Ye, Y. A. Pachepsky, and Y. Wu (2011). Sensitivity analysis of unsaturated flow and contaminant transport with correlated parameters. *Journal of Hydrology 397*(3-4), 238–249.

Pape, H., C. Clauser, and J. Iffland (1999). Permeability prediction based on fractal pore-space geometry. *Geophysics 64*(5), 1447–1460.

Plackett, R. L. and J. P. Burman (1946). The design of optimum multifactorial experiments. *Biometrika 33*(4), 305–325.

Pronzato, L. and W. G. Müller (2012). Design of computer experiments: Space filling and beyond. *Statistics and Computing 22*(3), 681–701.

Pujol, G. (2009). Simplex-based screening designs for estimating metamodels. *Reliability Engineering & System Safety 94*(7), 1156–1160.

Quan, N. T. (1988). The prediction sum of squares as a general measure for regression diagnostics. *Journal of Business & Economic Statistics 6*(4), 501–504.

Rabitz, H. and O. F. Aliş (1999). General foundations of High-Dimensional Model Representations. *Journal of Mathematical Chemistry 25*(2-3), 197–233.

Ratto, M., A. Pagano, and P. Young (2007). State dependent parameter metamodelling and sensitivity analysis. *Computer Physics Communications 177*(11), 863–876.

Razavi, S., B. A. Tolson, and D. H. Burn (2012). Numerical assessment of metamodelling strategies in computationally intensive optimization. *Environmental Modelling & Software 34*(0), 67–86.

Renard, P. (2007). Stochastic hydrogeology: What professionals really need? *Ground Water 45*(5), 531–541.

Renard, P. and D. Allard (2011). Connectivity metrics for subsurface flow and transport. *Advances in Water Resources 51*, 168–196.

Revil, A. and N. Florsch (2010). Determination of permeability from spectral induced polarization in granular media. *Geophysical Journal International 181*(3), 1480–1498.

Robert, C. and G. Casella (2005). *Monte Carlo Statistical Methods*. Springer Texts in Statistics. Springer New York.

Ruano, M. V., J. Ribes, A. Seco, and J. Ferrer (2012). An improved sampling strategy based on trajectory design for application of the Morris method to systems with many input factors. *Environmental Modelling & Software 37*(0), 103–109.

Rubin, Y. (2003). *Applied Stochastic Hydrogeology*. Oxford University Press.

Sacks, J., W. J. Welch, J. M. Toby, and H. P. Wynn (1989). Design and analysis of computer experiments. *Statistical Science 4*(4), 409–423.

Saltelli, A. (2002). Making best use of model evaluations to compute sensitivity indices. *Computer Physics Communications 145*(2), 280–297.

Saltelli, A., P. Annoni, I. Azzini, F. Campolongo, M. Ratto, and S. Tarantola (2010). Variance based sensitivity analysis of model output. Design and estimator for the total sensitivity index. *Computer Physics Communications 181*(2), 259–270.

Saltelli, A. and R. Bolado (1998). An alternative way to compute Fourier amplitude sensitivity test (FAST). *Computational Statistics & Data Analysis 26*(4), 445–460.

Saltelli, A. and S. Funtowicz (2014). When all models are wrong: More stringent quality criteria are needed for models used at the science-policy interface. *Issues in science and technology winter*, 79–85.

Saltelli, A., Â. Guimarães Pereira, J. P. Van der Sluijs, and S. Funtowicz (2013). What do I make of your latinorum? Sensitivity auditing of mathematical modelling. *International Journal of Foresight and Innovation Policy 9*(2), 213–234.

Saltelli, A., M. Ratto, T. Andres, F. Campolongo, J. Cariboni, D. Gatelli, M. Saisana, and S. Tarantola (2008). *Global Sensitivity Analysis: The Primer*. Wiley.

Saltelli, A., M. Ratto, S. Tarantola, and F. Campolongo (2006). Sensitivity analysis practices: Strategies for model-based inference. *Reliability Engineering & System Safety 91*(10-11), 1109–1125.

Saltelli, A. and I. M. Sobol' (1995). About the use of rank transformation in sensitivity analysis of model output. *Reliability Engineering & System Safety 50*(3), 225–239.

Saltelli, A. and S. Tarantola (2002). On the relative importance of input factors in mathematical models. *Journal of the American Statistical Association 97*(459), 702–709.

Saltelli, A., S. Tarantola, and F. Campolongo (2000). Sensitivity analysis as an ingredient of modeling. *Statistical Science 15*(4), 377–395.

Saltelli, A., S. Tarantola, F. Campolongo, and M. Ratto (2004). *Sensitivity Analysis in Practice. A Guide to Assessing Scientific Models*. John Wiley and Sons Ltd., Chichester, England, Chichester, UK.

Saltelli, A., S. Tarantola, and K. Chan (1999). A quantitative model-independent method for global sensitivity analysis of model output. *Technometrics 41*(1), 39–56.

Santiago, J., B. Corre, M. Claeys-Bruno, and M. Sergent (2012). Improved sensitivity through Morris extension. *Chemometrics and Intelligent Laboratory Systems 113*(0), 52–57.

Santner, T. J., W. B., and N. W. (2003). *The Design and Analysis of Computer Experiments*. Springer-Verlag.

Seber, G. A. F. (1977). *Linear Regression Analysis*. Wiley series in Probability and Statistics. New York: Wiley.

Shahkarami, P., L. Liu, L. Moreno, and I. Neretnieks (2015). Radionuclide migration through fractured rock for arbitrary-length decay chain: Analytical solution and global sensitivity analysis. *Journal of Hydrology 520*(0), 448–460.

Sobol', I. M. (1967). On the distribution of points in a cube and the approximate evaluation of integrals. *USSR Computational Mathematics and Mathematical Physics 7*(4), 86–112.

Sobol', I. M. (1993). Sensitivity analysis for non-linear mathematical model. *Math. Modell. Comput. Exp. 1*, 407–414.

Sobol', I. M. (2001). Global sensitivity indices for nonlinear mathematical models and their Monte Carlo estimates. *Mathematics and Computers in Simulation 55*(1-3), 271–280.

Sobol', I. M. (2003). Theorems and examples on High-Dimensional Model Representation. *Reliability Engineering & System Safety 79*(2), 187–193.

Sobol', I. M. and S. Kucherenko (2005). Global sensitivity indices for nonlinear mathematical models. Review. *Wilmott magazine 1*, 56–61.

Sobol', I. M. and S. Kucherenko (2009). Derivative-based global sensitivity measures and their link with global sensitivity indices. *Mathematics and Computers in Simulation 79*(10), 3009–3017.

Sobol', I. M. and S. Kucherenko (2010). A new derivative based importance criterion for groups of variables and its link with the global sensitivity indices. *Computer Physics Communications 181*(7), 1212–1217.

Sobol', I. M., S. Tarantola, D. Gatelli, and W. Kucherenko, S.and Mauntz (2007). Estimating the approximation error when fixing unessential factors in global sensitivity analysis. *Reliability Engineering & System Safety 92*(7), 957–960.

Sochala, P. and O. P. Le Maître (2013). Polynomial chaos expansion for subsurface flows with uncertain soil parameters. *Advances in Water Resources 62, Part A*(0), 139–154.

Soize, C. and R. Ghanem (2004). Physical systems with random uncertainties: Chaos representations with arbitrary probability measure. *SIAM Journal on Scientific Computing 26*(2), 395–410.

Stinnett, A. A., J. Mullahy, and N.B.E.R. (1998). *Net Health Benefits: A New Framework for the Analysis of Uncertainty in Cost-Effectiveness Analysis*. Technical Working Paper. National Bureau of Economic Research.

Stone, M. (1974). Cross-validatory choice and assessment of statistical predictions. *Journal of the Royal Statistical Society. Series B (Methodological) 36*(2), 111–147.

Storlie, C. B. and J. C. Helton (2008a). Multiple predictor smoothing methods for sensitivity analysis: Description of techniques. *Reliability Engineering & System Safety 93*(1), 28–54.

Storlie, C. B. and J. C. Helton (2008b). Multiple predictor smoothing methods for sensitivity analysis: Example results. *Reliability Engineering & System Safety 93*(1), 55–77.

Storlie, C. B., L. P. Swiler, J. C. Helton, and C. J. Sallaberry (2009). Implementation and evaluation of nonparametric regression procedures for sensitivity analysis of computationally demanding models. *Reliability Engineering & System Safety 94*, 1735–1763.

Sudret, B. (2008). Global sensitivity analysis using polynomial chaos expansions. *Reliability Engineering & System Safety 93*(7), 964–979.

Sun, X. Y., L. T. H. Newham, B. F. W. Croke, and J. P. Norton (2012). Three complementary methods for sensitivity analysis of a water quality model. *Environmental Modelling & Software 37*(0), 19–29.

Tarantola, S., W. Becker, and D. Zeitz (2012). A comparison of two sampling methods for global sensitivity analysis. *Computer Physics Communications 183*(5), 1061–1072.

Tarantola, S., D. Gatelli, and T. A. Mara (2006). Random balance designs for the estimation of first order global sensitivity indices. *Reliability Engineering & System Safety 91*(6), 717–727.

Touzani, S. and D. Busby (2014). Screening method using the Derivative-based Global Sensitivity Indices with application to reservoir simulator. *Oil & Gas Science and Technology – Rev. IFP Energies nouvelles 69*(4), 619–632.

Uffink, G. J. M. (1989). Application of the Kolmogorov's backward equation in random walk simulation of groundwater contaminant transport. *Contaminant Transport in Groundwater*, 283–289.

Van Doren, J. F. M., G. De Jager, J. D. Jansen, S. M. Luthi, and S. G. Douma (2007). Sensitivity of geostatistical modeling parameters on reservoir flow behavior.

Van Griensven, A., T. Meixner, S. Grunwald, T. Bishop, A. Diluzio, and R. Srinivasan (2006). A global sensitivity analysis tool for the parameters of multi-variable catchment models. *Journal of Hydrology 324*(1-4), 10–23.

Vincent, B. (2001). *Sédimentologie et géochimie de la diagenèse des carbonates : application au Malm de la Bordure Est du Bassin de Paris*. Ph. D. thesis, Université de Bourgogne.

Vinsot, A., J. Delay, R. de La Vaissière, and M. Cruchaudet (2011). Pumping tests in a low permeability rock: Results and interpretation of a four-year long monitoring of water production flow rates in the Callovo-Oxfordian argillaceous rock. *Physics and Chemistry of the Earth, Parts A/B/C 36*(17-18), 1679–1687.

Wold, H. (1982). Soft modeling: The basic design and some extensions. *Systems under indirect observation 2*, 589–591.

Xiu, D. and G. E. Karniadakis (2002). The Wiener-Askey polynomial chaos for stochastic differential equations. *SIAM J. Sci. Comput. 24*(2), 619–644.

Xu, C. G. and G. Z. Gertner (2008). Uncertainty and sensitivity analysis for models with correlated parameters. *Reliability Engineering & System Safety 93*(10), 1563–1573.

Ye, M., F. Pan, Y. Wu, B. X. Hu, C. Shirley, and Z. Yu (2007). Assessment of radionuclide transport uncertainty in the unsaturated zone of Yucca Mountain. *Advances in Water Resources 30*(1), 118–134.

Younes, A., T. A. Mara, N. Fajraoui, F. Lehmann, B. Belfort, and H. Beydoun (2013). Use of global sensitivity analysis to help assess unsaturated soil hydraulic parameters. *Vadose Zone Journal 12*(1).

Yue, W. Z. and G. Tao (2013). A new non-Archie model for pore structure: Numerical experiments using digital rock models. *Geophysical Journal International 195*, 282–291.

Zinn, B. and C. F. Harvey (2003). When good statistical models of aquifer heterogeneity go bad: A comparison of flow, dispersion, and mass transfer in connected and multivariate Gaussian hydraulic conductivity fields. *Water Resources Research 39*(3).

Zuniga, M. M., S. Kucherenko, and N. Shah (2013). Metamodelling with independent and dependent inputs. *Computer Physics Communications 184*(6), 1570–1580.

Appendix A

Backward elimination

Let us consider a regression meta-model based on $k = 2$ variables. The regressors are the linear effect of each variable and the interaction between the two, thus $P = 3$ regressors are considered in the full regression meta-model:

$$\widehat{\boldsymbol{y}} = \widehat{\beta}_0 + \widehat{\beta}_1\, x_1 + \widehat{\beta}_2\, x_2 + \widehat{\beta}_{1,2}\, x_1\, x_2 \qquad R^2_{adj} = 0.87 \tag{A.1}$$

Given that the experimenter is interested in finding the set of regressors that optimizes the criteria R^2_{adj}. The backward elimination procedure starts with the full model from Eq. A.1 and iterates upon the various sub-models of $Q = P - 1$ terms. At the first step of the algorithm, each regressor is discarded alternatively from Eq. A.1, hence the three iterations lead to the sub-models:

$$\begin{aligned}
\widehat{\boldsymbol{y}} &= \widehat{\beta}_0 + \widehat{\beta}_2\, x_2 + \widehat{\beta}_{1,2}\, x_1\, x_2 \qquad & R^2_{adj} &= 0.86 \\
\widehat{\boldsymbol{y}} &= \widehat{\beta}_0 + \widehat{\beta}_1\, x_1 + \widehat{\beta}_{1,2}\, x_1\, x_2 \qquad & R^2_{adj} &= 0.82 \\
\widehat{\boldsymbol{y}} &= \widehat{\beta}_0 + \widehat{\beta}_1\, x_1 + \widehat{\beta}_2\, x_2 \qquad & R^2_{adj} &= 0.89
\end{aligned} \tag{A.2}$$

The third sub-model yielding the highest selection criteria, with a $R^2_{adj} = 0.89$, is kept for the sequel. The next step consists in two iterations where each of the remaining regressors is removed alternatively:

$$\begin{aligned}
\widehat{\boldsymbol{y}} &= \widehat{\beta}_0 + \widehat{\beta}_1\, x_1 \qquad & R^2_{adj} &= 0.74 \\
\widehat{\boldsymbol{y}} &= \widehat{\beta}_0 + \widehat{\beta}_2\, x_2 \qquad & R^2_{adj} &= 0.77
\end{aligned} \tag{A.3}$$

The algorithm stops when the optimal sub-model of $Q = 2$ regressors is found, the mean $\widehat{\beta}_0$ being included in every sub-model. Then, all the possible sub-models are compared with regard to the selection criteria chosen by the experimenter. In this example, the interaction term $\widehat{\beta}_{1,2}\, x_1\, x_2$ reduces the goodness of the fit and, among all possible models, the third regression meta-model of Eq. A.2 provides the highest R^2_{adj} criteria. It can thus be used to perform an UA and/or a SA.

Appendix B

Permeability-porosity datasets and approximation functions

B.1 Empirical relationships

Many $\{K, \phi\}$ empirical relationships exist in the literature (Pape et al., 1999; Civan, 2011), the well-known Kozeny-Carman law (Kozeny, 1927; Carman, 1937, 1956) is one of the major ones to describe the relationship in granular medium. Others are found, such like the Archie's law (Archie, 1942) and its adapted versions (Revil and Florsch, 2010; Yue and Tao, 2013). In the context of carbonate rocks, Lucia (1995) provided a large set of empirical relationships, but which require knowledge regarding the class of carbonate rock-fabric.

For many layers comprised in the UPSILON model, the lack of explicit information regarding granulometry, pore type, tortuosity or mineral composition, lead to investigating various empirical functions and to measure the goodness of the fit. Besides, with regard to the large scale of the UPSILON model and the spatial scattering of datasets, it is assumed that any relationship can hold and be employed to relate the two parameters in this preliminary study. Eventually, empirical functions were confronted to polynomial functions and the approximation providing the best fit is employed in the following.

B.2 The confining layers

As mentioned in Section 4.2.4, very few datasets were obtained for the top layers K3 and K1-K2. The uncertainty bounds were extracted from literature (Fourre et al., 2011; Contoux et al., 2013) and a linear relationship for the $\{K, \phi\}$ couples, also referred to as *petrofacies*, is assumed. The approximation linear functions are not shown here while the uncertainty bounds for each layer is given in Table 4.3.

Figure B.1*a* presents permeability and porosity datasets found in the literature (Delay et al., 2006; Distinguin and Lavanchy, 2007) for layer C2, where the empirical relationship given in (Revil and Florsch, 2010) provides the best fit to relate the two factors following

$$k = \frac{{d_0}^2}{32\, m^2\, (F-1)^2 F} \tag{B.1}$$

where k is the intrinsic permeability [L^2], d_0 is the average grain diameter [L], $F = \phi^{-m}$ (Archie, 1942) is a shape factor depending on the pores' morphology and distribution, usually $10 \leq F \leq 30$ [-], and m is called the first Archie exponent or the cementation exponent which depends on the rock structure, or tortuosity, it is usually found in $1 \leq m \leq 3$ [-].

Note that the hydraulic conductivity K [LT^{-1}] is retrieved with

$$K = k\frac{\rho g}{\mu} \tag{B.2}$$

where μ is the dynamic viscosity of the fluid [$ML^{-1}T^{-1}$] and is assumed to be equal to 1.14E-02 kg/m/s in the whole study, which correspond to that of pure water at 15°C, ρ is the density of the fluid [ML^{-3}] and it equals 10^3 kg/m^3 in the whole study, and g is the acceleration due to gravity [MT^{-2}] and it equals approximately 9.81 kg/s^2.

Various combinations of factors d_0 and m were tested to find the optimal fit upon the data points. In definitive a coefficient of correlation $R^2 = 0.96$ was obtained for an average grain diameter $d_0 = 2.51\ 10^{-6}$ meters and an Archie exponent $m = 2.19$.

For the bottom layer, T, $\{K, \phi\}$ datasets were extracted from (Boisson et al., 2001) and a second-order polynomial function provides the best fit upon the data points with a coefficient of correlation $R^2 = 0.84$ (Figure B.1).

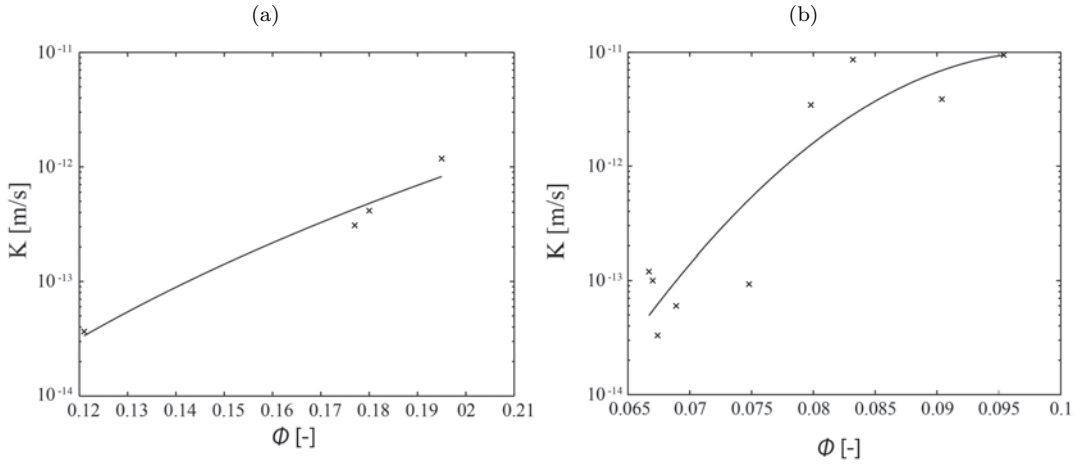

Figure B.1: Approximation of the $\{K, \phi\}$ dataset in layers (a) C2 and (b) T.

B.3 The Oxfordian limestone sequence

The datasets in each layer of the Oxfordian sequence were extracted from the well-documented article from Linard et al. (2011). Although various empirical approximation functions were tested in order to approximate the $\{K, \phi\}$ datasets, it was found that polynomial functions provided the best approximations.

Except for layer L2c for which a third-order polynomial function was employed (Figure B.2a), the other 5 layers of the sequence employ second-order polynomial functions to fit the $\{K, \phi\}$ datasets.

From Figure B.2e especially, two clusters of points appear. Depending on the borehole location from which the samples were obtained, large variations of the $\{K, \phi\}$ sets can be observed. Indeed, some boreholes are known to be situated in the vicinity of fractured zones where high porosity and hydraulic conductivity values are found with the presence of large groundwater volumes.

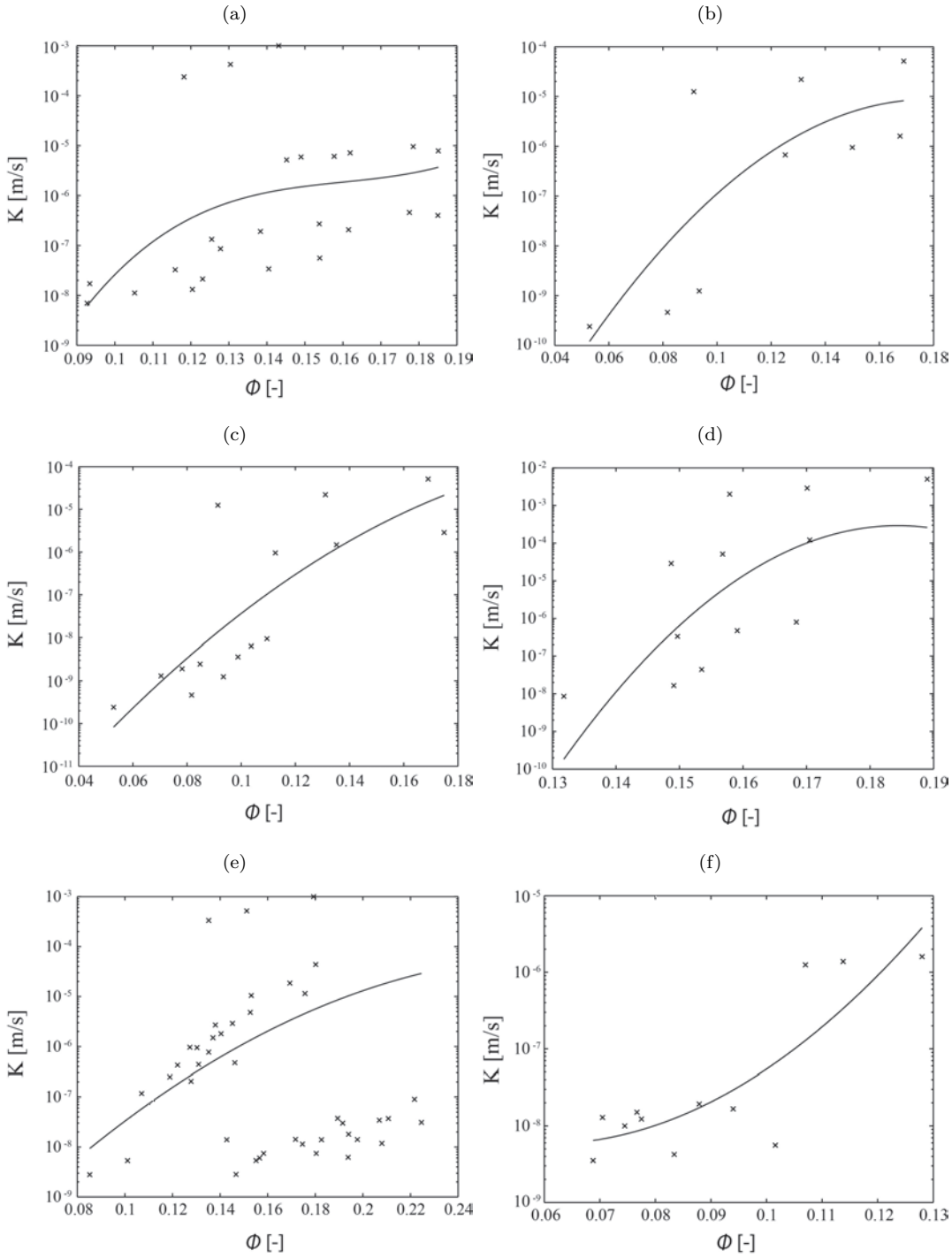

Figure B.2: Approximation of the $\{K, \phi\}$ dataset in layers (a) L2c, (b) L2b, (c) L2a, (d) L1b,(e) L1a and (f) C3ab.

B.4 The Dogger limestone sequence

Brigaud et al. (2010) provided the datasets for the 5 hydrogeological entities modelled in the synthetic numerical model as the Dogger sequence. Except for layer D1, for which the empirical relationship from (Revil and Florsch, 2010) (Eq. B.1) was employed, the other layers used polynomial functions.

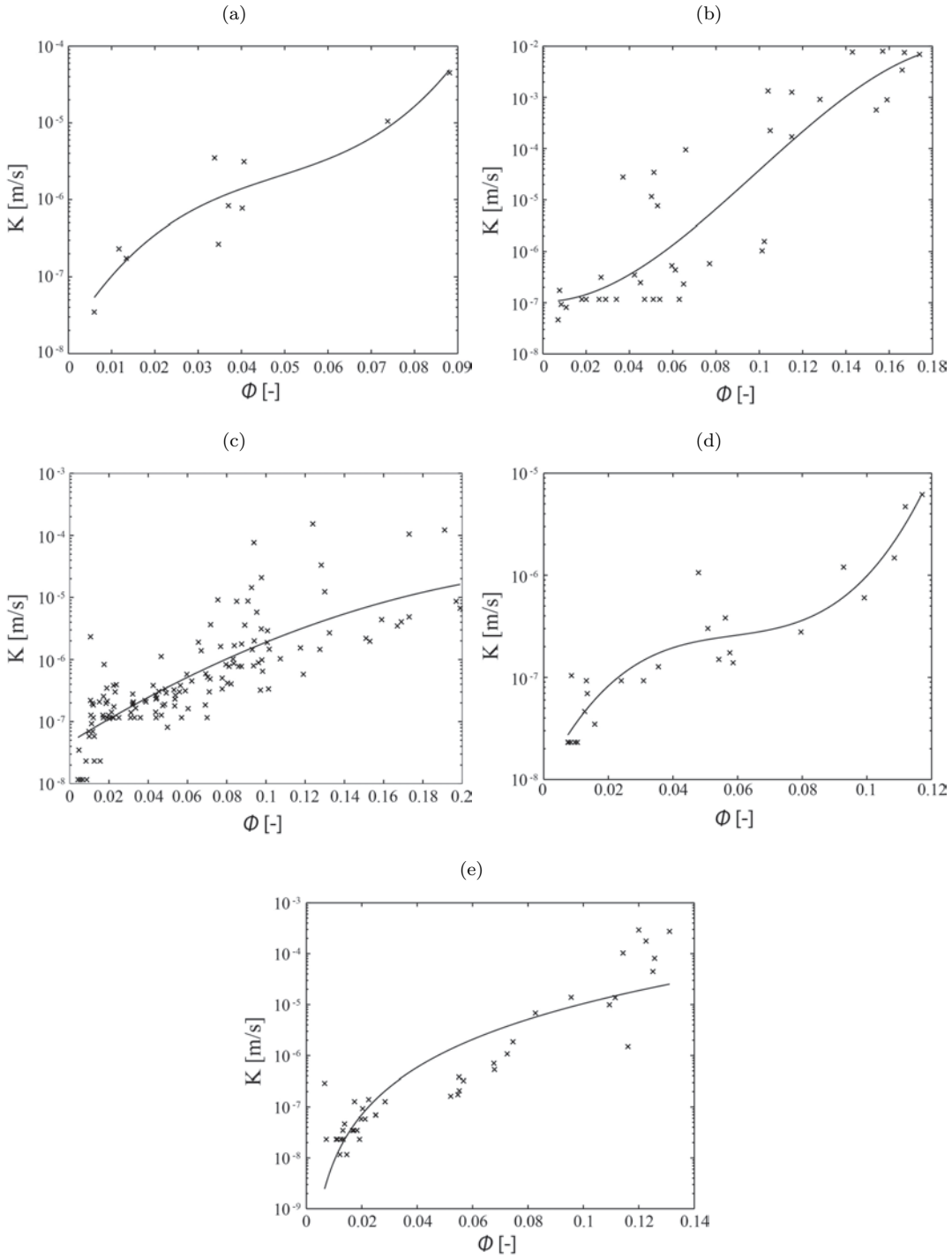

Figure B.3: Approximation of the $\{K, \phi\}$ dataset in layers (a) C1, (b) D4, (c) D3, (d) D2 and (e) D1.

Given as an information, the best fit ($R^2 = 0.77$) using Revil and Florsch (2010) empirical relationship on the dataset of layer D1 was obtained for an average grain diameter of 5.65 10^{-4} meters and an Archie exponent $m = 1$.

A major issue in fitting approximation functions is related to the small amount of data available for each individual hydrogeological layer. Although thicker than layer D3, layer D4 provides a much smaller amount of data (Figure B.3*c* and *b* respectively) displaying a wide range of values for K and for ϕ which makes it even more difficult to find any empirical function that fits the datasets. Nevertheless, it is assumed that at the general scale of the numerical model, and considering the scattering of the boreholes where measures were taken, empirical functions do not necessarily hold. In addition, most of the empirical functions found in the literature were employed to relate K and ϕ in granular media; which is not the type of material encountered in the subsurface of the Paris Basin.

Appendix C

Factor shifting in the multi-layer hydrogeological model

C.1 The petrofacies

As mentioned in Section 4.2.4, the term *petrofacies* designates the couple conductivity-porosity, $\{K, \phi\}$, which is considered in each homogeneous layer. According to the distribution of each $\{K, \phi\}$ dataset, a polynomial function is chosen to relate the two parameters and the K values are attributed to the principal component K_x of the hydraulic conductivity tensor in $\mathbf{K}_p$.

In Figure C.1 the MLE distributions in the whole model are illustrated when all the petrofacies P are set to their maximum values (top picture) or to their minimum values (bottom picture). These minimum and maximum values are listed in Table 4.3 and the two MLE distributions in Figure C.1 were obtained by setting every other uncertain variables at their mean, or reference, values.

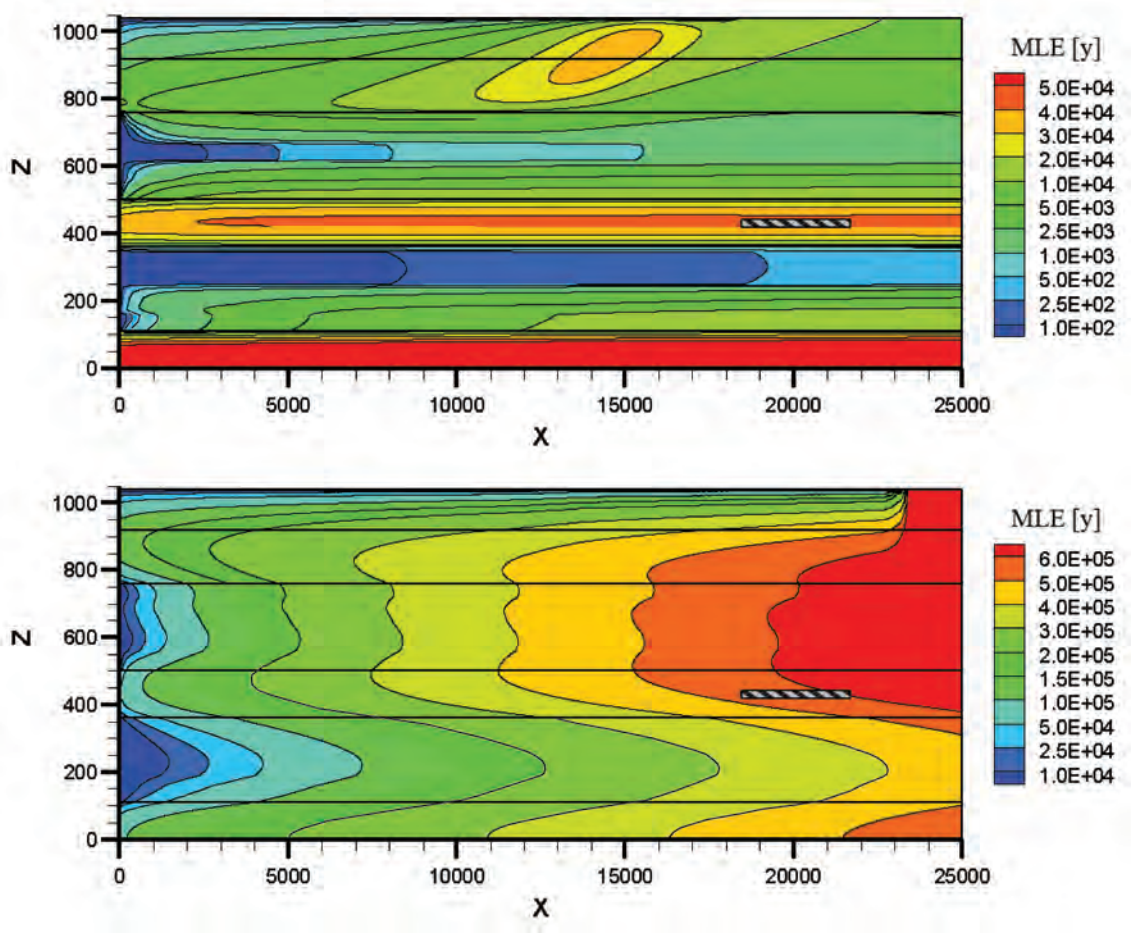

Figure C.1: Distribution of the MLE with the petrofacies set to their maximum values (top) or to their minimum values (bottom) in every layer (vertical exaggeration: 10)

When setting the maximum values of each petrofacies (top picture of Figure C.1), the effect of the two most conductive layers (L1b and D4) is clearly acknowledged. Viewed as highly conductive channels surrounded by less conductive ones, they play a major role in the transit time of solutes within each of the Oxfordian and Dogger sequence respectively. There is then a major difference in the MLE distributions in comparison to the reference case of Figure 4.3 which considers the mean values for each petrofacies. In the latter, the MLE from the target zone (TZ) is approximately 75'000 years whereas it is around 40'000 years when considering the maximum values of the petrofacies. Obviously, the greater the amount of solute entering layer D4 the lower the value of the MLE of solutes calculated at the TZ. The same reasoning could be made for the layer L1b but since it is more distant from layer C2, and also less conductive, it might have a lower influence on the output response quantity.

When considering the minimum values of the petrofacies (bottom picture of Figure C.1), the distribution of the MLE in the model is much more homogeneous than in the reference case (Figure 4.3) or when considering the maximum values of the petrofacies (top picture of Figure C.1). The effect of the conductive limestone sequences is still visible although it is not as distinct as in the case with the maximum values of the petrofacies. The MLE calculated at the TZ reaches approximately 550'000 years, which is much higher than in the reference case or when the maximum values of the petrofacies are considered.

Based on these observations it appears that the uncertainties characterizing the petrofacies P, *i.e.* the principal component of the conductivity tensor K_x and the porosity ϕ in each layer, have a very large influence on the variability of the MLE in the numerical model.

C.2 The anisotropy ratio in the hydraulic conductivity tensor

When accounting for the hydraulic conductivity tensor in each layer of the numerical model, the secondary component of the tensor, K_z, is retrieved as a function of the anisotropy ratio A_K considered in each layer. The uncertainty ranges are identical for each layer and they are uniformly distributed on [0.01 ; 1] (see Section 4.4.2).

Figure C.2 illustrates the distribution of the MLE in the whole model for a $A_K = 1$ (top picture) and for a $A_K = 0.01$ (bottom picture) with every other uncertain input factor set at its mean, or reference, value.

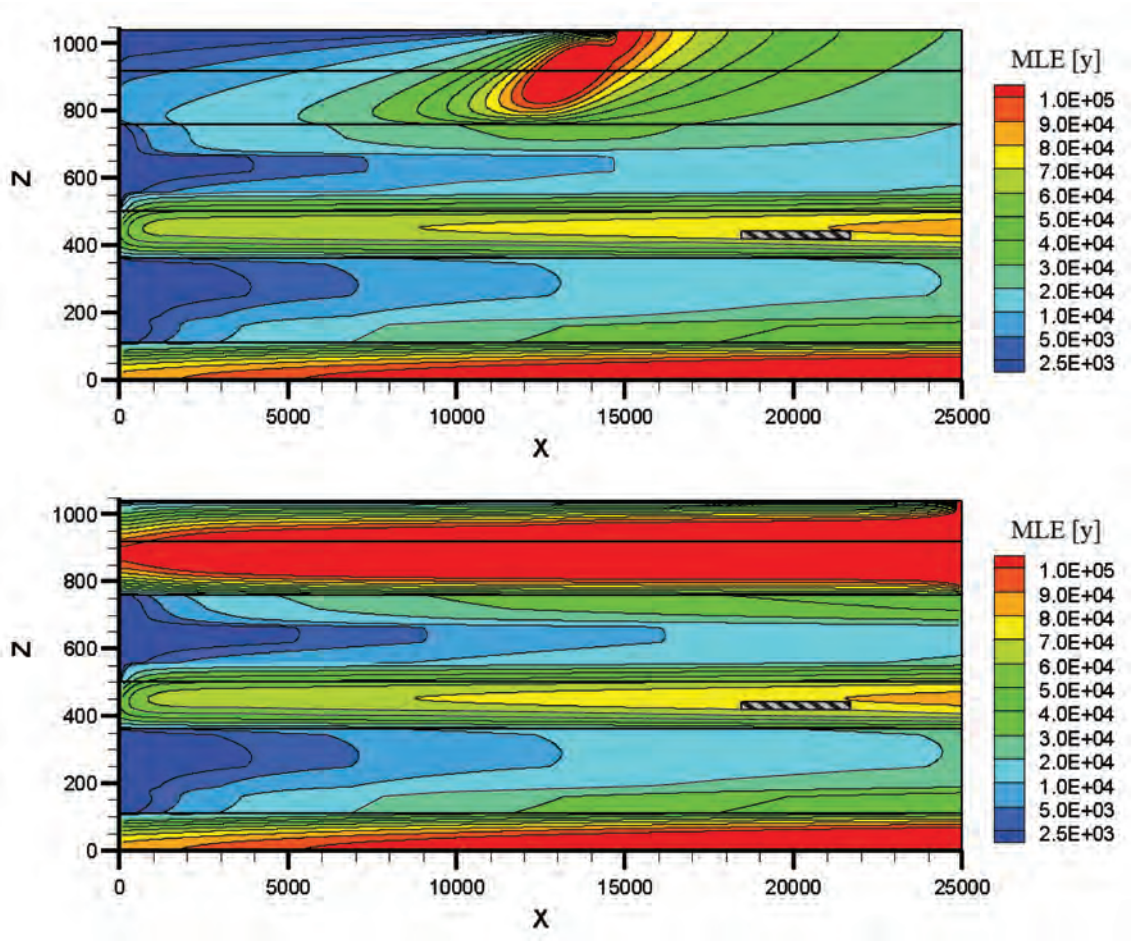

Figure C.2: Distribution of the MLE with the anisotropy ratio $A_K = 1$ (top) or $A_K = 0.01$ (bottom) in every layer (vertical exaggeration: 10)

Comparing Figure C.2 with the reference case of Figure 4.3, the distribution of the MLE in the model does not change drastically. The MLE calculated at the TZ remains stable around 75'000 years and only a small change is observable in the Oxfordian limestone sequences where a small anisotropy ratio (bottom picture) extends a little the fringes in the most conductive L1b layer. The main difference appears for the two low-permeability layers on top of the model (K3 and K1-K2) where the lower the anisotropy ratio the higher the MLE distribution within their volume. Indeed, reduced transverse groundwater fluxes occur with a K_z a hundred times lower than K_x. In these low-permeability layers, minor transverse advective fluxes would raise the time for any solute to reach either the underlying Oxfordian sequence, where higher advective fluxes occur, or the discharge boundary on top of the model.

C.3 The rotation matrix

As a reminder, in each layer of the numerical model, the hydraulic conductivity tensor $\mathbf{K}_p$ have components oriented along their principal direction X_p. The rotation matrix $\mathbf{R}$ applies to $\mathbf{K}_p$ in order to yield the orthotropic hydraulic conductivity tensor $\mathbf{K}$ implemented in each layer following the relationship:

$$\mathbf{K} = \mathbf{R}^T \, \mathbf{K}_p \, \mathbf{R} \tag{C.1}$$

In the numerical model, for each layer the Euler angle θ (in degree [°]) defines the rotation matrix as:

$$\mathbf{R} = \begin{pmatrix} \cos\theta & \sin\theta \\ -\sin\theta & \cos\theta \end{pmatrix} \tag{C.2}$$

In the sensitivity analysis of Section 4.4.2 the uncertainty ranges for the angle θ is equal in each layer and a uniform distribution on [-30 ; 30] (in degree [°]) is assumed.

In Figures C.3 and C.4 the angle θ is set to +30° and -30° respectively in every layer of the numerical model. Every other parameter is set to its mean, or reference, value and visual comparisons can be made with the nominal case of Figure 4.3. The resulting hydraulic gradient and the associated distribution of MLE in the whole model are depicted in the figures.

In comparison to the case where the angle $\theta = 0°$ (Figure 4.3) the heads contours and slightly tilted, especially in both limestone sequences. With an angle $\theta = -30°$ (Figure C.4) the groundwater fluxes are then oriented toward the lower formations in either sequence whereas with an angle $\theta = 30°$ (C.3) the advective fluxes are oriented toward the upper formations.

With concern on the middle (C2) layer, the orientation of the conductivity tensor does not influence much the orientation of the groundwater fluxes. Indeed, the hydraulic gradients implemented in the limestone sequences govern the flux orientation in the C2 layer. However, it must be noticed that an angle $\theta < 0°$ slightly shifts the groundwater flux inversion in layer C2 further toward the right side of the model whereas an angle $\theta > 0°$ tends to shift the groundwater inversion in the opposite direction, which may increase the amount of solutes departing from the target zone and entering the Dogger limestone sequence.

In the bottom pictures of Figures C.3 and C.4 the distributions of MLE are almost identical, but in comparison with the reference case of Figure 4.3 some differences appear. In layer C2, the reference case shows MLE value around 75'000 years whereas with extreme hydraulic conductivity tensor orientations the MLE reaches approximately 125'000 years. In the conductive formations of the limestone sequences, a raise of the MLE is also observed with maximum values of approximately 60'000 years and 80'000 years in the most conductive layers of the Oxfordian and Dogger sequences, L1b and D4 respectively, while in the reference case they reach approximately 20'000 years.

Thus, when the orientation of the principal component of the hydraulic conductivity tensor (K_x) in each layer is not oriented parallel to the x-axis, the MLE significantly raises. This is a consequence of groundwater fluxes oriented toward other, less conductive, layers rather than toward the discharge boundaries of either the Oxfordian or the Dogger sequences.

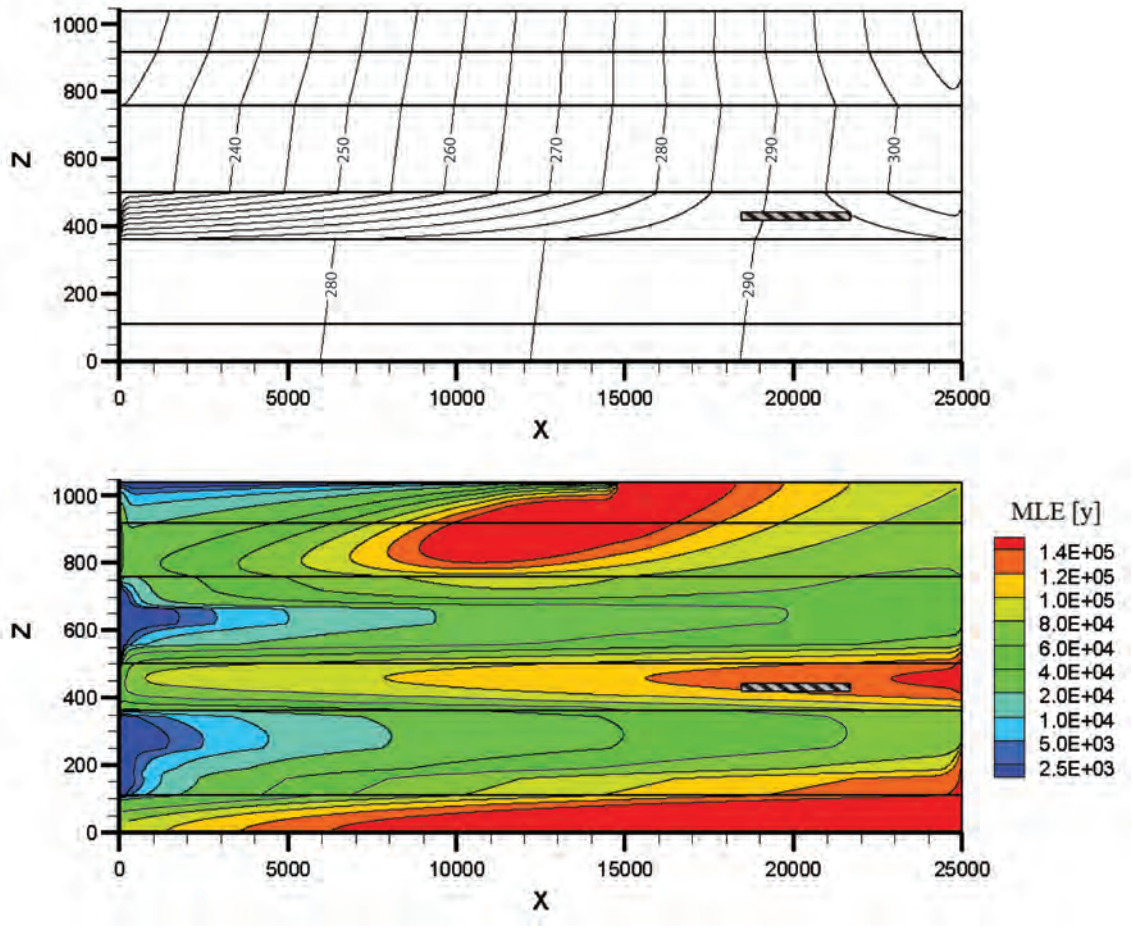

Figure C.3: (Top) heads contours and (bottom) MLE with an angle $\theta = +30^{\circ}$ in every layer (vertical exaggeration: 10)

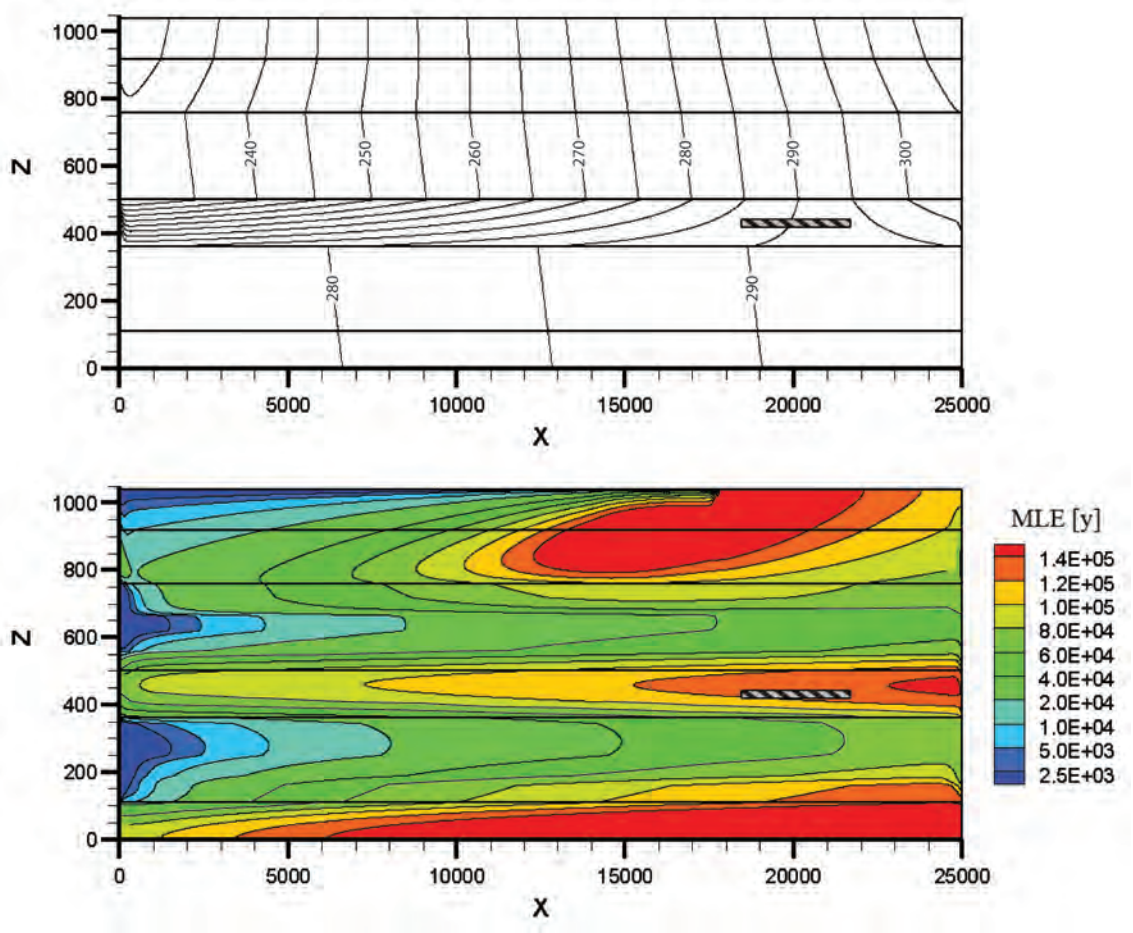

Figure C.4: (Top) heads contours and (bottom) MLE with an angle $\theta = -30^{\circ}$ in every layer (vertical exaggeration: 10)

C.4 The macro-dispersion tensor

In the formulation of the MLE (Eq. 4.6), the macro-dispersion tensor is represented through its principal and secondary components, the longitudinal α_L and the transverse α_T dispersivities respectively. In every layer, the principal component α_L is characterized by an uncertainty range uniformly distributed on [5 ; 25] (in meters) whereas the secondary component is retrieved by means of the anisotropy ratio A_α which is found in [0.01 ; 1].

Figure C.5 provides the distribution of the MLE in the entire model for a longitudinal dispersivity $\alpha_L = 25$m (top picture) or $\alpha_L = 5$m (bottom picture), every other uncertain variable being fixed to its mean, or reference, value. Note also that the anisotropy factor $A_\alpha = 0.1$ in both cases.

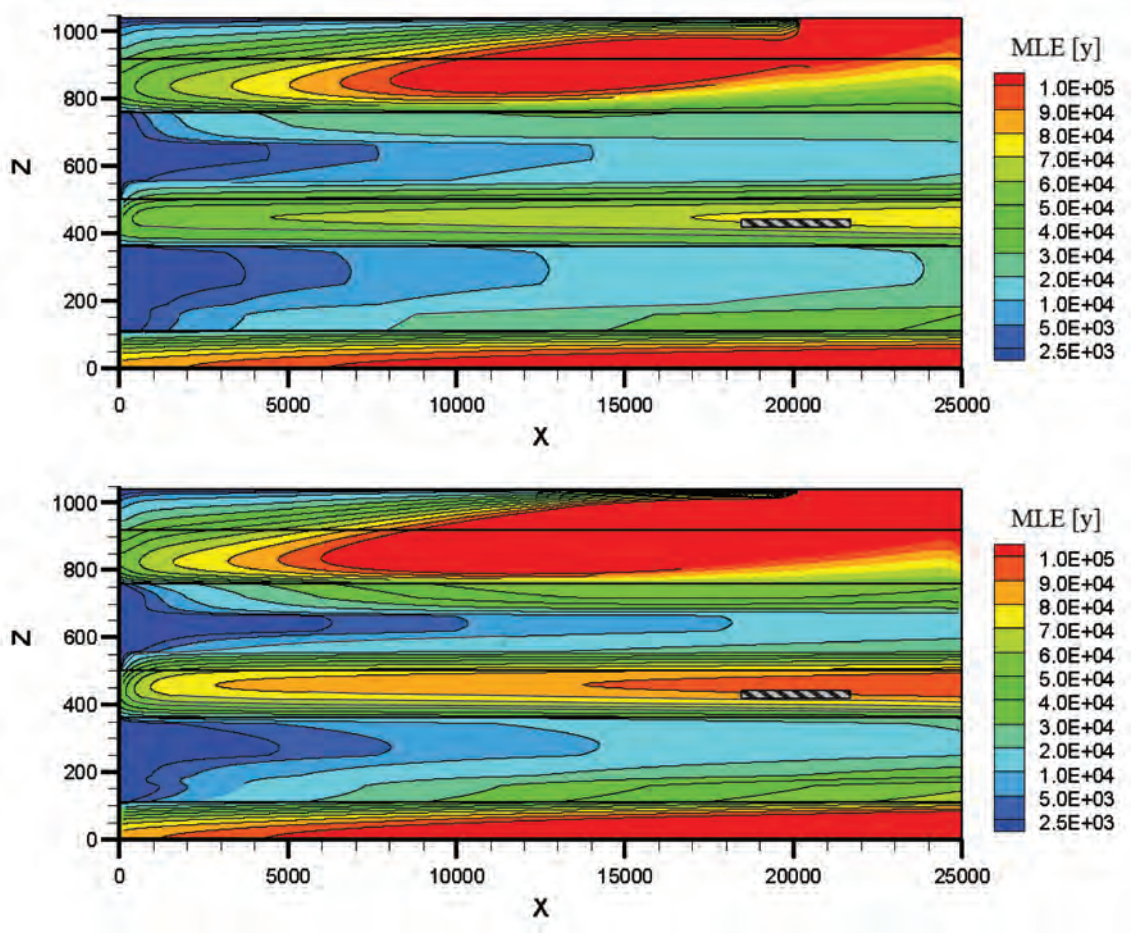

Figure C.5: Distribution of the MLE with the longitudinal dispersivity $\alpha_L = 25$m (top) or $\alpha_L = 5$m (bottom) in every layer (vertical exaggeration: 10)

In comparison to the reference case where $\alpha_L = 15$m (Figure 4.3) it can be observed that the lower the magnitude of the macro-dispersion tensor the higher the distribution of the MLE in the model. Obviously, dispersive effects add to the advective effects in the transport process (see Eq. 4.4) The effect of setting a low macro-dispersion tensor is observed for the conductive layers in both Oxfordian and Dogger sequences, for layers L1b and D4 respectively. It appears that the lower this parameter the more peculiar the effect of the conductive layer: the fringes extend preferably within the layers' volumes as the macro-dispersion tensor reduces; which means that advective effects dominate dispersive effects. With a strong magnitude of the macro-dispersion tensor, the MLE calculated at the TZ is approximately 70'000 years whereas it increases to approximately 90'000 years when setting a $\alpha_L = 5$m in the whole model, A_α still equals 0.1. This means that the magnitude of the macro-dispersion tensor has a little,

but not non-existent, effect on the target output response quantity considered in the sensitivity analysis of Chapter 4.

The changes in the distribution of the MLE in the model as a function of the anisotropy in the macro-dispersion tensor A_α has also been visualized when considering the extreme cases in all layers, *i.e.* $A_\alpha = 1$ and $A_\alpha = 0.01$. It appeared that these uncertain factors have no effect at all on the distribution of the MLE in the model, as discussed in Section 4.4.3. Hence, the figures representing the distribution of the MLE in the two above-mentioned cases are not illustrated here.

C.5 The hydraulic gradients

For the reference case, the hydraulic gradients in the three zones, namely , the Dogger ∇H^1 and the Oxfordian ∇H^2 limestone sequences, and the top of the model ∇H^3, were set according to values found in the literature. The uncertainty ranges were defined according to an arbitrary 20% perturbation of this reference case (Section 4.2.3).

In Figures C.6 and C.7 the three hydraulic gradients are set to their maximum and minimum values in the uncertainty ranges of Table 4.4 respectively. Every other uncertain variable is set to its mean, or reference, value. The resulting heads contour and the MLE distributions in the whole model are shown respectively in the top and in the bottom pictures of Figures C.7 and C.6.

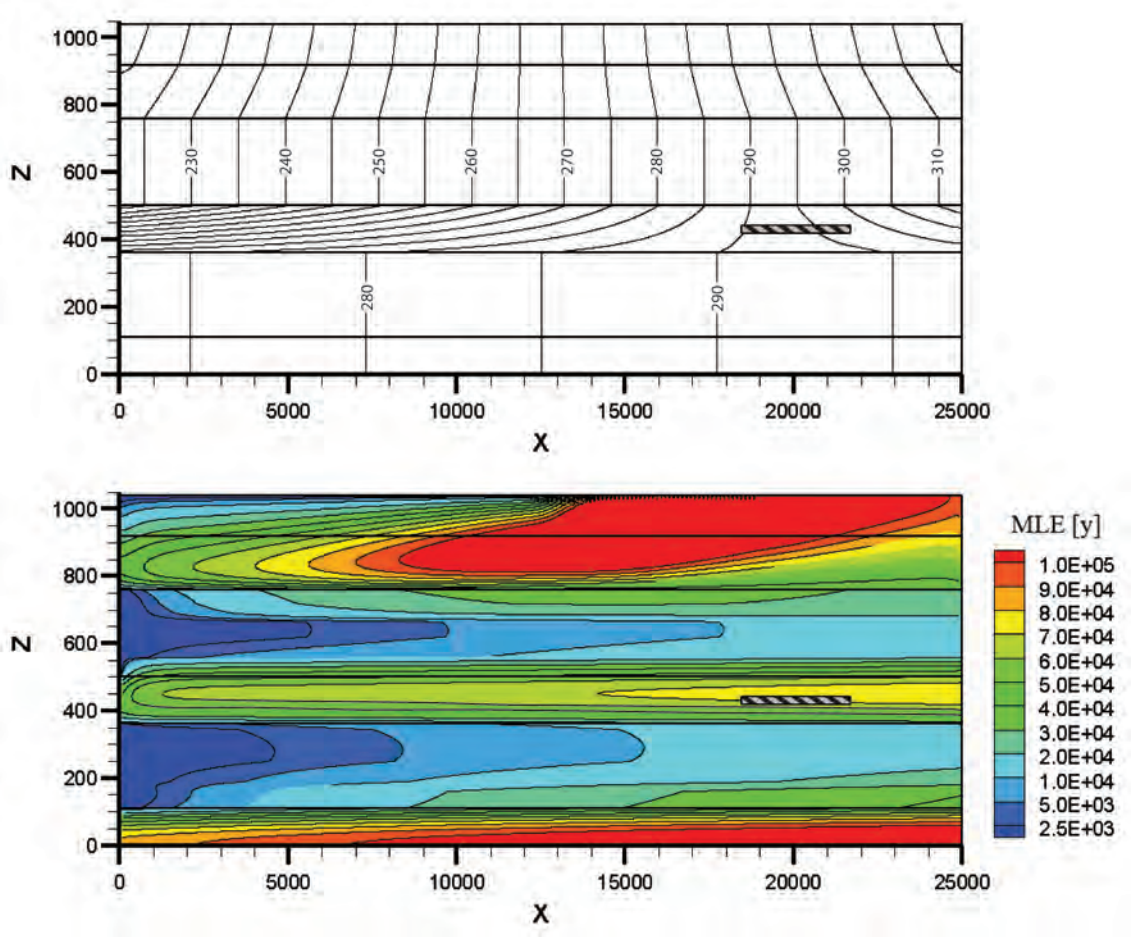

Figure C.6: (Top) heads contours and (bottom) MLE with the highest hydraulic gradients in the three zones (vertical exaggeration: 10)

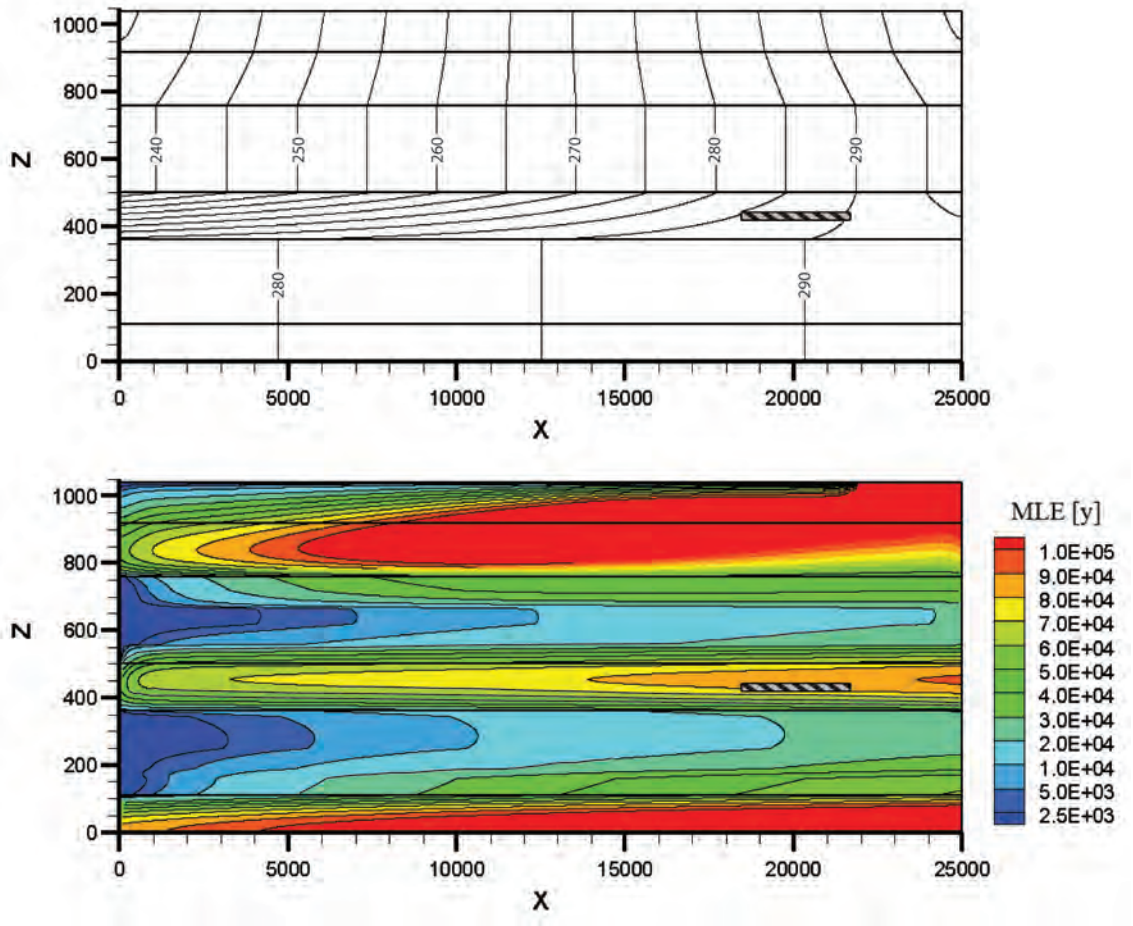

Figure C.7: (Top) heads contours and (bottom) MLE with the lowest hydraulic gradients in the three zones (vertical exaggeration: 10)

Perturbing the hydraulic gradients in each of the three zones significantly affects the contour heads in the model. Focusing on the position of the groundwater flux inversion in the C2 layer, it appears in the case with the lower gradients (Figure C.7) the inversion is positioned further to the right of the model. Hence, a larger proportion of the C2 layer has groundwater fluxes oriented upward and this may consequently reduce the amount of solute departing from the TZ to reach the Dogger sequence. Oppositely, implementing the upper bounds of the uncertainty ranges in Table 4.4 shifts the groundwater flux inversion in layer C2 toward the left of the model (Figure C.6), potentially raising the amount of solute departing from the TZ to reach the Dogger sequence.

The effect on the MLE distributions in the conductive layers of the Oxfordian and Dogger limestone sequences also appears since implementing the low boundary values of ∇H in each of the three zones reduces the advective fluxes. Comparing Figures C.6 and C.7 with the reference case of Figure 4.3, it can be observed that the lower the gradients the lesser the extension of the fringes in the limestone sequences. The MLE calculated at the TZ only slightly changes, with a value around 70'000 years for the case with the maximum ∇H and around 80'000 years for the case with minimum ∇H. So, the uncertainty on the hydraulic gradients in the three zones is thought to have a little effect on the variability of the output response quantity considered in the sensitivity analysis of Chapter 4. However, the combination of this effect with that of the petrofacies P or that of the orientation of the hydraulic conductivity tensor θ may emphasise the effect of the position of the groundwater flux inversion in the C2 layer by favouring a solute transport toward either the Oxfordian or the Dogger sequences.

Appendix D

Effects of the extreme values of the heterogeneity uncertainty bounds

D.1 Groundwater fluxes in the model

From Figure D.1 top to bottom, each aquifer sequence from the model was parametrized with the following Gaussian-variogram parameters:

Table D.1: Gaussian-variogram parameters of Figures D.1 and D.2

sub-Figure	λ_x	λ_z	$\mu_{log(K_g)}$	$\sigma^2_{log(K_g)}$
a & *b*	500m	15m	$inf[\mu_{log(K_g)}]$	$inf[\sigma^2_{log(K_g)}]$
c & *d*	2000m	30m	$nom[\mu_{log(K_g)}]$	$nom[\sigma^2_{log(K_g)}]$
e & *f*	8000m	60m	$sup[\mu_{log(K_g)}]$	$sup[\sigma^2_{log(K_g)}]$

where the values $\{inf[\mu_{log(K_g)}]$; $sup[\mu_{log(K_g)}]\}$ and $\{inf[\sigma^2_{log(K_g)}]$; $sup[\sigma^2_{log(K_g)}]\}$ for each aquifer sequences are the inferior and superior uncertainty bounds found in Table 5.2. The values $\{nom[\mu_{log(K_g)}]$; $nom[\sigma^2_{log(K_g)}]\}$ are the nominal values from Table 5.1. On the left side of Figure D.1, the $log(K_x)$ values were populated by making use of the turning-band method to produce one random multigaussian field. On the right side the multigaussian field was transformed into its connected form according to Eq. 5.8.

Implementing the lower bounds of the uncertainty ranges of Table 5.2 produces regular hydraulic head distributions within the layers, the isopiezes are rather linear in the heterogeneous fields. The spatial distribution of K parameters does not influence much the groundwater fluxes which are generally oriented from the inlet toward the outlet boundaries of the sequences. The connected form of the heterogeneous fields smoothers the isopiezes and are thus likely to stabilize the outflowing rates at the discharge boundaries.

In the nominal case, the hydraulic head distributions are quite irregular in the multigaussian case whereas the connected field diminishes the effect of the spatial distribution of K values. In the multigaussian case the position of the vertical groundwater flux inversion in the COX tends to drift from its position in homogeneous (Figure 4.2), or slightly heterogeneous (Figure D.1,*a*), models as a consequence of the spatial distribution of K values.

Then, implementing the upper bounds of the uncertainty ranges of Table 5.2 generates strong non-regularities in the hydraulic head distributions of both multigaussian and connected fields. Again, the position of the vertical groundwater flux inversion is strongly correlated to the spatial distribution of K values within the aquifer sequences of Dogger and Oxfordian ages.

From Figure D.1,*c*,*e* & *f*, it appears that the effect of the uncertainty on the Gaussian-variogram parameters modifies the groundwater fluxes inside the top-two layers of Kimmeridgian (K1-K2) and Tithonian (K3) ages. By augmenting the correlation lengths and variances (variogram parameters) of the distributions of K values, transverse fluxes raise within the heterogeneous sequences, influencing the orientation of groundwater fluxes within the thick impermeable layers, K1-K2 and K3. The spatial connectivity of high K values tends to lower this effect by homogenising the groundwater fluxes within the aquifer sequences. Nonetheless, the spatial distribution of K values has clearly a high contribution to the variability of the outflowing rates at the various discharge boundaries of the synthetic model; and the feature is emphasised at large correlation lengths and large variances of the K distributions.

D.2 Mean Lifetime Expectancy in the model

Figure D.2 presents the MLE distributions in the synthetic model for the six random fields illustrated in Figure D.1.

The distributions of the MLE throughout the aquifer sequences are more regular at the lower bounds of the uncertainty ranges of Table 5.2, and becomes more irregular as the uncertain Gaussian-variogram parameters get larger. The connected form always homogenises the distributions of the MLE, although at the upper bounds of the uncertainty ranges of Table 5.2 irregularities are still present. The spatial distribution of K values has an apparent effect on the irregularity of the distributions of the MLE throughout the aquifer sequences and also in the surrounding layers; this effect is augmented at high correlation lengths and variances.

The MLE from the TZ strongly reduces from the lower bounds of the uncertainty ranges ($\approx$ 120'000 years for the multigaussian and connected fields) to the upper bounds of the uncertainty ranges ($\approx$ 30'000 years for the multigaussian and connected fields).

From the observation of Figure D.2 it seems that between the lower and the upper bounds of the uncertainty ranges of Table 5.2, the MLE of water molecules calculated at the inlet of the limestone sequences varies from ≈ 110'000 years and ≈ 50'000 years, to ≈ 6'000 years and ≈ 4'000 years, in the Oxfordian and Dogger sequences respectively. Note that the spatial distribution of K values adds more variability to the above quantities as the Gaussian-variogram parameters are high.

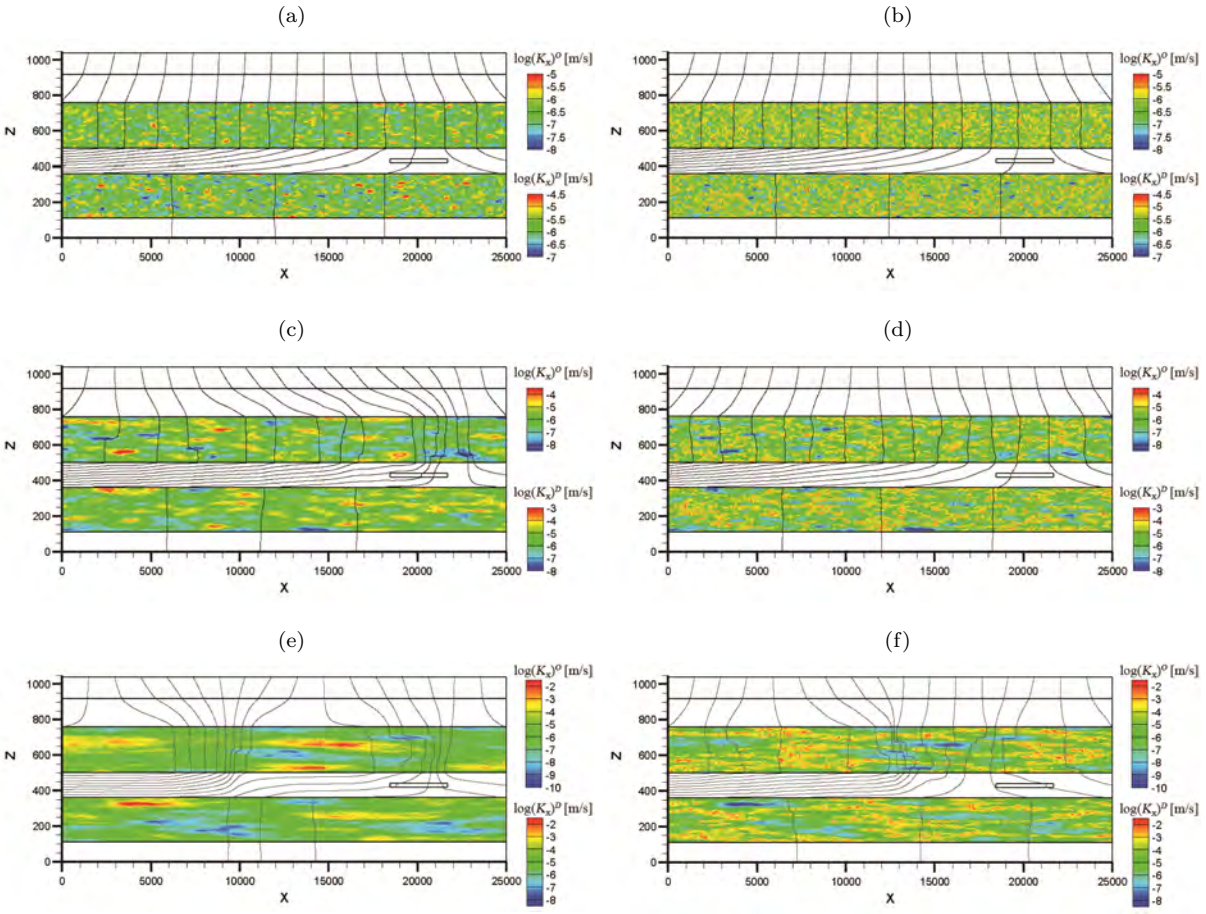

Figure D.1: Longitudinal conductivity $Log(K_x)$ for a multigaussian and connected field with inferior (a and b, resp.), nominal (c and d, resp.) and superior (e and f, resp.) values of the uncertainty bounds. Isopiezes in solid black lines - 5 m intervals. (vertical exaggeration: 10 m)

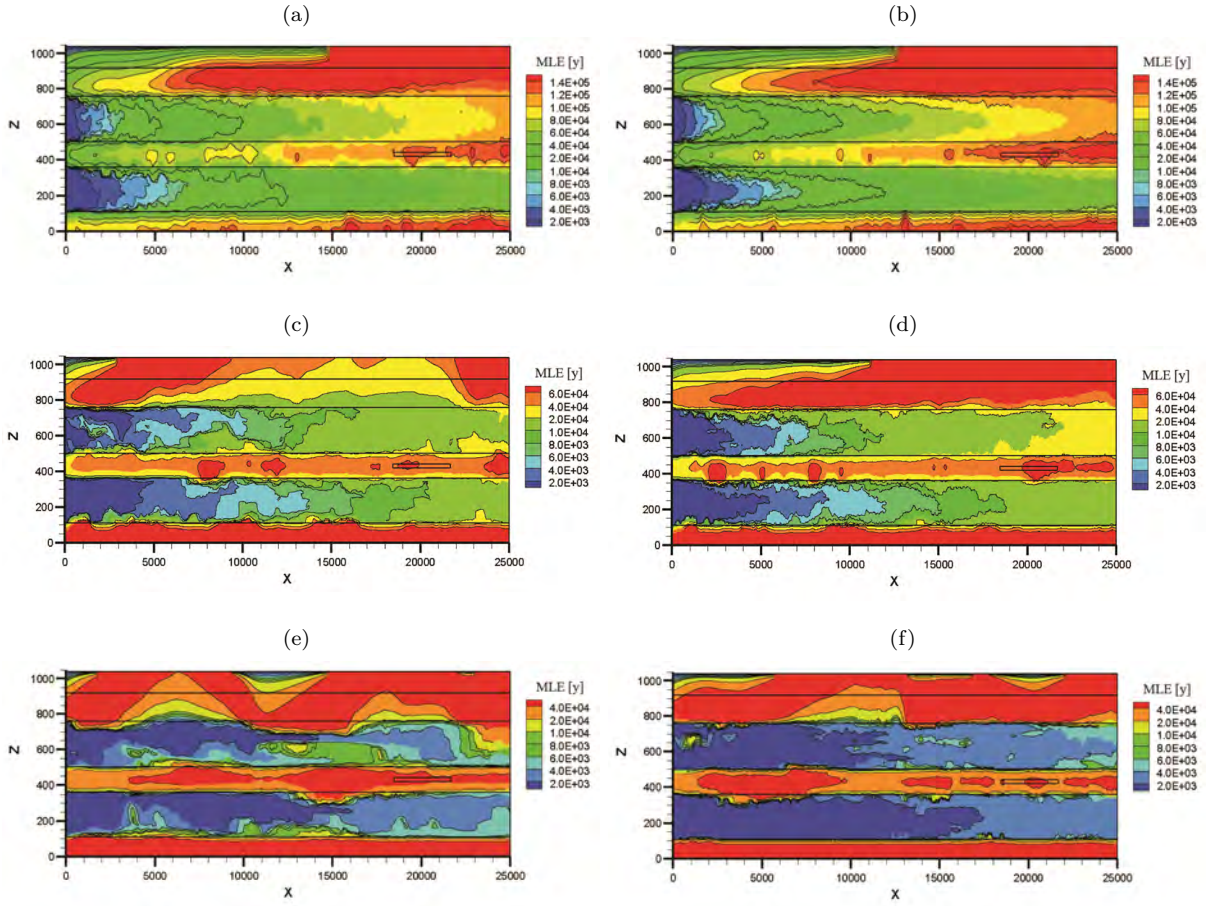

Figure D.2: Mean Lifetime Expectancy (MLE) for a multigaussian and connected field with inferior (*a* and *b*, resp.), nominal (*c* and *d*, resp.) and superior (*e* and *f*, resp.) values of the uncertainty bounds. Isopiezes in solid black lines - 5 m intervals. (vertical exaggeration: 10 m)

Appendix E

Modelling of predictive hydraulic impacts of a potential radioactive waste geological repository on the Meuse/Haute-Marne multilayered aquifer system (France)[1]

[1]This paper is published as: *H. Benabderrahmane, J. Kerrou, L. Tacher, G. Deman and P. Perrochet, 2014, Modelling of Predictive Hydraulic Impacts of a Potential Radioactive Waste Geological Repository on the Meuse/Haute-Marne Multilayered Aquifer System (France). Journal of Applied Mathematics & Physics, 2(12):1085-1090, doi: 10.4236/jamp.2014.212125.*

Journal of Applied Mathematics and Physics, 2014, 2, 1085-1090
Published Online November 2014 in SciRes. http://www.scirp.org/journal/jamp
http://dx.doi.org/10.4236/jamp.2014.212125

Modelling of Predictive Hydraulic Impacts of a Potential Radioactive Waste Geological Repository on the Meuse/Haute-Marne Multilayered Aquifer System (France)

Benabderrahmane Hakim[1*], Kerrou Jaouher[2], Tacher Laurent[3], Deman Gregory[2], Perrochet Pierre[2]

[1]Research & Development Department, ANDRA, 1-7 rue Jean Monnet, Châtenay-Malabry Cedex, France
[2]Centre of Hydrogeology and Geothermics (CHYN), University of Neuchâtel, Rue Emile Argand 11, Neuchâtel, Switzerland
[3]Laboratoire de Mécanique des Sols (EPFL-LMS), Ecole Polytechnique Fédérale de Lausanne, Lausanne, Switzerland
Email: [*]hakim.benabderrahmane@andra.fr

Received August 2014

Abstract

The French National Agency for Nuclear Waste Management (Andra) conducted a site investigations program within the project of a deep geological disposal of radioactive waste in the Meuse/Haute-Marne region. The construction of the tunnel of 5 Km length and the shafts of about 500 m depth to access the repository located in the clay host formation of Callovo-Oxfordian age, will lead to the perturbations of the groundwater flow fields. The prediction of the behaviour of these perturbations is needed to support: 1) the engineering and monitoring operations, and 2) the assessment of the consequences on groundwater resources. A variably-saturated flow model of a local multi-layered aquifer system is developed. It integrates the Oxfordian aquifer (limestone), the Kimmeridgianaquitard (marl) and the Barrois limestone aquifer including the karst conduits network. The variably-saturated flow Richard's equation is solved with a finite element simulator. Prior to the simulation of the predictive repository impacts, a transient flow model is calibrated with respect to Underground Research Laboratory (URL) construction data. The results are analysed and evaluated by the use of performance measures.

Keywords

Numerical Modelling, Variably-Saturated Flow, Karst, Repository, Hydraulic Impacts

[*]Corresponding author.

How to cite this paper: Hakim, B., Jaouher, K., Laurent, T., Gregory, D. and Pierre, P. (2014) Modelling of Predictive Hydraulic Impacts of a Potential Radioactive Waste Geological Repository on the Meuse/Haute-Marne Multilayered Aquifer System (France). *Journal of Applied Mathematics and Physics*, **2**, 1085-1090. http://dx.doi.org/10.4236/jamp.2014.212125

1. Introduction

Prior to the construction and the operation, by Andra (French Agency for Radioactive Waste), of the future deep geological repository for high and intermediate long lived radioactive waste, an analysis and evaluation of predictive hydraulic impacts which could be induced by the underground structures (shafts and tunnels) linking surface installations to the rad waste disposal located in the clay formation of Callovo-Oxfordian age (160 My) at depth of 500 m.The clay host formation of Callovo-Oxfordian age is found throughout the multilayered sedimentary fill of the Paris basin. The Callovo-Oxfordian layer is located between an overlying limestone of Oxfordian (Jurassic) age and an underlying limestone of Dogger (Jurassic) age. The potential repository emplacement is located in the Meuse/Haute-Marne sector which includes two nested zones: 1) transposition zone ZT and 2) the ZIRA. The transposition zone has been chosen as a suitable host domain based on 20 years of site investigations results; it extends over an area of approximately 250 km^2. In the transposition zone, the Callovo-Oxfordian formation is encountered at a depth of roughly 500 m, with a minimum thickness of approximately 130 m and a very small hydraulic conductivity (less than 10^{-12} m/s). Andra has carried out several investigation campaigns considering the chosen host domain and its surroundings and also carried out extensive site descriptive modelling. The aim of the site-descriptive modelling is to develop a discipline-integrated description of the past and present conditions at the site, by analysing, assessing, and modelling the data obtained from the investigation campaigns. "ZIRA" is an area extending over 30 Km^2 selected for further investigations, will be emplaced, five shafts with a diameter of 5 m to access the repository. Two access tunnels represented in the model by one ramp of over 5 Km length, 13 m of diameter and with a slope of about 12. This ramp will join the shafts in the host formation of the Callovo-Oxfordian at about 500 m of depth.

2. Conceptual Model and Mathematical Formulation

2.1. Geological Model, Engineered Structures and Data Monitoring

The hydrogeological conceptual model consists of 27 layers from the Triassic to Tertiary at the scale of the Paris basin and the 28 layers of the Triassic to Neocomian/Berriasian on the sector scale. The geological conceptual model represents the multilayered system including regional local faults and fracturing zone mainly located south west of the "ZIRA" which is the potential emplacement for the future repository. The construction of this geological concept was based on over 3300 drill holes data and about 2800 Km of seismic profiles.

Modelled domain is extracted from an integrated hydrogeological region-sector model which consists of the 1) 27 layers from the Triassic to the Quaternary on the scale of the Paris basin and 2) the 28 layers from the Triassic to the Portlandian on the scale of the sector. Lateral extend covers an area of about 3000 Km^2 which large enough to contain the hydraulic perturbation of repository construction. Vertically, only the geological layers above the Callovo-Oxfordian host formation which will host the underground structures (shafts and access tunnels) are represented. The first formation overlying the Callovo-Oxfordian is the Oxfordian formation considered as an aquifer and consists of limestones of Oxfordian age and early Kimmeridgian age and with a mean thickness at the repository potential emplacement of about 290 m. In the area of interest, this aquifer is split into two aquifer units separated by a marl layer called "sériegrise". Macro-pores zones identified through drill holes data and seismic survey results were characterized as relatively water productive with hydraulic conductivity ranging from 10^{-9} m/s to 10^{-7} m/s. Marne and limestone hydraulic conductivity are of 10^{-12} m/s and 10^{-9} m/s to 10^{-10} m/s respectively.

The 7 identified macropores zones are represented in the model by four relatively productive units:

- Hp1-4: lower unit located in deep Oxfordian with a mean thickness of 55 m;
- Hp5 confined by the marl;
- Hp6 and Hp7 belong to the Upper Oxfordien. Hp5, Hp6 and Hp7 have a mean thickness of about 5 m.

Kimmeridgianmarl layer overlying Oxfordian has men thickness of about 100 m and hydraulic conductivity estimated to 10^{-12} m/s. Measured specific storage values of the macro-pores zones ranges from 2.3×10^{-6} m^{-1} to 3.0×10^{-6} m^{-1}

For the simulations of the hydraulic impact of the access shafts to the Underground Research Laboratory (URL), it has been supposed that the perturbations of the flows will not affect the host formation northe underlying layers. It has thus been decided to uniquely model the layers on top of the Callovo-Oxfordian as a surface that comprises the sedimentary structures of the Oxfordian (the porous horizons and gray marl series).

2.2. Mathematical Formulation and Numerical Model

Variably Saturated Flow

Variably saturated groundwater flow is described by the modified form of Richard's equation which can be solved by Groundwater computer code in pressure head (ψ) form and in water content/hydraulic head form $(\theta\text{-}H)$.

$$\frac{\partial\theta}{\partial t}+\nabla\cdot q=\Delta Q$$

$$q=-k_r K\nabla H$$

$$c(\psi)\frac{\partial\psi}{\partial t}=\nabla\cdot k_r K\nabla(\psi+z)+\Delta Q$$

$$c(\psi)=S_w S_s+\theta\frac{\partial S_w}{\partial\psi}$$

$$\frac{\partial\theta}{\partial t}=\nabla\cdot k_r K\nabla(\psi+z)+\Delta Q$$

$H=\psi+z[\mathrm{L}]$, ψ : pressure head $[\mathrm{L}]$; z: elevation $[\mathrm{L}]$, q: Flux vector $\left[\mathrm{LT}^{-1}\right]$; t: time $[\mathrm{T}]$; ΔQ: source and/or sink term $\left[\mathrm{T}^{-1}\right]$; K : Tensor of saturated hydraulic conductivity $\left[\mathrm{LT}^{-1}\right]$; θ :water content [-]; $k_r=k_r(S_w)$: relative permeability of the medium with respect to degree of saturation [-]; $S_w=\theta/\theta_s$ [-]; θ_s: saturated water content [-]; $c(\psi)$: nonlinear capacitive coefficient.

The empirical law of dependence of the relative permeability and the pressure on the saturation is generally based on the experience achieved from the soil columns (granular porous media) on the decimeter to meter scale. A sensitivity of the variably saturated flow on the parameters of the model of Mualem (1976) [1]-Van Genuchten (1978) [2] allowed to test the parameters controlling the dependence of the relative permeability on the pressure or on the saturation with the aim to guarantee a rapid numerical convergence. The model of Mualem (1976) [1]-Van Genuchten (1978) [2] describes the dependence between the relative permeability and the saturation according to:

$$S_w=S_r+(S_m+S_r)\left[1+\|\alpha\psi\|^n\right]^{-m}\quad\text{for}\quad\psi<0$$

$$S_w=S_m\quad\text{for}\quad\psi\geq 0$$

$$k_r=S_e^{\nu}\left[1-\left(1-S_e^{1/m}\right)^m\right]^2,\quad m=1-\frac{1}{n},\quad n>1$$

$$S_e=\frac{S_w-S_r}{S_m-S_r}$$

S_r: residualsaturation [-]; S_m: maximum saturation [-]; S_e: effective saturation [-]; α [L^{-1}] and n [-] are fit parameters to experimental results; ν: pore connectivityparameter [-] equal to 0.5 for most soils [Mualem 1976].

The controlling coefficients of this model are α [1/L] and n [-], the coefficient υ being generally equal to 0.5. With S_w, S_m, S_r and $S_e=(S_w-S_r)/(S_m-S_r)$: the saturation with water, the maximum saturation, the residual saturation and the effective saturation, respectively. The parameter α could be considered as being the inverse of the thickness of the capillary zone. A low value of α is synonymous with a weak gradient of saturation, favorable for easy numerical convergence.

Figure 1 represents the range of van Genuchten curves utilized for parameterization of the unsaturated zone in the model under development. A α of 0.1 has been used for the semi-permeable formations so that they are twice as high as the aquifer formations (e.g.: the porous horizons).

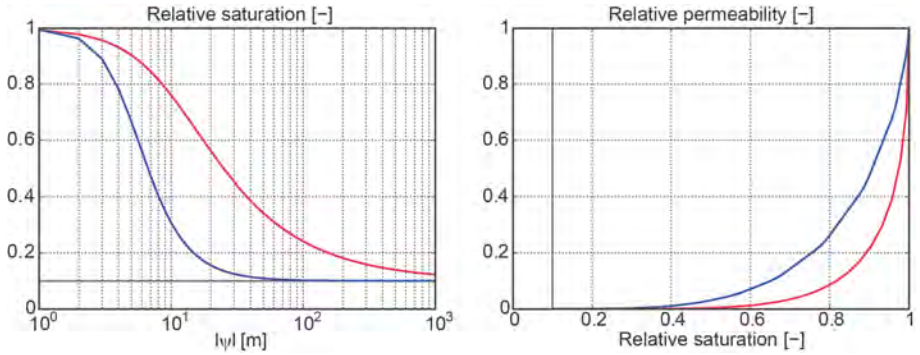

Figure 1. Range of van Genuchten curves utilized in the parameterization of the unsaturated zone. In red for α =0.1 [1/m] and n = 1.8 for the the semi-permeable units, in blue for α = 0.2 [1/m] and n = 3 for the aquifer units. The residual saturation of 0.1 is also shown in gray.

- **Meshing**

The multilayer conceptual model described above has been discretized in an unstructured 2D and 3D finiteelement mesh with a view to simulate flow and transport. The 3D mesh comprises 6'090'802 elements; the total number of nodes is 3'138'876. The major faults are discretized by means of 2D finite elements representing the fault planes. The diffuse fracturing is discretized as 3D elements and is represented as an equivalent porous medium. The flow solutions have been produced by means of the calculation code *Ground Water* (Cornaton, 2007) [3].

- **Boundary conditions**

In accordance with the hydrodynamics of regional hydrogeological system of the Paris Basin, boundary conditions for flow of the local model are applied to the geological medium or geosphere and to the engineered structures while they are in construction and later during the operational phase of the Underground Research Laboratory (URL) and the future Radwasterepository. Two types of boundary conditions are used to simulate first a steady state flow within the multilayered system before the construction of URL shafts in 2001 and prior to start the transient flow simulations. These boundary conditions are: 1) of Neumann type and correspond to the specified flux or recharge on the top of the model and 2) of Dirichlet type: constant hydraulic heads are assigned on the trace of the hydrographic network and at the lateral boundaries of the model. For the transient flow, the construction of the access shafts for the URL requires assignment of special boundary conditions that are variable in time. The boundary conditions applied at the level of the access shafts are seepage conditions: a hydraulic head equal to the elevation is attributed to the node (the pressure will be equal to the atmospheric pressure) while the flux is outward. Otherwise a null flux is assumed. The seepage conditions are variable in time in the sense that they are activated according to the calendar of advancement of the excavation.

3. Results of the Groundwater Flow Simulations

The analysis of the pressure records in multiple observation points shows that a quasi-steady state is obtained. This result has motivated an initial step of calibration for the local model which has consisted of calibrating the hydraulic conductivities of the different modeled units in the steady-state regime, supposing an instantaneous excavation of the main access shaft (PPA) to the URL and secondary shaft (PAX) where a seepage condition has been specified. The objective was to adjust the initial condition prior to excavation of the subterranean works but particularly calibration of the drainage flow rates for an equilibrium state. The values of hydraulic conductivity resulting from this calibration, along with the specific storage [coefficients] coming from the interpretation of hydraulic tests constitute the initial parameters for a transient-regime calibration. The calibration of the local model aims to better reproduce the measurements of hydraulic head in the monitoring drill holes of the perturbations and the flow rates of the water arrivals registered in the shafts PPA and PAX from October 2001 through August 2012, thus 11 years of continuous measurements. The method of calibration by "trial and error" is carried out by successive simulations and observation of the fit between the observed and modeled data. In each new simulation the user adjusts the hydrodynamic parameters to improve the fit of the measured values and those calculated. Computer code Ground Water (Cornaton, 2012) has been utilized to carry out the flow simula-

tion for a time period of 3957 days. The march in time is managed by an automatic estimation method with optimal time steps (predictor-corrector time integration algorithm). The time steps thereby are increased or reduced according to the convergence between two time steps. The calibration seeks to define the values of the parameters K and S of the 7 hydro geological entities that better reproduces the temporal records of the heads and flow rates in the porous horizons. One establishes for this purpose an objective function that represents the variable of interest. This function is the relative error squared between the measured data and the numerically simulated data. 14 records of head and 8 records of flow rates are used to calibrate the observed transient flow. The Objective Function is calculated for each simulation. The response surfaces method (RSM) allows establishing a mathematical approximation model from the values of the Objective Function. This polynomial model substitutes for the numerical model and thus allows evaluating values of the Objective Function for different combinations of the parameters. The RSM model is constructed by polynomial multiple regression based on the least squares criterion [4]. **Figure 2** represents the calibration of the transient flow based on the matching of the observed discharge and pressure/head time series. The predictive simulations of the hydraulic impacts rely on the quality of the transient flow calibration.

4. Results of the Predictive Impact Simulations

Predictive impact simulations were conducted based on the transient flow model reproducing the hydraulic perturbations induced by the URL construction and the drained shafts during 12 first years of the operational phase. Evaluation of the zone of hydraulic perturbation due to excavation of the access shafts has been carried out in the steady-state regime as well as in transient regime. The results have shown that the perturbation might at maximum exceed the extent of the transposition zone (steady-state regime). In the transient regime, the zone affected by the work of excavating the underground openings is less extensive with a maximum perturbation at the level of the lower Argovian around the tunnel/ramp [**Figure 3**]. After utilization of [the facility for] 100 years, it is expected to close and completely seal the underground infrastructure of the future repository. The predictive simulations of transient flow have been carried out to evaluate the time needed to return to a state of hydraulic equilibrium [as] prior to the perturbation. Tunnel and shafts construction induce hydraulic disturbance which is added to the one in place originated fromthe URL construction period and its present activity. Extensions and amplitudes of the hydraulic impact gradually evolve according to the schedule of the works. After six months of excavation of the first two shafts, it follows: 1) in the upper Oxfordian, a high amplitude perturbation localized around the tunnel while the shafts do not yet generate significant disruption, and 2) in the middle Oxfordian, the homogenized disturbance includes impacts of the tunnel and the shaft. At the end of construction, impacts: 1) in the upper Oxfordian indicate a local homogeneous perturbation with an amplitude of 40 m around the tunnel, discontinuous and very low extension and amplitude around the four shaft and 2) in the Middle Oxfordian a homo-

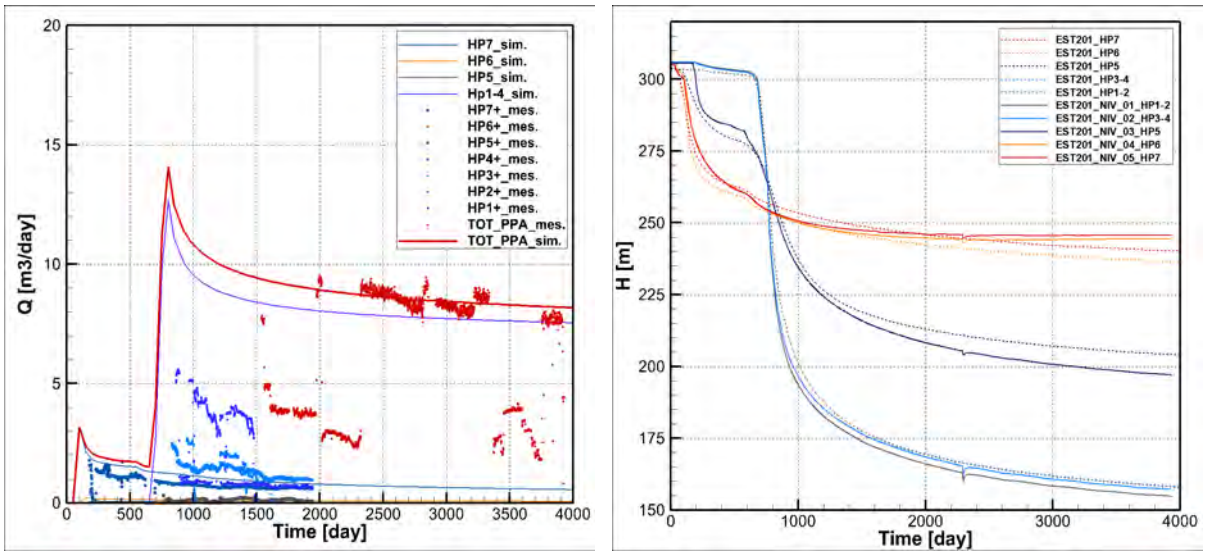

Figure 2. Measured and computed discharge (shafts) and pressure (monitoring borehole) time series.

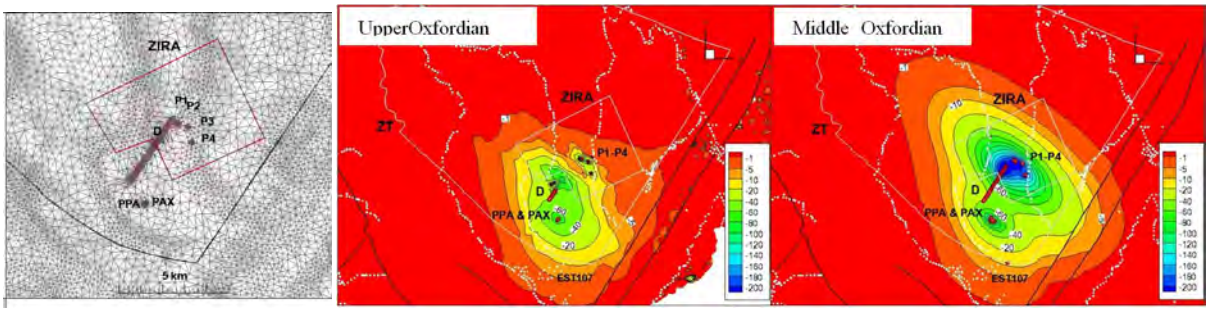

Figure 3. Meshing, layout of shafts and tunnels, and hydraulic impact at 100 years after the repository construction.

geneous disturbance of tunnel and shafts with maximum amplitude of about a hundred meters; at this stage the disturbance remains separated from that induced by underground laboratory.

The weak hydraulic response to shaft in the Upper Oxfordian is due to the absence of the porous horizons HP6 Hp7 in this area which is characterized by relatively low hydraulic diffusivity. During the operational phase: 1) in the Upper Oxfordian: disturbances of the tunnel and shafts as well as the Underground Laboratory are merged 50 years approximately; at 100 years approximately, the overall disturbance covers the South-West part of the transposition zone [**Figure 3**] and 2) in the Middle Oxfordian, the interference of the hydraulic disturbances occurs at the end of the construction phase. The overall impact covers the south-west part of the Transposition with maximum amplitude of 200 m.During the construction phase the maximum outflow rate of drained groundwater into the shafts, is about 20 m^3/day/shaft while the tunnel maximum water production is estimated to 150 m^3/day. Tunnel length crossing Oxfordian aquifer is of 3800 m. At the end of the operational phase (100 years approximately) of the repository, the water discharge developed by the macro-pores (Hp1-4, Hp5, Hp6) is about 4 m^3/day while the tunnel discharge is one order of magnitude greater.

5. Concluding Remarks

The results of predictive hydraulic impact of the underground structures of the future rad waste repository seek to be improved by reducing the conceptual and numerical uncertainties. One of the scopesis to compute the transient evolution of the unsaturated zone around the tunnel and the shafts under construction and during the operational phase. This will be achieved by: 1) refining the hydro geological concept of Barrois limestone aquifer system, 2) coupling the surface and subsurface flow and finally 3) refining the mesh around the tunnel and shafts in order to better control the unsaturated zone expansion during the construction and exploitation of the repository and its retreat induced by the closure of the facilities. The hydro-mechanical effect on the hydraulic overall hydraulic impact of the ramp and shaft construction will be investigated.

References

[1] Mualem, Y. (1976) A New Model to Predict the Hydraulic Conductivity of Unsaturated Porous Media. *Water Resources Research*, **12**, 513-522. http://dx.doi.org/10.1029/WR012i003p00513

[2] Van Genuchten, M.Th. (1978) Mass Transport in Saturated-Unsaturated Media: One-Dimensional Solutions. Research Rep. No. 87-WR-11, Water Resources Program, Princeton University.

[3] Cornaton, F. (2007) Ground Water: A 3-D Ground Water Flow, Mass Transport and Heat Transfer Finite Element Simulator. *Reference Manual*, 363 p. http://www1.unine.ch/chyn/php/softwares.php

[4] Kerrou, J., Deman, G., Tacher, L., Benabderrahmane, H. and Perrochet, P. (2015) Calibrating a 3D Numerical Model of Variably-Saturated Flow to Assess the Hydraulic Impacts of the Future Radwaste Repository on the Meuse/Haute-Marne Site. *The Clay Conference*, Brussels.

"C'est le propre des êtres vivants de faire aimer la vie,
même sous la forme d'une équation du second degré."

Comme un Roman - Daniel Pennac